Ab initio Calculations on the Ground and Excited States of Molecules

Charles Conor Ballard

B.Sc (Hons.)

A thesis presented for the degree of Doctor of Philosophy at the University of Edinburgh

1993

Declaration

This thesis was composed by myself and is based upon work performed as a Post-graduate student at the University of Edinburgh. Any results not obtained by myself but used in any subsequent discussion have been clearly indicated.

Abstract

In this work the results of highly correlated *ab initio* calculations on the low-lying states of propyne, furan, and the copper dimer are reported. The excitation energies obtained are used to interpret the electronic spectra of these molecules.

The electronic spectra of propyne and furan have been studied using multi-reference configuration interaction techniques. For both molecules the calculations comprise the low-lying valence and s, p, and d Rydberg states, all calculations being performed at the SCF optimised geometry. A variety of basis sets were used; the inclusion of diffuse polarisation functions in the basis set is found to improve the description of the excitation processes. In contrast, the use of polarisation functions optimised for the molecular ground state has negligible effect. The electronic spectrum of propyne is interpreted on the basis of these results to be similar to that of acetylene. The computed excitation energies for the valence states of furan differ drastically from earlier theoretical results. The present results are compared to new experimental data and found to give a consistent picture for the low-lying states.

The configuration interaction procedure was also utilised to determine the excitation energies of the *ungerade* states of Cu_2 arising from the $^2S+^2D$ asymptote. Much of the work took the form of a preliminary investigation to investigate the feasibility of the technique and applicability of a variety of basis sets. The calculations were performed at 2.20Å, arbitrarily, chosen to be close to the experimental equilibrium geometry. The inclusion of f-functions was found to be important in describing excitations involving states with different numbers of d electrons. Large reorganisation effects are found to accompany these excitations, which are not adequately described at the CISD level. Results are obtained which are in reasonable agreement with experiment and an interpretation is offered which states consistent with experimental data. The presence of a low-lying ion-pair state, with small amounts of valence character is confirmed.

The methods used were MRD-CI and Direct-CI, both within GAMESS-UK. Most of the work was performed on the Cray XMP28 and Convex 3840 machines at ULCC.

Acknowledgments

There are many people who deserve my thanks and acknowledgments for the contributions. First, I must thank the SERC for the award of a postgraduate studentship and providing the computer time. I must also thank my supervisors, Dr. Michael Palmer and Dr. Kenneth Lawley, for the assistance and encouragement provided, and sticking with me when the going got tough.

Thanks also go to those others who have in one way or another made major contributions to this work; these are in no particular order. Dr. Martin Guest, who was responsible for the extension and upkeep of GAMESS-UK, Dr. Isabel Walker for the electronic spectra and discussions on their assignment, and Dr. Hiroshi Tatewaki for discussions on basis sets for the transition metals.

I would also like to express my gratitude to Prof. Hiroshi Nakatsuji for the opportunity to work for a month at Kyoto University, and to the members of his research group, particularly Ehara-san and Sugimoto-san, for their hospitality during in my visit.

I would like to thank the various denizens of Rm. 6 and "the basement", for the friendship and camaraderie over the past few years. Also included in this category are my old drinking buddies (the names have been deleted to protect the not-so-innocent). I wish them well in all their endeavours.

I would also like to thank the people who have supported and encouraged me during the course of this work. I thank my parents,, without whom, of course, this would not have been possible ;-),, and family for their generous and open support. Their support, encouragement, and understanding were a great inspiration when the times got darkest. Last, but definitely not least, to Emi my deepest gratitude.

Thank you, and good luck, one-and-all.

Courses Attended:

Computers in Chemistry :Dr. K. Lawley
Dr. G.S. McDougall
Dr. R. Gould
Dr. P. Taylor
Prof. G.S. Pawley

Advances in Physical Chemistry :Dr. A. Jones
Dr. J. Tietze-Girault
Dr. S. Meach
Dr. B.M. Lowe

Computational Physics:Dr. R. D. Kenway (Physics)

Groups and Symmetries:Dr. D. J. Wallace (Physics)

Quantum Physics II:Dr. K. C. Bowler (Physics)

Advanced Quantum Theory:Dr. K. C. Bowler (Physics)

German for Scientists :German Department

Physical chemistry evening colloquia

Table of Contents

List of Tables

Chapter 1

Introduction

Quantum mechanical *ab initio* calculations on small molecules are widely used as an instrument in the study of problems in many fields of chemistry and physics. Most of these studies have dealt with ground state phenomena, *eg* structural properties of compounds, etc..., where a great deal of success has been obtained. A smaller body of literature exists for excited states, performed largely in connection with molecular spectroscopy, ionisation potentials, energy transfer, and reaction pathways via transition states.

With the advent of techniques which can be accurately applied to numerous systems these calculations have become complementary to the experimental work, aiding the interpretation of results which would otherwise be impossible. Ultimately another form of spectroscopy will be produced, one that is unhindered by selection rules and the stability of the system being studied.

This chapter contains a discussion on the basic techniques used in the field of quantum chemistry; including the Hartree-Fock model of a many electron systems, and the incorrect treatment of the interactions between electrons that are inherent in this model. Some of the more common methods for the overcoming the problem are discussed.

1.1 The Schrődinger wave equation

Non-relativistic approaches based upon the Schrődinger wave equation [1] have provided the basic theoretical framework for the treatment of atoms and molecules. As the stationary states of conservative systems are of interest, the time-independe nt form is used. For a system containing n electrons and N nuclei in the absence of any external fields:

$$\left\{-\sum_{A}^{N}\frac{\nabla_A^2}{2M_A}-\frac{1}{2}\sum_{i}^{n}\nabla_i^2-\sum_{iA}^{nN}\frac{Z_A}{r_{iA}}+\sum_{i>j}^{n}\frac{1}{r_{ij}}+\sum_{A>B}^{N}\frac{Z_AZ_B}{r_{AB}}\right\}\Psi(r,R)=E\Psi(r,R) \tag{1.1}$$

in atomic units. The first two bracketed terms are the nuclear and electronic kinetic energies, the third term is the electron-nuclear coulombic attraction, the fourth and fifth terms are the electron-electron and nuclear-nuclear repulsions respectively. The Schrődinger wave equation is often schematically simplified by gathering together the bracketed terms as $\hat{H}$, the Hamiltonian operator.

Non-relativistic quantum theory does not include any requirement that the particles have spin, this has to be introduced as a separate, but complementary, postulate. Electrons as spin $\frac{1}{2}$ particles are fermions and therefore obey Fermi statistics. This exhibits itself in the requirement that the wavefunction be anti-symmetric with respect to the interchange of any two indistinguishable particles and in the Pauli exclusion principle wherein no particles with the same quantum numbers may share the same point in coordinate space. As the non-relativistic Hamiltonian is independent of the spin of the particles it commutes with the spin operators S^2 and S_z.

The 3(N+n) degrees of freedom of the Schrődinger wave equation, and therefore the complexity of the problem, can be greatly reduced by the use of the Born-Oppenheimer approximation[2]. Due to the disparity in the masses of the electrons and nuclei, the electronic motion can accommodate almost instantaneously any change in the position of the nuclei; therefore the electrons experience the nuclei as being fixed force centers. This is valid if there is no coupling between the

electronic states induced by nuclear motion, and if no states are degenerate or near degenerate with the state of interest. The overall wavefunction can be separated into electronic Ψ_e and nuclear Ψ_n terms:

$$\Psi(r,R) = \Psi_e(r,R)\Psi_n(R) \tag{1.2}$$

where $\{r\}$ defines the electronic coordinates, $\{R\}$ the nuclear coordinates and Ψ_e obeys the electronic Schrődinger equation:

$$\hat{H}_e\Psi_e = E_e(R)\Psi_e \tag{1.3}$$

The nuclear kinetic energy term is small compared to the other terms and can be neglected when considering the electronic wavefunction, whilst the nuclear repulsion energy term is completely defined by the nuclear geometry. Therefore the electronic Hamiltonian is given by:

$$\hat{H}_e = -\frac{1}{2}\sum_{i}^{n}\nabla_i^2 - \sum_{iA}^{nN}\frac{Z_A}{r_{iA}} + \sum_{i>j}^{n} r_{ij}^{-1} \tag{1.4}$$

or as the sum of one- and two- electron terms:

$$\hat{H}_e = \sum_{i}^{n} h(i) + \sum_{i>j}^{n} r_{ij}^{-1} \tag{1.5}$$

The total energy for the system at a particular geometry, $E(R)$, is then given by the sum of the nuclear repulsion energy and the electronic energy, E_e.

The nuclear Schrődinger equation is given by:

$$\hat{H}_n\Psi_n(R) = E_n(R)\Psi_n(R) \tag{1.6}$$

where the nuclei are considered as moving in the averaged potential of the electrons acting through the nuclear Hamiltonian:

$$\hat{H}_n = -\sum_{A}^{N}\frac{\nabla_A^2}{2M_A} + \sum_{A>B}^{N}\frac{Z_A Z_B}{r_{AB}} + E_e(R) \tag{1.7}$$

The nuclear wavefunction Ψ_n describes the vibrational, rotational and translational motion of the system. The idea of a potential energy surface comes from the solution of the electronic problem, giving $E(R)$, for all nuclear configurations.

In practice the Born-Oppenheimer approximation is found to be excellent. Only in the most accurate calculations for molecules containing light atoms are the errors that arise from its use significant.

The relativistic contribution to the energy is proportional to Z^4c^{-2}, this term is large even for relatively light nuclei, however it has been noted [3] that for light atoms the relativistic portion of the energy is virtually independent of the number of valence electrons and that most of the relativistic energy is associated with the core electrons. As many molecular properties are largely determined by the valence electrons, the relativistic effect can be expected to be of little importance; indeed perturbation treatments can be used to approximate relativistic effects such as spin-orbit coupling. Thus the relativistic calculation for the binding energy of Li_2 is lower than the non-relativistic result by 0.04 eV [4]. However, this approximation does not hold for heavier nuclei ($\geq 70 a.m.u.$) where the valence region is significantly affected. Electrons occupying penetrating valence orbitals, those of low angular momentum, are substantially stabilised by the relativistic effect due to the fact that they spend a significant amount of time near the heavy nucleus and attain a velocity appreciable compared to the speed of light; here a full relativistic treatment is required [4, 5].

The non-relativistic Schrődinger equation can only be solved exactly for the simplest of systems such as H_2^+, for more complicated systems approximate solutions are employed to obtain Ψ_e.

1.2 Hartree-Fock Approximation

If the particles in a many-body system are considered as being independent, i.e. not depending on the instantaneous position of the other interacting bodies, the solution of the Schrődinger equation is greatly simplified. For atomic and molecular systems, by analogy with the solution for hydrogen, the concept of orbitals [6–8] is introduced. The most common independent electron model used in quantum chemistry is the Hartree-Fock approximation, where it is assumed that each

electron moves under the influence of the average field of the other electrons. This average field is the Hartree-Fock potential ν^{HF}. This reduces the many body Hamiltonian to a collection of (effective) one-electron terms, individually referred to as Fock operators:

$$\hat{f}(i) = -\frac{1}{2}\nabla_i^2 - \sum_A^N \frac{Z_A}{r_{iA}} + \nu^{HF}(i) \tag{1.8}$$

$$\hat{f}(i) = h(i) + \nu^{HF}(i) \tag{1.9}$$

The wavefunction is then taken as the product of n one-electron functions, ψ, with fermion symmetry enforced upon them. The simplest form that the wavefunction can take is a single Slater determinant:

$$|\Psi_e\rangle = \frac{1}{\sqrt{n!}} \begin{vmatrix} \psi_1(1) & \psi_2(1)\cdots & \psi_n(1) \\ \psi_1(2) & \psi_2(2)\cdots & \psi_n(2) \\ \vdots & \vdots & \vdots \\ \psi_1(n) & \psi_2(n)\cdots & \psi_n(n) \end{vmatrix} \tag{1.10}$$

or alternatively:

$$|\Psi_e\rangle = |\psi_1(1)\psi_2(2)\cdots\psi_i(i)\psi_j(j)\cdots\psi_n(n)\rangle \tag{1.11}$$

where each of the one-electron functions, or spin-orbitals, is composed of spatial and spin parts:

$$\psi_i(x_i) = \begin{cases} \phi_i(r_i)\alpha(\omega) \\ \phi_i'(r_i)\beta(\omega) \end{cases} \tag{1.12}$$

The Slater determinant formed from the n lowest orbitals is the Hartree Fock ground state, which is the best variational approximation to (and hence an upper bound to the energy of) the ground state of the system, in the single determinant form. The electronic energy is given by the expectation value of the Hamiltonian operator for the determinant:

$$\begin{aligned} E &= \langle\Psi_e|\hat{H}|\Psi_e\rangle \\ &= \sum_{i<j}\langle i|h|j\rangle + \sum_{i<j<k<l}\langle ij\|kl\rangle \end{aligned} \tag{1.13}$$

where

$$\langle i|h|j\rangle = \int dx_1 \psi_i^*(x_1) h(r_1) \psi_i(x_1) \tag{1.14}$$

and

$$\langle ij\|kl\rangle = \langle ij|kl\rangle - \langle ij|lk\rangle \tag{1.15}$$

$$\langle ij|kl\rangle = \int dx_1 dx_2 \psi_i^*(x_1)\psi_j^*(x_2) r_{12}^{-1} \psi_k(x_1)\psi_l(x_2) \tag{1.16}$$

As the electrons are indistinguishable any labels may have been used; by convention the equations are expressed in terms of electrons 1 and 2. The total energy cannot be identified with the expectation value of a single determinant in the case of degenerate wavefunctions.

Each of the spin-orbitals $\{\psi_i\}$ is an eigenfunction of the Hartree-Fock pseudo-eigenvalue equation with orbital energies $\{\varepsilon_i\}$. This is equivalent to the optimisation of the electronic energy with respect to variations in the orbitals under the constraint that the spin-orbitals are orthogonal $\langle \psi_i|\psi_j\rangle = \delta_{ij}$:

$$\hat{f}_i \psi_i = \varepsilon_i \psi_i \tag{1.17}$$

$$\left[h(i) + \sum_{j \neq i} \int dx_2 |\psi_j(2)|^2 r_{12}^{-1} - \sum_{j \neq i} \int dx_2 \psi_j^*(2)\psi_i(2) r_{12}^{-1} \right] \psi_i = \varepsilon_i \psi_i \tag{1.18}$$

where the second and third terms within the brackets are the coulomb, $\hat{J}_j$, and exchange, $\hat{K}_j$, operators respectively. The coulomb operator can be envisaged as the coulombic potential of an electron with density distribution $|\psi_j|^2$ acting upon another electron. The exchange operator has no such classical analogue.

The Slater determinant obeys the Pauli exclusion principle correlating the motions of electrons with the same spin through the exchange integral. Thus when the number of α and β electrons differ, the spatial components of the spin-orbitals cannot be expected to be the same for electrons of different spin, even if the quantum numbers, barring spin, are shared. If the spatial terms are considered to be the identical for paired electrons we have Restricted Hartree-Fock (RHF) for a closed shell system and Restricted Open-shell Hartree-Fock (ROHF) for a system with unpaired electrons; if the spatial term is allowed to differ we have the Unrestricted Hartree-Fock (UHF) single determinant.

The Hartree-Fock equations can be solved numerically for atoms and small diatomic molecules; for larger systems some form of algebraic approximation is required. This usually takes the form of expanding each of the molecular orbitals as a linear combination of a one particle basis:

$$\psi_i = \sum_\mu C_{\mu i}\chi_\mu \tag{1.19}$$

The χ_μ are usually referred to as atomic orbitals and the $C_{\mu i}$ as molecular orbital coefficients. This is commonly known as the linear combination of atomic orbitals (LCAO) method.

1.2.1 The Restricted Hartree-Fock Method

For many molecules the ground state near the equilibrium geometry is well described by the closed shell model. This is the justification of the RHF technique due to Roothaan [9]. The energy is minimised with respect to variation of the molecular orbital coefficients, subject to the constraint that the resulting molecular orbitals remain orthogonal. This leads to the Hartree-Fock-Roothaan system of equations. Within the approximation of a one particle basis this becomes a matrix problem:

$$FC = \varepsilon SC \tag{1.20}$$

where S and F are the overlap and Fock matrices in the atomic orbital basis:

$$S_{\mu\nu} = (\chi_\mu|\chi_\nu), \quad F_{\mu\nu} = (\chi_\mu|\hat{f}|\chi_\nu) \tag{1.21}$$

where $\hat{f}$ is an effective one electron Hamiltonian. In the closed shell case, where the spin terms have been integrated out:

$$\hat{f}(r_1) = h(r_1) + \sum_a^{\frac{n}{2}} [2J_a(r_1) - K_a(r_1)] \tag{1.22}$$

The system of equations is solved iteratively until self consistency is obtained.

The energy of an occupied orbital is given by

$$\varepsilon_a = \langle a|h|a\rangle + \sum_b \langle ab||ab\rangle \tag{1.23}$$

which is also by Koopmans' theorem, the ionisation potential of the orbital.

The total energy is then given by:

$$E = 2\sum_{a}^{\frac{n}{2}}(a|h|a) + \sum_{b}^{\frac{n}{2}}(a|\left[2\hat{J}_b(r_1) - \hat{K}_b(r_1)\right]|a) + \sum_{A>B}^{N}\frac{Z_A Z_B}{r_{AB}} \tag{1.24}$$

where the sum runs over occupied orbitals.

The general expression for the energy of a system containing any number of open shells is given by:

$$E = \sum_{i}\omega_i h_{ii} + \sum_{ij}\left(\alpha_{ij}\hat{J}_{ij} - \beta_{ij}\hat{K}_{ij}\right) \tag{1.25}$$

where the state parameters $\{\omega_i\}$, $\{\alpha_{ij}\}$ and $\{\beta_{ij}\}$ are related to the occupations of the orbitals i, j and upon the spins of the unpaired electrons. Orbitals within a shell have the same state parameters. For closed shell and high spin open-shell a single determinant can be used to describe the wavefunction ($c_p = 1$), *eg* for a closed shell wavefunction $\omega_i = 2$, $\alpha_{ij} = 2$ and $\beta_{ij} = 1$ for i,j doubly occupied, and for the open-shell high spin wavefunction:

$$\omega_i = \begin{pmatrix} 2 & 1 \end{pmatrix},\ \alpha_{ij} = \begin{pmatrix} 2 & 1 \\ 1 & \frac{1}{2} \end{pmatrix} \text{ and } \beta_{ij} = \begin{pmatrix} -1 & -\frac{1}{2} \\ -\frac{1}{2} & \frac{1}{2} \end{pmatrix} \tag{1.26}$$

If the total energy can be divided into the contributions from the different terms, then the use of a restricted wavefunction is valid. Using the method of Lagrangian multipliers $\{\lambda_{ij}\}$, under the condition that the molecular orbitals remain orthogonal, a series of equations is obtained with different Fock operators for each of the shells:

$$\hat{F}^i\psi_i = \sum_{j}\lambda_{ij}\psi_i \tag{1.27}$$

$$\hat{F}^i = \frac{1}{2}\omega_i\hat{h} + \sum_{j}\left(\alpha_{ij}\hat{J}_j - \beta_{ij}\hat{K}_j\right) \tag{1.28}$$

Unlike the closed shell Hartree-Fock theory, it is not possible to use the invariance of the total wavefunction under a unitary transformation, to eliminate the off-diagonal Lagrangian multipliers that are between orbitals in different shells. Ignoring these terms leads to the orbitals in different shells not being orthogonal.

The basis of the two operator method [10] is that the equations for the open and closed shells are solved separately. Thus

$$\hat{F}^c \phi_c = \varepsilon_c \phi_c \tag{1.29}$$

$$\hat{F}^o \phi_o = \varepsilon_o \phi_o \tag{1.30}$$

where

$$\hat{F}^c = h + 2\sum_j N_j (J_j - \frac{1}{2} K_j) \tag{1.31}$$

$$\hat{F}^o = h + \sum_j N_j (J_j - \frac{1}{2} K_j) - K_{os} \tag{1.32}$$

The orthogonality can be obtained using projection operators.

It was shown by Roothaan [10] that a single pseudo-eigenvalue equations can be obtained by defining certain coupling operators. There is a considerable literature on the formulation of eigenvalue equations which embody the conditions for a stationary expectation value of the energy [11]. The eigenvectors obtained in the solution of the ROHF equations are also eigenvectors of the spin operator $\hat{S}_z$. Linear combinations of restricted solutions can be taken to obtain eigenvectors of $\hat{S}^2$. The eigenvalues obtained cannot, however be related to the orbital energies.

Although successful for many systems near equilibrium, the constraint that the spatial orbitals be the same for paired electrons leads to an increasingly poor description away from equilibrium; this is particularly obvious for H_2 which when treated with a restricted wavefunction is found to incorrectly dissociate to $H^+ + H^-$. The unrestricted wavefunction, however, leads to the correct dissociation products for singly bonded systems, for H_2 one of the electrons is localised on each of the hydrogen atoms.

1.2.2 The Unrestricted Hartree-Fock Method

The Unrestricted Hartree-Fock method is the simplest theoretical method which is able to describe open-shell systems, and systems with broken or partially broken bonds. In UHF the electrons of α and β spin are described by different sets

of orthonormal spatial orbitals $\{\phi_i^\alpha\}$ and $\{\phi_i^\beta\}$ which themselves need not be orthogonal. The condition that the energy is stationary leads to coupled eigenvalue problems for the unrestricted orbitals of the form:

$$\hat{f}^\alpha|\phi_a^\alpha\rangle = \varepsilon_a|\phi_a^\alpha\rangle \tag{1.33}$$

$$\hat{f}^\beta|\phi_a^\beta\rangle = \varepsilon_a|\phi_a^\beta\rangle \tag{1.34}$$

where

$$\hat{f}^\alpha = h^\alpha + \sum_a^\alpha (J_a^\alpha - K_a^\alpha) + \sum_a^\beta J_a^\beta \tag{1.35}$$

The eigenvalues are the orbital energies of the various spatial orbitals. The total unrestricted electronic energy is then given by:

$$E_{UHF} = \sum_a^{N^\alpha} h_{aa}^\alpha + \sum_a^{N^\beta} h_{aa}^\beta + \frac{1}{2}\sum_a^\alpha \sum_b^\beta (J_{ab}^{\alpha\alpha} - K_{ab}^{\beta\beta}) + \sum_a^\alpha \sum_b^\beta J_{ab}^{\alpha\beta} \tag{1.36}$$

Introducing a basis set and expanding the unrestricted molecular orbitals yields:

$$\phi_i^\alpha = \sum_\mu c_{\mu i}^\alpha \chi_\mu \tag{1.37}$$

and

$$\phi_i^\beta = \sum_\mu c_{\mu i}^\beta \chi_\mu \tag{1.38}$$

This leads to the Pople-Nesbet equations for an unrestricted wavefunction [12]:

$$F^\alpha c^\alpha = S c^\alpha \varepsilon^\alpha \tag{1.39}$$

and

$$F^\beta c^\beta = S c^\beta \varepsilon^\beta \tag{1.40}$$

where $F_{\mu\nu}^\alpha = (\chi_\mu|f^\alpha|\chi_\nu)$, similarly for $F_{\mu\nu}^\beta$. These equations can be solved for the coefficients $c_{i\mu}^\alpha$, $c_{i\mu}^\beta$ in an equivalent manner to the RHF equations. At any iterative step the two matrix eigenvalue problems can be solved independently since the coupling is incorporated into the formation of the Fock matrices. However, a self consistent solution for the α equations cannot be obtained without simultaneously obtaining a solution for the β set. The solution of the Pople-Nesbet equations

yields the form of the two sets of molecular orbitals from which the energy of the system can be evaluated through (1.36). The molecular orbital energies obtained follow Koopmans' theorem.

When $N^\alpha \neq N^\beta$ there will always exist a unrestricted solution which is lower in energy than the corresponding restricted solution. When $N^\alpha = N^\beta$ there are two possible independent solutions of the Pople-Nesbet equations. The solution may be the same as the restricted solution to the Hartree-Fock Roothaan equations or there exists the possibility of a lower energy solution for which the electron densities of the α and β electrons are different. The second solution is important in the description of dissociation, since at large internuclear separations a degree of localisation of electrons of different spin is possible. In many cases the UHF potential minimum is found not to correspond to the RHF minimum [3].

Except in special cases, the unrestricted solutions are not eigenfunctions of $\hat{S}^2$ since there is contamination by spin states of higher multiplicity [13]. The expectation value of $\hat{S}^2$ for an unrestricted wavefunctions is given by [14]:

$$\langle S^2 \rangle_{UHF} = \langle S^2 \rangle_{Exact} + N^\beta - \sum_i^N \sum_j^N |S_{ij}^{\alpha\beta}|^2 \tag{1.41}$$

where it has been assumed that $N^\alpha \geq N^\beta$ and where:

$$\langle S^2 \rangle_{Exact} = \frac{S(S+1)}{2} = \left(\frac{N^\alpha - N^\beta}{2}\right)\left(\frac{N^\alpha - N^\beta}{2} + 1\right) \tag{1.42}$$

and $S_{ij}^{\alpha\beta} = \langle \phi_i | \phi_j \rangle$. For systems with a high degree of spin contamination the results may be suspect, especially when the unrestricted wavefunction is used as the basis for a correlated method, however for many open-shell systems at equilibrium there are no low-lying high-spin states and so the ground state has negligible contamination. Many techniques exist to remove the spin contamination and obtain pure spin states; these fall into two main categories. Those that operate spin projectors, or annihilators, upon the unrestricted wavefunction, such as Projected UHF (PUHF)[15] and Extended Hartree-Fock (EHF) [16], and those that act directly on the density matrices, such as the Spin constrained UHF (SUHF) [17]. The application of a spin projector introduces some multi-determinant character to the solution, removing one of the great advantages of the UHF method, the simplicity of the resulting wavefunction.

1.2.3 Basis sets

By virtue of being variational, the energy calculated by the LCAO procedure will decrease as the number of basis functions increases. As the basis set approaches completeness the SCF energy will converge toward that which would be obtained from a numerical calculation, the *Hartree-Fock limit.* The choice of basis set is important, often the largest error in a calculation is due to truncation in the one-particle basis. There is considerable freedom in the choice of basis function, any set of functions which form a complete set may be used. In reality the choice of functional form is governed by the rate of convergence of the orbitals when parameterised in terms of a particular basis set and the ease with which the integrals over the basis functions can be evaluated.

Exponential-type or Slater type functions[18], as suggested by atomic shielding constants, are given by:

$$\chi_{nlm}(r,\theta,\phi) = A_n r^{n-1} Y_{lm}(\theta,\phi) e^{-\zeta r} \tag{1.43}$$

where A_n is the normalisation constant and $Y_{lm}(\theta,\phi)$ are spherical harmonics. For this type of function the correct behavior is found at the nucleus (cusp behavior):

$$\left.\frac{\partial \chi}{\partial r}\right|_{r=0} \neq 0 \tag{1.44}$$

and far from the nucleus where the correct (r^{-1}) behavior for coulombic potentials is returned, leading to rapid convergence for atomic and molecular systems. However, using these functions, difficulties arise in the evaluation of multi-centre two electron integrals. Despite this, exponential basis functions are widely used for atoms and linear molecules, where the high degree of symmetry has allowed the use of efficient integral routines.

For polyatomic molecules the most common form of function is the Gaussian form as suggested by Boys [19]:

$$\chi_{nlm}(r,\theta,\phi) = N_n r^{n-1} Y_{lm}(\theta,\phi) e^{-\alpha r^2} \tag{1.45}$$

or in cartesian Gaussian form:

$$\chi_{lmn}(x,y,z) = N_{lmn} x^l y^m z^n e^{-\alpha r^2} \tag{1.46}$$

The Gaussian functions are not well suited to the description of the eigenfunctions of Hamiltonians involving coulomb potentials as they have an inappropriate form near the nucleus (do not have the correct cusp like behavior):

$$\left.\frac{\partial \chi}{\partial r}\right|_{r=0} = 0 \tag{1.47}$$

and at long ranges where r^{-2} behavior is found; thus a larger number of Gaussian functions is required to describe an orbital than Slater functions. The necessity of computing a larger number of integrals is more than offset however by the ease of computing the multi-centre integrals. The number of integrals required to be stored for a basis sets composed of Gaussian functions can be reduced by taking linear combination of functions with fixed expansion coefficients, known as contracted Gaussian type functions [20]. In the cartesian form additional functions are introduced in the description of higher angular momentum states, *eg* 6 *d*-type functions are used, which combine to give a further diffuse *s*-function. This *s*-function can lead to problems with near-linear dependence for large basis sets.

A great deal of effort has gone into the optimisation of basis set exponents for use in molecular calculations. The optimisation is performed for atoms, with empirical investigation of the additional requirements for the description in the molecular environment. A recent development is the Atomic Natural Orbital (ANO) contraction scheme in which a large basis set is contracted so as to mimic the molecular environment [21] by averaging over several atomic states, positive and negative ions, and atoms in an external field.

The use of large basis sets is required for the accurate description of molecular properties, especially in the description of excited states. Indeed in highly correlated calculations the limiting factor is the error due to the size of the one-particle basis. The need to store the two electron integrals on external disk proved to be a bottleneck, however, the development of direct SCF techniques [22], in which the integrals are evaluated in each iteration, has eliminated the storage problem, although the computation time is increased by the repetitive calculation of the integrals.

1.2.4 The breakdown of the Hartree-Fock method

The Hartree-Fock method yields approximately 98% of the total electronic energy of the molecule, unfortunately the error is of the order of magnitude of the chemical energy differences which are of interest, *eg* the calculation for N_2 gives 99.5% of the total energy compared to a binding energy of 0.2% [3]. The approximation ignores the correlation of electrons with different spins, especially those which occupy the same orbital which can be expected to have a large interaction. This error is approximately 1 eV for each electron pair, the electron correlation energy for He [23]. This is especially problematic for processes which involve changes in the numbers of electron pairs, such as bond formation. A well known example is that for F_2 Hartree-Fock calculations have the molecule unbound by 130 kJ mol^{-1} (5.35 eV) with respect to the atoms [24]. To recover this error it is necessary to introduce the effects of electron correlation.

Symmetry breaking problems are known to occur for the RHF method for such systems as CO_2 ($^3A_2$) [25] and Cu_2^+ ($^2\Sigma_u$) [26,27] where a lower energy solution is given by a calculation with a lower symmetry than the molecular framework. This is the result of the localisation of the unpaired electrons, since in such situations RHF only describes one of the resonance structures. The single reference Hartree-Fock methods also neglect the non-dynamical correlation which arises from the near degeneracy of configurations.

For systems which are well described by one configuration in the region of equilibrium, the Hartree-Fock method yields good qualitative results and is useful as a first approximation and as a starting point for more accurate calculations. The method in its limit generally predicts bond lengths which are too short by 0.01-0.02 Å, and harmonic vibrational frequencies that are overestimated by $\approx$ 10 % for molecules containing first period elements [28].

1.3 Correlated Methods

The correlation energy is defined, according to Löwdin [29], as the difference between the exact eigenvalue of the non-relativistic Hamiltonian and its expectation value in the Hartree-Fock approximation for the state under consideration, within the fixed nucleus approximation.

There are two types of correlation effect; "non-dynamical correlation", which arises when several configurations are nearly degenerate and interacting, and "dynamical correlation" which is due to the cusp condition in the inter-electron interaction that must be satisfied by the exact wavefunction. In situations when there is a large amount of non-dynamical correlation, the single determinant HF method gives qualitatively incorrect results and a multi-determinant wavefunction, such as that generated by Multi-Configuration SCF, is required. The dynamical correlation is obtained by mixing excited states into the wavefunction, separating the electron pairs. Convergence with the inclusion of the excited determinants is fairly rapid [30]. The major techniques for the computation of this effect are configuration interaction (or mixing), coupled cluster, and perturbation theory.

1.3.1 Configuration Interaction

The method of configuration interaction (CI) is the most widely used approach for the solution of the problem of electron correlation. In CI the total wavefunction is expanded as a variable linear combination in an n-particle basis

$$\Psi = \sum_I c_I \Phi_I \tag{1.48}$$

where the n-particle functions Φ_I are Slater determinants, or spin and symmetry adapted combinations of Slater determinants (Configuration State Functions, or CSF chosen to be eigenvectors of S^2 and S_z) and the c_I are coefficients to be determined. The CSF may be generated using Yamanouchi-Kotani spin functions [31], or using Unitary Group theory [32, 33].

The CI energy, $E = \langle\Psi|H|\Psi\rangle$, is variationally optimised with respect to the CI coefficients, c_I. The coefficients are determined as the eigenvectors of the linear eigenvalue equation

$$\left\langle \Phi_I|H|\sum_J c_J\Phi_J \right\rangle = Ec_I \tag{1.49}$$

where the Hamiltonian element can be expanded, in terms of molecular orbital one- and two- electron integrals, and coupling coefficients, as

$$H_{JI} = \sum_{pq}\gamma_{pq}^{IJ}\,(p|h|q) + \sum_{pqrs}\Gamma_{pqrs}^{IJ}\,(pq||rs) \tag{1.50}$$

The coupling coefficients depend only upon the occupation and spin coupling of the molecular orbitals p, q, $(r,\ s)$ in the CSFs I, J, and not on such factors as the molecular geometry, external fields, etc... The coupling coefficients are most often obtained using group theory [34, 35].

In the limit of a complete, or full, n-particle basis, termed full-CI, the basis set correlation energy is returned for a particular one-particle basis. As the one-particle basis becomes infinite the basis set correlation energy approaches the exact correlation energy for the system. The CI method, being variational, the lowest eigenvalue of (1.49) is an upper bound to the exact ground state energy. This also applies for excited states. According to MacDonald's Theorem [36], $(i-1)^{\text{th}}$ and i^{th} eigenvalues with M expansion functions, E_{i-1}^{M} and E_i^M, bracket E_i^{M+1}.

All the CSFs in the full n-particle space can be generated by successively exciting one, two, three,.. electrons from the zeroth order, reference, wavefunction; *ie* equation (1.48) can be expressed in terms of excitation operators from a single reference function

$$\Psi = (c_0 + \sum_{ia} c_i^a\{a_i a_a^\dagger\} + \sum_{ijab} c_i^a\{a_i a_j a_a^\dagger a_b^\dagger\} + \ldots)\Phi_0 \tag{1.51}$$

using creation, $a_a^\dagger$, and annihilation, a_i, operators. The two-body nature of the Hamiltonian, coupled with the orthogonality of the n-particle basis, ensures that

only configurations which at most differ by two orbitals can interact [37, 38], therefore, only singly and doubly excited states can interact directly with reference function [1]. When the reference function is a closed shell HF wavefunction, Brillouin's theorem states that the singly excited states cannot interact through the Hamiltonian ($\langle 0|H|i\rangle = 0$), thus, the correlation energy of a closed shell HF state depends, explicitly, only on the doubly excited configuration

$$E_C = \sum_{i>j,a>b} c_{ij}^{ab} \left\langle \Phi_0|H|\{a_i a_j a_a^\dagger a_b^\dagger\}\Phi_0 \right\rangle \tag{1.52}$$

although the coefficients c_{ij}^{ab} are affected by the presence of other excited configurations. In contrast, for non-HF reference functions singly excited configurations are found to be of importance when computing the correlation energy [14, 33]. Singly excited configurations are also vital for the accurate treatment of one-electron properties, such as the dipole moment [3].

The number of terms in the full-CI expansion grows factorially. The number of determinants is given by the number of ways of distributing the N_α, and N_β electrons amongst the M orbitals,

$$\left(\begin{array}{c} M \\ N_\alpha \end{array} \right) \left(\begin{array}{c} M \\ N_\beta \end{array} \right) \tag{1.53}$$

Ignoring the point group, the number of CSFs is given by the Weyl formula [39],

$$\frac{2S+1}{M+1} \left(\begin{array}{c} M+1 \\ \frac{1}{2}N - S \end{array} \right) \left(\begin{array}{c} M+1 \\ M - \frac{1}{2}N - S \end{array} \right) \tag{1.54}$$

for N electrons in M spatial orbitals, with total spin $S{=}N_\alpha - N_\beta$. Therefore, even using the most efficient "direct" procedures [40, 41], and exploiting the sparseness

---

[1] In a term borrowed from perturbation theory this is often called the first order interacting space.

of the Hamiltonian matrix [42] it is not usually possible to perform full-CI for a basis which accurately reproduces experimental properties. Nevertheless, calculations with small, but reasonable one-particle basis sets can be used as a benchmark against which to compare the performance of more approximate methods [30]. In general these calculations employ direct-CI methodology, this avoids the explicit construction of the Hamiltonian by computing and storing the residual vector, $\sigma_K = \sum_l H_{kl} c_l$ [30, 41].

The application of the CI method to chemically significant problems invariably involves a truncated expansion of the n-particle basis. Commonly the expansion is limited to those terms singly and doubly excited with respect to the reference function(s) (CISD). These truncated CI techniques rely on the zeroth-order wavefunction being an adequate description of the the exact wavefunction. When this is not the case, *eg* in bond breaking, where a CISD calculation fails to describe phenomena correctly when applied to a RHF wavefunction [3, 14]. For molecules which can be well described by a single reference function CISD returns a significant proportion of the correlation energy, for example ~94 % for NH_3 and H_2O at equilibrium geometries [43]. When the SCF configuration is not dominant a significantly lower percentage of the correlation energy is obtained by CISD, 80 % for H_2O at $2R_e$ [43]. The failure of CISD in these situations is largely caused by the neglect of quadruple excitations, CISDTQ returns a consistently high percentage of the correlation energy throughout the potential energy surface, ~ 99 % [43]. Further, as the size of the molecule being studied increases the importance of the higher excitations in turn increases. Indeed Čársky and Urban note that for large molecules it is expected that the majority of the correlation energy will be derived from quadruple and higher terms [3]. The CISD method scales as M^6 with the number of basis functions. The inclusion of quadruply excited states, and triply excited states, which are also found to be important in the description of multiply bonded systems, is desirable, although only feasible for small systems. The truncated expansions which include the quadruply excited configurations, CISDQ and CISDTQ, scale as M^8, and M^{10}, respectively. The alternative approach is to include the configurations required to provide an adequate first order description of

the wavefunction, as reference configurations and to perform multireference (MR) CISD. These MR-CI(SD) calculations are found to give reliable results for most systems which have been studied [30].

The major bottleneck in the use of MR-CI methods is the rapid increase in the length of the expansion with the number of reference configurations. This leads to the requirement that either the number of references is kept small, or that the number of variational parameters in the CI be reduced. A variety of procedures have been proposed to do this; amongst these are, the selective techniques [13, 44–52] , the external contraction scheme of Siegbahn [53, 54], and the internal contraction scheme of Werner and Meyer [55, 56].

The selective routines work by estimating the effects of the generated CSFs upon the roots being calculated, either perturbatively [13, 48, 49, 52, 57], or through the diagonalisation of a small interaction matrix [50, 51]. Often the effects of the discarded configurations is estimated and included in the final result [50, 52, 57]. The necessarily random nature of the selected CSFs, however, precludes the use of many of the efficient routines developed for full-CI. The application of the selective procedures has been found to give accurate results economically [57]. A further discussion of the MRD-CI program of Buenker is given in Section 1.3.2.

The externally contracted CI method [53, 54] contracts together all the CSFs which differ in the external space. The contraction coefficients are estimated perturbatively. The contraction process reduces the number of variational parameters by ~2-3 orders of magnitude with a loss of only ~3-4 % of the correlation energy, as compared to the fully uncontracted procedure.

The internally contracted scheme [55, 56] treats the reference (internal) space as a single entity, the SD excitations are from the internal space not the individual reference configurations. All the CSF with the same external components, but which differ internally, are contracted. The weighting in the contractions are usually determined in an MCSCF computation. This is a particularly efficient technique as the number of terms in the CI expansion is independent of the number of reference configurations employed, however, the coupling coefficients become matrices of high order, and the resulting contracted terms are non-orthogonal.

Some of these problems are solved by selectively uncontracting the large number of singly excited states [56]. Highly accurate results have been obtained with this contraction scheme, to within 0.5 % of the uncontracted correlation energy.

The truncated CI solution is neither size extensive, nor size consistent. In thermodynamics, a size extensive property is one that is proportional to the size of the system. This problem has been discussed in detail by Bartlett and co-workers [58–61]. The closely related property of size consistency requires that the energies of the components of a system be the same if calculated at infinite separation, or separately [33, 60]. For a CISD wavefunction with a large number of electrons, N, the energy is proportional to $\sqrt{N}$. The unphysical scaling with the number of particles can be traced to the explicit energy dependence of the CI coefficients in equation (1.49). This $\sqrt{N}$ behavior has been discussed by various workers [33, 62]. The energy dependence is canceled by the inclusion of higher order excitations, for example, a CID or CISD wavefunction would require quadruple excitations. Although multi-reference CI procedures including all single and double excitations relative to several well chosen reference configurations would introduce the important quadruple excitations, these methods are not rigorously size extensive or consistent.

Several authors have incorporated corrections into the CISD procedure to account for higher excitations [63–65]. The single reference Davidson correction [63],

$$E_D = (1 - C_0^2)E_c \tag{1.55}$$

is a simple perturbative estimate of the energy effects of higher than double excitations. Here E_c is the correlation energy from CID, or CISD, and C_0 is the coefficient of the reference configuration. This has been extended for MR-CI by replacing C_0 by $\sum_R C_R$ [66]. A slightly different route has been taken in the development of the Coupled Pair Functional (CPF) method [67–69]. In this procedure the (MR)-CISD equations are modified to cancel the energy term through the use of normalisation denominators, and so bring about size extensivity and consistency to a high degree.

1.3.2 The MRD-CI

Since its introduction in the mid-1970's the MRD-CI program of Buenker and Peyerimhoff [50, 70–73] has been successfully applied to a wide range of applications, especially the calculation of the excited states of molecules for which the multi-reference multi-root nature of the code is a major requirement. The version employed in the present studies is that as included in the quantum chemistry package GAMESS-UK [74, 75], which could latterly handle up to 80 reference CSFs and a final secular equation of dimension up to 20,000 CSFs[2].

The selection procedure used is of the A_k type [76, 77], the contribution to the full MR-CISD energy being estimated employing perturbation theory for the individual CSF, or spin blocks.

$$\epsilon_j = \frac{|H_{j0}|^2}{(E_0 - E_j)} \tag{1.56}$$

where

$$H_{j0} = \langle \Phi_j | H | \Psi_0 \rangle = \sum_i H_{ji} a_i \tag{1.57}$$

for zeroth order root Ψ, composed of reference CSFs i. Those CSF with estimated contributions to the energy lowering of any of the zeroth order roots greater than threshold T are included in the secular equation. The individual estimates can be combined to furnish an estimate of the total effect of the rejected CSF [50, 78]

$$\Delta E^r(T) = \sum_j \epsilon_j \tag{1.58}$$

however, this relies on the zeroth order function, Ψ_0, providing a good description of the wavefunction at $T = 0$, which is usually not the case for large multi-root calculations.

MRD-CI uses an extrapolation procedure based upon the estimated lowerings and the results of the secular equations at various thresholds.

$$E(T=0) = E(T_A) + \left(\frac{E(T_A) - E(T_B)}{\Delta E^r(T_A) - \Delta E^r(T_B)} \right) \Delta E^r(T_A) \tag{1.59}$$

---

[2]Program expansions undertaken by M. F. Guest, Daresbury Lab..

This is equivalent to the original extrapolation procedure of Buenker and Peyerimhoff [50, 70], with the assumption that λ is given by the value in parentheses, and similar to the extrapolation method of Langhoff and Davidson [79] where the fractional error made in estimating the energy correction of the rejected CSFs by $\Delta E^r(T)$ is assumed to be the same as in the corresponding estimate for the selected CSFs.

The extrapolation method has been shown to give results in good agreement with the complete MR-CISD [80, 81]. Serious errors can, however, be introduced into the extrapolation if the character of the root undergoes substantial change between the thresholds used for the extrapolation, therefore the step size must be chosen to be small enough to prevent this, and also large enough that any irregularities in the convergence to $T = 0$ are smoothed out. In the extreme case, the order of the roots (in a density sense) may not be the same at different thresholds. Under these circumstances, since the program uses the canonical order, unlike roots can be extrapolated together, leading to bogus energies. Jackels and Shavitt noted that in MR-CI calculations, the effect of the large number of CSFs with small contributions is underestimated by these extrapolation procedures [57].

1.3.3 Multi-Configuration Self-Consistent Field

MCSCF [82, 83], in which the wavefunction is optimised with respect to variations in the CI coefficients and in the orbitals, can be viewed as an extension of Hartree-Fock theory [84]. The concept of orbitals is conserved, although occupation numbers are non-integer, and the idea of an orbital energy is maintained through the use of the extended Koopmans' theorem [85]. Provided all the necessary configurations are included in the expansion, the method should give a qualitatively good description of the electronic structure, and account for much of the non-dynamical correlation energy. The Complete Active Space (CAS) SCF method [86, 87] considers wavefunctions in which the CI expansion is complete within a set of active orbitals. A modification of CASSCF, whereby the occu-

pancy of groups of orbitals are constrained is the Restricted Active Space (RAS) SCF [88].

With the MCSCF wavefunction expanded as a linear combination of CSFs, as in CI, the energy takes the form,

$$E = \left\langle \sum_I c_I \Phi_I | H | \sum_J c_J \Phi_J \right\rangle \tag{1.60}$$

Hence, using the definition of the Hamiltonian in equation (1.50)

$$E = \sum_{pq} \gamma_{pq} h_{pq} + \sum_{pqrs} \Gamma_{pqrs} (pq|rs) \tag{1.61}$$

where the one particle density matrix is $\gamma_{pq} = \sum_{IJ} c_I c_J \gamma_{pq}^{IJ}$ and the two particle density matrix is $\Gamma_{pqrs} = \sum_{IJ} c_I c_J \Gamma_{pqrs}^{IJ}$, with γ_{pq}^{IJ}, Γ_{pqrs}^{IJ} the spin coupling coefficients as before.

The energy is made stationary with respect to variations in the CI coefficients and the orbitals, subject to the constraints that the total wavefunction is normalised ($\sum_I c_I = 1$), and that the MOs remain orthogonal ($\langle \psi_I | \psi_J \rangle = \delta_{IJ}$). The secular equation for the CI coefficients is the same as for CI, equation (1.49).

The orbital convergence conditions are obtained by considering the variation of the energy expression caused by mixing between the MOs [89]. The orbitals are divided into two classes; internal orbitals, which are occupied in the reference configurations, and external orbitals which are unoccupied. The external orbitals play no role in the final (orbital optimised) wavefunction, but are used during the optimisation procedure to improve the internal space. A new set of orthogonal MOs may be obtained by an orthogonal transformation:

$$\psi_t = \sum_p U_{pt} \psi_p \tag{1.62}$$

The transformation operator U is often represented in exponential form, $U = e^x$, with x an antisymmetric matrix ($x^{\mathrm{T}} = -x$), constituting the variational parameters for the orbital rotations. The derivative of the energy with respect to x_{rs}, mixing orbitals ϕ_r and ϕ_s, which is zero for the converged wavefunction, is given

by:

$$\frac{\delta E}{\delta x_{rs}} = \left\{ \sum_u \gamma_{su} h_{ru} + \sum_{uvw} \Gamma_{suvw}(ru|vw) \right\} - \left\{ \sum_u \gamma_{ru} h_{su} + \sum_{uvw} \Gamma_{ruvw}(su|vw) \right\} \quad (1.63)$$

This condition is equivalent to the satisfaction of the generalised Brillouin theorem [90]. For some orbital rotations the variational condition is always obeyed automatically; for example if r, s are both external then the density matrix elements are all zero, the same can occur for certain internal-internal rotations, these redundant parameters do not change the first order energy and are usually removed from the optimisation [91]. For CASSCF the internal-internal rotations are all redundant [87] which lead to a simplification of the orbital optimisation.

The form of the MOs is then given by the solution of the set of coupled Fock equations:

$$\sum_s F_{rs} \, |\psi_s\rangle = \sum_r \epsilon_{rs} \, |\psi_s\rangle \quad (1.64)$$

subject to the MCSCF convergence conditions. The MCSCF Lagrangian matrix is given by, $\epsilon_{rs} = \langle \psi_r | \sum_u F_{su} | \psi_s \rangle$, and the MCSCF Fock operator can be written as:

$$F_{rs} = \gamma_{rs} h(1) + \sum_{vw} \Gamma_{rsvw} \int dr_2 \psi_v(2) \psi_w(2) \quad (1.65)$$

The energy expression is fourth order in the orbitals and infinite order in x, since the orbitals are periodic functions due to the orthogonality constraint. There are many orbital optimisation procedures including the Fock operator method of Hinze [89], super-CI methods [92, 93], and second-order Newton-Raphson procedures [82, 83, 94, 95]. The optimisation of the orbitals is performed iteratively until self-consistency is obtained. The optimisation of the CI coefficients proceeds simultaneously in a"one-step" process, or in a separate step after each improvement in the orbitals, a "two-step" process. In general the one-step methods give quicker convergence as there is found to be strong coupling between the orbitals and the CI coefficients far from the solution.

The calculation of MCSCF excited states is made difficult due to the phenomena of "root flipping" [92]. During the optimisation of the excited state the orbitals may become poorer for the description of the ground state, which can

ultimately lead to a switch in the order so that the solution is no longer that desired but instead a saddle point. This is undesirable as the resulting root is not an upper bound to the energy of the state. The problem is solved by averaging the wavefunctions of several roots, State Averaged MCSCF [96, 97].

The ability of the MCSCF procedure to include the non-dynamical correlation energy makes the resulting wavefunction an excellent zeroth-order approximation for MR-CISD [53–55, 82], perturbation theory [98–100], or coupled cluster [101–104] methods.

1.3.4 Perturbation Theory

Another approach to the computation of the correlation energy is through the application of perturbation theory. The two forms of perturbation theory most commonly used in quantum chemistry are Møller-Plesset (MP) [105] and the closely related Many-Body Perturbation Theory (MBPT) [106–109]. MP and MBPT give equivalent energy expressions when expressed in the algebraic approximation [110, 111], though the derivations are different. MP theory is a first quantised form of the Rayleigh-Schrödinger perturbation theory, derived with respect to a Hartree-Fock wavefunction, RHF for closed shells and usually UHF for open shell systems. MBPT is more general, being a second quantised theory based upon a Fermi vacuum state, which can conveniently be expressed in diagrammatic form.

These methods are, unlike CI, size-consistent and extensive, although non-variational, *ie* the property of an upper bound for the energy does not apply.

MP theory involves the separation of the Hamiltonian [3],

$$H + H_0 + V \tag{1.66}$$

such that the zeroth order Hamiltonian, H_0, is the sum of the one-electron Fock operators and the perturbed Hamiltonian, V, is the difference between the electronic

[3] This is known as the Møller-Plesset separation.

Hamiltonian, H, and H_0, including a significant part of the electron repulsion:

$$H_0 = \sum_i^n f(i) = \sum_i^n \left[h(i) + v^{HF}(i)\right] \tag{1.67}$$

$$V = \sum_{i>j}^n r_{ij}^{-1} - \sum_i^n v^{HF}(i) \tag{1.68}$$

The zeroth order expression is therefore,

$$H_0|\Phi_0\rangle = E_0|\Phi_0\rangle \tag{1.69}$$

with the E_0 the sum of the orbital energies, ϵ_i,

$$E_0 = \sum_i \epsilon_i = \sum_i (i|h|i) + \sum_{i,j} (ij||ij) \tag{1.70}$$

and the first-order energy correction is the action of the perturbation upon the zeroth-order wavefunction,

$$E^{(1)} = \langle\Psi_0|V|\Psi_0\rangle \tag{1.71}$$

The Hartree-Fock energy is

$$E_{HF} = E_0 + \langle\Phi_0|V|\Phi_0\rangle = E_0 + E^{(0)} \tag{1.72}$$

Electron correlation is therefore introduced at second order, MP2 and MBPT(2).

In MBPT the n^{th} order wavefunction and energy are given by,

$$\Psi_n = (1+V)|\Phi_0\rangle + \sum_{k=1}^n \left[(E_0 - H_0)^{-1}V\right]^k |\Phi_0\Big\rangle_L \tag{1.73}$$

$$E_n = \sum_n E^{(n)} = E_0 + \sum_{k=0}^n \Big\langle \Phi_0|V\left[(E_0 - H_0)^{-1}V\right]^k |\Phi_0\Big\rangle_L \tag{1.74}$$

the subscript L indicating that the terms are limited to linked diagrams following the Linked Diagram Theorem [106–108]. Similar expressions exist for MP theory without the restriction to linked diagrams, the "unlinked" terms being canceled explicitly for the energy expressions at each order.

In perturbation theory based upon HF orbitals, all the excited determinants are eigenfunction of H_0. The perturbation causes mixing between these and the

zeroth order wavefunction. The n^{th} order wavefunction can, therefore, be written as linear combinations of these eigenfunctions.

The second-order perturbation to the energy is given by

$$E^{(2)} = -\sum_{m} \frac{\langle 0|V|m\rangle \langle m|V|0\rangle}{E_m - E_0} \tag{1.75}$$

where $E_m = \langle m|H_0|m\rangle$. For a closed shell HF zeroth order function the two-body nature of the Hamiltonian and Brillouin's theorem [112] ensure that the summation is over doubly excited states only. Equation (1.75) can be expanded in terms of canonical orbitals to yield [33, 105]

$$E^{(2)} = -\frac{1}{4}\sum_{ij,ab} \frac{|\langle ij||ab\rangle|^2}{\epsilon_a + \epsilon_b - \epsilon_i - \epsilon_j} \tag{1.76}$$

where $\langle ij||ab\rangle$ is an antisymmetrised two-electron integral, and ϵ is an SCF eigenvalue. The third order energy correction for MP is similarly restricted to doubly excited configurations,

$$E^{(3)}(MP) = \sum_{mn} \frac{V_{0m}V_{mn}V_{no}}{(E_m - E_0)(E_n - E_0)} - E^{(1)}\sum_{m} \frac{V_{0m}V_{m0}}{(E_m - E_0)^2} \tag{1.77}$$

using the notation $V_{nm} = \langle n|V|m\rangle$. Single, triple, and quadruple excitations are introduced at fourth order,

$$\begin{aligned} E^{(4)}(MP) \;=\; & -\sum_{mn}^{D}\sum_{t}^{SDTQ} \frac{V_{0m}V_{mt}V_{tn}V_{n0}}{(E_m - E_0)(E_t - E_0)(E_n - E_0)} \\ & + \sum_{mn} \frac{V_{0m}V_{m0}}{(E_m - E_0)} \frac{V_{0n}V_{n0}}{(E_n - E_0)^2} \\ & + 2V_{00}\sum_{mn} \frac{V_{0m}V_{mn}V_{n0}}{(E_m - E_0)^2(E_n - E_0)} \\ & - V_{00}^2 \sum_{m} \frac{V_{0m}V_{mn}}{(E_m - E_0)^3} \end{aligned} \tag{1.78}$$

where the sum t corresponds to all unique single, double, triple, and quadruple excitations. The expression for the MP4 energy can be partitioned into its various contributions, $E_S^{(4)} + E_D^{(4)} + E_T^{(4)} + E_Q^{(4)}$, the first three parts arising from the S, D, T summations in equation (1.78), and the final part includes the Q sum and the renormalisation term $(E^{(2)}\sum V_{0m}/(E_m - E_0))$.

The size consistency and extensivity can be demonstrated by examining the formulae and applying them to a set of N (identical) isolated molecules. The

$E^{(2)}$ summation (1.75) will give S terms for one molecule and NS terms for N molecules, where S represents the number of unique excitations. The first term in the $E^{(3)}$ expression, equation (1.77), for $m \neq n$ will give S^2 terms for one molecule and NS^2 terms for N molecules, the second term, however, gives S terms from one molecule and N^2S for N. Similarly, for $E^{(4)}$, (1.78), the second and third terms scale as N^2, and the fourth as N^3. These expressions with unphysical behavior cancel, so that the energy scales with N as required. The second term in $E^{(3)}$ is canceled by the portion of the first term with $m = n$, and in $E^{(4)}$ the renormalisation term (second) cancels with certain quadruple contributions, whilst the third and fourth terms cancel with part of the contribution from double excitations in the first term [14, 58]. The canceled terms in MP theory correspond to unlinked diagrams in MBPT.

The formalism based upon the UHF Hamiltonian is similar to the RHF case. Again the UHF energy is returned through first order in the perturbation series, $E^{(0)} + E^{(1)}$. In terms of spin and spatial orbitals the second order correction to the energy is given by,

$$\begin{aligned} E^{(2)}_{UHF} = & -\frac{1}{4}\sum_{ij}^{\alpha}\sum_{ab}^{\alpha}\frac{|\langle ij||ab\rangle|^{\alpha\alpha^2}}{\epsilon_a^\alpha + \epsilon_b^\alpha - \epsilon_i^\alpha - \epsilon_j^\alpha} - \frac{1}{4}\sum_{ij}^{\beta}\sum_{ab}^{\beta}\frac{|\langle ij||ab\rangle|^{\beta\beta^2}}{\epsilon_a^\beta + \epsilon_b^\beta - \epsilon_i^\beta - \epsilon_j^\beta} \\ & -\frac{1}{4}\sum_{i,a}^{\alpha}\sum_{j,b}^{\beta}\frac{|\langle ij||ab\rangle|^{\alpha\beta^2}}{\epsilon_a^\alpha + \epsilon_b^\beta - \epsilon_i^\alpha - \epsilon_j^\beta} \end{aligned} \tag{1.79}$$

UHF-based perturbation series converge very slowly when the reference function exhibits a large degree of spin contamination [113, 114]. Recently open shell formalisms based upon the restricted wavefunction have been developed [115–118].

Perturbation treatments are valid only if the perturbation is small compared to the zeroth order term. This implies that the state should be well described by a single configuration. It is also desirable that the perturbation series converges rapidly, so that a large proportion of the correlation energy is returned for the low orders. For suitable molecules, typically, up to 90 % of the total correlation energy (as obtained for full-CI) can be returned at second order for a given basis set, up to 96 % through third order, and in excess of 99 % for full fourth order [113, 119]. The

non-variational nature of the technique, though, means that the full-CI correlation energy can be exceeded, *eg* 102 % is obtained at the MBPT(4) level for F^- [119]. For systems which are less well described by a single configuration the perturbation series is slower to converge, and may even be divergent [113]. This restriction has limited the application of the perturbation methods to mostly ground state properties.

Second order perturbation theory is the simplest method for the inclusion of correlation energy, it scales as M^5 with the number of basis functions. The third order scales as M^6, the same as CISD, however, as the perturbation method is non-iterative, it is more computationally efficient. The calculation of the fourth order correction scales as M^7. This is mostly due to the computation of the contribution of the triply excited states, the contributions of the remaining terms scale as M^6, therefore, the triple contribution is often neglected.

1.3.5 Coupled Cluster

The coupled cluster (CC) approach [4] for solving the Schrödinger wave equation, in electronic structure, originates with the exponential ansatz of Coester and Kümmel [120, 121], which acts on an independent particle reference function,

$$|\Psi\rangle = e^T |\Phi_0\rangle \tag{1.80}$$

T is a cluster operator, which is separated into n-body cluster terms, $T = T_1 + T_2 + T_3 + \ldots + T_m + \ldots$, each of which is composed of an amplitude, t, and a series of excitation operators,

$$T_m = \frac{1}{m!} \sum_{ijk\ldots abc\ldots} t_{ijk\ldots}^{abc\ldots} a_a^\dagger a_b^\dagger a_c^\dagger \ldots a_i a_j a_k \ldots \tag{1.81}$$

[4] The coupled cluster method is also known as the **exp S** method in nuclear physics.

Expanding the exponential as a power series, the CC wavefunction can be written as,

$$\Psi\rangle = \left\{(1) + (T_1) + (T_2 + \frac{1}{2!}T_1^2) + (T_3 + T_2T_1 + \frac{1}{3!}T_1^3) + \ldots\right\} \Phi_0\rangle \qquad (1.82)$$

with terms of the same excitation level collected together in parentheses. Defining C_I by these excitation levels yields the CI wavefunction: $1 + C_1 + C_2 + C_3 + \ldots$ $|\Phi_0\rangle$. When T includes clusters up to T_n for n electrons the full-CI wavefunction is obtained for a given basis set. As for the other correlated methods, a complete solution of the CC wavefunction is not practical, it is, therefore necessary to truncate the series at a level of T_p [60, 104, 122–126] . Due to the exponential nature of the wave operator, selected higher excitations are included, *eg* for $T \sim T_2$ (coupled cluster doubles [123] or coupled pairs many electron theory [122]) certain quadruple, sextuple, etc,... terms: $e^{T_2} = 1 + T_2 + \frac{1}{2}T_2^2 + \frac{1}{6}T_2^3 + \ldots$. Single cluster operators are often referred to as "connected", and products of two or more cluster operators as "disconnected". The truncated CC wavefunction differs from the CI counterpart by the inclusion of these disconnected terms.

The variational minimisation of the energy expectation value for e^T leads to equations that are too complicated to be solved. The equations for the correlation energy and cluster amplitudes are, therefore, derived by the method of moments, projecting the Schrödinger equation:

$$(H_N - E_C)\,|e^T\Phi_0\rangle = 0 \qquad (1.83)$$

onto the reference function and the set of excited configurations chosen to represent the operators T_n [125, 127]. H_N is defined as $H - \langle\Phi_0|H|\Phi_0\rangle$. The resulting equations are:

$$\langle\Phi_0|H_N - E_C|e^T\Phi_0\rangle = 0 \qquad (1.84)$$

$$\langle{}^{ijk\ldots}_{abc\ldots}|H_N - E_C|e^T\Phi_0\rangle = 0 \qquad (1.85)$$

The explicit energy terms in equation (1.85) are eliminated by the substitution of equation (1.84). Another derivation of the CC equations which is often used in

CC theory eliminates the energy dependence of the cluster equations through the use of a transformation suggested by Coester [120, 121]. The Schrödinger equation (1.83) is premultiplied by e^{-T}, which when projected as above, yields:

$$\left\langle \Phi_0 | e^{-T} H_N e^T | \Phi_0 \right\rangle = E_C \tag{1.86}$$

$$\left\langle {}^{ijk\ldots}_{abc\ldots} | e^{-T} H_N e^T | \Phi_0 \right\rangle = 0 \tag{1.87}$$

The equivalence of these equations has been demonstrated for the full CC operator [128] and for certain truncated cluster operators [129]. Čížek showed that only linked diagrams of MBPT contribute to the CC equations [130], which guarantees the size-extensivity of the method. This is a feature of the product separability of the exponential ansatz. That the energy terms in equation (1.85) exactly cancels the unlinked diagrams has been explicitly shown for CCSD by Paldus *et al.* [129]. In terms of MBPT, CC theory may be viewed as the summation of certain energy diagrams through infinite order [60]. The CCD model is correct through fourth order MBPT for double and quadruple excitations, the methods differ due to the inclusion of higher order disconnected contributions in CCD. Correspondingly CCSD is correct through fourth order for singles, doubles, and quadruples, and CCSDT through full MBPT(4).

The CC equations for the cluster amplitudes are solved iteratively, the arrays generated, particularly in connection with the disconnected terms, are generally too large to allow solution by matrix manipulation. The CCD and CCSD methods scale as M^6 with the number of basis functions, the same as CISD, although the necessity of an iterative solution of the non-linear equations means that the calculation takes 2-8 times longer [131]. CCSDT scales as M^8 [126], making the method more efficient than the comparable CISDTQ. Several approximations exist that include the effects of the T_3 clusters without the expensive iterative solution of the full CCSDT equations, such methods have derived and applied by Bartlett and co-workers [126, 132–135]. Other methods simplify the calculation of the cluster amplitudes by using approximate treatments for the disconnected terms. The simplest of these are the linear CC methods which remove the disconnected terms and linearise the CC equations [14]. Another approximation originally proposed by

Meyer [136] is to include only certain important disconnected terms, the Coupled Electron Pair Approximation (CEPA).

The CC methods are equally applicable to UHF and ROHF reference functions [124, 137]. The CCD method is effectively restricted to the use of HF orbitals optimised for the state being investigated due to the lack of a treatment of single excitations, and is not suitable for the description of bond breaking, excited states, and other situations were there is much non-dynamical correlation. The CCSD method is predicted to return a major portion of the correlation energy, *ie* up to 99 %, within a basis set for well behaved systems described satisfactorily by a single reference function. CCSDT has been found to give results in excellent agreement with full-CI [126], and to be applicable even in cases where there is a large degree of degeneracy in the wavefunction [138].

The extension of the CC approximation to the treatment of states which are ill described by a single reference function is not straight forward. The simplest of these methods is the Linear Response Theory, or Equation of Motion, CC [139–146] , which describes the excited state wavefunction as [147],

$$|\Psi_k\rangle = We^T\,|\Phi_0\rangle \tag{1.88}$$

where W is a linear combination of excitation operators corresponding to the reference space for the excited states, and $e^T|\Phi_0\rangle$ corresponds to the exact wavefunction of the reference, normally ground state, wavefunction. The LRT-CC method benefits from the simplicity of the description of the reference state in terms of the single reference CC approximation. The ground state cluster operator, e^T is included with the electronic Hamiltonian to give an effective Hamiltonian, $\bar{H}_N = e^{-T}H_N e^T$. The excitation energy and coefficients, W_I, are obtained by diagonalising the effective Hamiltonian. The method implicitly relies on the approximation that the major portion of the correlation energy is transferable between the vacuum state and the excited states, therefore, the validity of ansatz is limited to situations in which the transition from Φ_0 to Ψ_k does not lead to extensive reconstruction of the wavefunction [147], and the presence of a state which can be well described by a single reference function. LRT-CC is core extensive, the valence electrons are

not treated in a strictly size-extensive manner [148]. Despite this the method has been applied successfully to a wide range of systems [149–152].

The extension of the CC approximation to include a full CC treatment of the excited states in a multireference environment faces the problem of redundancy in the wavefunction operator; the complete set of cluster amplitudes cannot be determined by a wave operator of the form e^T [138, 153], in particular the partitioning of T into the various n-body components is not defined and additional conditions are required. This requirement has lead to the development of two distinct form of MR-CC theory: Fock space, or valence universal [153–168] , and Hilbert space, or state universal [101–103, 138, 147, 165, 169].

In the Fock space method the wave operator, Ω, is parameterised within the complete Fock space, for all possible occupancies of the active orbitals [154, 156, 157]. The most commonly employed ansatz in the Fock space formalism is that of Lindgren [157],

$$\Omega = \left\{e^T\right\} P \tag{1.89}$$

where $\{A\}$ denotes a normal ordered form of A and P is the projection onto the reference space. The normal ordering condition prevents the operators in T contracting amongst themselves and decouples the different Hilbert spaces [153]. The various Hilbert spaces, or sectors [170], are treated in a hierarchical manner, the vacuum state is computed as in single reference CC, then the unique cluster amplitudes are determined in each successive Hilbert space. The Fock space equations for sector (m, n), m electrons and n holes, are obtained from [170]:

$$H\Omega P^{(m,n)} - \Omega \bar{H} P^{(m,n)} = 0 \tag{1.90}$$

where $\bar{H}$ is the effective Hamiltonian,

$$\bar{H} = P^{(m,n)} \Omega^{-1} H \Omega P^{(m,n)} \tag{1.91}$$

The eigenvalues of the Hamiltonian determine the energies of the system, and the eigenvectors give the linear expansion coefficients within the reference space. The cluster amplitudes are obtained by projecting equation (1.90) onto the complementary space in sector (m, n), $Q^{(m,n)} = 1 - P^{(m,n)}$.

The Hilbert space wave operator was proposed by Jeziorski and Monkhorst [147]:

$$\Omega = \sum_K e^{T(K)} P_K \tag{1.92}$$

where the operator is defined with respect to each of the reference determinants in P, therefore the summations in the T_n do not overlap and are strictly defined. The equations to be solved for the cluster amplitudes are similar to those of the single reference CC methods, with the addition of a renormalisation term, reflecting the coupling of the reference determinants [147, 169, 171]. The energies of the states and the expansion coefficients within the reference space are determined through diagonalising the effective Hamiltonian,

$$\bar{H} = PH\Omega P \tag{1.93}$$

The Fock and Hilbert space CC methods are easier to apply within a complete model space, one that includes all possible distributions of electrons within the active orbitals, however, the effective Hamiltonian for a complete space can suffer from problems with intruder states [167, 169]. This occurs when a non-reference configuration becomes almost degenerate with the reference functions, and can cause convergence difficulties. The problem is overcome by employing an incomplete model space, this, however, greatly complicates the methods as excitations within the active orbitals have to be allowed for in the wave operator. Recent progress has been made in the study of incomplete model spaces for both Fock [153, 172–174] and Hilbert [169, 175] methods. The calculations in the Fock space are simplified by the presence of "quasicomplete" spaces [153], these include the particle-hole states (singly excited states).

The Fock space CC method has been applied to a wide variety of atoms and small molecules [104, 167, 168, 170]. Due to difficulties associated with the coupling of the reference configurations there have been few calculations employing the full Hilbert space procedure. An approximation which has been used is to fix the contraction coefficients for the reference space in an MCSCF. Bartlett [104] used this procedure on the ground states of F_2 and N_2 obtaining results close to MR-CISD and superior to single reference CC. More recently Balková *et al.* applied the

full Hilbert space CC on the potential energy surfaces for the ground and low-lying states of the model system H_4 [171], which display regions of degeneracy and non-degeneracy. The MR-CCSD performed well for the degenerate region, although agreement with full-CI was less satisfactory for the non-degenerate region.

Chapter 2

The Electronic Spectra of Propyne

Propyne, or methylacetylene, is the second member in the alkyne series of molecules, possessing as their major characteristic a carbon-carbon triple bond, the presence of which dominates both the physics and chemistry of the smaller alkynes. The molecule is a minor constituent of the atmosphere of Titan [176] and interstellar clouds [177,178].

In comparison with the parent molecule of the series, acetylene, there have only been a small number of published experimental studies on the electronic spectra of propyne. In common with acetylene the interpretation of the spectrum is made difficult by the large number of transitions, both of valence and Rydberg type that occur in a narrow energy range, with the associated problems of mixed valence and Rydberg character and intensity borrowing. Further complication is caused by the existence of strong vibrational progressions. The diffuse nature of the observed bands has prevented the unequivocal assignment of the transitions.

Despite the small size of the molecule there have been, to the best of my knowledge, no theoretical studies reported on the Rydberg series and only one on the valence electronic spectrum. In the present work *ab initio* calculations were performed using a variety of basis sets, including extensive Rydberg functions, with the aim of providing guidance in this assignment of the low-lying Rydberg and valence states.

2.1 Molecular orbital description of propyne

In the discussions that follow use will be made of the molecular orbital description of the molecule with symmetries being described in terms of both the molecular point group and, for convenience, in the "local symmetry" of the triple bond, *ie* use will be made of the terms π and σ even though these do not exist in the molecular point group. The point group of the propyne ground state is C_{3v}.

The carbon skeleton can be described by the hybridisation scheme $sp^3 - sp - sp$ with two mutually perpendicular "π", e pair, MOs arising from p-orbitals giving the triple bond. The highest occupied molecular orbitals and therefore the most active for the low-lying states in the electronic spectrum are the pair of π MOs.

Classifying the MOs according to their behavior under the symmetry operations of this point group the corresponding SCF single configuration occupancy is $1-7a_1^2, 1-2e^4$ (X^1A_1). In the ground state no orbitals of a_2 symmetry are occupied, indeed these can only be generated by the inclusion of orbitals with higher than p angular momenta on the methylenic hydrogens.

The excited states fall into two categories, valence and Rydberg, the low lying transitions arising from excitation out of the highest e. The low-lying valence virtual states are derived from the $\ldots 2e^3(e^*)^1$ configuration, where the e^* MOs are the complement of the $2e$ MOs, configuration. This occupancy gives rise to six states, ${}^2E * {}^2E = {}^{1,3}A_1 + {}^{1,3}A_2 + {}^{1,3}E$. Under C_{3v} symmetry transitions of A_2 type are both dipole and quadrupole forbidden.

With distortion from the "linear" C_{3v} nuclear arrangement the MOs of propyne undergo significant alterations. Upon planar distortions the molecular symmetry is reduced to C_S. In this point group all transitions are dipole and quadrupole allowed. On *cis*-planar or *trans*-planar deformation the e type MOs are no longer degenerate; the HOMO $2e$ splits into in-plane "σ" and out-of-plane "π" components of a' and a'' symmetry respectively. Using arguments put forward by Walsh for HAAH, a situation is found similar to acetylene [179]. The energy of the a' (σ)

state is slightly stabilised relative to the linear e state by *cis* bending, the a'' state is unaffected. On the other hand the a'' state is greatly stabilised by *trans* bending. For the e^* state the energies and symmetries are such that $a'(\sigma^*) \ll a''(\pi^*) \sim e^*$ for both *cis* and *trans* deformations.

2.2 Experimental and theoretical background

2.2.1 Ground state geometry and properties

The ground state of propyne has a symmetric top arrangement [180, 181], the carbon chain in a linear configuration. The molecule has a permanent dipole moment, aligned along the carbon chain, of approximately 0.78 Debye [182, 183].

The experimental structure has been determined by a variety of techniques, Table 2–1. In general even relatively low level theoretical methods give reasonable agreement with the experimental values, Table 2–8 and Section 2.4.1. The observed C-C single bond length of $\sim$1.46 Å is significantly shorter than the single bond in ethane, $\sim$1.54 Å [184, 185], furthermore the bond dissociation energy, as calculated from the heats of formation of propyne, CH_3, and CCH, predicted that the bond will be significantly stronger than that in ethane, 124$\pm$1.0 compared to 87.8$\pm$0.3 kcal mol^{-1} (5.10 and 3.61 eV)[186]. Observation of propyne and other hydrocarbons led Stoicheff to formulate an empirical relation in which the bond length varies nearly linearly with the number of atoms attached to the carbon atoms forming the bond [187]. The C$\equiv$C triple bond and acetylenic C-H bond lengths are similar to those found in acetylene, in the case of the C-H bond this is $\sim$ 0.03 Å shorter than the corresponding bond length in methane. The reduction of the C-C single bond and acetylenic C-H bond lengths with respect to the saturated hydrocarbons reflects the change in hybridisation of the carbon atoms from sp^3 to sp, the decrease in p character in the bond having a corresponding effect on the internuclear separation.

Table 2–1: Ground state geometries of propyne.

Method[a]	Bond lengths (Å)				Angles (deg)		
	C≡C	C-C	C-H	C-H_{methyl}	HCC	HCH	ref.
IR	1.204[b]	1.462	1.057[b]	1.093[a]	109.5[b]	-	[184]
IR	1.207	1.458	1.059	1.110	-	108.5	[188]
IR	1.2073	1.4577	1.060	1.096	-	108.3	[189]
ED	1.20	1.46	-	-	-	-	[190]
MW r_0	1.207	1.460	1.056	1.097	-	108.2	[181]
MW r_0	1.2073	1.4577	1.0602	1.1124	110.5	-	[191]
MW r_s	1.2066	1.4586	-	-	-	-	[192]
MW r_s	1.2062	1.4589	1.0562	1.1054	110.2	-	[193]

[a] IR=infra-red; ED=electron diffraction; MW=microwave; r_0=structure obtained from rotational constant B_0; r_s=substituted structure.

[b] assumed

An alternative explanation for the shortened C-C bond was proposed by Mulliken [194]; through analogy with the alkyl radical, that hyperconjugation imparts a degree of double bond character through the interaction of the C-H bond in the methyl group with the "π" orbitals on the central carbon atom. Trambarulo and Gorby estimated that to explain the observed shortening would require approximately 12 % double bond character [181]. An additional effect of the hyperconjugation would be the weakening of the adjacent methyl C-H and C≡C bonds, although the increase in C≡C bond length would not be expected to be large. Experimental evidence for a large amount of hyperconjugation in the neutral propyne molecule is not strong, especially when the necessary comparisons are between molecules with greatly differing bonding environments and steric interactions. Of the bond dissociation energies only the methyl C-H energy has been directly determined and found to be 89.4 kcal mol^{-1} at 300 K (3.68 eV), this is 9 kcal mol^{-1} (0.39 eV) less than in ethane as would be expected from the hyperconjugation model, however the difference has been explained in terms of the resonance stabilisation of the radical product [195, 196]. Bauschlicher and Langhoff [186] used *ab initio* methods to determine the bond dissociation energies of propyne. The results obtained were consistent with hyperconjugation; the acetylenic C-H and the C≡C

bonds being predicted to be weakened by the substitution of the methyl group, by as much as 8 kcal mol^{-1} (0.35 eV) for the triple bond. The computed effects on the other bonds were again due to the resonance stabilisation in the resulting fragments. This result for the bond dissociation energy of the triple bond was contrary to the earlier results of Wiberg [197, 198] who predicted that the triple bond would be stabilised by ~5 kcal mol^{-1} (0.22 eV), the methyl group acting as a σ and π donor to the adjacent atom. Wiberg also noted a minor increase in the π electron density at the remote atom.

The fundamental vibrational frequencies of propyne, and deuterated analogues, have been extensively studied by infra-red spectroscopy [199–207] , Table 2–2. The stretching vibrations in the methyl group are found to undergo a transition from normal-mode vibrations, the symmetric ν_2 and antisymmetric ν_6, to a single local-mode vibrations, ν_m in higher vibrational levels[208]. The presence of the carbon chain allows low frequency vibrations to occur, there are four fundamental frequencies below 1100cm^{-1} all of which have appreciable populations at room temperature. The first excited level of the carbon skeleton bending mode, ν_{10}, having an occupation 41% as large as that of the vibrational ground state whilst the acetylenic group bend, ν_{10}, has 9.4%, as estimated using Boltzmann's statistics [209]. For the interpretation of the electronic spectra the most important modes of vibration are those concerned with changes in the carbon skeleton, particularly bond lengths, ie the carbon-carbon triple bond stretching mode, ν_3, and the single bond stretching mode, ν_5.

The UV-photoelectron spectrum has been given for ionisation by irradiation by both the He(I) line at 21.215 eV [212, 213], and the He(II) line at 40.78 eV [214]. Six main bands occur in the IP region from 10 to 25 eV (bands $\tilde{X}$-$\tilde{E}$), Table 2–3. The first two spectral features, $\tilde{X}$ and $\tilde{A}$ are assigned to ionisations of E type from the -C≡C- and methyl groups respectively. The vibrational structure observed on band $\tilde{X}$, 940 cm^{-1} and 1940 cm^{-1}, demonstrates the excitation of vibrations in the carbon skeleton, similar to the ground state ν_3 and ν_5 vibrations. The angular dependence of the electron ejection in the first band is also consistent with the loss of a π electron [215]. The 1290 cm^{-1} progression of the $\tilde{A}$ band is similar to

Table 2–2: Fundamental vibrational frequencies of propyne.

Mode	Frequency /cm^{-1}	Intensity /km mol^{-1}[a] [205]	Experimental Assignment	Ref.
		a_1 modes		
ν_1	3335.1	45.1±3.1	acetylenic C-H stretch	[201]
ν_2	2941.4	14.9±3.6	symmetric methyl C-H stretch	[199]
ν_3	2137.9	5.3±0.3	C≡C stretch	[210]
ν_4	1385.0	1.5±1.0	methyl deformation	[206]
ν_5	930.3	1.0±0.5	C-C stretch	[211]
		e modes		
ν_6	2980.8	17.7±3.5	antisymmetric methyl C-H stretch	[199]
ν_7	1450.3	17.9±1.6	methyl skeletal deformation	[206]
ν_8	1036.1	0.4±0.3	methyl skeletal rock	[211]
ν_9	628.1	87.3±4.5	C≡C-H bend	[199]
ν_{10}	327.5	16.7±1.0	C-C≡C bend	[199]
		local modes		
ν_m	3037	-	methyl C-H stretch	[208]

[a] $= (1/nl)\int_{band} log(I_0/I)d\nu$, the integral of the extinction coefficient over the band.

that of the ground state methyl group deformations, ν_4, ν_7, and ν_8. The order of ionisation is then $1E$ <$2E$ <$1A_1$ <$2A_1$ .... Beyond the first two bands, the assignment differs between Kimura *et al.* [213] and Bieri *et al.* [214]. Kimura *et al.* assign bands $\tilde{A}$ and $\tilde{B}$ to arise to the Jahn-Teller splitting of the $1e$ MO with the $1A_1$ ionisation being assigned to the shoulder observed at 15.8 eV. The spectrum of Bieri *et al.* showed no evidence of this feature; the $\tilde{B}$ band was therefore assigned to the $7A_1$ ionisation. The most complete theoretical study of the UV-PES comes from the Green's function work of von Niessen *et al.* [216], which in common with the result of Koopmans' theorem on SCF calculations, yields the ionisation order from the MOs $2e$ <$1e$ <$7a_1$ <$6a_1$ ... in agreement with the experimental assignments. Using a qualitative arguments based on the hyperconjugation model Bock *et al.* [217, 218] obtained an alternative ordering, e <$7a_1$ <$1e$ <$6a_1$ ..., the $\tilde{B}$ band being resolved into two features, due to the Jahn-Teller splitting of the 1E state, at 15.3 and 15.5 eV.

Propyne has a negative electron affinity; a resonance variously reported at 2.8

Table 2–3: Vertical ionisation potentials of propyne

State	He(I) [213] /eV	He(II) [214] /eV	Vibrations /cm^{-1}
$\tilde{X}$	10.37	10.54 (10.37)[b]	1940[c], 940[d]
$\tilde{A}$	14.70	14.6 (13.91)[b]	1290[c]
$\tilde{B}$	15.50	15.4	
	(15.8)[a]		
$\tilde{C}$	17.49	17.4	
$\tilde{D}$		22.4	
$\tilde{E}$		23.9	

[a] shoulder

[b] adiabatic ionisation energies [219, 220]

[c] [219]

[d] [214]

[221] and 3.14 eV [222] on the electron transmission spectrum. The state, due to electron attachment to an antibonding MO predominantly formed from the triple bond e* MOs [221], is unstable with respect to electron autodetachment, with a lifetime of less than 1 ms [223].

2.2.2 Excited states and electronic spectra

The molecular geometries for the excited states are not known. Theoretical calculations on the lowest valence $^3A'$ [179] and $^{1,3}A''$ [179, 224] states support the idea that the geometries are, like those of acetylene [225–229], non-linear. By analogy with acetylene [230–233] the Rydberg states are expected to be linear[1].

The energies of the most prominent features in the optical [234, 235] and electron impact [236–240] spectra are given in Table 2–4. For ease of interpretation the electron impact studies have been sub-divided into three categories, the threshold electron impact studies [236, 237], those electron impact studies at higher energies

[1]Definitions of valence and Rydberg states are given in Appendix A.

[238, 239], and the variable angle study of Flicker *et al.* [239]. As will be outlined in the following discussion the two optical studies do not agree. The VUV and electron energy loss spectra of propyne are shown in Figure 2.2.2.

The longest wavelength absorption system of the ultraviolet spectrum of propyne consists of a broad structureless dissociation feature extending from 220 to 160 nm (5.5-7.6 eV) [234, 235, 241]. The feature was first studied by Price and Walsh [234] who resolved two bands, 195-188 nm (6.37-6.59 eV) and 175-160 nm (7.08-7.75 eV) with maxima at 192 (6.45 eV) and 165 (7.51 eV) (the $\tilde{A}$ and $\tilde{B}$ bands of Herzberg [242]) which by analogy with the spectrum of acetylene were assigned to be valence transitions. A subsequent UV study by Nakayama and Watanabe [235] failed to confirm the existence of the two bands, instead a single broad band was observed a maximum at 176 nm (7.05 eV) with a secondary feature at 172 nm (7.20 eV). As part of a fluorescence study Hamai and Hirayama [241] investigated the absorption spectra of propyne in the vapour phase, between 230 and 160 nm (5.40-7.75 eV). The maximum absorption was found to occur at 173 nm (7.17 eV) in good agreement with Nakayama and Watanabe. The feature was assigned to the optically allowed $e \rightarrow e^*$ transition to the $\tilde{B}$ state of E symmetry. Evidence of the $\tilde{A}$ state was first reported by Dance and Walker [237] who observed a shoulder in the electron energy loss spectrum at 6.7 eV, corresponding to a weak feature in the optical spectrum of Nakayama and Watanabe [235]. On this evidence the feature was assigned to an optically forbidden transition.

A weak transition ($\tilde{X} \rightarrow \tilde{C}$) is observed at $\sim$7.85 eV which has no analogue in the spectra of acetylene [234, 235, 239, 240]. Fridh [240] assigned the peak as being due to the first member of the $np\sigma$ Rydberg series.

Above 154 nm (8.05 eV) Price and Walsh [234] reported rich Rydberg structure ascribing it to two Rydberg series, the R and R', converging to a limit of 11.25 eV. These series were similar, with a constant shift of $\sim$850cm^{-1} (0.11 eV), to those known in acetylene [243] and assigned accordingly as being due to excitation form a π, or e, orbital. The diffuseness of the observed peaks prevented any analysis of the symmetries of the excited states.

Nakayama and Watanabe [235] also studied the absorption spectrum of propyne

Table 2–4: Excited electronic states of propyne

	Vertical transition energy /eV			
		Electron impact		
State	Optical [235]	Threshold [237]	Other [240]	Variable angle [239]
$\tilde{a}$	...	5.2	...	5.2
$\tilde{b}$	...	5.8	...	5.85
...	...	6.1^{BM}, 6.3	...	(6.4)
$\tilde{A}$	$6.7, 6.45^{PW}$	6.7	...	6.7
...	7.04	7.0, 7.1	...	...
$\tilde{B}$	7.2	7.2	$7.18, 7.25^{S}$	7.18
...	...	...	7.44^{S}	7.38
...	7.51	...	...	...
$\tilde{C}$	7.86	...	7.86, 7.87	7.88
3R′	$8.05, 8.04^{PW}$	8.1	8.05	8.06
3R′+ν_5	8.17	8.2	8.16	...
3R′+ν_3	8.29	$8.35, 8.3^{BM}$	$8.29, 8.28^{S}$	8.30
3R″	8.45	...	$8.44, 8.45^{S}$	...
3R′+2ν_3	8.54	...	8.53	...
3R″+ν_3	8.69	...	8.69	...
4R	8.83	...	$8.83, 8.81^{S}$	8.84
3R″+2ν_3	8.93	8.9	...	...
4R+ν_3	$9.07, 9.12^{PW}$	...	$9.07, 9.08^{S}$	9.08
4R′	9.21	9.23	9.21	9.25
4R″	9.36	...	$9.37, 9.39^{S}$	9.36
4R′+ν_3	9.45	...	9.45	9.44
5R	9.51	9.5	...	...
5R′	9.66	...	9.66	...
4R′+2ν_3	9.69	...	...	9.71
5R″	9.75	...	9.75	...
6R′	9.91	...	9.92	...
6R″	9.94		$9.92, 9.93^{S}$	9.96
7R	9.99	...	...	...
7R′	10.03	...	10.04	...
	10.10	...	10.10^{S}	...
	10.17	...	$10.17, 10.16^{S}$	...
	10.18	...	...	10.19
	10.22	...	10.24^{S}	...
	10.30	...	10.30	10.28

^{PW} [234]

^{BM} [236]

^{S} [238]

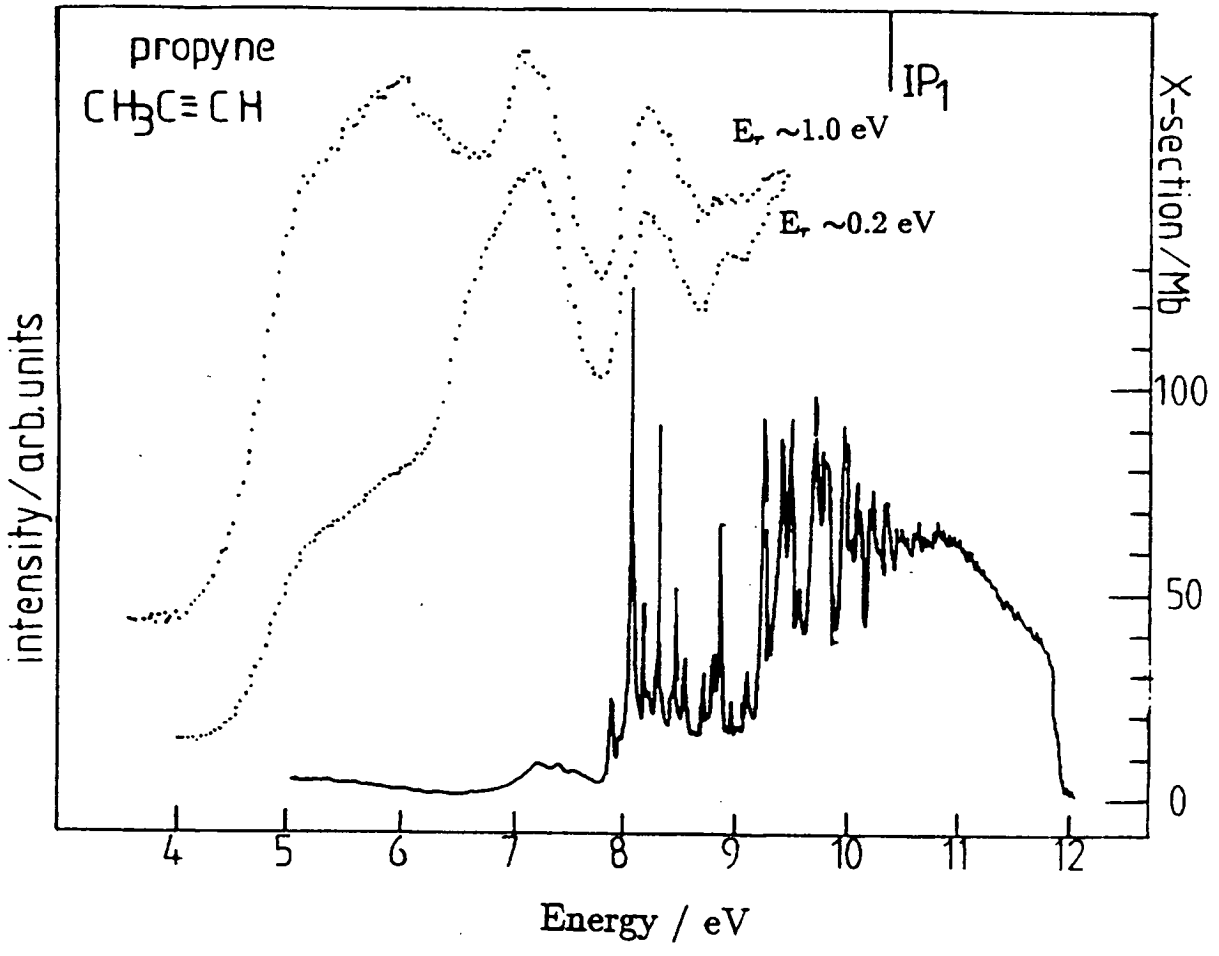

Figure 2–1: The electron energy loss and VUV spectra of propyne.

... Electron Energy Loss spectra of propyne at stated residual electron energies (E_r).

— VUV spectrum.

Spectrum courtesy of Dr. I. C. Walker, Heriot-Watt University.

in the region 160-105 nm (7.75-11.80 eV). Unlike the spectrum of Price the majority of the observed bands were found to be below 120 nm (10.33 eV), where almost continuous absorption was found. The presence of three Rydberg series, R, R' and R'' was postulated converging to the same limit of 10.56 eV (see Figure 2.2.2), in good agreement with the ionisation potential: $\nu_0(\mathrm{cm}^{-1})$=83570-R/(n-0.98)^2, n=4,5,...; $\nu_0(\mathrm{cm}^{-1})$=83580-R/(n-0.57)^2, n=3,4,5,...; $\nu_0(\mathrm{cm}^{-1})$=83600-R/(n-0.33)^2, n=3,4,5,.... By comparison with similar series in acetylene, the R and R' Rydberg series were assigned as the ns and nd series respectively. The n=3 member of the R series was not observed, from the quantum defect the transition would be expected to lie under the $\tilde{X}\rightarrow\tilde{B}$ valence transition. The term value associated with the $\tilde{B}$ state is 3.3 eV, a value close to that of the lowest $3s$ Rydberg state in acetylene [244].

Many of the early members of the Rydberg series exhibited strong vibrational progressions, especially with spacing $\sim$1970cm^{-1} corresponding to C$\equiv$C ν_3' stretching mode (*cf* 1849cm^{-1} for the analogous ν_2' symmetric stretch for the $\pi\rightarrow$3s state of acetylene [230]) and consistent with a large relaxation of the C$\equiv$C bond length associated with a change of bond order from three to two-and-a-half due to excitation from the triple bond. The lack of bending modes provides strong evidence that the Rydberg states be assigned as being linear or near linear. No information on the rotational spectra was forthcoming from the study, preventing the experimental determination of the excited state symmetries.

Betts and McKoy [245], using a model potential method to calculate the Rydberg series, also assigned R and R' as being due to transitions to ns and nd, with quantum defects of 0.90 and 0.54 respectively. No suitable candidate was found for R''.

Electron impact studies at higher energies and low scattering angle [238–240] reveal Rydberg structure similar to the UV spectrum of Nakayama and Watanabe. As a result of a high resolution electron impact energy loss spectra, at energies of 500 eV and 25-75 eV, Fridh [240] re-interpreted the R, R' and R'' as being excitations to ns, $np\pi$ and $nd\sigma$ MOs respectively.

The position of the second IP at approximately 14.8 eV, almost 3.5 eV above

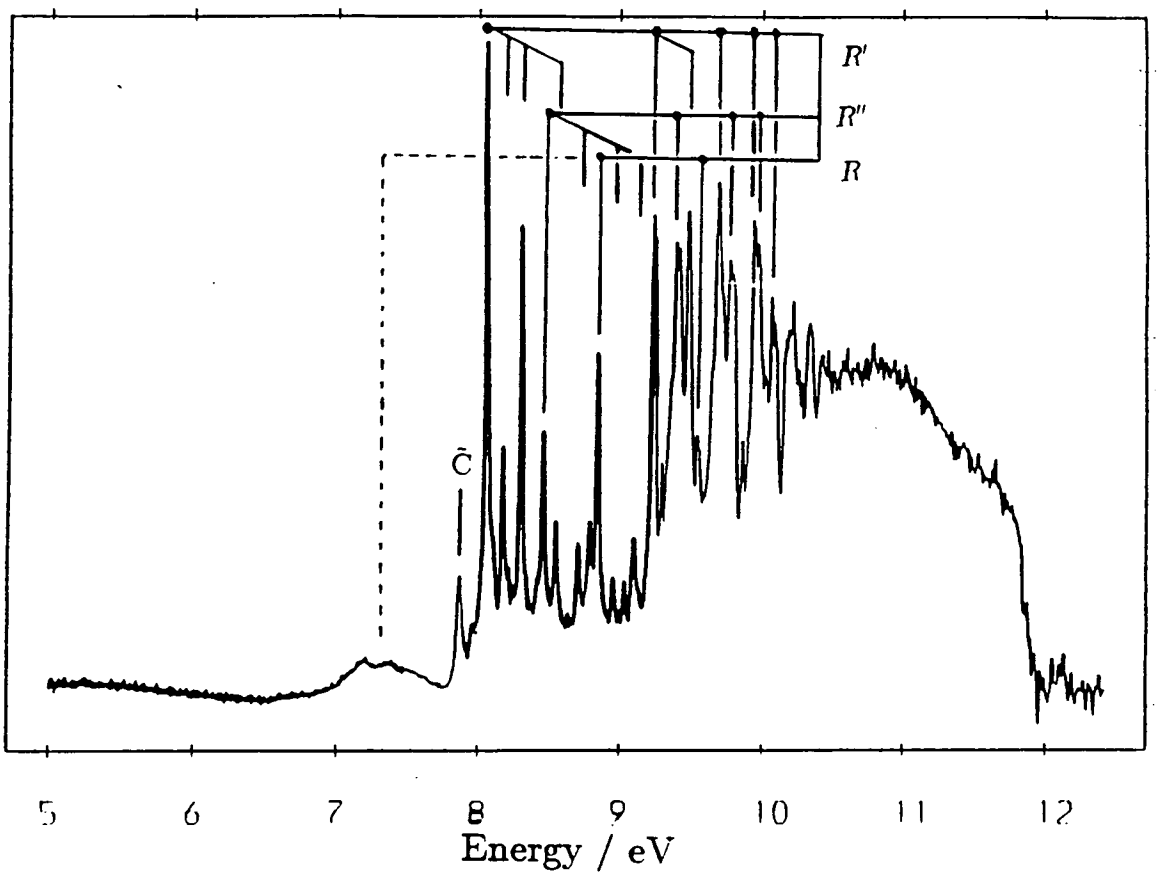

Figure 2–2: The VUV spectrum of propyne with the Rydberg series marked. Spectrum courtesy of Dr. I. C. Walker, Heriot-Watt University.

the first IP, in conjunction with the estimated position of the first Rydberg transition, suggests strongly that no transitions from other than the HOMO e pair will be observed in the electronic spectrum below 10 eV. Flicker *et al.* [239] observed super-excited states at 10.57, 10.72, 12.7, and 14.7 eV. The first two of these were assigned to be members of Rydberg series converging to vibrationally excited states of the first molecular ion. The other peaks were interpreted as converging to the third and fourth molecular ions.

The electron energy loss studies of Knoop, and Dance and Walker [237] located transitions below the onset of optical excitation, at 5.2 and 5.8 eV. These were assigned as being of singlet-triplet in character. The features occur at similar excitation energies to the corresponding $\tilde{X}\rightarrow\tilde{a}$ and $\tilde{X}\rightarrow\tilde{b}$ transitions in acetylene [237, 246, 247]. The triplet nature of the excited state was confirmed by variable angle electron impact study of Flicker *et al.* [239]. Knoop also detected a feature at 6.3 eV which he suggested might be due to the third singlet-triplet transition; an earlier electron impact study by Bowman and Miller [236] had identified a peak at 6.1 eV. Neither Dance and Walker nor Flicker *et al.* found strong evidence of a transition in this region, although Flicker *et al.* reported that an occasional feature was found at 6.4 eV. In addition Flicker *et al.* noted an unexpected intensity dependence upon scattering angle in the singlet-singlet features at 8.30 eV, suggesting the presence of a previously unidentified underlying singlet-triplet transition.

Fridh performed semiempirical calculations upon the low-lying singlet and triplet valence states arising from $e \rightarrow e^*$ using the HAM/3 method parameterised upon dinitrogen [240]. The results agreed with the experimental ordering for the excitation energies, $^3A_2 <^3 E <^3 A_1$ and $^1A_1 <^1 E <^1 A_2$, with the third triplet and first singlet states predicted to arise at the same energy, see Table 2–12.

Hamai and Hirayama [241] studied the fluorescence spectra of several of the alkynes, including propyne. Propyne, in common with the other 1-alkynes, exhibited a broad fluorescence emission with a maximum at 370 nm (3.35 eV) in nitrogenated cyclohexane solution. The vapour spectrum, obtained at atmospheric pressure, was found to be identical to the solution fluorescence, but shifted to the

blue by ~5 nm, when excited at 180 nm (6.89 eV), however as the wavelength of the exciting radiation was decreased the fluorescence sharply yield decreased. Fluorescence was not observable at wavelengths below 175 nm (7.08 eV), a value close to the maximum absorption in the UV spectrum. This compared to acetylene with a fluorescence maximum at approximately 320 nm (3.87 eV) for the same exciting radiation. Given the similarity of the spectra for the 1-alkyne series Hamai and Hirayama interpreted the chromophore as being the H−C≡C− group with the emissions originating from the neutral excited $\tilde{A}$ state. The large Stokes shift (shift to lower energy) of ~26600cm^{-1} (3.3 eV) combined with the featureless emission spectrum and the relatively large spectral width, ~6500cm^{-1} (0.8 eV), lead them to conclude that there was a large disparity in the nuclear configurations of the ground and excited states. The sudden cut-off in fluorescence is consistent with the existence of a dissociative state, *cf* acetylene where a decrease in the fluorescence yield was observed by Fujii *et al.* 11.8-12.8 kcal mol^{-1} (0.51-0.56 eV) above the 0-0 transition [248] to the *trans*-isomer of the lowest excited state, an energy comparable to the linear geometry.

The photolysis of propyne has been performed at 206 nm (6.02 eV) by Galli *et al.*[249], at 193 nm (6.42 eV) by Seki and Okabe [250] and Satyapal and Bersohn [251], at 147 nm (8.43 eV) by Stief *et al.* [252], and at 123.6 nm (10.03 eV) by Payne and Stief [253]. At 206 nm, in the lower reaches of the dissociation continuum observed in the UV spectrum, the main photolysis products are 1,5-hexadiyne, propylene, hydrogen and acetylene [249]. As no isotopic labeling was performed the initial processes involved were not determined. At 193 nm and 147 nm, within the dissociation band and in a region of strong Rydberg structure respectively, the main primary processes were determined to be the loss of the acetylenic hydrogen atom [250, 252]. On the assumption that the absorption at these wavelengths was most likely to occur in the -C≡C- group Seki and Okabe [250] concluded that the process of hydrogen elimination must occur on a timescale of less than one molecular vibration, before the photon energy could propagate to the weaker methyl C-H bonds. Thus the broad dissociation feature observed in the optical spectrum of propyne is interpreted as being due to the rapid loss

of the acetylenic hydrogen. The higher energy study at 123.6 nm had the loss of molecular hydrogen as the dominant process [253]. Seki and Okabe [250] suggested that this might be due to the absorption being predominantly in the region of the methyl group.

2.2.3 The excited states of acetylene

The electronic spectrum of acetylene has been the subject of many investigations, both experimental [225–227, 230, 235, 237, 243, 247, 254–260] and theoretical [228, 229, 231–233, 261–265]. The point group of the acetylene molecule is $D_{\infty h}$, which is reduced upon *trans* and *cis* deformations to C_{2h} and C_{2v}, respectively.

Four valence transitions have been identified in the electronic spectra of acetylene, the singlet $\tilde{X}\rightarrow\tilde{A}$ and $\tilde{X}\rightarrow\tilde{B}$ and the triplet $\tilde{X}\rightarrow\tilde{a}$ and $\tilde{X}\rightarrow\tilde{b}$ [225–227, 237, 247, 254, 256]. The $\tilde{X}\rightarrow\tilde{A}$ consists of a number of weak bands at 240-210 nm (5.17-5.90 eV) [225, 226, 254]. Detailed analysis of the vibrational and rotational structure has been performed by Ingold and King [225] and Innes [226] who concluded that the upper electronic state was of ^1A_u ,*trans*-bent, equilibrium structure (C_{2h} molecular symmetry), corresponding to $^1\Sigma_u^-$ at the linear geometry. The 0-0 transition energy, T_{00}=5.23 eV, and the excited state structural parameters, r(C-C) 1.38 Å, r(C-H) 1.08 Å, and θ(CCH) 120° have also been experimentally determined [225]. *Ab initio* calculations have confirmed the existence of this minimum [229, 231, 232, 263] and also predict the existence of a stable *cis*-bent isomer, $^1A_1$ (C_{2v} molecular symmetry). However, the transition to the *cis*-state, like the linear state, is forbidden. A second complex and diffuse band system, $\tilde{X}\rightarrow\tilde{B}$, is situated around 195-155 nm (6.37-8.00 eV). The transition was investigated by Foo and Innes [227] who ascribed a *trans*-bent equilibrium geometry, ^1B_u, corresponding to a $^1\Delta_u$ linear asymptote. The value determined for T_{00} was 6.71 eV. Again theoretical studies predict the existence of a stable *cis*-bent, $^1B_2$, isomer [229, 231, 232, 263]. The other *trans*,^1A_u, component of the $^1\Delta_u$ state has not been observed experimentally; this state has been predicted to either have a small minima or to have a linear geometry [229, 231, 232, 263]. The triplet states have been

studied by electron impact experiments [237, 247, 256] with vertical excitation energies of 5.3 eV for the $\tilde{X}\rightarrow\tilde{a}$ transition corresponding to a $^3\Sigma_g^+$ excited state and 6.0 eV for $\tilde{b}^3\Delta_g^+$ state. These states are also found to have non-linear equilibrium geometries in calculations [228, 232].

At linear geometry, spin and symmetry restrictions mean that only four of the possible Rydberg series resulting from excitations out of the HOMO π_u orbital have been observed and identified in the one photon absorption spectrum. These allowed transitions result from promotions to *s*- and *d*-type orbitals, specifically there are the $^1\Pi_u$ associated with $\pi_u^4 \rightarrow \pi_u^3 ns\sigma_g$, $\pi_u^4 \rightarrow \pi_u^3 nd\sigma_g$, and $\pi_u^4 \rightarrow \pi_u^3 nd\delta_g$, and the $^1\Sigma_u^+$ arising from $\pi_u^4 \rightarrow \pi_u^3 nd\pi_g$. In addition to these series a further state $^1\Phi_u$ from $\pi_u^4 \rightarrow \pi_u^3 nd\delta_g$ has been identified.

The lowest energy Rydberg state ($\tilde{C}$) occurs in the 153-140 nm region with an absorption origin at 152 nm (8.16 eV). This state has been experimentally [230, 235, 243] and theoretically [232, 233, 262, 264] assigned to the linear $^1\Pi_u$ state arising from $\pi\rightarrow 3s$ transition. The n=4 and n=5 members of this series have been identified at 9.93 and 10.57 eV respectively [259]. Hollas and Sutherley [255] determined the Franck-Condon factors for the n=4 transition and concluding that the upper state was linear with bond C-C and C-H bond lengths of 1.26 and 1.07 Å, approximately 0.05 Å and 0.01 Å longer than the ground state, respectively.

The assignment of the $\tilde{X}\Sigma_g^+ \rightarrow^1 \Pi_u$ transition, associated with the electronic promotion $\pi_u^4 \rightarrow \pi_u^3 nd\delta_g$, to the $\tilde{G}$ band at 9.97 eV [257] has bent confirmed by Herman and Colin [259] using rotational analysis. The two further dipole allowed transitions arising from promotion to a *d*-type Rydberg orbital , the $\pi_u^3 3d\pi_g(^1\Sigma_u^+)$ and the $\pi_u^3 3d\sigma_g(^1\Pi_u)$, have been identified as occurring at around 9.25 eV. Three spectra features have been observed in this region, the $\tilde{D}$, $\tilde{E}$, and $\tilde{F}$ bands at 9.24, 9.25, and 9.27 eV [230, 235, 257, 259]. The $\tilde{D}$ and $\tilde{F}$ bands are found to be considerably stronger than the $\tilde{E}$ band, therefore they were assigned as being the allowed transitions with the $\tilde{E}$ an as yet unidentified forbidden transition. Experimentally the unambiguous assignment has been hindered by the lack of resolvable rotational structure, however theoretical studies predict the $^1\Pi_u$ state to have the lower energy [232, 233]. Ashfold *et al.* [260] located the $^1\Phi_u(\pi_u^3 3d\delta_g)$

state at 9.91 eV using 3+1 multiphoton ionisation spectroscopy. The rotational structure and observed line strengths lead to the conclusion that the upper state possessed a linear geometry.

It is possible to get an idea of the likely transition energies in propyne by assuming that the excitations in propyne will occur with the same term values as the corresponding Rydberg transitions in acetylene. As the first IP in propyne occurs at a lower energy than in acetylene, 10.37 eV as compared to 11.41 eV, the Rydberg series that converge to this IP will arise at correspondingly lower energies. Using this the experimental energies of the identified Rydberg transitions in acetylene the lowest Rydberg transition in propyne, the $2e3s$ of E symmetry, would be expected to arise at 7.13 eV (π3s, 8.16 eV in acetylene) with the second and third members of this series arising at 8.90 (π4s, 9.93 eV) and 9.54 eV (π5s, 10.57 eV). The other identified transitions are to d-type Rydberg states, therefore the E symmetry transition to the $d\sigma_g$ is predicted at 8.22 eV (9.25 eV) close to the A_1 transition to $d\pi_u$ at 8.24 eV (9.27). The transitions corresponding to excitation to the $d\delta_g$ orbital are predicted to occur at 8.88 eV (9.91 eV) for the E and 8.94 eV (9.97 eV) for the A_1. All these excitations are expected to be active in the UV spectrum of propyne.

2.3 Theoretical methods employed

The present study on the excited states of the propyne molecule employed a variety of different basis sets to investigate the dependence of the valence (π, π^*) excitation energies. The smallest used was Dunning-Huzinaga (9s5p/5s)/[4s2p/2s] double zeta, DZ, basis (38 GTOs) [266, 267]. Two basis sets of double zeta plus polarisation, DZP, standard (68 GTOs) were generated by the addition of p-functions to the hydrogens and d-functions to the carbons with exponents 1.0 (H), 0.72 (C) , and 0.25 (H), 0.20 (C)[2]. The triple zeta, TZ, basis of Dunning (57 GTOs) [268] was also employed and additionally augmented by the addition of two polarisation functions on each atom; 2.0, 0.5 (H), and 1.44, 0.36 (C), TZ2P(117 GTOs). For the investigation of the electronic spectrum the DZ and DZP-type bases were augmented by the addition of a large Rydberg set, $3s2p2d$, to the centre of the triple bond, with exponents 0.021, 0.008, 0.0025(s), 0.017, 0.009(p), 0.015, and 0.008(d). This set of Rydberg functions has previously been successfully employed in the assignment of the azine series of molecules [269–272]. All six components arising from the Gaussian d-functions were retained in the SCF and subsequent calculations, including the pseudo s-type functions of the from $d_{x^2+y^2+z^2} = d_{r^2}$.

The equilibrium structures (r_e) were determined for all the basis sets at the SCF level and for the DZ, DZP, and TZ2P bases at the MP2 level. The calculations employing the Rydberg augmented sets were performed using the optimised geometries of the respective unaugmented basis set.

The highest point group accessible in MRD-CI is D_{2h}, therefore the CI calculations on propyne were performed in C_s symmetry with the identities $A'(A_1 + E)$ and $A''(A_2 + E)$, symmetric and antisymmetric with respect to reflection in, in this case, the yz-plane of symmetry.

---

[2]These are denoted DZP for the standard polarisation functions and DZP$_l$ for the diffuse functions to remove ambiguity.

The single configuration SCF wavefunctions were used to provided the MO basis for all-valence electron ground state and excited state CI calculations. In all these the "core" carbon C1s MOs were kept doubly occupied at all times, also in order to keep the calculation within reasonable dimension a group of the highest virtual orbitals, in aufbau order, were discarded. For the calculations on the Rydberg space, the maximum of 20 roots were generated, this being required due to the low number of symmetries being available to cover the desired energy range. There were up to 56 main reference configurations, leading to the maximum 80 reference CSFs once spin combinations had been taken into account; this is 56M20R in the conventional MRD-CI nomenclature [71–73]. The largest calculations performed generated in excess of 10^7 CSFs. The selection threshold in the MRD-CI module was used to reduce the number of CSFs in the final diagonalisation to below 18000. Information regarding the numbers of active orbitals and electrons employed in the calculations, along with the numbers of reference functions and roots, and the associated computation dimensions are given in Tables 2–5 and 2–6, with and without Rydberg functions, respectively. The oscillator strengths of the transitions in the DZP_I singlet manifold were determined.

As part of the investigation on the energies of the valence states, iterative natural orbital (INO) calculations were performed on the ground state and low-lying A_2 (A'') valence state to determine if the SCF MO basis was adequate for describing the transition. In general the ground state wavefunction is found to be an adequate MO basis for the description of the states in the electronic spectrum, especially if the complete MO space is active. This approach breaks down when the excited state has a radically different electron density from the ground state, in such circumstances the use of the excited state SCF or MCSCF is required, or alternatively the density of the sate can be iterated in an iterative natural orbital calculation. For Rydberg transitions and most valence transitions the improvement gained by using the state specific wavefunction is usually small.

All the computations, apart from the MP2 calculations, used the GAMESS suite of programs [74] which contain the MRD-CI program of Buenker [71–73]. The MP2 calculations were performed using CADPAC [273]. The calculations

Table 2–5: MRD-CI dimensions for the calculation of propyne without Rydberg functions

Basis	States	Electrons/ Orbitals	Ref./ Roots	No. CSF	Threshold /μH	Diagonaliser Dimension
DZ	gs	16/32	29M1R	436160	1	6723
DZ	^{1}A′	16/32	60M5R	1130099	7	17756
DZ	^{1}A″	16/32	66M5R	1135495	7	17800
DZ	^{3}A′	16/32	53M5R	1710396	10	17368
DZ	^{3}A″	16/32	52M5R	1773371	10	17166
DZP	gs	16/62	19M1R	1715967	4	10561
DZP	^{1}A′	16/62	26M3R	3142952	7	17966
DZP	^{1}A″	16/62	60M5R	6776108	13	16448
DZP	^{3}A′	16/62	34M3R	5689973	7	14896
DZP	^{3}A″	16/62	32M3R	4714588	6	18485
DZP$_l$	gs	16/62	6M1R	1715967	3	13862
DZP$_l$	^{1}A′	16/62	29M3R	3313235	8	18226
DZP$_l$	^{1}A″	16/62	22M3R	2190294	7	19920
DZP$_l$	^{3}A′	16/62	36M3R	6021569	8	15397
DZP$_l$	^{3}A″	16/62	24M3R	3841356	7	19578
TZ	gs	16/57	6M1R	505415	1	14487
TZ	^{1}A′	16/57	46M3R	4263238	9	18023
TZ	^{1}A″	16/57	44M5R	1135495	7	17800
TZ	^{3}A′	16/57	47M3R	7816951	6	17287
TZ	^{3}A″	16/57	44M3R	7434941	6	17939
TZ2P	g.s.	16/74	6M1R	903724	4	15612
TZ2P	^{1}A′	16/74	40M7R	5601322	16	18071
TZ2P	^{1}A″	16/74	29M10R	4122539	19	19207

Table 2–6: MRD-CI dimensions for the calculation of propyne with Rydberg functions

Basis	States	Electrons/ Orbitals	Ref./ Roots	No. CSF	Threshold /μH	Diagonaliser Dimension
DZ+R	g.s.	16/53	6M1R	424687	1	8493
DZ+R	^{1}A′	16/53	63M20R	4400193	21	19792
DZ+R	^{1}A″	16/53	69M20R	4448419	24	18199
DZP$_I$+R	g.s.	16/67	10M1R	1049357	1	13636
DZP$_I$+R	^{1}A′	16/67	63M20R	8023832	15	18618
DZP$_I$+R	^{1}A″	16/67	69M20R	7919519	19	18804
DZP$_I$+R	^{3}A′	16/67	52M20R	$>10^7$	17	19984
DZP$_I$+R	^{3}A″	16/67	55M20R	$>10^7$	17	17411
DZP$_I$+R	g.s.	16/83	6M1R	1176007	2	15601

were performed on the Convex C3840 and C240 machines at ULCC and on the Cray X-MP/48 at RAL.

2.4 Results

2.4.1 Ground state

The present molecular energies and optimised geometries are compared with previous theoretical work in Table 2–7 and Table 2–8 (the experimental data is shown in Table 2–1). The energies and geometries obtained for calculations at the same level are in general in good agreement. The notable exception to this being the difference between the DZ SCF energies as obtained by the Nomura and Iwata [224], and the present author. The reason for this discrepancy is the shorter C-H bond lengths as calculated in the present work, although both geometries are supposedly optimised. The previous calculations with the greatest inclusion of correlation effects are the MP4 calculations of Kellö *et al.* [274] performed at the experimental geometry, and the SDCI+Q work of Honjou *et al.* [275] both using the DZP basis.

Table 2–7: Theoretical propyne ground state energies

Basis	Method	Geometry	Energy /au	Ref.
STO-3G	SCF	optimised	-114.4490	[276]
3-21G	SCF	optimised	-115.225	[179]
4-31G	SCF	optimised	-115.7085	[221]
DZ	SCF	optimised	-115.7341	[224]
DZ	CI (6/6[a] 95CSF)	SCF	-115.7928	[224]
6-31G	SCF	STO-3G	-115.8216	[277]
DZ+D_C	MP2	SCF	-116.2767	[278]
6-31G*	SCF	STO-3G	-115.8634	[277]
6-31G*	SCF	4-31G	-115.8693	[221]
DZP	SCF	MW[b]	-115.8858	[274]
DZP	MP2	MW[b]	-116.2801	[274]
DZP	MP3	MW[b]	-116.3025	[274]
DZP	MP4	MW[b]	-116.3234	[274]
DZP	SCF	optimised	-115.8926	[275]
DZP	SDCI (16/62[a] 48729CSF)	SCF	-116.2695	[275]
DZP	SDCI+Q	SCF	-116.3138	[275]
DZ	SCF	optimised	-115.8347	-
DZ	CI (29M1R 16/32[a])	SCF	-116.1176	-
DZ	MP2	optimised	-116.1359	-
DZ+R(3s2p2d)	SCF	DZ SCF	-115.8352	-
DZ+R(3s2p2d)	CI (6M1R 16/53[a])	DZ SCF	-116.1182	-
DZP	SCF	optimised	-115.8882	-
DZP	CI (19M1R 16/62[a])	SCF	-116.3048	-
DZP	MP2	optimised	-116.3246	-
DZP_I	SCF	optimised	-115.8495	-
DZP_I	CI (19M1R 16/62[a])	SCF	-116.1937	-
DZP_I+R(3s2p2d)	SCF	DZP_I SCF	-115.8499	-
DZP_I+R(3s2p2d)	CI (10M1R 16/67[a])	DZP_I SCF	-116.0995	-
DZP_I+R(3s2p2d)	INO	DZP_I SCF	-116.1020	-
DZP_I+R(3s2p2d)	CI (19M1R 16/83[a])	DZP_I SCF	-116.1834	-
TZ	SCF	optimised	-115.8565	-
TZ	CI (6M1R 16/57[a])	SCF	-116.1708	-
TZ2P	SCF	optimised	-115.9082	-
TZ2P	CI (6M1R 16/74[a])	SCF	-116.3096	-
TZ2P	MP2	optimised	-116.4041	-

[a] active electrons / active orbitals

[b] microwave structure [193]

The previously reported *ab initio* ground state geometries [186, 224, 275, 276, 278, 279] have been obtained at the SCF level. As noted, even relatively low levels of theory can return results that are are in reasonable agreement with the experimental microwave, r_s, structure [193]. The methyl C-H and the carbon-carbon triple bond length are underestimated by all the basis sets at the SCF level, whilst carbon-carbon single bond is overestimated. The effect on the ground state geometry of increasing the basis set size varies depending on the type of basis function which is added. The addition of further valence functions leads to a reduction of most of the bond lengths, a larger effect for the carbon-carbon bonds. For the addition of polarisation functions carbon-carbon triple bond and the acetylenic C-H bond show increases, however the carbon-carbon single bond length is slightly reduced. The continued reduction in the carbon-carbon triple bond length with increasing basis set dimension leads to this bond length being underestimated by $\sim$0.025 Å with respect to the experimental value by the largest basis used in the present study, TZ2P; this is the largest error for this bond of all the listed basis except the smallest , STO-3G. The methyl C-H bond is largely unaffected by the addition of extra functions, whilst the HCC bond angle is slightly reduced by the inclusion of polarisation functions and increased by the transition from DZ to TZ. The inclusion of electron correlation through perturbation theory increases all the bond lengths as calculated using the DZ basis by at least 0.02 Å, the largest increment being 0.04 Å for the triple bond, as would naively be expected due to the inclusion of greater anti-bonding character. This leads to a relatively large error in the computed bond lengths of the carbon skeleton. It has previously been noted that this size of basis is insufficient for the accurate determination of geometrical parameters [3]. For the larger DZP and TZ2P basis smaller increases are obtained, with a slight decrease in the computed value for the carbon-carbon single bond length, this brings the results into better agreement with the experimental values. The smallest increases, and correspondingly the largest decrease, in bond length are obtained for the TZ2P basis. The MP2 optimised geometry for the TZ2P basis is in excellent agreement with experiment for the carbon skeleton and for the acetylenic C-H, agreement is somewhat poorer for the methyl group. The findings at the SCF and MP2 level for the C≡C bond are in accordance with

Table 2–8: Ground state geometries of propyne.

	Bond lengths (Å)				Angles (deg)		
Method	C≡C	C-C	C-H	C-H_{methyl}	HCC	HCH	Ref.
STO-3G SCF	1.170	1.484	1.064	1.088	110.5	-	[276]
DZ SCF	1.201	1.475	1.065	1.093	108.9	109.5	[224]
4-31G SCF	1.191	1.464	1.052	1.083	111.0	-	[221]
SCF	1.191	1.460	1.052	1.082	110.9	-	[279]
DZ+D_C SCF	1.192	1.476	1.059	1.082	-	108.7	[278]
DZP SCF	1.191	1.472	1.060	1.084	110.2	-	[275]
DZP SCF	1.190	1.474	1.059	1.084	-	-	[186]
DZ SCF	1.201	1.472	1.053	1.082	110.6	108.4	-
DZP SCF	1.191	1.475	1.058	1.083	110.4	108.7	-
DZP_I SCF	1.198	1.472	1.058	1.087	110.6	108.4	-
TZ SCF	1.190	1.462	1.051	1.082	110.8	108.1	-
TZ2P SCF	1.181	1.466	1.053	1.081	110.4	108.5	-
DZ MP2	1.245	1.492	1.070	1.102	110.6	108.3	-
DZP MP2	1.226	1.471	1.065	1.090	110.6	108.6	-
TZ2P MP2	1.211	1.461	1.059	1.086	110.6	108.3	-
Exptl	1.206	1.459	1.056	1.105	110.2	108.7[a]	[192, 193]

[a] [191]

those of Simandiras *et al.* for acetylene [280]. Simandiras *et al.* obtained values for the C-H bond length within 0.002 Å of the experimental result for TZ2P at the MP2 level. The experimental results quoted in Table 2–8 are for the substituted structure, r_s, which is known to be somewhat larger than the equilibrium geometry, r_e, an effect particularly pronounced for hydrogen.

The SCF-MO energies are shown in Table 2–9. The energies of the occupied orbitals are maintained throughout all the basis sets. Using Koopmans' theorem the order of ionisation is expected to be $2e < 1e < 7a_1 < 6a_1 \ldots$, with the first four IPs 10.6, 16.2, 16.9, and 19.6 eV using the orbital energies from the TZ2P calculation. The energy of the lowest valence e^* (π^*) state is similarly unaffected by the addition of Rydberg functions, although the expected trend of reducing energy with increasing basis set dimension is shown. It should be noted that for the basis sets of TZ quality this e^* pair is not the lowest of the virtual valence states.

Table 2–9: Propyne ground state SCF MO energies at linear geometry (au)

	Basis						
Orbital	DZ	DZP	DZP_l	TZ	TZ2P	DZ+R	DZP_l+R
$1a_1$	-11.2558	-11.2532	-11.2566	-11.2539	-11.2467	-11.2567	-11.2573
$2a_1$	-11.2520	-11.2450	-11.2498	-11.2449	-11.2287	-11.2527	-11.2511
$3a_1$	-11.2364	-11.2273	-11.2302	-11.2252	-11.2112	-11.2372	-11.2315
$4a_1$	-1.0644	-1.0576	-1.0611	-1.0675	-1.0608	-1.0653	-1.0621
$5a_1$	-0.9681	-0.9603	-0.9653	-0.9715	-0.9637	-0.9690	-0.9662
$6a_1$	-0.7197	-0.7177	-0.7170	-0.7201	-0.7199	-0.7206	-0.7178
$7a_1$	-0.6212	-0.6173	-0.6195	-0.6256	-0.6223	-0.6221	-0.6204
$1e$	-0.5949	-0.5938	-0.5924	-0.5945	-0.5950	-0.5956	-0.5931
$2e$	-0.3890	-0.3874	-0.3866	-0.3902	-0.3895	-0.3899	-0.3874
$a_1(s)$						0.0029	0.0029
$a_1(s)$						0.0136	0.0133
$a_1(p_z)$						0.0181	0.0180
$e(p_x/p_y)$						0.0196	0.0195
$a_1(d_{z^2})$						0.0236	0.0235
$e(d_{xz}/d_{yz})$						0.0239	0.0239
$e(d_{x^2-y^2}/d_{xy})$						0.0246	0.0246
$a_1(s)$						0.0348	0.0341
$a_1(s)$						0.0697	0.0688
$a_1(d_{z^2})$						0.0721	0.0714
$e(d_{xz}/d_{yz})$						0.0758	0.0753
$e(d_{x^2-y^2}/d_{xy})$						0.0764	0.0764
$e(p_x/p_y)$						0.0794	0.0788
$a_1(p_z)$						0.0795	0.0772
$a_1(s)$						0.1463	0.1441
a_1				0.1479	0.1372		
a_1					0.1752		
e	0.2012	0.2034	0.2004	0.1841	0.1827	0.2061	0.2060
a_1	0.2444	0.2431	0.2029	0.1923	0.2061	0.3054	0.2793

The energy lowering of the single configuration SCF wavefunction by configuration interaction for the basis sets without Rydberg functions increase from ~0.28 au for the DZ basis to ~0.40 au for the TZ2P basis, which includes polarisation functions and a wider range of valence functions. In all cases the three lowest occupied MOs, corresponding to the C2s, were frozen, leaving 16 active electrons. In all of the ground state CI calculations the SCF single configuration amounts to about 89 % of the total wavefunction. The other principal configurations consist of the SCF configuration with the $2e$ MO either singly or doubly replaced by the lowest virtual e^* orbital, these however amount to less than 1 % of the wavefunction and play a lesser role for the larger basis sets (less than 0.25 % for TZ2P). The presence of Rydberg functions in the basis set has little effect on the ground state SCF energies and the lowering obtained through the inclusion of correlation, *eg* the present results for the DZ+R basis set. However, a marked reduction in the returned correlation energy is found when the active space is truncated; for example the lowering obtained for the DZP_I+R basis set with 67 active orbitals is ~0.25 au compared to the ~0.35 au for the DZP_I calculation. Increasing the active space to 83 MOs greatly reduces the discrepancy.

A considerable lowering in energy is achieved by the MP2 calculations relative to the single configuration SCF energies, ranging from ~0.3 au for the DZ basis to ~0.5 au for the larger TZ2P basis. That the MP2 energies are lower than the CI energies for the same basis set despite the inclusion of the effects of single, triple, and quadruple excitations in the later, reflects to a large extent the inclusion of the correlation of the core electrons in the MP2 calculations. The lowering due to the optimisation of the geometry is considerably less than this effect, less than 0.05 au for the DZ basis. The weight of the single SCF configuration decreases with increasing basis set dimension from near 89 % for the DZ basis to approximately 86 % for the basis sets including polarisation functions.

The Mulliken charge distribution and dipole moments as obtained at the SCF and MP2 levels are shown in Table 2–10, the numbering system has $HC_{(1)}$ and $H_3C_{(3)}$. The introduction of correlation markedly (10 %) reduces the calculated dipole moments. The good agreement between the DZ SCF dipole moment and

Table 2–10: Theoretical propyne ground state properties

	Basis and Method							
	DZ		DZP		DZP_l	TZ	TZ2P	
properties	SCF	MP2	SCF	MP2	SCF	SCF	SCF	MP2
charge on atoms[a]								
q_H	+0.232	+0.214	+0.154	+0.151	-0.0946	+0.257	+0.151	+0.155
q_{C_1}	-0.411	-0.368	-0.373	-0.355	+0.071	-0.199	-0.098	-0.111
q_{C_2}	+0.142	+0.157	+0.169	0.194	+0.008	-0.165	-0.151	-0.116
q_{C_3}	-0.581	-0.604	-0.381	-0.451	-0.254	-0.457	-0.240	-0.340
$q_{H_{methyl}}$	+0.206	+0.143	+0.154	+0.090	+0.200	+0.185	+0.113	+0.137
dipole moment[b]								
μ_D	0.7834	0.7100	0.7745	0.7286	0.8024	0.8098	0.7903	0.7425

[a] Mulliken charge analysis

[b] Experimental dipole moment 0.781 Debye [183]

experiment is clearly fortuitous, but is useful, since for many molecules DZ may be the highest level of calculation possible.

The harmonic frequencies of propyne and predicted IR intensities, calculated using MP2 on the TZ2P basis at r_e, are listed in Table 2–11. The definitions of the modes and references for the experimental data are given in Table 2–2. The largest error of +6.0 %, 180 cm^{-1}, is for the antisymmetric methyl C-H stretch, ν_6. The low frequency bending modes associated with the C≡C and acetylenic C-H are found to be underestimated with respect to experiment, a feature noted for acetylene by Simandiras *et al.* [280] who found that the C≡C, especially, was calculated low by ~17 % using TZ2P at MP2. Most of the deficiency was corrected by the inclusion of f- functions in the basis set.

Table 2–11: Computed fundamental vibrational frequencies of propyne.

	Theoretical		Experimental		
Mode	Frequency /cm^{-1}	Intensity /km mol^{-1}	Frequency /cm^{-1}	Intensity /km mol^{-1}	Percent[a]
		a_1 modes			
ν_1	3501.6	53.25	3335.1	45.1	105.0
ν_2	3075.1	13.27	2941.4	14.9	104.5
ν_3	2142.2	3.6	2137.9	5.3	100.2
ν_4	1436.5	0.05	1385.0	1.5	103.7
ν_5	935.0	0.66	930.3	1.0	100.5
		e modes			
ν_6	3160.4	9.61	2980.8	17.7	106.0
ν_7	1514.6	16.46	1450.3	17.9	103.7
ν_8	1075.0	0.54	1036.1	0.4	103.8
ν_9	628.1	100.52	633.3	87.3	99.2
ν_{10}	317.5	15.34	327.5	16.7	96.9

a percentage of experimental frequency returned

2.4.2 Excited States

The vertical excitation energies for the valence and Rydberg states are given in Tables 2–12 and 2–13.

Valence States

The ordering of the valence excited states in propyne is found to be identical to that of acetylene, in agreement with the HAM/3 calculation of Fridh [240], with the transitions arising from excitations from the HOMO e pair of MOs to the complementary e^*. The lowest triplet state is calculated to be of symmetric A_1 symmetry with the ^3E state computed to arise ~1 eV higher in energy, whilst the first valence singlet state is of antisymmetric A_2 symmetry. The second singlet state is predicted to lie ~0.3 eV higher in energy. The calculated separation between the optically forbidden $^1A_2 \leftarrow \tilde{X}^1A_1$ and allowed $^1E \leftarrow \tilde{X}^1A_1$ transitions supports the assignment of the feature observed at 6.7eV to the $\tilde{A}^1A_2$ [237, 239]. The second and third singlet-triplet transitions, E and A_2 respectively, are predicted to be

Table 2–12: Propyne valence states vertical excitation energies, eV

	Present work							Fridh[a]
State	DZ	DZ+R	DZP	DZP$_l$	DZP$_l$+R	TZ	TZ2P	HAM/3
$^3\pi\pi^*$								
$^3A_1$	6.0066	-	6.0793	5.8104	5.8405	5.5954	-	6.2
^3E	7.1665	-	7.0206	6.8616	6.8895	6.7136	-	6.7
$^3A_2$	7.8249	-	7.6323	7.5751	7.5886	7.3553	-	7.2
$^3\pi\sigma^*$								
^3E	10.4564	-	-	-	-	8.2354	-	-
$^1\pi\pi^*$								
$^1A_2$	8.0510	8.0247	7.8488	7.6514	7.5771[b]	7.6062	7.6886	7.2
^1E	8.3927	8.1686	8.1764	7.9877	7.8231	7.9896	7.9156	7.7
$^1A_1$	11.6100	-	11.3028	11.1257	-	11.7703	10.5958	10.8
$^1\pi\sigma^*$								
^1E	10.9383	-	-	9.9494	-	8.6552	8.6373	-
^1E	-	-	-	-	-	-	9.6515	-

[a] [240]

[b] INO energy 7.5604 eV.

separated by ~0.7 eV, leading to the prediction that the third transition is to be found at ~6.55 eV near a feature observed at 6.45 eV by Knoop [237, 239].

The calculated energies are high by 0.4-1.4eV compared to the experimental values of the identified singlet and triplet valence states (Table 2–4) the best agreement being obtained for the lowest triplet state. Clearly the addition of diffuse basis functions to the basis set reduces the error, going from DZ to TZ level calculations lowers the computed transition energies by 0.4 eV. The addition of Rydberg functions has little effect on the transition energies. INO calculations were performed on the ground state and the first $^1A_2$ for the DZP$_l$+R basis set. The result was little changed (7.5604 eV) from the direct calculation of the transition energy. The current results for propyne yield excitation energies similar in value to calculations of approximately the same level in acetylene, where several authors have noted a similar failure to reproduce adequately experimental excitation energies [231, 233, 262]. In acetylene much of the discrepancy is due to the

optically forbidden nature of transitions to the linear valence states, that is, theory and experiment are not focusing on exactly the same phenomena. However, large errors, comparable to those in this study are observed for the singlet-triplet transitions which are vertical in nature.

The valence $^1A_1$ state is predicted to occur in the region of 10.6-11.8 eV by the calculations employing basis sets without Rydberg functions, the most accurate being the TZ2P result of 10.60 eV. Given the degree of overestimation found for the other valence states it is probable that this is anywhere between 0.5 and 1 eV high. This state is, however, not obtained in the calculations including Rydberg functions, the estimated energy lying outside the energy range of the roots studied (see discussion of Rydberg states), although the reference configurations allowed the possibility of the root occurring. For the DZ+R/DZP$_l$+R basis no valence-valence transitions other than ee^* were located.

The lowest "$\pi\sigma^*$" ($e \rightarrow a_1$) transition is computed at the DZ level to arise at nearly 10.9 eV, an energy which drops to 8.6 eV for the TZ and TZ2P bases sets. In the latter calculations there is a change in the LUMO at the SCF level, the e^* complement of the HOMO being replaced by an a_1 MO, Table 2–9. The presence of a low-lying $\pi\sigma^*$ in the singlet manifold in the TZ basis has an analogue for the triplet manifold, the state predicted to occur at 8.14 eV. Whether this calculated energy would be returned if Rydberg states were included in the basis set is questionable as the state occurs in a region where a lot of Rydberg transitions are expected. The triplet state arises in the same energy region as Flicker *et al.* [239] reported behavior in their electron impact study which was consistent with an underlying triplet state, whether this state is the one computed would require calculations including a full Rydberg set.

The addition of Rydberg functions has little effect on the calculated energy of the $^1A_2$ state. A slight increase is found for the DZ basis (8.05 eV) and a decrease for the DZP$_l$ basis (7.58 eV). Correspondingly, the state has little Rydberg character. The energies of the symmetric (A') and antisymmetric (A'') components of the ^1E state are found to be significantly lowered by the inclusion of Rydberg functions for both the basis sets used. The energy of the ^1E computed transition

is 8.16 eV for the DZ basis and 7.82 eV for the DZP_I basis, the lowering being slightly larger for the smaller basis set. A large amount of Rydberg character is predicted for this state, predominantly of p_x/p_y type. The oscillator strengths, Table 2–13, are consistent with what is expected with the premise that the A_2 transition is forbidden, the predicted transition probability being low compared to that of the allowed E state. The triplet states are energetically uneffected by the Rydberg functions and the calculated states are almost exclusively valence in nature.

Rydberg States

The computations lead to reasonable values for the quantum defect, δ, when n=3 for the ns, np, and $nd\sigma$ series (Table 2–13). The first members of the $nd\pi$ and $nd\delta$ series have δ values which are calculated to be slightly larger than 3 a common problem when low quantum defects exist. More erratic behavior is obtained for the higher (n=4 and occasionally n=5) Rydberg states. Since there are generally only two Rydberg AOs for each of the p- and d-type functions, this is to be expected. In general to obtain a good value for the excitation to state n it is required that at least a reasonable value be obtained for the state $(n+1)$. The density of the observed Rydberg states is predicted to rapidly increase in the region of 9 eV. An increase in the size of the Rydberg set used would in general lead to a lowering of the excitation energies and produce more states, particularly in this region.

The lowest singlet states of $p\pi$ type are found to be almost even combinations of p_x and p_y, with strong valence mixing for all the singlet states except the $^1A_2$, for the triplet states this is reversed. The wavefunctions for states associated with transitions to Rydberg orbitals with σ local symmetry at the triple bond, *eg* s, p_z, and d_{z^2}, are found to have give linear combinations. The definitions used in the following discussion refer to the leading terms in the CI expansion.

The lowest ns Rydberg state has not been experimentally identified, although it is expected by analogy with the corresponding transition in acetylene, and through arguments based on the quantum defect, to underlie the broad $\tilde{B}$ valence band at

Table 2–13: Propyne vertical excitation energies for valence and Rydberg states (eV)

State		DZ+R(3s2p2d) singlet	DZ+R(3s2p2d) (n-δ)[a]	DZP$_l$+R(3s2p2d) singlet	DZP$_l$+R(3s2p2d) (n-δ)[a]	DZP$_l$+R(3s2p2d) triplet	oscillator strength
Valence							
ee^*	A_1	-		-		5.8405	
	A_2	8.0247		7.5771		7.5886	0.022
	E	8.1686		7.8231		6.8895	0.578
Rydberg							
$e3s$	E	7.5048	2.18	7.3085	2.11	7.0767	0.018
$e4s$	E	9.1852	3.39	9.4130	3.76	8.8341	0.057
$e5s$	E	9.5427	4.05	9.8053	4.91		0.008
$e3p\sigma$	E	8.0457	2.42	8.0533	2.42	7.9936	0.232
$e4p\sigma$	E	9.0953	3.27	9.3749	3.70	-	0.214*
$e3d\sigma$	E	8.8179	2.96	8.6254	2.79	8.8799	0.933
$e4d\sigma$	E	9.5903	4.18	9.5985	4.20	-	0.910
$e3p\pi$	A_1	8.2976	2.56	8.4052	2.63	8.0263	1.090
	A_2	8.5644	2.74	8.3882	2.62	8.4859	0.000
	E	8.6084	2.78	8.5588	2.74	8.6464	0.069
$e4p\pi$	A_1	9.4912	3.93	9.6622	4.40	-	0.796
	A_2	9.6837	4.45	-	-	-	-
	E	9.5917	4.18	9.6662	4.40	-	0.999
$e3d\pi$	A_1	8.9863	3.13	9.2860	3.54	9.1562	0.151
	A_2	9.1451	3.33	9.2407	3.53	8.2088	0.007
	E	8.9829	3.13	8.9762	3.12	8.8799	0.761
$e4d\pi$	A_1	9.9457	5.66	-	-	-	-
	A_2	10.1235	7.43	9.7772	4.79	-	0.052
	E	9.9882	5.97	10.1316	7.55	-	0.085
$e3d\delta$	A_1	9.2360	3.46	9.0826	3.21	9.0485	0.058
	A_2	9.1587	3.35	9.1121	3.29	8.9778	0.003
	E	9.2206	3.44	9.1497	3.34	9.3096	0.029
$e4d\delta$	A_1	9.6989	4.50	10.0338	6.36	-	0.071
	A_2	9.9576	5.74	10.1444	7.76	-	0.009
	E	9.9202	5.50	9.9331	5.58	-	0.057

* only a single component calculated.

[a] (n-δ)^2=13.595/(IP-E); IP=10.37 eV [213]

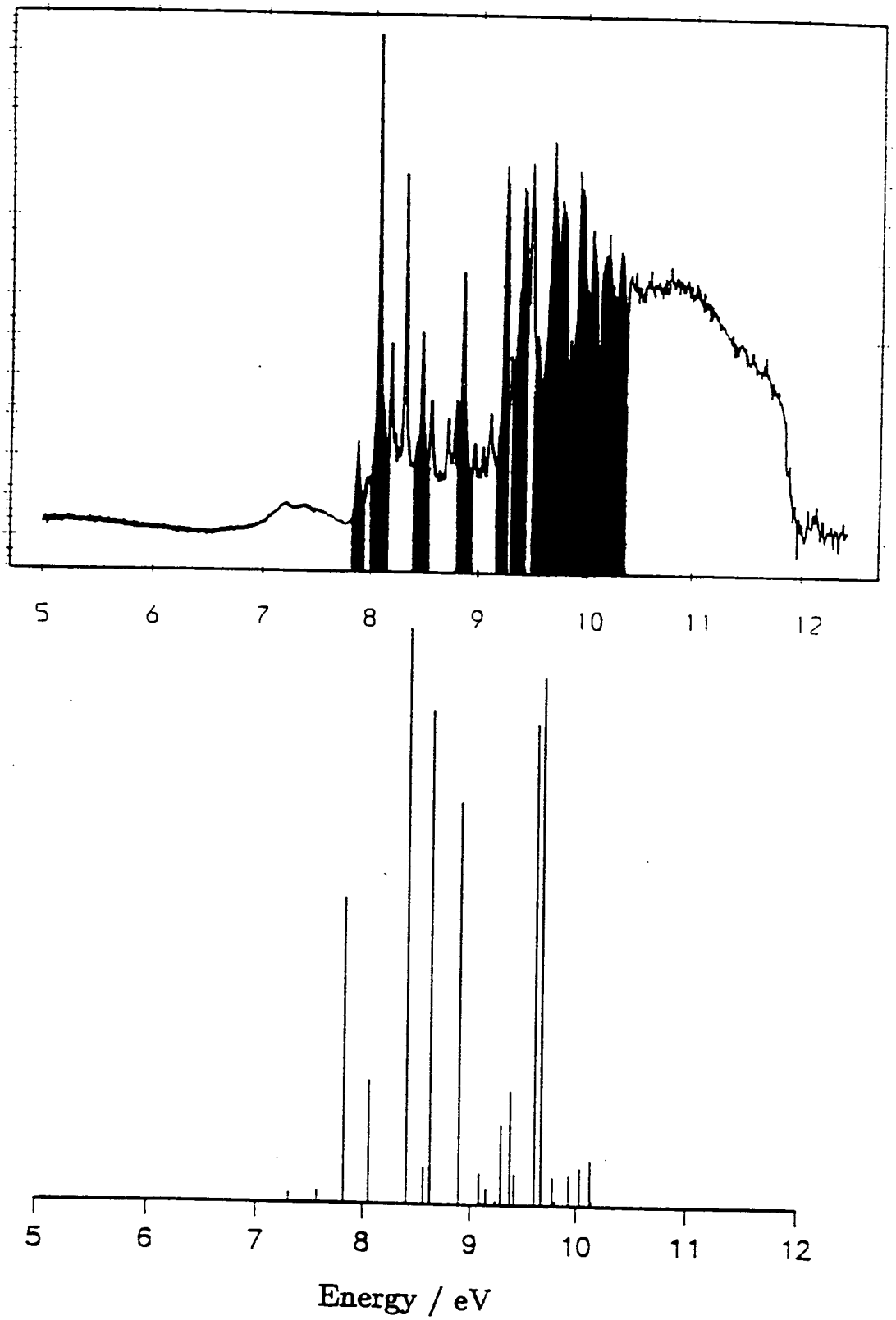

Figure 2–3: The oscillator strengths of propyne.
Experimental (top) and theoretical (bottom) excitation spectra for propyne. The VUV spectrum is identical to Figure 2–2. The theoretical excitation energies are for the DZP_I+R basis and are given in Table 2–13.

approximately 7.1 eV. The present results support this assignment, the $2e3s$ (E) transition placed at 7.50 eV in the DZ+R and 7.31 eV in the DZP$_l$+R computations. The oscillator strength estimated for this state is consistent with the a very weak absorption in the UV spectrum (Figure 2–3). The energies obtained for the corresponding $2e4s$ and $2e5s$ states using the DZP$_l$+R basis, 9.41 eV and 9.81 eV, are somewhat higher than would be expected by comparison with acetylene and the measured energies of the $4R$ and $5R$ features, 8.83 and 9.51 eV respectively, which have been assigned as being the second and third member of the Rydberg s-series. The values from the DZ+R, 9.18 and 9.54 eV, are in better agreement especially for the $e5s$ state. The oscillator strengths (f) calculated for both these excitations are low, 0.057 for $e4s$ and 0.008 for $e5s$, would suggest that these would be weak spectral features, in contrast to the prominent peak observed for the $4R$ transition. An alternative assignment of the R Rydberg series will be given.

The $2e3p_z$, or $2e3p\sigma$ (E), is found to be the first of the $2e3p$ Rydberg types calculated to lie at 8.05 eV. This compares to 7.86 eV for the $\tilde{\text{C}}$ band, the lowest feature assigned to a Rydberg transition, and 8.05 eV for $3R'$. The oscillator strength of 0.232 is consistent with a moderately strong absorption.

The three "π" $2e3p$ (p_x/p_y) states, A_1+A_2+E, are calculated to lie within 0.3 eV, at about 8.4 eV. Experimentally this is a region which contains much structure assigned to vibrational progressions associated with $3R'$ and $3R''$ at 8.45 eV. The ordering of the three states is problematic. The DZ+R basis yields the order $A_1 < A_2 < E$ in contrast the DZP$_l$+R gives $A_2 < A_1 < E$. Of the optically allowed A_1 and E both bases place the A_1 lower in energy, 8.30 and 8.41 eV . The oscillator strength calculations predict that these three states will give rise to a single intense band associated with the A_1 (f=1.09). The E state is predicted to be only a weak absorption and the A_2, as expected for a forbidden transition, has a singularly low oscillator strength.

The first of the $2e3d$ transitions, $2e3d_{z^2}$ (E), arises at 8.63 eV (DZP$_l$) and 8.82 eV(DZ+R). The corresponding oscillator strength is consistent with the presence of a strong UV absorption. The DZ+R energy is close to the $4R$ feature, 8.83 eV, with the DZP$_l$+R energy found to lie between the $4R$ and the $3R''$. Comparison

with acetylene would seem to support the lower assignment, a similar feature being predicted from the turn value at 8.22 eV, Section 2.2.3.

With the assignment of $3R''$ as being due to promotion to $3d_{z^2}$ the assignment of the $2e3p$ Rydbergs to the $\tilde{C}$ band, 7.86 eV, to $2e3p_z$ (E) and $3R'$, 8.05 eV, to $2e3p_\pi$ (E) is made. This is in agreement with the previous assignment of Fridh [240], but contrary to that of Nakayama and Watanabe [235].

The six other states arising form $e^4 \rightarrow e^3d$ transitions, $2e3d\pi$ (d_{xz}/d_{yz}) and $2e3d\delta$ ($d_{xy}/d_{x^2-y^2}$), are predicted to occur at approximately 9.1 eV, within 0.4 eV of each other. The large number of states arising in such a small interval would be expected to lead to a complex spectrum, four of the transitions would be UV allowed, however the transitions to the $2e3d\delta$ states are predicted to be weak features. The ordering of the two UV active $2e3d\pi$ states (the A_2 has a small oscillator strength consistent with the forbidden nature of the transition) is uncertain. The calculation employing the DZ+R basis places the A_1 and E both at 8.98 eV whilst the DZP$_l$+R computes them to be separated by 0.3 eV with the E state at the lower energy, 8.98 eV. The oscillator strengths associated with these transitions, 0.761 for E and 0.151 for A_1, predict that these should be observed as prominent features in the UV spectrum. Given that the ns Rydberg series is expected to produce only weak features it would seem reasonable to re-assign the $4R$ peak, 8.83 eV, to be due to the first member of the $nd\pi$ Rydberg series, probably of E symmetry. Support for this assignment comes form the quantum defects of the experimental $4R$ and $5R$ states which are found to be $\sim$1.03 for transitions to n=4 and 5, or $\sim$0.03 for n=3 and 4.

In comparison with the term values of the $\pi 3d\pi$ Rydberg states of acetylene this assignment does not seem unreasonable, indeed the transitions predicted to occur at $\sim$8.24 eV (Section 2.2.3), some 0.6 eV lower than the transition assigned here. A strong possibility is that this marked difference in the excitation energy of the $d\pi$-series Rydbergs is due to the methyl group perturbing the state in propyne. The computed energies for the $2e3d\delta$ states are, in contrast, in close agreement with the predictions using the term values of the corresponding transitions in acetylene.

2.5 Conclusion

Highly correlated *ab initio* calculations have been performed on the vertical transition spectrum of propyne. Despite the poor energies found for the valence transitions the ordering of the states is found to be identical to that in acetylene. Investigations on the failure to reproduce the transition energies suggest that increasing the dimension of the basis set will provide at least a partial solution, although the composition of the E valence state leads to the conclusion that a full Rydberg set should be included in the calculation if reasonable results are to be obtained.

In the light of the present result the R Rydberg series is re-assigned as being due to a promotion to a $d\pi$ state, probably E for $3R$, and not a s as previously believed. The other assignments of the R' to $np\pi$, R'' to $nd\sigma$, and $\tilde{C}$ to the first member of $np\sigma$ are in agreement with the earlier work of Fridh [240].

Chapter 3

The Electronic Structure of Furan

Furan (C_4H_4O) is a five-membered aromatic ring which forms the basis for a series of heterocyclic compound of importance in biochemistry [281, 282] and synthetic chemistry [283, 284]. Applications extend into a wide variety of areas including synthetic fuel products, pharmaceuticals, dye solvents, insecticides, and coal conversion technology. The accurate description and assignment of the ground and excited states are important in the understanding of the role and behavior of the molecule in chemical environments.

The electronic spectrum of the molecule has been studied many times since the 1930's and the experimental spectrum is well characterised. Despite the large volume of experimental studies a satisfactory theoretical description of the low-lying valence excitations has not been forthcoming. A particular motivation for this work is the availability of a new VUV study, carried out on the Daresbury synchrotron by Dr. I. C. Walker. In this chapter the result of large scale *ab initio* calculations are reported for the furan molecule, results are obtained for the valence states which are in accordance with the experimental spectrum. Reasons for the failure of previous theoretical work are proposed.

3.1 The Background to the Present Work

3.1.1 The Molecular Ground State of Furan

The ground state of the furan molecule is believed to be planar, having C_{2v} symmetry. The principal axis passes through the oxygen and the centre of the opposite C_β-C_β bond. Experimental support for the planar nature of the molecule is found in the small inertial defects detected in the rotational spectrum [285, 286].

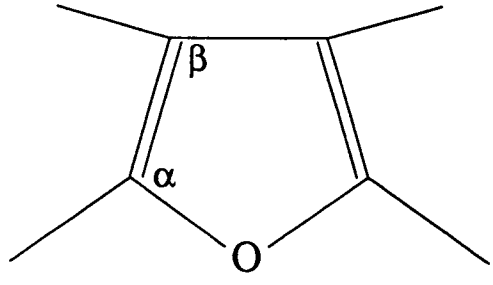

Figure 3–1: The furan molecule

Classifying the MOs according to the symmetry operations of the molecular point group, the out-of-plane, or π, orbitals are b_1 and a_2, and the in-plane, or σ, orbitals are a_1 and b_2. Five π MOs can be generated from the out-of-plane p orbitals of the ring atoms, as in benzene three of these are doubly occupied in the electronic ground state. In the single configuration ground state eighteen of the MOs are doubly occupied, up to $9a_1$, $2b_1$, $6b_2$, $1a_2$.

The ground state geometry, within the assumption of the above molecular symmetry, has been determined in the gas [285–287] and crystalline phases [288]. In the microwave and electron diffraction studies the C-O and C_α-C_β bond lengths are found to be similar, both ~1.36 Å. In contrast, the X-ray diffraction study has the C-O bond longer by more than 0.04 Å [288]. Cordell and Boggs have suggested that the disparity between these experimental results is to be explained as an experimental artifact, probably due to a combination of disorder in the crystal lattice and thermal motion [289]. The C_β-C_β bond is found to be the longest of

the bonds in the penta-atomic ring; this is consistent with the notion that this is largely a single bond. The molecule is only weakly aromatic, six electrons π-electrons delocalised in a planar ring consistent with the Hückel $4n + 2$ rule [289]; it undergoes substitution rather than addition in many reactions [290]. Also the magnetic susceptibility is consistent with a conjugated system [291]. Cordell and Boggs concluded that there was strong delocalisation over the diene portion of the ring, but that the delocalisation did not continue around the C-O-C region [289].

The ionisation energies of a molecule have great consequences for the interpretation of the electronic spectrum, especially regarding the assignment of the Rydberg states. Numerous experimental [213, 219, 292–300] and theoretical [213, 301–308] studies have been performed on the ionisation spectrum of furan. The valence region has been studied using irradiation by He I (58.4 nm, 21.22 eV), He II (30.4 nm, 40.82 eV), and variable wavelength synchrotron from 90 to 200 eV. This has allowed the accurate identification of the major ionisation processes that occur below 35 eV. The core carbon and oxygen $1s$ orbitals have been investigated using XPS [309].

The experimental IPs as obtained by Kimura *et al.* using the He I line [213], Derrick *et al.* using He II [293], and Bawagan *et al.* [300] are listed in Table 3–2. Seven bands are observed in the UV-photoelectron spectrum below 18 eV, the lowest, the $\tilde{X}$ band, is observed at approximately 8.9 eV. The lowest shake-up, or correlation state, is located at 21.9 eV [300]. Historically the most controversial feature of the photoelectron spectrum has been the assignment of the three π MOs, particularly that associated with the inner $1b_1$ MO. Experimentally it is possible to differentiate between σ and πMOs through the comparison of the relative band intensities for different energies of ionising radiation, an alternative method involves the angular dependence of the emission of the ionised electron. Using the former technique the features at 8.9 eV ($\tilde{X}$), 10.4 eV ($\tilde{A}$), and 15.6 eV were assigned as being due to ionisation from π MOs [298, 300]. Through the investigation of the angular dependence of the resulting electron, Sell and Kuppermann arrived at a different assignment for the lowest $^2B_2$ state correlating this to the band at 17.5 eV [296]. However, the angular dependence was found to be not as

Table 3–1: Experimentally determined geometries of ground state furan

	Bond lengths Å					Bond angles (deg)					
Method	OC_α	$C_\alpha C_\beta$	$C_\beta C_\beta$	$C_\alpha H_\alpha$	$C_\beta H_\beta$	$C_\alpha\hat{O}C_\alpha$	$O\hat{C}_\alpha C_\beta$	$C_\alpha\hat{C}_\beta C_\beta$	$O\hat{C}_\alpha H_\alpha$	$C_\alpha\hat{C}_\beta H_\beta$	Ref.
MW	1.362	1.361	1.431	1.075	1.077	106.5	110.7	106.0	115.9	127.9	[285]
MW	1.362	1.361	1.430	1.075	1.077	106.6	110.7	106.7	116.0	127.8	[287]
X-ray	1.368	1.322	1.428	-	-	106.2	110.1	106.8	-	-	[288]
ED	1.364	=r(CO)	1.44	1.09	=r(CH)	105.7	-	-	119	131	[286]
MW+ED+NMR	1.364	1.364	1.430	1.086	1.086	106.7	110.5	106.1	117.3	127.9	[286]

Table 3–2: Valence ionisation of furan ground state (eV)

	Radiation		
Orbital [303]	He I [213]	He II [293]	Synchrotron[a] [300]
$2a_1$	8.87	8.883 (8.883)	9.0
$2b_1$	10.38	10.308 (10.308)	10.4
$9a_1$	12.94	13.0 (12.6)	13.0
$8a_1$	13.84	13.8 (~13.3)	13.6
$6b_2$	14.47	14.4 (~13.9)	14.2
$5b_2$	15.20	15.1 (~14.6)	15.2
$1b_1$	(15.2)	15.6 (~14.7)	15.6
$7a_1$	17.77	17.5 (17.4)	17.5
$6a_1$		19.0 (~18)	18.7
$4b_2$		19.5 (~19)	19.8
$3b_2$		~23 (~21.5)	23.1
$4a_1$		~25 (~23)	24.6
$6a_1$			33.5

() adiabatic ionisation energies

[a]calibrated using $^2A_2$ in He II spectrum of [297].

prominent as that observed for the first two orbitals and therefore the assignment was tentative. The theoretical work on the UV-PES has not yielded a consistent ordering for the ionisations. The most complete theoretical study is the Green's function calculation of von Niessen *et al.* [303], the assignments of which are listed in Table 3-2. Recently the assignment of the $\tilde{B}$ state as $^2A_1$ has been questioned by Seth-Smith *et al.* [299], who observing fluorescence to the molecular ion ground state, $\tilde{X}^2A_2$, but not to the $\tilde{A}^2B_1$ state, in a laser induced fluorescence experiment, and assuming that the excited molecular ion retains C_{2v} symmetry, reassigned the band as $^2B_2$. In addition a new term value for the $\tilde{B}\rightarrow\tilde{X}$ transition was located at 3.06 eV, considerably lower than previously. This has the effect of lowering the adiabatic IP of the $\tilde{B}$ state to 11.94 eV, just 1.64 eV above that of the 2^2B_2 state.

3.1.2 Experimental and Theoretical Studies on the Electronic Spectrum of Furan

The low-lying transitions in the electronic spectrum are expected to be the result of excitations from the highest occupied π MOs, $1a_2(\pi_3)$ and $2b_1(\pi_2)$, into empty valence MOs, also of π symmetry, or neighbouring Rydberg states[1]. Despite the apparent presence of lone pair (non-bonding) electrons on the oxygen no transitions of $n \rightarrow \pi^*$ have been positively identified.

The C_{2v} point group of the ground state molecule means that vertical transitions of A_2 symmetry are dipole and quadrupole forbidden; thus promotion from the a_2 HOMO to upper orbitals of a_1 such as occurs for the ns Rydberg series are expected to be low intensity features in the one photon UV spectrum.

Strong evidence is found experimentally for the presence of three singlet-singlet valence transitions below 8 eV. The lowest energy of these are associated with a broad band in the UV spectrum with maximum intensity at 48800 cm^{-1} (6.05 eV) first identified by Pickett [310] and assigned as $N \rightarrow V_1$ by Robin [244]. Pickett noted the presence of three members of a vibrational series on the low energy side of this feature; which were assigned by Robin as the optically forbidden $\pi_3 \rightarrow 3s$ Rydberg. On the evidence of an analysis of the band using magnetic circular dichroism, Nordén *et al.* [311] suggested the presence of two singlet-singlet valence transition at 48500 cm^{-1} (6.01 eV) and ~50000 cm^{-1} (6.2 eV). Roebber *et al.* studied the UV absorption over the 220-195 nm (5.63-6.36 eV) energy range in cyclohexane solution [312]. Their results supported the conclusion of Nordén *et al.*; the spectrum was found to be red shifted but otherwise identical to the vapour phase, as would be expected for transitions of valence nature [2]. Roebber *et al.* tentatively assigned the vibrational progression of Pickett, beginning at 45960 cm^{-1} (5.7 eV), to the valence $N \rightarrow V_2$ ($\pi \rightarrow \pi^*$) transition. Using multiphoton ionisation

---

[1] Definitions of valence and Rydberg states are given in Appendix A.

[2] Transitions to states Rydberg in nature are strongly attenuated in solution.

(MPI) the $\pi_3 3s$ singlet Rydberg state was located at 5.91 eV [312]. The near UV spectra of several furan derivatives were studied by Nyulászi in the vapour and liquid phases [313]. The findings were consistent with the presence of two valence transitions. The third low-lying valence state was identified by Pickett with a broad absorption region with a maximum located at 62800 cm^{-1} (7.79 eV) [310], a conclusion also reached by Robin [314]. The presence of two low-lying valence transitions is confirmed by the electron energy loss and VUV studies of Dr. I. C. Walker, see Figure 3–2, and a further singlet valence state has been tentatively identified at ~8.7 eV [315].

Two transitions have been reported occuring at excitation energies below the first optically active singlet-singlet band with maxima at ~4.0 and ~5.2 eV in electron impact studies [316–319]. The singlet-triplet nature of the transitions was confirmed by the angle and energy dependence of the observed features. At higher energies two further triplet-singlet transitions have been located and assigned to valence transitions by Dr. I. C. Walker at 6.5 and 8.0 eV [315].

The Rydberg transitions as assigned in furan by Dr. Walker are listed in Table 3–3 based upon VUV/UV, low energy electron impact studies and a review of the current literature. The VUV/UV spectrum of furan is shown in Figure 3–3. These assignments will be used as the basis of the following discussion on the Rydberg states of the molecule.

An extensive review of the Rydberg series of furan in the 6.4 to 9.8 eV range was published by Derrick *et al.* in 1971 [294], drawing upon the reported UV work of Pickett [310], Price and Walsh [320], Pickett, Hoeflich and Liu [321], and Watanabe and Nakayama [322]. Three Rydberg series were resolved converging to the first and second IPs, accounting for all the observed spectroscopic features:

$$E_n = 8.883 - R/(n - 0.55)^2 \tag{3.1}$$

$$E_n = 8.883 - R/(n - 0.04)^2 \tag{3.2}$$

$$E_n = 10.308 - R/(n - 0.82)^2 \tag{3.3}$$

The identification of the appropriate ionisation asymptote was aided by using the similarity of the observed vibrational structure to the corresponding photoionisa-

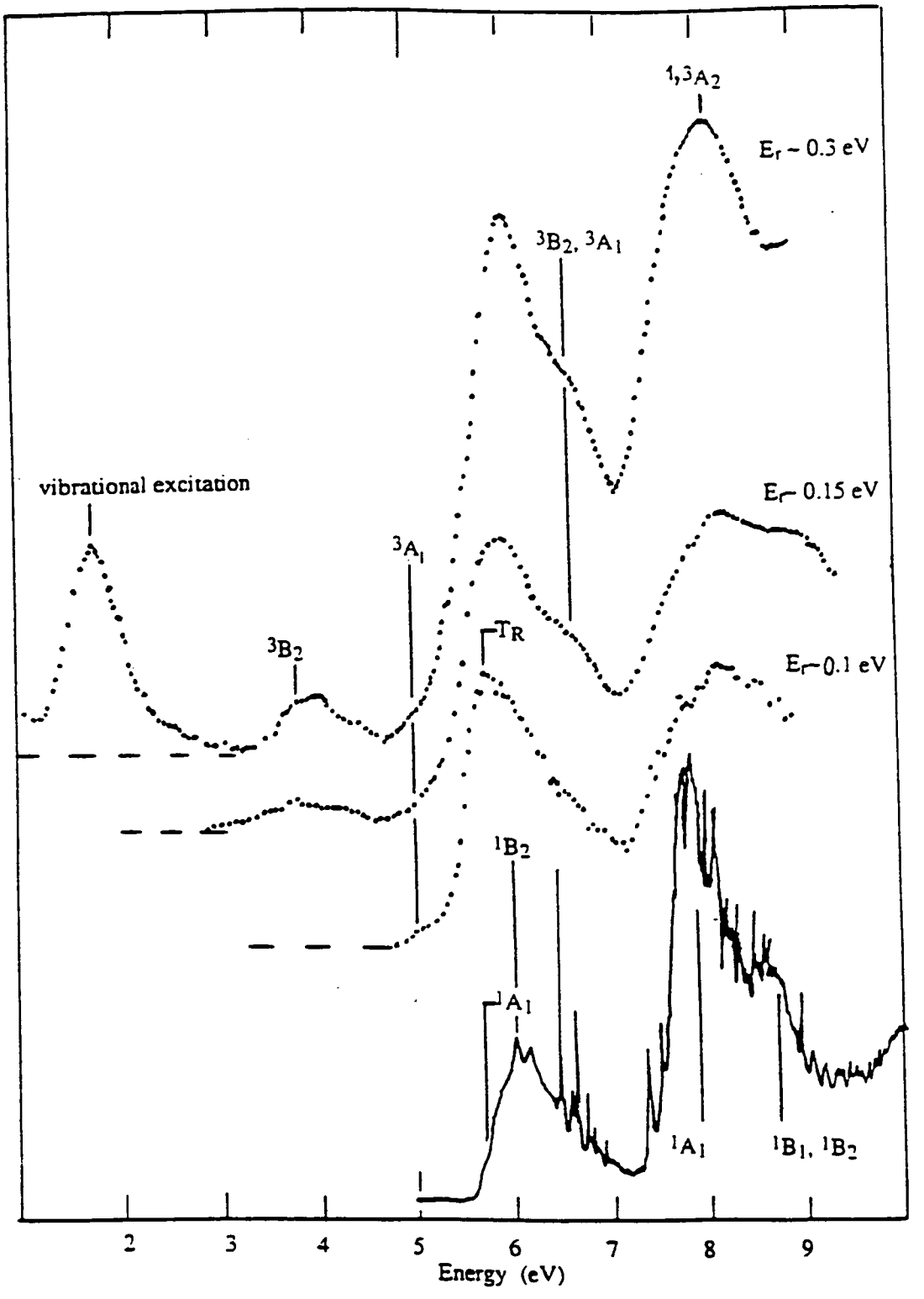

Figure 3–2: The electron energy loss and VUV spectra of the valence states of furan.

... Electron Energy Loss spectra of furan at stated residual electron energies (E_r).

— VUV spectrum.

T_R Rydberg triplet state ($a_2 3s$); all other states are valence $\pi\pi^*$.

Spectrum courtesy of Dr. I. C. Walker, Heriot-Watt University.

Table 3–3: Rydberg series in furan

(a) converging to $1a_2^{-1}$ (IP$_1$=8.883 eV)

n	R(ns)	R(np)		R(nd)		R(nd/f)
3	5.910*(0.87)	6.472 (0.62)	6.752 (0.47)	7.283 (0.00)	7.427* (-0.06)	[7.377] (0.08)
4	7.515 (0.85)	7.706 (0.60)	7.787 (0.48)		8.043 (-0.03)	8.011 (0.05)
5	8.103 (0.82)	8.191 (0.57)	8.226 (0.45)		8.343 (-0.02)	8.321 (0.04)
6	8.377 (0.81)	8.435 (0.49)	8.461 (0.33)			8.499 (0.03)
7	8.528 (0.81)	8.566 (0.45)				8.601 (0.02)
8		8.633 (0.62)				8.671 (0.00)
9		8.702 (0.33)				
10		8.738 (0.32)				

(b) converging to $2b_1^{-1}$ (IP$_2$=10.308 eV)

n	R(ns)	R(np)	R(np/d)	R(d)
3	[7.377] (0.85)	8.101 (0.52)	8.461 (0.29)	8.772 (0.00)
	[7.520] (0.79)			
4	8.964 (0.82)	9.206 (0.49)	9.341 (0.24)	9.461 (0.00)
5	9.534 (0.81)	9.642 (0.48)	9.713 (0.22)	9.761 (0.01)
6	8.964 (0.82)			9.927 (-0.05)
7	8.964 (0.82)			

() are δ values from E=IP-13.595/(n-δ)

[] are uncertain assignments

* one-photon forbidden

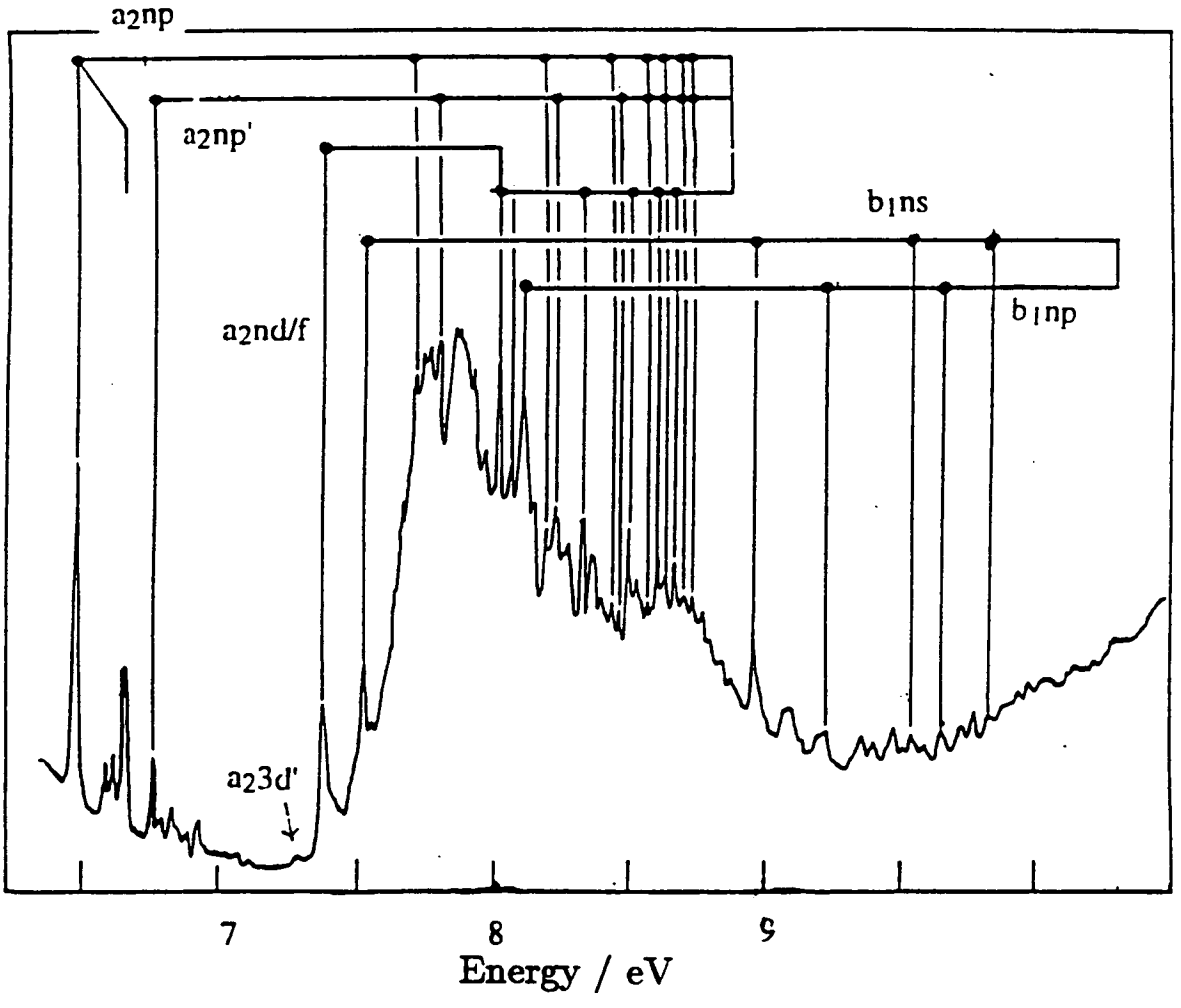

Figure 3–3: The VUV spectrum of furan with the Rydberg series marked. Spectrum courtesy of Dr. I. C. Walker, Heriot-Watt University.

tion peak. Through comparison with the quantum defects found for benzene the Rydberg series were identified as $\pi_3 np$, $\pi_3 nd/f$, and $\pi_2 ns$. The uncertain identification of the second Rydberg series was due to the difficulty the authors found in locating the n=3 member of the series, eventually placed at 7.284 eV by comparison with pyrrole [3]. The first members of the $\pi_3 np$ and $\pi_2 ns$ Rydberg series were located at 6.47 and 7.38 eV. In contrast to the earlier analysis of the spectrum by Watanabe and Nakayama [322], and Herzberg [242] no ns Rydberg series was identified as converging to the first IP, consistent with the a_2 HOMO.

Utilising resonance enhanced multiphoton ionisation Cooper *et al.* [323] studied two and three photon absorption using radiation in the 360-680 nm range, covering 3.65-10.3 eV. The study lead to the identification of four Rydberg series all converging to the first IP, associated with promotion to s, p (previously identified by Derrick *et al.*[294]), d, and f (Derrick *et al.*'s d/f[294]) Rydberg orbitals. The first observed members of the $\pi_3 ns$ (n=4) and $\pi_3 nd$ (n=3) were found at 7.52 and 7.43 eV. Major differences were found between the one- and three-photon spectra at 52230-57325 cm^{-1} (6.47-7.10 eV); in the one-photon spectrum all the transitions in this region could be assigned as vibrational excitations of the $\pi_3 3p$ at 6.47 eV [310], however from the three-photon spectrum another band with vibronic structure was identified at 54509 cm^{-1} (6.77 eV). This band was tentatively assigned as a $\pi \rightarrow \pi^*$ transition. Robin later questioned the assignment to a valence feature suggesting instead that the observed band was due to $\pi_3 3p'$ [314]. Through the study of the term values of the corresponding transitions in furan derivatives and the using the associated reduction in the molecular symmetry to observe promotions optically forbidden in the parent molecule, Nyulászi was able to strongly support the interpretation of Robin [313].

The Rydberg series identified by Dr. Walker as converging to the first IP agree for the most part with those of Derrick *et al.* [294] and Cooper *et al.* [323], including the identification of further series members. The band at 6.77 eV (6.752 eV) is assigned as $\pi_3 3p'$ in accordance with Robin, and Nyulászi [313, 314]. In

---

[3]The absence of an n=3 member of the Rydberg series would be consistent with nf.

addition the band that was suggested as a possible n=3 member of the nd/f series of Derrick *et al.* [294] has been re-assigned as the first member of an $\pi_3 nd$ Rydberg series. Converging to the second IP three further series corresponding to promotion to p and d Rydberg states are listed with first members at 8.101, 8.461, and 8.772 eV. Watanabe and Nakayama [322], and Flicker *et al.* [317] have previously associated peaks at 8.01 and 8.50, and 8.05 and 8.52 eV with these Rydberg series the asymptotes corresponding to the second IP, these transitions can however be identified as members of the Rydberg series converging to the first IP.

Theoretical calculations on the excited states of furan have mostly been restricted to semiempirical work on the valence states [305, 324–328], the Rydberg states being tackled in the *ab initio* works of Thunemann *et al.* [306] and of Nakatsuji et al. [308]. Although these have been of great assistance in the assignment of the experimentally observed Rydberg excitations, the results are found to be contradictory for the valence states, the *ab initio* results especially failing to produce results consistent with experiment.

The majority of the cited semiempirical computations place the $^1B_2$ valence state below the $^1A_1$ by less than 0.5 eV, although with the inclusion of double excitations in the calculation, the order is reversed [327, 328]. Satisfactory results for the triplet excitation levels have not been generally accessible by the application of semiempirical techniques [325, 328]. Mirsha and Jug [326] used the semiempirical SINDO1 with limited configuration interaction to compute the non-vertical transition energies. The lowest singlet and triplet valences state were found to be B_2 symmetry [4]. The $^1A_1$ state was computed to be only the fourth of the singlet valence states, and assigned to the experimental feature at ~7.8 eV; a $^1B_1$ and the second $^1B_2$ states were placed at lower excitation energies. Mirsha and Jug found that there was a large change in the character associated with the transition to

[4]The authors quote the results in terms of the symmetry of the corresponding planar, C_{2v} state.

the lowest excited valence state, the single and double bonds being reversed with respect to those of the ground state [326].

Thunemann *et al.* employed multireference CI to investigate the valence and Rydberg transitions from the π_3 and π_2 MOs [306]. By using, where possible, the MOs from the corresponding SCF, both the static and dynamic correlation of the state could be well described using a limited number of reference configurations. The $^1A_1$ state was found to occur at 7.08-6.79 eV, depending on the MO set used in the calculation (the open shell SCF for this state could not be converged), whilst the $^1B_2$ state was calculated at 7.58 eV. No other valence singlet-singlet transitions were found occur below 8 eV. Correspondingly the experimental $N \rightarrow V_1$ transition at 6.05 eV was assigned as being a single transition of $^1A_1$. The $N \rightarrow V_3$ at 7.75 eV was assigned as $^1B_2$. Thunemann *et al.* found that the valence states were not admixtures of valence and Rydberg character; however, as the Rydberg set employed in their calculations only included one of the *d* functions (a_2) such an interaction between the valence and Rydberg functions could not be completely ruled out. Excellent agreement was found between the calculated Rydberg states and the experimental assignments of Derrick *et al.* [294], the $\pi_3 3p$, $\pi_3 3d$, and $\pi_2 3s$ having estimated vertical excitation energies of 6.52, 7.46, and 7.27 eV. Two further Rydberg series, the $\pi_2 np$ and $\pi_2 nd$ were predicted to have first members in the region of 7.85 and 8.50 eV. The low-lying triplet valence states were also computed, the energies being in good agreement with the experimental results. The lowest state was assigned as $^3B_2$ due to promotion from the a_2 (π_3) HOMO, calculated at 4.08 eV, whilst the experimental feature at 5.22 eV was assigned as $^3A_1$, calculated at 5.44 eV, a combination of excitations from π_2 and π_3.

Nakatsuji *et al.* [308], utilising the Symmetry Adapted Cluster-CI (SAC-CI) method, also found that the singlet valence $\pi \rightarrow \pi^*$ excitation of $^1A_1$ symmetry was lower than the $^1B_2$, 7.32 and 7.50 eV respectively, and assigned the experimental spectrum in accordance with Thunemann *et al.* [306]. The ordering of the computed Rydberg states (an identical Rydberg set was used), was found largely to be the same as that obtained by Thunemann *et al.* [306]. Triplet state calculations were performed for the full set of Rydberg and valence transitions, the results

confirming the assignments made by Thunemann *et al.* for the valence states. A small singlet triplet splitting was computed for the Rydberg states.

Through comparison with earlier work on butadiene, Thunemann *et al.* suggested that the remaining difference between the experimental and theoretical data was not due to the frozen core nor to an inadequate basis set being employed, but due to the non-vertical nature of the transition [306], as also proposed by Mirsha and Jug [326]. Nakatsuji *et al.*, whilst agreeing with the possibility of a non-vertical transition, reasoned that the problem could be that the basis set employed by themselves and Thunemann *et al.* could not well describe the reorganisation of the electron cloud along the z-axis along which the transition moment of the $^1A_1$ was found to lie [308]. The molecular dipole moment obtained, also aligned along the z-axis was found to be poorly reproduced. The addition of a single d-function to the oxygen atom was found to reduce the excitation energy, in a π only calculation by 0.1 eV, however it should be noted that the HOMO π_3 has a node at the oxygen atom and that this would not be expected to significantly lower the excitation energy.

An obvious defect in the previous *ab initio* computations performed on the Rydberg state of furan, is the selective choice of only one of the d-type Rydberg functions, the a_2, which, due to its symmetry, would not normally be expected to mix with the valence or Rydberg functions which are of different symmetry. In the current work the full set of d-type Rydberg functions is retained.

3.2 The Present Work

3.2.1 Method

The present calculations were performed under the assumption of a C_{2v} furan molecule, the alignment being such that the principle axis of symmetry is the z-axis. All the calculations were performed using the GAMESS suite of programs

Table 3–4: MRD-CI dimensions for the calculation on furan

Basis	States	Electrons/ Orbitals	Ref./ Roots	No. CSF	Threshold /μH	Diagonaliser Dimension
DZ+R	gs	26/69	11M1R	1606006	8	10377
DZ+R	$^1A_1$	26/69	48M9R	9165195	30	12770
DZ+R	$^1B_1$	26/69	37M14R	6022556	35	14163
DZ+R	$^1B_2$	26/69	53M8R	$>10^7$	30	12644
DZ+R	$^1A_2$	26/69	34M14R	6643066	35	14748
DZP$_l$	gs	26/75	8M1R	1085873	10	11297
DZP$_l$	$^1A_1$	26/75	69M4R	$>10^7$	11	12583
DZP$_l$	$^1B_1$	26/75	62M5R	$>10^7$	19	14471
DZP$_l$	$^1B_2$	26/75	58M4R	$>10^7$	17	14850
DZP$_l$	$^1A_2$	26/75	64M5R	$>10^7$	18	14371
DZP$_l$	$^3A_1$	26/75	36M3R	$>10^7$	9	13971
DZP$_l$	$^3B_2$	26/75	52M4R	$>10^7$	16	16373
DZP$_l$+R	gs	26/84	11M1R	2383524	7	11570
DZP$_l$+R	$^1A_1$	26/84	63M9R	$>10^7$	18	13542
DZP$_l$+R	$^1B_1$	26/84	47M13R	$>10^7$	20	14148
DZP$_l$+R	$^1B_2$	26/84	59M8R	$>10^7$	18	13342
DZP$_l$+R	$^1A_2$	26/84	52M13R	$>10^7$	22	13534
DZP$_h$+R	gs	26/84	11M1R	2383524	7	11530

[74, 75]. The post-Hartree-Fock treatments used the MRD-CI package of Buenker [71–73] to include correlation effects and obtain excitation energies.

The initial basis set employed in this study was a double zeta basis (DZ) of Gaussian type orbitals (GTOs), using the GTOs of Huzinaga [266] contracted according to the Dunning procedure (9s5p/5s)/[4s2p/2s] [267]. For the description of the Rydberg states the DZ basis was augmented by $3s2p2d$ functions placed at the molecular centre of mass, with exponents 0.021, 0.008, 0.0025(s), 0.017, 0.009(p), 0.015, and 0.008(d), to yield a total of 79 GTOs. In order to improve the description of the singlet-singlet valence transitions, which according to Nakatsuji *et al.* [308] are poorly defined by the DZ+R basis, two basis sets of DZ plus polarisation (DZP) quality were investigated, with exponents of 0.85 (O), 0.75 (C), and 1.00 (H) and a diffuse set of 0.30 (O), 0.20 (C), and 0.25 (H), a total of

121 GTOs [5]. The higher exponent set are those typically used for the description of the ground state, geometry and properties, and are considered near optimal for this purpose. It has previously been noted that such a tight set of polarisation functions may not necessarily be the best for describing excitation processes, and hence the use of the more diffuse set. No attempt was made to optimise these functions. For the calculation of the excited states the DZP basis sets were also augmented by the $3s2p2d$ Rydberg functions. In order to test the effectiveness of the two DZP basis sets, calculations were performed upon the $^1A_1$ excited states. It was found that the DZP$_h$+R basis offered little improvement upon the energies obtained using the DZ+R basis, therefore this basis set was reluctantly abandoned and only passing mention of the results obtained for the $^1A_1$ excited states will be made. The DZP$_l$+R basis set, as for propyne (see also Section 2.4), showed immediate signs of selective lowering of the valence states, therefore this work was continued for the other symmetries. An extended set of singlet and triplet valence states was calculated using the DZP$_l$ basis set (100 GTOs). The equilibrium structure (r_e) was obtained at the SCF level for the DZ, DZP$_l$, and DZP$_h$ basis sets, and the calculations for the excited states using the DZ+R, DZP$_l$+R, and DZP$_h$+R bases used the appropriate non-Rydberg augmented basis set r_e values.

After a single configuration SCF study, all valence electron ground state CI calculations were performed for the DZ+R, DZP+R, and DZP$_l$ MOs. The five core MOs due to the carbon and oxygen $1s$ orbitals were frozen; after excluding the core complements and some of the higher virtual orbitals, but retaining all the π MOs for the DZP+R bases, this led to a total of 26 active electrons in 69, 84, and 75 MOs respectively. In the corresponding open shell singlet and triplet states, up to 69 main reference configurations were used to generate up to 14 roots of each symmetry, 69M14R in MRD-CI terminology [71–73]. The dimensions of the computations along with the thresholds employed are given in Table 3–4.

---

[5]These basis sets will be referred to as DZP$_h$ for the normal exponent polarisation functions and DZP$_l$ for the low exponent polarisation functions to avoid ambiguity.

3.2.2 The ground state

The ground state equilibrium structures as obtained theoretically are listed in Table 3–5. These should be compared to the experimental geometries in Table 3–1. The present results follow the trend noted by Cordell and Boggs [329], whereby the smaller basis set, in this case DZ, yields bond lengths for O-C_α and C_α-C_β which differ by a significant amount (in this case ~0.02 Å), in contrast to experiment where these bond lengths are found to be almost identical [285, 286], an error which is reduced with increasing basis set dimension. The current DZP_h calculation correctly reproduces this experimental finding, however the computed bond lengths are approximately 0.02 Å shorter than experiment. In agreement with the experimental structure [285, 286], all the theoretical results predict that the C_β-C_β (formally single) bond is the longest of those in the penta-atomic ring, although at the SCF level this bond length is somewhat overestimated. Simandiras *et al.* demonstrated, using MP2, that these errors for the ring bond lengths are primarily due to the lack of correlation effects at the SCF level [280]. The C-H bond lengths are underestimated by all the studies listed, the best results being obtained by the MP2 calculation of Simandiras *et al.* [280] and (perversely) the smallest basis set study (STO-3G) [330]. This is not entirely unexpected as these bonds incorporate light atoms and are particularly prone to experimental errors introduced by the assumption of no variation of bond length with isotopic substitution [286]. The bond angles are in general in reasonable agreement with experiment, although again large errors are found for the experimental determination of bond angles including light atoms. The structure obtained for the DZP_l basis set is similar to that of the DZ basis, and clearly inferior to the DZP_h r_e structure. As the main purpose of using the DZP_l basis was to investigate excitation energies this failure to describe the ground state geometry was not considered a problem.

The ground state SCF valence MO energies are listed in Table 3–6. The energies of the occupied orbitals are largely unaffected by the addition of the Rydberg functions. Using Koopmans' theorem, the ionisation potentials of the $1a_2$ (π_3), and $2b_1$ (π_3) MOs are 8.83 and 10.78 eV, as calculated for the DZP_h+R basis set, in reasonable agreement with the experimental values of 8.883 and 10.308 ev [293].

Table 3–5: Theoretically determined geometries of ground state furan

Method	Bond lengths Å					Bond angles (deg)					Ref.
	OC_α	$C_\alpha C_\beta$	$C_\beta C_\beta$	$C_\alpha H_\alpha$	$C_\beta H_\beta$	$C_\alpha\hat{O}C_\alpha$	$O\hat{C}_\alpha C_\beta$	$C_\alpha\hat{C}_\beta C_\beta$	$O\hat{C}_\alpha H_\alpha$	$C_\alpha\hat{C}_\beta H_\beta$	
CNDO	1.364	1.351	1.429	1.114	1.110	103.6	112.8	105.4	114.5	126.2	[331]
STO-3G SCF	1.376	1.340	1.445	1.082	1.077	105.4	111.2	106.1	116.5	127.2	[330]
3-21G SCF	1.380	1.340	1.450	1.065	1.062	107.0	109.8	139.5	123.5	133.7	[332]
4-21G SCF	1.386	1.338	1.451	1.063	1.064	106.8	109.7	106.8	116.1	127.0	[329]
4-21G+P_O SCF	1.365	1.339	1.445	1.065	1.065	106.3	110.8	106.0	116.3	126.9	[329]
4-21G+P_{OC} SCF	1.352	1.335	1.443	1.070	1.072	106.4	111.1	105.7	116.1	126.8	[329]
DZ SCF	1.375	1.353	1.451	1.063	1.065	107.6	109.7	106.5	116.7	126.6	-
DZP_l SCF	1.371	1.346	1.453	1.069	1.071	106.9	110.4	106.2	116.3	127.1	-
DZP_h SCF	1.345	1.345	1.444	1.069	1.070	107.2	110.9	105.5	116.5	126.6	-
DZP_h MP2	1.364	1.374	1.433	1.078	1.079	106.9	110.5	106.0	115.7	127.9	[280]

Table 3–6: Energies of valence SCF MOs (au)

	Basis set					
MO	DZ	DZP_l	DZP_h	DZ+R	DZP_l+R	DZP_h+R
$1a_1$	-20.6171	-20.6173	-20.6192	-20.6181	-20.6194	-20.6206
$1b_2$	-11.3061	-11.2993	-11.2916	-11.3068	-11.3010	-11.2925
$2a_1$	-11.3061	-11.2993	-11.2916	-11.3067	-11.3009	-11.2925
$3a_1$	-11.2504	-11.2415	-11.2358	-11.2511	-11.2431	-11.2366
$2b_2$	-11.2496	-11.2406	-11.2349	-11.2503	-11.2422	-11.2357
$4a_2$	-1.4675	-1.4565	-1.4714	-1.4683	-1.4582	-1.4727
$5a_1$	-1.0968	-1.0881	-1.0860	-1.0977	-1.0897	-1.0871
$3b_2$	-1.0229	-1.0124	-1.0134	-1.0236	-1.0139	-1.0144
$4b_2$	-0.8120	-0.8069	-0.8144	-0.8127	-0.8084	-0.8155
$6a_1$	-0.7897	-0.7815	-0.7794	-0.7904	-0.7829	-0.7804
$7a_1$	-0.7485	-0.7415	-0.7459	-0.7491	-0.7430	-0.7467
$1b_1$ (π_1)	-0.6324	-0.6276	-0.6399	-0.6331	-0.6291	-6409
$5b_2$	-0.6158	-0.6062	-0.6147	-0.6165	-0.6076	-0.6156
$6b_2$	-0.5927	-0.5847	-0.5804	-0.5933	-0.5861	-0.5813
$8a_1$	-0.5660	-0.5588	-0.5662	-0.5666	-0.5603	-0.5671
$9a_1$	-0.5401	-0.5378	-0.5371	-0.5408	-0.5393	-0.5381
$2b_1$ (π_2)	-0.4028	-0.3962	-0.3953	-0.4035	-0.3976	-0.3963
$1a_2$ (π_3)	-0.3358	-0.3271	-0.3237	-0.3363	-0.3283	-0.3245
b_1 (π_4^*)	0.1380	0.1479	0.1536	0.1444	0.1533	-0.1600
a_2 (π_5^*)	0.2091	0.2157	0.2166	0.2084	0.2144	-0.2158

Inspection of the atomic orbital contributions to the highest two MOs demonstrates that the $1a_2(\pi_3)$ orbital is based upon the diene portion of the molecule; the C_{2v} symmetry of the molecule causes there to be a node at the oxygen. In contrast, $2b_1(\pi_2)$ is delocalised; around the whole ring, with especially large components on the oxygen and β-carbons. The oxygen "lone pair" electrons are also delocalised, the π lone pair mixes with the p functions on the neighbouring α-carbons (the $1b_1$ MO), whereas the σ lone pair contributes strongly to $8a_1$ and $9a_1$, to such an extent that it cannot really be called a lone pair as noted by Thunemann *et al.* [306]. Furthermore, $8a_1$ and $9a_1$ are very close in energy for two MOs of the same symmetry. For the SCF without Rydberg functions, the π_5^* (a_2), and π_4^* (b_1) MOs are found to be similar to the π_3 and π_2 MOs, with an increase in the number of nodes in the ring, from two to four going from π_3 to π_5^* and two to three for π_2 to π_4^*. The composition of the π_5^* (a_2) MO like the occupied MOs, is not effected by the switch to basis sets including Rydberg functions; the π_4^* (b_1) MO on the other hand becomes an admixture of valence and Rydberg character, with particularly large components of p_x and d_{xz}. The Rydberg functions are found to yield linear combinations with respect to the C_2 axis, typical examples being $(s+p_z+d_{z^2})$, (p_y+d_{yz}), and (p_x+d_{xz}); particularly, this was found for the tighter p_y/d_{yz} Rydberg states. This suggests that the inclusion of Rydberg functions in the basis set may be necessary if an adequate description of excitations is to be obtained, particularly in the case of of promotions to the π_4^* MO. In the discussion which follows the assignments will be based upon the major components in the configurations.

The ground state energies as obtained in this, and for comparison, in previous theoretical studies are tabulated (by basis set) in Table 3–7; further information regarding the MRD-CI calculations are given in Appendix C. The lowering in energy associated with moving from the experimental structure to the optimised structure for a particular basis set is amply demonstrated by the present DZ basis results and those of Niessen *et al.* [303], and Hehenberger [304]. The addition of Rydberg functions, as expected, has negligible effect (<0.002 au) on the ground state energies at the SCF level. In all of the ground state CI calculations the

Table 3–7: Theoretical ground state energies of furan (au)

Method	Basis	Geometry	Energy	Ref.
SCF	STO-3G	optimised	-225.7513	[330]
SCF	3-21G	optimised	-227.3501	[332]
SCF	4-21G	optimised	-228.1210	[329]
SCF	4-21G+P_O	optimised	-228.1587	[329]
SCF	4-21G+P_{OC}	optimised	-228.2314	[329]
SCF	DZ	MW	-228.4869	[303]
SCF	DZ	MW	-228.5556	[304]
SCF	DZ	optimised	-228.5564	-
SCF	DZ+P_H	MW	-228.5738	[302]
SCF	DZP$_l$	optimised	-228.5968	-
CI (8M1R[a] 75/26[b])	DZP$_l$	SCF	-229.0869	-
SCF	DZP$_h$	MW	-228.5937	[333]
SCF	DZP$_h$	optimised	-228.6739	-
SCF	DZ+R(2s2p1da_2)	MW	-228.5572	[308]
SAC	DZ+R(2s2p1da_2)	MW	-228.8106	[308]
SCF	DZ+R(3s2p2d)	DZ	-228.5583	-
CI (11M1R[a] 69/26[b])	DZ+R(3s2p2d)	DZ	-229.0232	-
SCF	DZ+B(s)+R(2s2p1da_2)	MW	-228.6005	[306]
CI (54/16[b])	DZ+B(s)+R(2s2p1da_2)	MW	-228.8382	[306]
SCF	DZ[c]+B(s)+R(2s2p)	MW	-228.6011	[334]
SCF	DZP$_l$+R(3s2p2d)	DZP$_l$	-228.5982	-
SCF	DZP$_h$+R(3s2p2d)	DZP$_h$	-228.6747	-
CI (11M1R[a] 84/26[b])	DZP$_l$+R(3s2p2d)	DZP$_l$	-228.9818	-
CI (11M1R[a] 84/26[b])	DZP$_h$+R(3s2p2d)	DZP$_h$	-228.9755	-

[a] main reference and roots

[b] active molecular orbital/electrons

[c] DZ set on O decontracted to give triple zeta valence

SCF, single configuration amounts to about 88 % of the total wavefunction, see Appendix C for further details, the other contributions were found to be less than 1 %. The doubly excited configurations with the largest contribution consists of the SCF configuration, with π_2/π_3 replaced by either π_4^* or π_5^*. The energy lowering compared to the single configuration SCF wavefunction by CI shows ~0.47 au for the DZ+R basis set with 69 active orbitals and 26 electrons, and ~0.48 au for the DZP_l basis set with 26 electron in 75 MOs. Substantially less of the correlation energy is returned when the number of virtual orbitals excluded from the active MO set is increased, ~0.3 au and ~0.39 au for the DZP_h+R and DZP_l+R bases, respectively. This reduction in correlation energy associated with the truncation of the active MO set leads to the DZP_l ground state being computed 0.1 au lower than the DZP_l+R CI ground state. Surprisingly the DZP_l+R CI set yields a lower ground state energy than the DZP_h+R CI despite the SCF energies being separated by 0.08 au in favour of the DZP_h+R basis.

3.2.3 Excited states

The results of the present calculations for the singlet excited valence states of furan are given in Tables 3–8, 3–9, and 3–10 for the DZ+R, $DZP_l + R$, and DZP_l basis sets, respectively. For comparison with previous theoretical and experimental work they are again listed in Table 3–11. Further details of the MRD-CI results are given in Tables C–2 to C–9 in Appendix C.

Valence excitations

The lowest $^1A_1$ valence state is the antisymmetric linear combination of the $\pi_2(b_1) \rightarrow \pi_4(b_1)$ and $\pi_3(a_2) \rightarrow \pi_5(a_2)$ transitions. The second $^1A_1$ valence state is the symmetric linear combination of these, and also includes mixing from the doubly excited configuration $\pi_3^2(a_1) \rightarrow \pi_4^2(b_1)$.

The computed excitation energies of the first two valence states in the DZ+R basis set, 6.80 and 7.55 eV, are very close to those obtained by Thunemann *et*

Table 3–8: Transition energies computed with the DZ+R(3s2p2d) basis set

Symmetry	Type	Energy[a]	(n-δ)[b]	Symmetry	Type	Energy[a]	(n-δ)[b]
$^1A_1$	$\pi\pi^*$	6.7952	-	$^1B_2$	$\pi\pi^*$	7.5501	-
	$\pi\pi^*$	9.2824	-		$\pi\pi^*$	9.9973	-
	$\pi_3 d_{xy}$	7.6383	3.30		$\pi_3 p_x$	6.3955	2.34
	$\pi_2 p_x$	8.1151	2.49		$\pi_3 d_{xz}$	6.7609	2.53
	$\pi_2 d_{xz}$	8.3059	2.61		$\pi_3 p_x$	7.8462	3.62
	$\pi_3 d_{xy}$	8.3411	5.01		$\pi_3 d_{xz}$	8.7801	-
	$\pi_2 p_x$	9.1228	3.39		$\pi_2 d_{xy}$	8.8246	3.03
	$\pi_2 d_{xz}$	10.5371	-		$\pi_2 d_{xy}$	9.7498	4.94
$^1A_2$	$\pi_3 s$	5.9606	2.17	$^1B_1$	$\pi_3 p_y$	6.7553	2.53
	$\pi_3 p_z$	6.7750	2.54		$\pi_3 d_{yz}$	7.2132	2.85
	$\pi_3 d_{x^2-y^2}$	6.8305	2.57		$\pi_3 p_y$	7.3536	2.98
	$\pi_3 d_{z^2}$	7.3560	2.98		$\pi_2 s$	7.5102	2.20
	$\pi_3 s$	7.4416	3.07		$\pi_2 p_z$	8.0599	2.46
	$\pi_3 p_z$	7.7336	3.44		$\pi_2 d_{x^2-y^2}$	8.5832	2.81
	$\pi_2 p_y$	7.9911	2.42		$\pi_2 d_{z^2}$	8.6745	2.88
	$\pi_3 s$	8.1664	4.36		$\pi_2 s$	8.7696	2.97
	$\pi_2 d_{yz}$	8.7360	2.94		$\pi_3 d_{yz}$	8.7809	-
	$\pi_3 d_{x^2-y^2}$	8.8484	-		$\pi_2 p_z$	9.3913	3.85
	$\pi_2 d_{yz}$	8.8611	3.07		$\pi_2 s$	9.5608	4.27
	$\pi_3 d_{z^2}$	9.5951	-		$\pi_2 d_{z^2}$	9.9660	6.30
	$\pi_2 p_y$	9.6157	4.43		$\pi_2 d_{x^2-y^2}$	10.7105	-
	$\pi_3 s$	10.4227	-		$\pi_2 s$	11.7054	-

[a] energies in eV.

[b] $(n-\delta)^2 = 13.595/(IP-E)$; IP_1=8.883 eV, IP_2=10.308 eV from [293].

Table 3–9: Transition energies computed with the DZP$_l$+R(3s2p2d) basis set

Symmetry	Type	Energy[a]	(n-δ)[b]	Symmetry	Type	Energy[a]	(n-δ)[b]
$^1A_1$	$\pi\pi^*$	6.6322	-	$^1B_2$	$\pi\pi^*$	6.8788	-
	$\pi\pi^*$	9.3597	-		$\pi\pi^*$	9.4773	-
	π^{*2}	9.8396	-				
	$\pi_3 d_{xy}$	7.7503	3.46		$\pi_3 p_x$	6.6589	2.47
	$\pi_2 p_x$	8.1481	2.51		$\pi_3 d_{xz}$	7.7115	3.41
	$\pi_2 d_{xz}$	8.3269	2.62		$\pi_3 p_x$	7.8244	3.58
	$\pi_3 d_{xy}$	8.5806	6.82		$\pi_3 d_{xz}$	8.8911	-
	$\pi_2 p_x$	9.3196	3.71		$\pi_2 d_{xy}$	8.9357	3.15
	$\pi_2 d_{xz}$	9.9160	5.89		$\pi_2 d_{xy}$	9.7713	5.03
$^1A_2$	$\pi_3 s$	5.9500	2.15	$^1B_1$	$\pi_3 p_y$	6.6386	2.46
	$\pi_3 p_z$	6.4096	2.37		$\pi_3 p_y$	6.6517	2.47
	$\pi_3 d_{x^2-y^2}$	7.1478	2.84		$\pi_3 d_{yz}$	6.9884	2.68
	$\pi_3 d_{z^2}$	7.4047	3.03		$\pi_2 s$	7.1430	2.07
	$\pi_3 d_{z^2}$	7.5628	3.21		$\pi_2 p_z$	8.0398	2.45
	$\pi_3 s$	7.5944	3.25		$\pi_3 d_{yz}$	8.0645	4.08
	$\pi_3 d_{x^2-y^2}$	7.8292	3.59		$\pi_2 d_{x^2-y^2}$	8.3585	2.64
	$\pi_2 p_y$	7.9007	2.38		$\pi_2 d_{z^2}$	8.3949	2.67
	$\pi_2 d_{yz}$	7.9987	2.43		$\pi_2 d_{x^2-y^2}$	8.9835	3.20
	$\pi_3 p_z$	8.4954	5.92		$\pi_2 s$	9.2854	3.65
	$\pi_3 s$	8.8442	-		$\pi_2 p_z$	9.9740	6.38
	$\pi_3 s$	9.5722	-		$\pi_2 d_{z^2}$	10.0054	-
	$\pi_2 d_{yz}$	11.7063	-		$\pi_2 s$	12.0326	-

[a] energies in eV.

[b] $(n-\delta)^2 = 13.595/(IP-E)$; IP_1=8.883 eV, IP_2=10.308 eV from [293].

Table 3–10: Valence transition energies computed with the DZP_l basis set

Symmetry	Type	Energy[a]	f(r)	Symmetry	Type	Energy[a]	f(r)
$^1A_1$	$\pi_3 \rightarrow \pi_4^*/\pi_2 \rightarrow \pi_5^*$	6.4935	0.027	$^1B_2$	$\pi_3 \rightarrow \pi_5^*$	6.8566	0.213
	$\pi_2 \rightarrow \pi_5^*/\pi_3 \rightarrow \pi_4^*$	8.5728	0.273		$\pi_2 \rightarrow \pi_4^*$	9.3901	0.060
	$\pi_3^2 \rightarrow \pi_4^{*2}$	10.0315	0.038		$\pi_3 \rightarrow \pi_6^*$	12.2270	0.255
	$\pi_1 \rightarrow \pi_4^*$	11.9418	0.008		$\pi_3^2 \rightarrow \pi_4^*\pi_5^*/\pi_2 \rightarrow \pi_5^*$	12.2471	0.027
$^3A_1$	$\pi_2 \rightarrow \pi_5^*/\pi_3 \rightarrow \pi_4^*$	5.2563		$^3B_2$	$\pi_3 \rightarrow \pi_4^*$	4.2298	
	$\pi_3 \rightarrow \pi_4^*/\pi_2 \rightarrow \pi_5^*$	7.3040			$\pi_2 \rightarrow \pi_5^*$	6.7702	
	$\pi_1 \rightarrow \pi_4^*$	10.8223			$\pi_3 \rightarrow \pi_6^*$	10.8020	
$^1A_2$	$\pi_3 \rightarrow \sigma_{17}^*$	9.2653		$^1B_1$	$\pi_3 \rightarrow \sigma_{19}^*/\sigma_{16}^*$	8.9573	
	$\pi_3 \rightarrow \sigma_{18}^*$	9.4015			$\pi_3 \rightarrow \sigma_{16}^*/\sigma_{19}^*$	9.6637	
	$\sigma_{15} \rightarrow \pi_4^*$	9.2662			$\pi_2 \rightarrow \sigma_{17}^*$	9.7335	
	$\pi_2 \rightarrow \sigma_{19}^*/\sigma_{16}^*$	9.8299			$\pi_3 \rightarrow \sigma_{20}^*$	9.7335	
	$\pi_2 \rightarrow \sigma_{16}^*/\sigma_{19}^*$	10.5097			$\pi_2 \rightarrow \sigma_{18}^*$	10.8725	

[a] energies in eV.

al. [306] and would tend to support their assignment of only one valence transition, the $^1A_1$, to the experimental band at ~6 eV. Thunemann *et al.* assigned the experimental transition at 7.8 eV as being due to the $^1(\pi,\pi^*)$ $^1B_2$ which was calculated at 7.58 eV. The result quoted in Table 3–11 from the paper of Thunemann *et al.* [306] was the lowest obtained and involved an iterative natural orbital computation on the $^1A_1$ state based on MOs from the ground state. Without the INO calculation this state was computed in the region of 7.0 eV. In contrast no attempt has been made in the present work to optimise the MO basis for the description of this, or any other state. As previously stated, the present work differs from that of Thunemann with respect to the Rydberg states in that the complete set of *d*-functions is retained. The $^1A_1$ is found, as reported by Thunemann *et al.* and Nakatsuji *et al.* [306, 308], not to be an admixture of valence and Rydberg states; therefore, the slight lowering in excitation energy obtained between these two cases is taken to be due to the greater inclusion of higher excited states in the present computation, and the reduction in the number of uncorrelated core orbitals from ten to five. The energy lowering obtained by Thunemann *et al.* through the use of an INO procedure is also evidence of the effect of multiply excited states.

The $^1B_2$ valence state is found, contrary to the results of the previous theoretical work [306, 308], to be an admixture of valence and Rydberg transitions, particularly d_{xz} is found to be a large component in the final wavefunction. The mixing of valence and Rydberg character for this state resulted in a strong dependence being found for the energy upon the reference set employed in the calculation.

Two other singlet-singlet valence transitions were located using the DZ+R basis at 9.28 ($^1A_1$) and 10.00 eV ($^1B_2$). The energy of the $^1A_1$ transition compares to a possible valence feature observed experimentally at ~8.7 eV, the discrepancy between the two energies being approximately the same as the error found in the calculation of the 1^1A_1, $N \rightarrow V_1$, transition. As the two previous *ab initio* studies on furan by Thunemann *et al.* and Nakatsuji *et al.* [306, 308] only calculated the lowest two singlet valence states, no comparison is possible.

The assignments arrived at through the use of the DZ+R basis set, and the earlier theoretical results, are questioned by the present work, due to results ob-

Table 3–11: Valence excited states of furan (eV)

	Present			Literature	
Experiment[a]	DZP$_l$	DZ+R	DZP$_l$+R	Thunemann[b]	Nakatsuji[c]
~5.8 $^1A_1$ $\pi\pi^*$	6.49 $^1A_1$ $\pi\pi^*$		6.63 $^1A_1$ $\pi\pi^*$		
6.0 $^1B_2$ $\pi\pi^*$	6.86 $^1B_2$ $\pi\pi^*$	6.80 $^1A_1$ $\pi\pi^*$	6.88 $^1B_2$ $\pi\pi^*$	6.79 $^1A_1$ $\pi\pi^*$	7.32 $^1A_1$ $\pi\pi^*$
7.8 $^1B_2$ or $^1A_1$ $\pi\pi^*$	8.57 $^1A_1$ $\pi\pi^*$	7.55 $^1B_1$ $\pi\pi^*$	9.35 $^1A_1$ $\pi\pi^*$	7.58 $^1B_2$ $\pi\pi^*$	7.50 $^1B_2$ $\pi\pi^*$
		9.28 $^1A_1$ $\pi\pi^*$			
	8.96 $^1B_1$ $\pi\sigma^*$				
	9.27 $^1A_2$ $\pi\sigma^*$				
	9.27 $^1A_2$ $\sigma\pi^*$				
~8.7	9.39 $^1B_2$ $\pi\pi^*$	10.00 $^1B_2$ $\pi\pi^*$	9.48 $^1B_2$ $\pi\pi^*$		
	9.40 $^1A_2$ $\pi\sigma^*$				
	9.66 $^1B_1$ $\pi\sigma^*$				
	9.73 $^1B_1$ $\pi\sigma^*$				
	9.73 $^1B_1$ $\pi\sigma^*$				
	9.83 $^1A_2$ $\pi\sigma^*$				
	10.03 $^1A_1$ $\pi^0\pi^{*2}$		9.84 $^1A_1$ $\pi^0\pi^{*2}$		

[a] see Section 3.1.2 for details.

[b] [306]

[c] [308]

tained using a larger DZP basis. A significantly different situation is found for the singlet valence states in the DZP$_l$/DZP$_l$+R calculations. The $^1A_1$ and $^1B_2$ $^1(\pi,\pi^*)$ states are both computed at lower energies. This is especially the case for the $^1B_2$ state which is computed in both calculations at approximately 6.8 eV, closer to the valence transition at 6.0 eV than to that at 7.8 eV. In the DZ+R computation, the two lowest singlet valence states were found to be split by ~0.75 eV, this splitting is reduced to less than 0.4 eV for both the DZP$_l$ and DZP$_l$+R. This small separation for the valence states is not unprecedented, the two lowest valence states are only 0.18 eV apart in the SAC-CI calculation of Nakatsuji *et al.* [308]. The lowering of excitation energy leads to a change in the assignment of the electronic spectra compared to the DZ+R calculation, and to previous theoretical work. In agreement with experiment two valence transitions are proposed to occur at about 6 eV, with the $^1A_1$ predicted to be the lower and assigned to the experimental feature at ~5.8 eV, and the $^1B_2$ assigned to 6.0 eV. The oscillator strengths calculated for the DZP$_l$ basis set support this conclusion, the $^1A_1$ state is found to have a low oscillator strength and the $^1B_2$ is predicted to be a significantly stronger absorption, see Table 3–10.

With the assignment of the two lowest computed singlet valence states to experimental transitions at or below 6 eV, the feature at 7.8 eV has to be reassigned. Experimentally the symmetry of this transition has not been determined but is expected to be either A_1 or B_2, and due to a $\pi \rightarrow \pi^*$ promotion [317]. In both the DZ+R and DZP$_l$+R calculations the second $^1A_1$ valence state is placed at about 9.3 eV, some 1.5 eV above the experimental feature, with the next $^1B_2$ valence state placed at 10.00 eV, and 9.48 eV respectively. A further valence state, $^1A_1$, generated by a double excitation, and therefore one-photon forbidden, is predicted to occur at 9.84 eV due to the DZP$_l$+R calculation. This doubly excited state was found not to be an admixture of valence and Rydberg states. On the basis of the results for the basis sets including Rydberg functions it is felt that it is not possible to assign unambiguously the other two valence transitions observed experimentally, although tentative assignment of the 7.8 eV feature as $^1A_1$ is suggested with the ~8.7 eV feature 2^1B_2.

In both the DZ+R and DZP$_l$+R computations only low-lying valence states of A_1 and B_2 symmetries due to $\pi \rightarrow \pi^*$ promotions were found, no transitions involving σ or σ^* states were obtained. Through comparison with the DZP$_l$ calculation these states would be expected to onset in the region of 9 eV. It is possible that states of this kind were "swamped" by the large number of Rydberg states involved in the former computations.

The assignment of the transition at 7.8 eV as being the 2^1A_1 state is supported by the valence only calculation using the DZP$_l$ basis set, computed at 8.57 eV, *cf* an error of ~0.8 eV obtained for the other low-lying valence states for this basis set. The oscillator strength is also consistent with this assignment, predicting a strong absorption for this state, Table 3–10. The assignment of the experimental valence transition at ~8.7 eV is complicated by the presence of several optically allowed valence transitions within a relatively small energy range, and the knowledge that the present results are probably high by an unspecified amount. The next $^1(\pi,\pi^*)$ state is found at 9.39 eV, *cf* 9.48 eV for the analogous state in the DZP$_l$+R calculation, and three $^1B_1$ stated generated from the excitation of a π electron to a σ^* MO are calculated at within about 1 eV of the experimental transition, the lowest at 8.9 eV. The lowest transition due to promotion from a σ MO, in this case the "delocalised" oxygen lone pair ($9a_1$), is computed as arising at approximately 9.3 eV, although this state is of $^1A_2$ symmetry and therefore the transition is one-photon inactive. The first transition form the π lone pair oxygen MO is computed at nearly 12 eV ($^1A_1$), above the first two IPs and the first of the doubly excited states at ~10 eV ($^1A_1$).

Rydberg series

The low-lying Rydberg states of furan can be described theoretically as excitations out of the two highest valence orbitals, π_2 and π_3, into diffuse *s*, *p*, *d*, and *f* (not included in these calculations) orbitals. The first two IPs of furan are ascribed to $^2A_2$ (band $\tilde{\mathrm{X}}$) and $^2B_1$ ($\tilde{\mathrm{A}}$); the corresponding vertical IPs are 8.883 and 10.308 eV [293]; the adiabatic IPs have identical values. The controversial third IP, the $\tilde{\mathrm{B}}$ band, has a vertical IP of 12.96 eV [293] and an adiabatic IP of 11.94 eV according

to Seth Smith *et al.* [299]. From the adiabatic IPs and the normal ranges of the quantum defect (δ) for the Rydberg series approximate lower limits can be set for the anticipated Rydberg singlet states using the Rydberg formula. This was important in the present case because an inappropriate choice of reference configurations was found to lead to linear dependence, with very low excitation energies obtained for certain states states. The normal range of δ values appears to be ~0.75-0.90 for s states, 0.3-0.6 for p states, and below 0.3 for d states. The very low δ values for the d states can lead to negative δs being obtained. The lowest virtual orbitals of each symmetry in C_{2v} are: a_1 (s), b_1 (p_x), b_2 (p_y), and a_2 (d_{xy}). It was not found possible to remove the strong mixing between the s and p_y in the DZP$_l$+R $^1B_1$ calculation, and for the DZ+R some important configurations could not be included due to this effect on the $^1A_2(\pi_3, s)$ state. The excitation energies obtained using the DZ+R and DZP$_l$+R basis sets are listed along with the associated $(n - \delta)$ values in Tables 3–8 and 3–9, respectively.

The δ values obtained for the lowest, n=3, members of the Rydberg series are reasonable for the s and p in both computations. The 3s have δ at ~0.8, the 3p δ values lie in the 0.6-0.4 range for DZ+R, and the 3s are at 0.9 to 0.8, the 3p 0.6-0.4 for DZP$_l$+R. The values obtained for the 3d cover somewhat larger ranges, 0.4 to -0.3 and 0.6 to -0.5 for the DZ+R and DZP$_l$+R respectively. Those states calculated at the limits of these ranges, especially the $\pi_2 d_{yz}$ in the DZP$_l$+R calculation can be considered suspect on this evidence. The results for the higher, n=4 and sometimes 5, members of these series are found to be erratic. This is not entirely unexpected since the current description of most of the Rydberg series includes usually only two functions, and to obtain a good energy for the n$^{\text{th}}$ state requires that reasonable description is possible for the (n+1)$^{\text{th}}$ state. The difficulties in describing the n=4 members of the Rydberg series are demonstrated by the second $\pi_3 p_y$ state of $^1B_1$ symmetry in the DZP$_l$+R calculation. This state is computed at 6.65 eV, just 0.02 eV above the first member of this series and has a δ value of 1.53. The reason for the low energy obtained for this state can be ascertained from Table C–7, the state is found to be an un-physical linear

combination of p_y and s, therefore the energies of this state and the $\pi_2 3s$ at 7.14 eV are of to be treated with some scepticism.

The present results for the Rydberg states to a large extent confirm the findings of Thunemann *et al.* [306], although the present study extends that work to include a greater number of Rydberg states, see Table 3–12 for comparisons with the previous *ab initio* studies of Thunemann *et al.* and Nakatsuji *et al.*[306, 308], and the experimental assignments of Walker [315].

The lowest of the Rydberg excitations is found, as expected, to correspond to an excitation out of π_3 (a_2) into $3s$ (a_1), and hence is a $^1A_2$ species. The calculated excitation energies of approximately 5.95 eV are in excellent agreement with the experimental value of 5.91 eV, and the assignment of this feature to the dipole forbidden $^1A_2(\pi_3, 3sa_2)$ Rydberg state underlying the $N \rightarrow V_1$ transition [323]. The corresponding $^1B_1(\pi_2, 3sa_2)$ excitation is predicted to arise at 7.51 eV in the DZ+R computation and 7.14 eV in the DZP$_l$+R computation (this value although in close accordance with the 7.27 eV obtained by Thunemann *et al.*[306] is not taken with full confidence for the reasons given above). The error of ± 0.4 eV estimated for the extrapolation procedure in the MRD-CI calculation, however, prevents the unambiguous assignment of the $^1B_2(\pi_2, 3sa_2)$ state in the experimental spectrum.

The DZ+R and DZP$_l$+R calculations result in excitation energies for the $\pi_3 \rightarrow 3p$ in the range of 6.4-6.8 eV in good agreement with the experimentally determined features at 6.47 and 6.75 eV, especially the DZ+R results, which reproduce these values to within 0.1 eV for the optically allowed states. The separation between the optically allowed transitions is found to be larger than the 469 cm^{-1} suggested by Robin and used by Thunemann *et al.*[306], who computed the energy of the respective p Rydberg states originating from excitation to p_y and estimated the likely energy of the other states. The optically forbidden $^1A_2(\pi_3, 3p_z)$ is predicted to arise close to the allowed states, 6.78 eV in DZ+R and 6.41 eV in DZP$_l$+R. The $3p$ Rydberg states arising from excitation from the π_2 MO are predicted to have energies around 8 eV by both calculations, 8.0-8.1 eV for DZ+R and over a slightly wider range for DZP$_l$+R. In both cases the $^1A_2(\pi_2, 3p_y)$ state is predicted

Table 3–12: Singlet Rydberg excited states of furan (eV)

	Theoretical				
State	DZ+R	DZP$_l$+R	Thunemann[a]	Nakatsuji[b]	Experimental[c]
$\pi_3 3s\ ^1A_2$	5.96	5.95	5.94	6.27	5.91
$\pi_3 4s\ ^1A_2$	7.44	7.59			7.52
$\pi_3 3p_x\ ^1B_2$	6.40	6.66	6.52	6.80	6.47
$\pi_3 3p_y\ ^1B_1$	6.75	6.63	6.52	6.74	6.75
$\pi_3 3p_z\ ^1A_2$	6.78	6.41		6.98	
$\pi_3 3d_{xz}\ ^1B_1$	7.21	6.99			(7.28)
$\pi_3 3d_{xy}\ ^1A_1$	7.63	7.75	7.46	7.59	(7.38)
$\pi_3 3d_{xz}\ ^1B_2$	6.76	7.71			(7.38)
$\pi_3 3d_{x^2-y^2}/3d_{z^2}\ ^1A_2$	6.83/7.36	7.14/7.40			7.43
$\pi_2 3s\ ^1B_1$	7.51	7.14	7.27	7.62	(7.52)
$\pi_2 4s\ ^1B_1$	8.76	9.28			8.96
$\pi_2 3p_z\ ^1B_1$	8.06	8.04		8.24	
$\pi_2 3p_x\ ^1A_1$	8.12	8.14		8.27	8.1
$\pi_2 3p_y\ ^1A_2$	7.99	7.90	7.85	8.19	
$\pi_2 3d_{xz}\ ^1A_1$	8.31	8.33			
$\pi_2 3d_{x^2-y^2}/3d_{z^2}\ ^1B_1$	8.58/8.67	8.36/8.39			(8.46)
$\pi_2 3d_{xy}\ ^1B_2$	8.82	8.93	8.60	8.91	(8.77)
$\pi_2 3d_{yz}\ ^1A_2$	8.73	8.00			

[a] [306]

[b] [308]

[c] see Table 3–3 [315]

to be the lowest. The energies obtained for the optically allowed transitions are in excellent agreement with the experimental results, falling within 0.06 eV of the observed transition at 8.1 eV.

The excitation energies for the *d* Rydberg states are found to cover surprisingly large ranges, as much as 0.9 eV. As the previous calculations of Thunemann *et al.* and Nakatsuji *et al.* [306, 308] only employed a single *d*-type Rydberg function, it is not possible to make a comparison. As previously stated, the SCF MOs were found to be were found to be linear combinations with respect to the symmetry axes, ie p_x/d_{xz} and p_y/d_{yz}. In general where strong interactions between configurations with upper *p* and *d* Rydberg orbitals occurs, the energies of the resulting *d* states are found to be poor; the *p* states seem to be affected to a much smaller extent. Particular difficulty was found for the $^1B_1(\pi_3, d_{yz})$ states which were found to interact strongly with the p_y, and the $^1B_2(\pi_3, d_{xz})$, especially for the DZ+R basis set, which interact strongly with the p_x and to some extent with the valence state of the same symmetry. It is quite possible that this interaction has caused the valence state to be raised and the Rydberg state to be correspondingly lowered in energy. The same interactions occur for the DZP$_l$+R basis set, therefore there is the possibility of the reverse occurring. For these reasons it is probable that the most reliable energies are to be found for the *d* Rydberg orbitals of a_2 (d_{xy}) which has no *p*-type function of the same symmetry species with which to interact, and the a_1 (d_{z^2} and $d_{x^2-y^2}$), which although showing mixing for the higher members in the series have n=3 members that are not admixtures of states. The $^1A_1(\pi_3, 3d_{xy})$ Rydberg state is placed around 7.7 eV in the present work, this compares to promotions assigned to optically allowed transitions occurring in the 7.3-7.4 eV range. Excellent agreement is found between the computed values for $^1A_2(\pi_3, 3d_{z^2})$ and the one-photon forbidden process observed at 7.43 eV by Cooper *et al.* [323], the other $^1A_2(\pi_3, 3d_{x^2-y^2})$ state is predicted to occur at lower excitation energies. With the large spread of energies obtained for promotions from the π_3 orbital to *d*-type Rydbergs it is not possible to offer assistance in the assignment of the $\pi_2 \rightarrow 3s$ transition, which is found to occur in the same energy region. The earlier calculations of Thunemann *et al.* [306] and Nakatsuji *et al.* [308] have placed

this state below and almost degenerate with the d Rydberg states respectively. For transitions from π_2 the energies obtained for promotion to the $3d_{xy}$, $3d_{z^2}$, and $3d_{x^2-y^2}$ are found to be in close agreement with the experimentally determined energies at 8.46 and 8.77 eV. Again the proximity of the excitations prevents any definite ordering from being obtained.

3.3 Concluding remarks

Calculations have been performed on the lowest valence and Rydberg excited states of the Furan molecule. The excitation energies and assignments of the valence states are very different from the earlier theoretical predictions. Two valence states, the lowest of the $^1A_1$ and $^1B_2$, are assigned to the experimental feature at 6 eV. This reassignment reflects the substantial lowering obtained for the $^1B_2$ state when the DZ basis is augmented by diffuse polarisation functions. The usual polarisation functions optimised for the ground state are found to have little effect on the excitation energies of the valence states, mirroring the situation found for propyne (Section 2.4.2). Despite the improved description of the differential correlation between the states obtained by using these polarisation functions the calculated energies for both the singlet valence states are approximately 0.8 eV higher than experiment. There exist several possibilities for this remaining discrepancy; that the discarded virtual MOs have a large effect for the valence states relative to the ground state, that there is significant reorganisation of the MOs upon the valence transition, or that further polarisation is required to return dynamic correlation for the excited states. This obviously requires further investigation, although the author feels that the remaining differences are probably caused by the requirement of further polarisation functions, perhaps the original ground state functions. In other systems of interest to theoreticians there has been considerable work in obtaining basis sets to describe the differential correlation between valence states, such work is clearly required for the organic molecules, especially in conjunction with the necessary use of small basis sets that can be applied to larger systems. An

interesting alternative is the use of large highly contracted basis sets as proposed by Almlöf *et al.* [21].

Despite the improvement found for the lowest valence states, disappointing results are obtained for the other valence states in particularly those including Rydberg functions. Excluding these functions leads to an improvement and would suggest that the prominent experimental feature at ~7.8 eV be assigned as $^1A_1$, this is supported by the large transition moment calculated. Such calculations are, however, unsatisfactory due to the possibility of valence- Rydberg mixing.

The energies computed for the Rydberg states are in reasonable agreement with experiment, although difficulties encountered, especially concerning linear combinations, prevent the unambiguous assignment of the experimental spectra.

3.3.1 Addendum

After this study was completed a further paper by Serrano-Andrés *et al.* [JACS, **115**, 6184, 1993.] appeared. Many of the results and conclusions are similar to the present study, however, they did not have access to new experimental data. Serrano-Andrés *et al.* employed the CASPT2 (second order perturbation theory acting upon a CASSCF reference function) method upon a large ANO basis, including four polarisation functions in the contraction $4d/1d$. As in the present work two valence transitions, $^1A_1$ and $^1B_2$, are assigned to the experimental feature at 6.00 eV. The ordering of these states is reversed with the $^1B_2$, 6.04 eV, placed below the $^1A_1$, 6.16 eV, although the use of different ground state energies for the two manifolds has the effect of lowering the $^1B_2$ by 0.2 eV relative to the $^1A_1$. The author feels that the lower excitation energies obtained by Serrano-Andrés *et al.* reflect the improved polarisation functions. The excitation energy of the second $^1A_1$ valence state is found to be in excellent agreement with experiment at 7.74 eV.

Chapter 4

The Low-lying Excited States of Dicopper

The electronic structures of transition metal clusters are of considerable interest on several grounds. From the theoretical point of view, there is the role played by the s and d electrons in the bonding; from the practical point of view, in the role these systems have as models for heterogeneous catalysts; and there is the need to address the question of the onset of metallic properties in a cluster. There has been an explosion of experimental work in the last fifteen years, particularly due to the development of molecular beam methods which have allowed the investigation of properties at low temperatures and the resolution of spectral features [335].

The copper dimer is the one of simplest examples of a transition metal cluster. Copper is the lightest member of the Group IV atoms, the atomic ground state possess a closed shell of d-electrons with a single unpaired electron occupying an s orbital, therefore the dimer, Cu_2, is expected to be closely related to the alkali metal dimers. Due to the relatively large separation between the Cu atomic states there is a low density of states in the Cu_2 molecular spectrum. There exists a wealth of experimental data on the ground and excited states of this molecule.

The ground state has been extensively studied by *ab initio* means and is well characterised. There has, however, been little work on the excited states, which have not yet been unambiguously assigned. There is, also, the question about the existence of a low-lying ion-pair state [336].

4.1 The copper atom

The ground state of the copper atom has the electronic configuration [Ar]$3d^{10}4s^1$, where [Ar] represents the electronic occupancy of an argon atom, $1s^22s^23s^22p^63p^6$. This Cu configuration yields one atomic term, ^2S. Excitation of a single $3d$ electron to the $4s$ shell gives rise to the first excited term ^2D, with electronic configuration [Ar]$3d^94s^2$. Spin orbit coupling in the ^2D term is quite large, the $^2D_{3/2}$ lying 2043 cm^{-1} above the $^2D_{5/2}$ state; the [Ar]$3d^94s^2$ ^2D states lie 11203 and 13245 cm^{-1} (1.39 and 1.64eV) above the [Ar]$3d^{10}4s^1$ ground state respectively (Table 4–1). The spin-orbit coupling constant $\zeta(3d)$ for the d^94s^2 configuration is given by the Landé interval rule [337] as 817 cm^{-1}.

$$\zeta(3d) = \frac{2}{5}\left|E(^2D_{3/2}) - E(^2D_{5/2})\right| \tag{4.1}$$

The next highest term is the $^2P^0$ arising form the excitation of the $4s$ electron to a $4p$ orbital. The corresponding electronic configuration is [Ar]$3d^{10}4p^1$. This term suffers a relatively small spin orbit splitting (248 cm^{-1}, $\zeta(4p)\approx$166 cm^{-1}), with the lowest component, $^2P^0_{1/2}$, lying 30535 cm^{-1} (3.79 eV) above the ground state. Several quartet states lie a further 9000 cm^{-1} (1.12 eV) higher in energy.

The dissociation energy of the copper dimer has been measured as 16760±200 cm^{-1} (2.08±0.03 eV)[339]. Relative to the molecular ground state the ^2D appear in the 28000-30000 cm^{-1} (3.47-3.72 eV) region, and the $^2P^0$ at approximately 47500 cm^{-1} (5.89 eV) (Table 4–1).

The bonding of the transition metal dimers, particularly the tendency to form multiple bonds is governed by the relative sizes of the nd and $(n+1)d$ orbitals [335]. In copper the $3d$ orbitals is relatively contracted; the $< r_{4s} > / < r_{3d} >$ ratio is calculated by numerical Dirac-Hartree-Fock as 3.27 for the ^2S ground state [341], and 3.15 for ^2D [342]. Therefore, there is expected to be little overlap of the d orbitals for the molecular states arising from these asymptotes, with the result that the bonding results mostly from the s orbitals.

Table 4–1: Atomic terms of copper

Configuration	Term	Energy /cm^{-1}	Interval /cm^{-1}
[Ar]$3d^{10}4s^1$	$^2S_{1/2}$	0.000 (16760$^{a b}$)	
[Ar]$3d^9 4s^2$	$^2D_{5/2}$	11202.565 (27962^b)	
	$^2D_{3/2}$	13245.423 (30005^b)	−2042.858
[Ar]$3d^{10}4p^1$	$^2P^0_{1/2}$	30535.302 (47295^b)	
	$^2P^0_{3/2}$	30783.686 (47544^b)	+248.384
[Ar]$3d^9 4s^1 4p^1$	$^4P^0_{5/2}$	39018.652 (55779^b)	
	$^4P^0_{3/2}$	40113.99 (56874^b)	−1095.34
	$^4P^0_{1/2}$	40943.73 (57703^b)	−829.74
[Ar]$3d^{10}$	$^1S_0$ (IP)	62317.2 (79977^b)	
[Ar]$3d^{10}4s^2$	$^1S_0$ (EA)	−9961^c (6799^b)	

Data from [338], except [a] the dissociation energy of the copper dimer, 16760±200 cm^{-1} from Rohlfing and Valentini [339].

[b] energy relative to the ground state of the dimer.

[c] 1.235±0.005 eV from [340].

4.2 The electronic spectrum of Cu_2

A summary of present state of the experimental knowledge of the electronic states of the copper dimer is given in Table 4–2. The potential energy curves corresponding to these constants are illustrated in Figure 4–1. Also included for completeness are low-lying atomic asymptotes and the attractive limb of an ion-pair state as estimated using the coulombic interaction, Section 4.3.

The earliest observations of the emission spectrum of the copper dimer were reported in 1954 by Kleman and Lindqvist [350] and, Ruamps [351]. Two bands were observed, the $X \rightarrow A$ with its origin at 20396 cm^{-1} (2.53 eV), and the

Table 4–2: Electronic states of Cu_2

State	T_e [a] /cm^{-1}	ω_e /cm^{-1}	$\omega_e X_e$ /cm^{-1}	B_e /10^{-3}cm^{-1}	α_e /10^{-8}cm^{-1}	r_e /Å	ν_{00} /cm^{-1}
J	37437.7[c] (4.6417)[b]	288.4	0.64	0.1165[b]	10[b]	2.15[b]	37451.1[c]
I	~35000 (4.3395)[c]	280[c]	1[c]				
H	~36782 (4.5604)[c]						36559.0[c]
(c $^3\Delta$)	~34870 (4.3234)	100	0.5				
(b $^3\Delta$)	~33120 (4.1064)	90	0.5				
G	~30702 (3.8066)[d]	116.0[c]	0.046[c]			2.73[d]	
F	~28560 (3.5410)[c]	248.0[c]	0.90[c]				
E	~27153 (3.3666)	231.5	-4.25				27136
D ($^3\Delta$)	~25560 (3.1691)	~160				~2.38	25508
C $^1\Pi_u$ (1_u)	21866.4 (2.7111)[b]	221.4[b]	1.76[b]	0.1045[b]	0.92[b]	2.26[b]	21484
B $^1\Sigma_u^+$ (0_u)	21747.88 (2.6964)	246.317[e]	2.231[e]	0.09889[f]	0.606[f]	2.3281[e]	21747.9[f]
A $^1\Sigma_u^+$ (0_u)	20430.98 (2.5331)[g]	193.11[g]	0.606[g]	0.1034[g]	1.38[g]	2.2832[h]	20396.0
a $^3\Sigma_u^+$	~15420 (1.9118)[i]	~125[i]				~2.48[i]	15350[i]
X $^1\Sigma_g^+$	0	266.459[e]	1.0350[e]	0.10874	0.614	2.21927[e]	

[a] energies in parentheses are in eV.

[b] from Page and Gudeman [343].

[c] from Powers *et al.* [344].

[d] from Rohlfing and Valentini [339].

[e] from Ram *et al.* [345].

[f] from Åslund *et al.* [346].

[g] from Doverstål et al [347].

[h] from Lochet [348].

[i] from Bondybey [349].

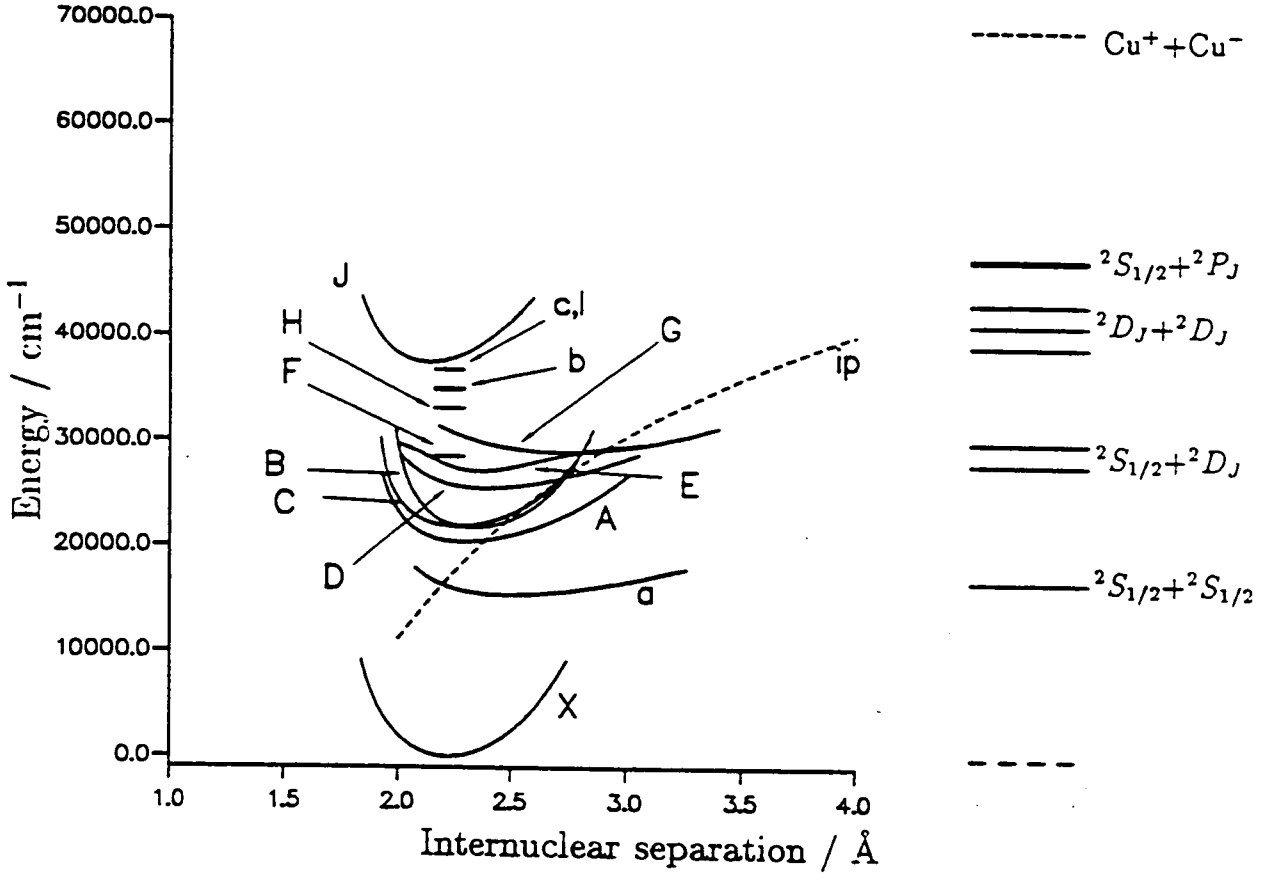

Figure 4–1: Potential energy curves of dicopper determined using experimental data

The states are defined in Table 4–2.

ip demonstrates the ion-pair attractive limb.

$X \rightarrow B$ at 21748 cm^{-1} (2.70 eV). These are known as the "green" and "blue" bands respectively.

The first high resolution study of Cu_2 was performed by Åslund *et al.* in 1965 [346]. The B-X system was analysed for rotationally structure and found to be a parallel transition, $^1\Sigma - ^1\Sigma$. Through the consideration of the correlation of the ground and lowest excited terms of the copper atom to form molecular states, Section 4.3, the states were identified as $^1\Sigma_g^+$ and $^1\Sigma_u$. Equilibrium internuclear separations were obtained as 2.3274 and 2.2195 Å for the excited and ground states respectively.

Pesič and Weniger [352] identified apparent Q branches in the A-X system and thereby assigned the A state as $^1\Pi_u$. Subsequent work by Lochet [348], using laser-induced fluorescence, on this system, resolved only P and R branches, and the A state was accordingly assigned as $^1\Sigma_u$. The Σ nature of the B-state was confirmed by McCaffrey *et al.* [353], who also found evidence that the v' level was perturbed by a previously unidentified state.

Preuss *et al.* [354] identified a spectral feature approximately 100 cm^{-1} to the blue of the B-X origin. The presence of this system was confirmed independently by Powers *et al.* using resonant two photon ionisation [355], and Gole *et al.* employing laser induced fluorescence [356]. The origin of the band was found at ~21870 cm^{-1} (2.71 eV). The rotationally resolved study of Page and Gudeman [343] identified Q as well as P and R branches, assigning the C-state as Π symmetry.

McCaffrey *et al.* [353] observed large electronic isotope shifts for the A- and B-states. The magnitude of these shifts was found to be similar to the "specific mass shifts" found in the optical spectrum of atomic copper for transitions involving states differing in the number of d electrons, especially the ^2D states derived from the $3d^9 4s^2$. On the basis of this observation the A- and B-states were interpreted as both arising from the low-energy $^2D + ^2S_{1/2}$ asymptote of the copper dimer. This assignment is not consistent with Hund's case (a) coupling of angular momenta; under this coupling scheme only one $^1\Sigma_u^+$ states is generated from the $^2D + ^2S_{1/2}$ asymptote. However, considering the coupling between the total angular momenta

in the $^2D_{5/2}+^2S_{1/2}$ and $^2D_{3/2}+^2S_{1/2}$ asymptotes in Hund's case (c) two molecular states of 0_u^+ symmetry are obtained. The C-state is also found to exhibit an electronic isotope shift, approximately half as large as the A- and B- state [357].

Studies have also revealed information on the lifetimes and photoprocesses of the excited states. Steele [358] measured the lifetimes of several vibrational levels of the A- and B-states at a selection of buffer gas pressures. The B-state lifetime was found to be shorter than that for the A-state. In addition to the expected decrease in lifetimes with increasing buffer gas pressure, the B-state luminescence showed evidence of a second longer lived process with a lifetime corresponding to that of the A-state, suggesting efficient collisional relaxation between these states. In later work, Bondybey *et al.* [349] reported the gas phase lifetimes of the A-, B-, and C-states. The lifetimes of the three lowest vibrational levels of the A-state were found to shorten rapidly with excitation (~115, 75, and 40 ns for v'=0,1,2, respectively) but, in contrast to Steele, were independent of helium pressure in the range 0.5 to 15 torr. At low pressures the decay lifetimes of the v'=0 level of the B-state was measured as ~40 ns. At higher pressures the same double exponential decay was observed, as found by Steele, however the coupled state was identified as the C-state. The lifetime of the C-state is found to be considerably greater than either the A- or the B-states, the collision free estimate being 800 ns. This long lifetime is consistent with the assignment of the C-state as Π symmetry and the resulting optically forbidden nature of the transition to the $^1\Sigma_g^+$ ground state.

Cu_2 has also been investigated trapped in inert gas matrices. Ozin *et al.* [359] published results which suggested that when Cu_2 was trapped in argon, krypton, or xenon matrices, that the matrix induced shifts of the spectral transitions to the A- and B- states were large, approximately 5000-7000 cm^{-1} (0.62-0.87 eV) to the blue. Gole *et al.* [356], however, found that the matrix induced shift of these electronic transitions in neon was small. Excitation at 26000 cm^{-1} (3.22 eV) yielded fluorescence from a long vibrational progression with a 0-0 band near 25508 cm^{-1} (3.16 eV), the system assigned by Ozin as the blue shifted A- (or B-) state. The emission from this system, designated $X \rightarrow D$ was long lived with an estimated lifetime of approximately 6.5 μs. This is considerably longer than

the matrix isolated lifetimes of either the A- or B-states, both of which have been measured as shorter that 10 ns, and is consistent the the assignment of the D-state as triplet excited state of Cu_2. On the basis of a Franck-Condon fit to the observed fluorescence intensities the equilibrium internuclear separation of the D-state was estimated as 2.38 Å [360].

Gole *et al.* [356] reported that excitation of either the A or B bands resulted in fluorescence from a long lived system (lifetime of 27 ms) at longer wavelengths. This long lived system exhibited a 0-0 transition at 15350 cm^{-1} (1.90 eV) and a long vibrational progression to the red of this origin. On the basis of the long lifetime, Bondybey [360] assigned the transition as originating from the lowest triplet state of Cu_2. This was designated $a^3\Sigma_u^+$, formed by the predissociation of either the A- or B- states followed by a cage recombination of atoms in the ground state ($^2S_{1/2}$+$^2S_{1/2}$). Comparison with the dissociation energy of the copper dimer, 16760 cm^{-1} [339], demonstrated that this state was weakly bond by 1000-1500 cm^{-1} (0.12-0.19 eV). Through the analysis of the vibrational band intensities, the r_e was estimated as 2.48 Å.

At higher excitation energies five bands have been observed by Powers *et al.* [344], using the resonant two photoionisation method, and assigned as Cu_2 transitions from the ground state. The two lowest of these states, the F- and G- states of Morse [335], are found to perturb each other strongly, and exhibit long progressions in the excited state frequencies. The bond length of the G-state was obtained by Rohlfing and Valentini [339] using the Franck-Condon envelope and found to be considerably longer, 2.73 Å, than that of the ground state. The vibrational frequency for the next transition, the $X \rightarrow H$ with an origin at 36559 cm^{-1} (4.53 eV), is the highest of any reported for Cu_2, and indeed for any of the $3d$ transition metal dimers [335]. According to Morse [335] such a difference in vibrational frequency between the upper and lower states "would require considerable electronic rearrangement and appears quite dubious".

Powers *et al.* [344] also reported two additional band systems in the 37000-38600 cm^{-1} (4.59-4.79 eV) region, the I-X and J-X systems. Through the rotational analysis of the J-state, Page and Gudeman [343] determined the bond

length to be shorter than the ground state at 2.138 Å. The resolution obtained was not sufficient to obtain the symmetry of the state.

Sappey *et al.* [361] used the lowest vibrational levels of the J-state as intermediate resonant steps in a two-photon study of Cu_2^+. The molecular ionisation potential was determined as 7.899 eV for $^2\Sigma_g^+$ (cf the Cu atomic IP of 7.73 eV) with an associated adiabatic dissociation energy of 1.84 eV, to be compared with 2.08 eV for the molecular ground state. Two excited-ionic-state progressions were found beginning at T_0=1.143 and 1.256 eV, which were assigned, through comparison with the atom and atomic ion, as spin orbit components of the $^2\Pi$ state, $^3\Pi_{3/2}$ and $^3\Pi_{1/2}$, respectively. The $^2\Pi$ ion state was estimated to have a dissociation energy of 2.08 eV, and a bond length of 2.23 Å [343]. Following the observation that the $^2\Pi$ state was due to direct ionisation from the J-state, it was concluded that the molecular state contained a d-hole of the same symmetry as the ion. The similarity between the dissociation energies of the excited $^2\Pi$ ion state and the molecular ground state led Sappey to conclude that a d hole in the ion either does nothing or increases the bonding slightly by reducing $3d$ core repulsion.

Further transitions attributed to the copper dimer have been observed in emission from the study of copper arcs [362], and from the flames of copper sulphides [363]. Of these band systems only one is found to emit to a state with the same vibrational frequency as the ground states of the molecule. This emission is now known as the $X \rightarrow E$, and has an electronic origin at 27136 cm^{-1} (3.36 eV). Morse [335] tentatively assigned two of the remaining bands as belonging to the triplet manifold, terminating on the $a^3\Sigma_u^+$ state; the bands exhibiting ω'' values in agreement with Bondybey's [360] estimated vibrational frequency of that state. The spectra of these states have not been rotationally analyzed and there exists some doubt concerning their attribution to the copper dimer [343].

4.3 The correspondence of molecular states and atomic asymptotes for dicopper

The low-lying states of the copper dimer are expected to arise from the $^2S_{1/2}$+$^2S_{1/2}$, $^2S_{1/2}$+$^2D_{3/2}$($^2D_{5/2}$), $^2D_{3/2}$($^2D_{5/2}$)+$^2D_{3/2}$($^2D_{5/2}$) and $^2S_{1/2}$+$^2P_{1/2}$($^2P_{3/2}$) atomic copper asymptotes. A controversial feature of the assignment of the electronic spectrum of dicopper is the possible intrusion of an ion-pair state into the bonding region and the effects of this upon the explanation of the observed spectra. The molecular states corresponding to these atomic asymptotes, and the ion-pair limit, under Hund's case (a) and (c) coupling are tabulated in Table 4–3. These separated atom limits are also shown in Figure 4–1.

The ground state of copper, like the alkali metal dimers, corresponds to $^2S_{1/2}$+ $^2S_{1/2}$, with effectively non-bonding d electron shells, and a $3d^{10}3d^{10}4s\sigma_g^2 4s\sigma_u^0$ molecular orbital configuration. This is confirmed by numerous theoretical calculations, and is discussed further in Section 4.4. This atomic asymptote also generates a molecular triplet state with $3d^{10}3d^{10}4s\sigma_g^1 4s\sigma_u^1$ configuration, identified as the $a^3\Sigma_u^+$ experimental state.

In contrast with the alkali dimers the presence of a low-lying excited state corresponding to ^2D greatly increases the number of possible low-lying states in the copper dimer. Through the separated atom limit a total of 20 molecular states are predicted to be generated from the ^2S+^2D. Under Hund's case (a) coupling three types of state, Σ^+, Π, and Δ, are produced each of which can exist as singlet or triplet [1] and *gerade* or *ungerade* forms. Of these states, two are accessible from the ground state ($^1\Sigma_g^+$) by one-photon transitions with significant dipole moments, the $^1\Sigma_u^+$ and the $^1\Pi_u$ with configurations $3d\sigma_g^1 \ldots 4s\sigma_g^1 4s\sigma_u^1$ and $3d\pi_g^3 \ldots 4s\sigma_g^1 4s\sigma_u^1$.

---

[1] The molecular terms have degeneracies of three for the triplets, and two from states other than Σ, thus: $^1\Sigma$ (1 state); $^1\Pi$, $^1\Delta$, etc.. (2 states); $^3\Sigma$ (3 state); $^3\Pi$, $^3\Delta$, etc.. (6 states).

Table 4–3: Correspondence of atomic and molecular states in Hund's case (a) and (c).

Atomic States	Molecular States	
	Hund's (a)	Hund's (c)
$^2S_{1/2}+^2S_{1/2}$	$^1\Sigma_g^+$	0_g^+
	$^3\Sigma_u^+$	$0_u^-,1_u$
$^2S_{1/2}+^2D_{5/2},^2D_{3/2}$	$^1\Sigma_{g/u}^+$	$0_{g/u}^+$
	$^1\Pi_{g/u}$	$1_{g/u}$
	$^1\Delta_{g/u}$	$2_{g/u}$
	$^3\Sigma_{g/u}^+$	$0_{g/u}^-,1_{g/u}$
	$^3\Pi_{g/u}$	$0_{g/u}^-,0_{g/u}^+,1_{g/u},2_{g/u}$
	$^3\Delta_{g/u}$	$1_{g/u},2_{g/u},3_{g/u}$
$^2D_{5/2},^2D_{3/2}+^2D_{5/2},^2D_{3/2}$	$^1\Sigma_g^+(3)\ ^1\Sigma_u^-(2)$	$0_g^+(3)\ 0_u^-(2)$
	$^1\Pi_{g/u}(2)$	$1_{g/u}(2)$
	$^1\Delta_g\ ^1\Delta_u(2)$	$2_g\ 2_u(2)$
	$^1\Phi_{g/u}$	$3_{g/u}$
	$^1\Lambda_g$	4_g
	$^3\Sigma_g^-(2)\ ^3\Sigma_u^+(3)$	$0_g^+(2),1_g(2)\ 0_u^-(3),1_u(3)$
	$^3\Pi_{g/u}(2)$	$0_{g/u}^-(2),0_{g/u}^+(2),1_{g/u}(2),2_{g/u}(2)$
	$^3\Delta_g\ ^3\Delta_u(2)$	$1_{g/u},2_{g/u},3_{g/u}\ 1_{g/u}(2),2_{g/u}(2),3_{g/u}(2)$
	$^3\Phi_{g/u}$	$2_{g/u},3_{g/u},4_{g/u}$
	$^3\Lambda_u$	$3_u,4_u,5_u$
$^2S_{1/2}+^2P_{1/2}^0,^2P_{3/2}^0$	$^1\Sigma_{g/u}^+$	$0_{g/u}^+$
	$^1\Pi_{g/u}$	$1_{g/u}$
	$^3\Sigma_{g/u}^+$	$0_{g/u}^-,1_{g/u}$
	$^3\Pi_{g/u}$	$0_{g/u}^-,0_{g/u}^+,1_{g/u},2_{g/u}$
$Cu^{+1}S_0+Cu^{-1}S_0$	$^1\Sigma_{g/u}^+$	$0_{g/u}^+$

From Figure 4–1 it is evident that the *A*-, *B*-, *C*-, *D*-, and *E*-states would be expected to correlate with the $^2S+^2D$ limit. Of these states both the *A*- and *B*- have been experimentally assigned as $^1\Sigma_u^+$, and the *C*-state is identified with Π_u. Given this, and the relatively large atomic spin-orbital splitting between the $^2D_{3/2}$ and $^2D_{5/2}$ terms, McCaffrey *et al.* [353] argued that the low-lying excited states should be interpreted in terms of the mutual coupling of the total angular momenta of the constituent atoms as described by Hund's case (c). Under this coupling scheme 20 states are again derived [2] (Table 4–3). The $^2S_{1/2}+^2D_{3/2}$ asymptote gives rise to $0^+, 0^-, 1, 1, 2$, and $0^+, 0^-, 1, 1, 2, 2, 3$ associated with the $^2S_{1/2}+^2D_{5/2}$ asymptote, where the *gerade/ungerade* symmetry has been omitted. For an electric dipole transition coupling these molecular states to the 0_g^+ ground state, six are allowed, involving $0_u^+, 2*1_u$ states associated with each of the asymptotes. McCaffrey *et al.* [353] connected the two 0_u^+ (*A* and *B*) states with the $^2D_{5/2}$ and $^2D_{3/2}$ asymptotes, respectively. The *C*-state is then assigned as being due to one of the four 1_u [343].

The next highest energy asymptotes are the three $^2D+^2D$, which gives rise to 30 molecular terms under Hund's case (a); restrictions imposed by the Pauli exclusion principle forbid certain combinations between identical states of a homonuclear diatomic. As a result of these restrictions no molecular states of $^1\Sigma_u^+$ symmetry are formed. The allowed transitions involve the two $^1\Pi_u$ states. For Hund's (c), 59 terms are found, of which, twelve can one-photon couple to the ground state; namely two 0_u^+ derived from the $^2D_{3/2}+^2D_{5/2}$ asymptote [3] and ten 1_u. All the states possess the $3d^{18}4s\sigma_g^2 4s\sigma_u^2$ electronic configuration, generated by double excitations from the ground state. As the atomic 4*s* orbitals are completely filled, it is expected that any bonding in the molecule will be through the *d*-shell and will be essentially negligible due to the highly contracted nature of this shell, Section 4.1.

---

[2] $\Omega \neq 0$ terms are doubly degenerate.

[3] No 0_u^+ are obtained from the $^2D_{3/2}+^2D_{3/2}$ and $^2D_{5/2}+^2D_{5/2}$ pairs due to restrictions when the atomic *J* values are equal.

The $^2S+^2P$ asymptote is located 30600 cm^{-1} above (3.79 eV) the ground state asymptote, and approximately 47500 cm^{-1} (5.89 eV) above the molecular ground state. The states that can couple radiatively to a $^1\Sigma_u^+$ ground state are $^1\Sigma_u^+$ with electronic configuration $3d^{10}3d^{10}4s\sigma_g^1 4p\sigma_u^1$, and $^1\Pi_u$ corresponding to $3d^{10}3d^{10}4s\sigma_g^1 4p\pi_u^1$. Hund's case (c) treatment of the $^2S+^2P$ states gives rise to two 0_u^+ and two 1_u. McCaffrey *et al.* [353] noted that the Hund's (c) treatment of these molecular states was probably inappropriate due to the small spin orbit splitting observed for the atomic $[Ar]3d^{10}4p^1$ configuration.

The ion-pair limit lies at 70016 cm^{-1} (8.68 eV), relative to the molecular ground state, but due to the strong coulombic attraction, the energy drops to below that of the $^2S+^2P^0$ atomic limit when the ions are still 5.37 Å apart [357]. The attractive limb of the potential is included in Figure 4–1 as a simple coulomb $(-e^2/R)$ attraction, ignoring the possibility of stronger attractions due to the polarisability of the ions, and interactions with molecular states. Neither is the repulsive interactions arising from the Pauli repulsions of the filled orbitals as the ions approach each other included, hence the curve displays the unphysical behavior of going to $-\infty$, and having no repulsive limb. It is clear from Figure 4–1 that the ion pair state will pass close to the low-lying excited states in their bonding region, indeed the majority of the published *ab initio* works, Section 4.4, identify this state with either the A- or B-state. A similar situation exist for CuAg where Bishea *et al.* [364] have assigned the low-lying B-state as corresponding to an ion-pair.

4.4 Previous theoretical work on Cu_2

Dicopper has been of considerable interest to theoreticians for many of the same reasons as the systems has appealed to experimentalists. In addition, the abundance of experimental data on the ground state has meant that Cu_2 is viewed as a bench mark molecule for *ab initio* techniques, and as a test case for theories on transition metal bonding. Most of the published work has concentrated on obtain-

ing an adequate description of the molecular ground state, as such there has been a concerted effort by many groups to investigate the variation of the one-particle basis [365–369], the inclusion of different degrees of correlation [365, 370–372] and the effect of relativity [371–374].

The ground state is universally predicted to be of $^1\Sigma_u^+$ symmetry corresponding to the $^2S+^2S$ separated atomic limit. The bonding has been found to be predominantly through the interaction of the $4s$ atomic orbitals [365, 371, 375]. This is contrary to the suggestion of Pauling [376] based on empirical observation, that the relatively short bond (the nearest neighbour distance in the metal is 2.56 Å) might be due to the existence of a triple bond caused by significant mixing of the $3d^{10}4s^14p^1$ configuration with the atomic ground state. The $3d$ orbitals remain essentially atomic in nature in the bonding region, as expected given the relative sizes of the $3d$ and $4s$ orbitals, see Section 4.1.

The Hartree-Fock limits for the bond length and dissociation energy of dicopper, as computed by numerical H-F are 2.447 Å and 0.52 eV [369]. As the basis set limit is reached the SCF results approach these values from below.

The effects of correlating different groups of electrons have been investigated by Bauschlicher and co-workers [365, 375], and Jordan and co-workers [366, 367]. Similar results were reported by both groups. The inclusion of the $4s\sigma_g^2 \rightarrow 4s\sigma_u^2$, required to describe the correct dissociation of the molecule, through MCSCF lead to an increase in the calculated bond length. Correlating just the two bonding $4s$ electrons was found to give a bond length similar to the SCF, 2.44 Å [366], although a large improvement was obtained for the dissociation energy, 1.24 eV [366]. The configurations associated with the double excitation $4s\sigma_g^2 \rightarrow 4s\pi_u^2$ are found to be important, accounting for angular correlation of the HOMO, especially since the near degeneracy of the $4s$ and $4p$ orbitals in the atom. Although the d electrons do not play a significant role in the bonding, an adequate description of the potential energy curve requires that they be correlated; the inclusion of the d electrons reduced the computed bond length by 0.15 Å to 2.29 Å [366], and increased D_e by 0.1 eV. The further expansion of the number of correlated electrons to include the $3p$ was found to have little effect on either the dissociation energy or

Table 4–4: Previous theoretical work on the ground state of Cu_2

Method	Basis	r_e[a]	D_e[b,c]	Ref.
numerical-HF		2.447	0.52	Partridge *et al.* [369]
SCF	$(15s11p6d2f)/[9s6p4d2f]$	2.44 (2.39)	0.51 (0.58)	Werner and Martin [372]
CISD+Q[d]	$(15s11p6d2f)/[9s6p4d2f]$	2.28 (2.24)	1.14 (1.24)	Werner and Martin [372]
CEPA-1	$(15s11p6d2f)/[9s6p4d2f]$	2.37 (2.24)	1.69 (1.80)	Werner and Martin [372]
SCF	$(14s11p6d3f)/[8s6p4d2f]$	2.423	0.56	Scharf *et al.* [371]
CPF	$(14s11p6d3f)/[8s6p4d2f]$	2.28 (2.24)	1.727 (1.841)	Scharf *et al.* [371]
CPF	$(14s11p6d)/[8s6p4d]$	2.297	1.766	Langhoff *et al.* [377]
CPF	$(14s11p6d4f)/[8s6p4d3f]$	2.267	1.789	Langhoff *et al.* [377]
CPF	$(14s11p6d4f1g)/[8s6p4d3f1g]$	2.260	1.806	Langhoff *et al.* [377]
SCF	$(14s11p6d2f)/[6s5p3d1f]$	2.400	0.52	Raghavachari *et al.* [366]
CISD+Q[d]	$(14s11p6d2f)/[6s5p3d1f]$	2.270	1.76	Raghavachari *et al.* [366]

[a] internuclear separation in Å.

[b] terms in parentheses include relativistic correction.

[c] dissociation energy in eV.

[d] includes Davidson correction.

the bond length [365]. The inclusion of the *d* electrons is required by the necessity of including correlation *d-d* to describe the repulsion of the *d* cores and allow the closer approach of the nuclei. Excellent results have been obtained by treating Cu_2 as a two electron system, describing the "core" using a psuedopotential and including core-valence polarisation through perturbation theory [378–380]

Much discussion has centred on the importance of the inclusion of *f*-functions in the basis set, and the relative contributions of tight and diffuse functions [366, 367, 377, 381]. The extension of the basis set to include *f*-functions is found to be desirable in that it leads to an increase in percentage of the *d-s* correlation obtained. This is important since it is differential over the potential energy surface, increasing the well depth and decreasing the bond length. In the atom, the increased correlation of the *d* orbitals afforded by the extension of the basis set to include *f*-functions, leads to an increase in the "size" of the *d* orbitals, as measured by their expectation value $\langle r_{3d}^2 \rangle$, and a reduction in the size of the 4*s* orbital due to the reduced shielding of the nucleus [382]. Langhoff *et al.* [377] found that the inclusion of *f* orbitals lead to a reduction in the calculated bond length of 0.03 Å.

Several authors have noted the problem of size consistency when correlating such a large number of electrons (in this case 22) when using truncated CI. The inclusion of higher excitations, *eg* through the Davidson [63] correction, results in an reduction of the computed bond length of about 0.03 Å, and an increase in the value of D_e by up to 0.2 eV. This has been attributed to the difficulty in describing the *d-d* correlation at large internuclear separations and the resulting error swamping the differential *s-d* correlation [375]. The size consistency problem is reduced, though not removed, through the use of multireference CI; Raghavachari *et al.* [366] obtained r_e=2.27 Å and D_e=1.76 eV, in error with respect to experiment by 0.03 Å and 0.3 eV, using a reference space for SDCI consisting of the double excitations from the $4s\sigma_g$ HOMO into $4s\sigma_u$, and the various 4*p* based orbitals. Bauschlicher [383] suggested that the neglect of the *d-d* correlation would remove this swamping effect. Employing a modified CI method with the restriction that only one electron could be excited from the 3*d*-shell on each atom 1.99 eV, was obtained for the dissociation energy; the bond length of

2.35 Å, was however significantly poorer than that calculated using SDCI. Fully size-consistent methods, such as the coupled pair functional (CPF), the coupled electron pair approximated (CEPA), and coupled cluster techniques, yield shorter bond lengths and greater dissociation energies than CISD [366, 371, 372, 377, 384], the average in bond length being approximately 2.27 Å [372].

The importance of including the effect of relativity for reproducing accurately the experimental bond length of Cu_2 was demonstrated by Pelissier [385] who using CI with relativistic effective core potentials obtained an r_e of 2.25 Å[4], ~0.05 Å shorter than non-relativistic all-electron calculations. The contraction of the atomic 4*s* orbital on taking into account relativistic effects was reported by Desclaux [341] as ~0.035 Å at the SCF level. Martin [374] included the relativistic effects, as the first-order correction arising from the Cowan-Griffin operator [386], on the basis of a two-reference MCSCF wavefunction. This led to a bond shortening of ~0.05 Å (from 2.48 to 2.42 Å). A slightly smaller correction of 0.04 Å is obtained for the correlated wavefunction, for both SDCI and various size consistent methods [371, 372]. The reduction is primarily through the mass-velocity stabilisation of the kinetic energy in the 4*s*-4*s* bond [372]. The dissociation energy is increased by approximately 0.1 eV [371].

Density functional treatments based on various local [387–391] and non-local [392] exchange functionals have also been applied successfully to the ground state of the copper dimer. The various local-spin-density (LSD) approximation calculations give results for the bond length in good agreement with experiment, r_e lying in the range 2.17 to 2.28 Å, despite the exclusion of the relativistic effects which are found to be important in *ab initio* work. There is a tendency for these methods to overestimate the binding energy, $2.10 < D_e < 2.65$ eV [387–391]. In a review, Jones and Gunnarsson [393] reported that the best results for the spectroscopic constants were obtained with the X_α method, and not the more refined electron gas functionals. Delley *et al.* [388] computed a bond length of

---

[4]Due to an omission in the original paper it was long believed that this calculation was non-relativistic [373].

2.22 Å, and a dissociation energy of 2.10 eV employing X_α with a numerical basis. Painter and Averill [389] put the apparent superiority of X_α in the computation of D_e down to the fortuitous cancellation of errors in the atom and dimer. They also pointed out that LSD methods tend to favour energetically the d electrons, and, furthermore, that the short bond lengths were consistent with the reduced Wigner-Seitz radii found in LSD approximation calculations for the crystals of first series transition metals. It is indicative of the preference for d bonding associated with these methods, that strong interactions are found between the $4s$ and $3d\sigma$ orbitals. This results in a substantial increase in the stabilisation of the $4s$-$4s$ bond, and significant σ bonding for the d orbitals. The $4s\sigma_g$ MO is predicted to lie below the $3d$ band and the $4s\sigma_u$ MO is found embedded in the $3d$ band, whilst the HOMO is $3d\sigma_u$[389, 390]. Despite this the first IP is still predicted to be due to the removal of an s electron. Ziegler *et al.* [394] have shown that relativistic effects in LSD-X_α calculations result in a reduction of r_e of 0.02 Å (2.26 to 2.24 Å). With the inclusion of this correction, the tendency of the LSD results to give bond lengths shorter than experiment is increased. Much of the discrepancy between the density functional and *ab initio* results is removed when a non-local approach, such as the generalised gradient approximation (GGA), is used. Kobayashi *et al.* [392] obtained an increase in the bond length of 0.07 Å (2.18 to 2.25 Å) and a decrease in D_e of 0.4 eV (2.60 to 2.20 eV) on moving from LSD to GGA, bringing the results into good agreement with high level *ab initio* calculations, and into excellent agreement with experiment, if the relativistic bond shortening of Ziegler [394] is included.

A smaller body of work exists for the excited states [27, 389, 395–399], which is certainly not at the same level of computation as that of the ground state. As many of the calculations were performed before the positive experimental identification of the A-state as $^1\Sigma_u^+$ and the C-state as $^1\Pi_u$ the results will be reinterpreted in the light of these findings.

The most extensive work is that of Witko and Beckmann [398], who calculated the potential energy surfaces of the most of the states arising from the ^2S+^2S and ^2S+^2D asymptotes at the CI level using a basis set of DZ quality. On the basis of

Table 4–5: Previous theoretical work on the excited states of Cu_2

State	Semiempirical				Non-empirical			
Hund's (a)	Anderson[a]		Amos[b]	Ozin[c]	Joyes[d]	Miyoshi[e]	Witko[f]	Painter[g]
	A	**B**						
$^3\Sigma_u^+(s\sigma_g \rightarrow s\sigma_u^*)$						1.09	1.89	
$^3\Sigma_g^+(d\sigma_u \rightarrow s\sigma_u^*)$							2.82	
$^3\Pi_u(d\pi_g \rightarrow s\sigma_u^*)$						~2.4	3.02	
$^1\Sigma_u^+(s\sigma_g \rightarrow s\sigma_u^*)$	2.41	2.15	2.26	3.29	~4	2.41	3.09	2.12 2.31
$^1\Sigma_g^+(d\sigma_u \rightarrow s\sigma_u^*)$				2.55			3.13	
$^3\Delta_g(d\delta_u \rightarrow s\sigma_u^*)$							3.27	
$^1\Pi_u(d\pi_g \rightarrow s\sigma_u^*)$	2.85	2.18	2.54	2.99		~2.4	3.29	2.30 2.50
$^3\Sigma_u^+(d\sigma_g \rightarrow s\sigma_u^*)$							3.50	
$^3\Delta_u(d\delta_g \rightarrow s\sigma_u^*)$							3.53	
$^1\Delta_u(d\delta_g \rightarrow s\sigma_u^*)$			3.01				4.03	
$^3\Pi_g(d\pi_u \rightarrow s\sigma_u^*)$							4.37	
$^1\Delta_g(d\delta_u \rightarrow s\sigma_u^*)$			2.85				4.39	
$^1\Pi_g(d\pi_u \rightarrow s\sigma_u^*)$			3.40				4.37	
$^1\Sigma_u^+(d\sigma_g \rightarrow s\sigma_u^*)$	3.59	2.85	3.78					
$^1\Pi_u(s\sigma_g \rightarrow p\pi_u^*)$	4.38	4.05	4.31	4.61				
$^1\Sigma_u^+(d\pi_u \rightarrow p\pi_g^*)$	4.81	4.24	4.59	4.36				
$^1\Sigma_u^+(d\sigma_u \rightarrow p\sigma_g^*)$	5.44	4.76	4.60	5.42				
$^1\Phi_u(d\delta_u \rightarrow p\pi_g^*)$	5.16	4.43	5.06	4.89				

The energies are in eV.

[a] [396];[b] [399];[c] [397]; [d] [395];[e] [27];[f] [398]; [g] [389]. See text for further details.

their results the authors identified the experimental *A*- and *B*- states as $^1\Sigma_u^+$, arising from $4s\sigma_g \rightarrow 4s\sigma_u^*$ at short bond lengths, and $^1\Pi_u$, from $3d\pi_g \rightarrow 4s\sigma_u^*$, although the computed separation of 0.20 eV between the states was small enough that the ordering could not be determined. The lowest $^1\Sigma_u^+$ was found to change character from predominantly $4s\sigma_g^1 4s\sigma_u^1$ in the bonding region to $3d\sigma_g^3 4s\sigma_u^1$ at longer bond lengths. The $^3\Pi_u$ state is placed at 3.02 eV, below the $^1\Sigma_u^+$, consistent with the assignment of either the *A*- or the *B*-state to the 0_u^+ component of this state. Although the $^1\Sigma_u^+$ corresponding to $3d\sigma_g^1 4s\sigma_u^1$ was not computed, the corresponding triplet is placed at 3.50 eV, arguing against this being the *A* or *B*. With the assignment of the *A*-, *B*- *C*- states as being due to $^3\Pi_u(3d\pi_g^3 4s\sigma_u^1)$, $^1\Sigma_u^+(4s\sigma_g 4s\sigma_u^1)$,

and $^1\Pi_u(3d\pi_g^3 4s\sigma_u^1)$, a consistent pictures is obtained with respect to experiment. The $^3\Sigma_u^+$ derived from the $^2S+^2S$ asymptote is predicted at 1.89 eV in excellent agreement with the findings of Bondybey [360].

In the early 1970s Joyes and Leleyter [395] performed LCAO-STO-SCF calculations for the $^{1,3}\Sigma_g^+$ and $^{1,3}\Sigma_u^+$ states arising for the $^2S+^2S$ asymptotes associated with the atomic ground states, cations, and anions. The ion-pair limit was found to give rise to a $^1\Sigma_u^+$ state at 4 eV. The $^3\Sigma_u^+$ complement of the ground state was repulsive in nature.

Miyoshi *et al.* [27] used the ΔSCF method to obtained excitation energies for the lowest $^{1,3}\Sigma_u^+$ and $^{1,3}\Pi_u$ states. The $^1\Sigma_u^+$ state arising from the $s\sigma_g \rightarrow s\sigma_u^*$ excitation was predicted at 2.41 eV, and the $^{1,3}\Pi_u(3d\pi_g^3 4s\sigma_u^1)$ at 4.07 and 4.21 eV. The energy of the $^1\Sigma_u^+$ state is close the *A*- and *B*-states, however the energy of the $^{1,3}\Pi_u$ would argue against the assignment of these to either of the experimental states. Considerable lowering of the excitation energy was found when the symmetry was broken, allowing the localisation of the *d*-hole onto one of the copper atoms. Moving from $D_{\infty h}$ to $C_{\infty v}$ brought both the $^3\Pi_u$ and $^1\Pi_u$ below the $^1\Sigma_u^+$, 1.24 and 1.46 eV. The figures quoted in Table 4–5 were then obtained including an empirical correction, noting that the SCF procedure placed the ^2D state of the atom below the ^2S. The new energies of ~2.4 eV are in good agreement with experiment. The reorganisation energies associated with the localisation of the resulting hole upon ionisation from the 4*s* and 3*d* shells in the dimer were also calculated. The effect was found to be small (0.4 eV) for the 4*s* shell, and much larger for the loss of a *d* electron (5.7-6.2 eV) in agreement with the earlier work of Cox *et al.* [26].

Although the density functional method is not strictly formulated for states other than the ground state, reasonable transition energies have been obtained for excited states which are the lowest for a particular set of quantum numbers. Painter and Averill applied two functionals, LSD-X_α and VWM, to the calculation of the $^1\Sigma_u^+(4s\sigma_g^1 4s\sigma_u^1)$ and $^1\Pi_u(3d\pi_g^3 4s\sigma_u^1)$ states [389]. The $^1\Sigma_u^+$ was placed below the $^1\Pi_u$ by approximately 0.2 eV, again suggesting that if the $^1(s\sigma_u, s\sigma_u^*)$ is to be found in the same energy region as the *A*- and *B*-states.

The remaining published work on the excited states of dicopper is semi-empirical and for the most part only includes the calculation of singlet states. The three studies quoted here extend the theoretical treatment to include transitions to $4p$ based MOs [396, 397, 399].

Ozin *et al.* [397] applied the SCF-X_α-SW method parameterised for the calculation of excitation energies. On the basis of these results, the A-state was assigned to $d\pi_g \rightarrow s\sigma_u^*$ and the B-state to $s\sigma_g \rightarrow s\sigma_u^*$. Also calculated were the states due to the $^2P^0$ atomic limit which were found in the 4.3-5.4 eV range.

Extended Hückel Theory (EHT) calculations have been performed by several groups [396, 399]. The earliest by Anderson [396] found the $^1\Sigma_u^+(4s\sigma_g^1 4s\sigma_u^1)$ state to be dissociative in nature, corresponding to the $^2S+^2S$ separated atom limit. The restrictions placed upon the wavefunction by the requirement of antisymmetry with respect to the interchange of electrons means that this is an un-physical result, there is not a $^1\Sigma_u^+$ state that corresponds to these limits (Section 4.3). The technique for the calculation of the singlet-singlet excitation energies involves the determination of the singlet-triplet energy and the energy of the average transition to the singlet or triplet state, hence the $^1\Sigma_u^+$ behavior reported by Anderson is an artifact of the method of computation, mirroring the real behavior of the corresponding $^3\Sigma_u^+$ state. With a supposedly nonbonding $^1(s\sigma_g, s\sigma_u^*)$, and the separation between the $^1\Sigma_u^+(3d\sigma_g^1 4s\sigma_u^1)$ and the $^1\Pi_u(3d\pi_g^3 4s\sigma_u^1)$ states of ~0.7 eV (2.85 as compared to 3.59 eV) far larger than the respective difference in the low-lying experimental states, Anderson assigned the A- and B-state to be the 0_u^+ and 1_u of the $^3\Pi_u$. The lowest transition to a $4p$ based MO was placed at 4.38 eV, corresponding to $^1\Pi_u(s\sigma_g \rightarrow p\pi_u^*)$. A second series of calculations was also performed using a value for the IP of the d orbitals lowered by 0.7 eV; this result is also listed, as B in Table 4–5. The agreement obtained between theory and experiment is good for the lower states, although this may be due to the use of relatively accurate experimental data. The validity of the findings for higher states must remain questionable, as it must for a calculations of this type, due to the lack of good experimental data on which to base the state energetics. In order to tackle this shortcoming, Amos *et al.* [399] included parameters from theoretical calcula-

tions [397]. The $s\sigma_g \rightarrow s\sigma_u^*$ transition is again placed at a lower energy than the $d\pi_g \rightarrow s\sigma_u^*$, with the $d\sigma_g \rightarrow s\sigma_u^*$ at considerably higher energy. The states involving $^2P^0$ are computed in the range 4.3-5.1 eV, with the lowest, due to $s\sigma_g \rightarrow p\pi_u^*$ at 4.31 eV. Again the calculation is only as good as the parameters used in defining the problem, therefore the same reservations are expressed regarding the results of Amos *et al.* as apply to the earlier work of Anderson.

Although the theoretical work does not reproduce accurately the experimental excitation energies, strong evidence is found in many of the calculations that either the *A*- or the *B*-state is due to the intrusion of a state with a higher energy asymptote. The semi-empirical results would seem to suggest that this state is not from the $^2S+^2P^0$ or $^2D+^2P^0$, but is rather a state which corresponds to the ion-pair limit as predicted by Witko and Beckmann [398].

4.5 The present study

Preliminary investigations of the excited states of dicopper were performed at 2.20 Å. The choice of 2.20 Å, whilst arbitrary, was made after a survey showed that operating at r_e for the basis set at the SCF-level, would have led to a bond length near 2.4 Å, unacceptably long.

4.5.1 Basis sets

The choice of basis set for the calculation of excitation energies is an art rather than a science; in the case of dicopper the chosen basis set must be flexible enough in the valence space to describe the radically different distributions that arise when the *d* shell is opened up, and return approximately the same percentage of the total correlation energy for each of the states of interest. The *spd* portion of the present basis set is obtained from a $11s8p4d$ contraction of a $15s11p6d$ Gaussian-type orbital basis set, generated by adding a single *s* function, α_s=0.33 to span the large gap between the functions used to describe the 3*s* and 4*s* orbitals [377],

and the diffuse d function (α_d=0.1491) of Hay [400] to Wachters' 14s11p5d basis set [401][5]. The contraction schemes used were 51111111111 for s, 41111111 for p, and 3111 for d; leading to a total of 118 GTOs.The 6d/4d contraction of the d set is as recommended by Langhoff and Bauschlicher for the description of the ground state and to obtain the $d^2 \rightarrow (d')^2$ component of the d-d correlation energy. Also it is noted that the Wachters found that the optimal exponents for the description of the ^2D state of atomic copper were significantly different from those for the ^2S.

The inclusion of f functions in the basis set has been found to be important for the computation of the properties of the ground state of the copper dimer, resulting in a decrease in the bond length and an increase in the dissociation energy (Section 4.4). Two important forms of correlation involve these functions, $sd \rightarrow p'f'$ (s-d correlation) and $d^2 \rightarrow f^2$ (a further component of d-d correlation). Jordan and co-workers [366, 367, 382] demonstrated that a good description of the s-d correlation was required for the accurate determination of the ionisation potentials and excitation energies of atomic copper. The major component of the correlation energy of the Cu atom is due to transitions from the d MOs, ~92 % [402]. Although non-differential for the ground state of Cu_2, d-d correlation is found to be very important for those transition metals with unfilled d shells, and especially when comparisons are made between states with different d occupancies [403]. The basic spd basis set was therefore supplemented with f polarisation functions. In total three exponents were employed for the f functions either singly or in combination, with values 0.40, 0.3375, and 2.89. Calculations were performed for the following basis sets; 11s8p4d, 11s8p4d1f(0.40), 11s8p4d1f(1.3375), 11s8p4d1f(2.89), 11s8p4d2f(0.40,1.3375), and 11s8p4d2f(0.40,2.89). The inclusion of a single f function results in a basis set dimension of 138 GTOs, and two f functions in 158 GTOs.

The most diffuse function, α_f=0.40, is that recommended by Langhoff and Bauschlicher [377] and is similar to the more diffuse of the pair of functions used by

---

[5] 14s9p5d augmented by the two p functions optimised for Cu(^2P) and scaled for the molecule.

Sunil and Jordan [382] for the description of $ds \rightarrow f'p'$ correlation (two exponents of 1.48 and 0.37) in Cu. The α_f=1.3375 is the lowest exponent member of the STO-3G for a $4f$ with exponent 5.0, optimised for the energy of the Cu atomic ground state [365]. The value is similar to the tighter of the pair of functions of Sunil and Jordan for *s-d* correlation, and to the diffuse member of the pair of functions recommended by the same authors for *d-d* correlation (1.32 and 5.28). Although the α_f=1.3375 was originally included to provide the $d^2 \rightarrow f^2$ correlation, it was pointed out to the author [404] that the exponent was probably too low for the purpose. The other function, α_f=2.89, is as used in the computation of the excited states of CuO by Hippe *et al.* [405], this exponent is close to the 2.64 recommended by Sunil and Jordan for the Cu atom, although lower than the 3.49 reported by Werner and Martin [372].

The s components of the Cartesian d functions ($d_{x^2+y^2+z^2}$) and the p components of the Cartesian f functions (f_{xxx}, f_{yyy}, and f_{zzz}) are retained. This results in four additional s and one p set for each f included in the calculation.

4.5.2 SCF calculations and discussion

The MO and total SCF energies of the copper dimer at 2.20 Å are listed in Table 4–6. The addition of the f functions is found, unsurprisingly, to have negligible effect on the MO energies. The lowering in the total energy is larger than that reported by Sunil *et al.* [367] for the addition of a single f function [6]. Whether the changes observed are due to shifts in the potential surface energy or in the position of the minima cannot of course be determined from a single point calculation. Analysis of the Mulliken electron populations shows that the f functions play only a minor role in the SCF wavefunction, the largest population, mostly negative, occurring for the α_f=2.89 function, which has the largest overlap with the d orbitals. The 1.3375 leads to a small positive population.

---

[6] Calculation performed at 2.22 Å.

Table 4–6: SCF-MO energies of the Cu_2 ground state at 2.20Å as calculated with various basis sets (au)

	Basis set					
	$11s8p4d$		$11s8p4d1f$		$11s8p4d2f$	
MO		(0.40)[a]	(1.3375)[a]	(2.89)[a]	(1.3375,0.40)[a]	(2.89,0.40)[a]
$1s\sigma_u$	-328.7971	-328.7970	-328.7969	-328.7971	-328.7968	-328.7969
$1s\sigma_g$	-328.7971	-328.7970	-328.7969	-328.7971	-328.7968	-328.7969
$2s\sigma_u$	-40.8226	-40.8225	-40.8224	-40.8225	-40.8223	-40.8224
$2s\sigma_g$	-40.8226	-40.8225	-40.8224	-40.8225	-40.8223	-40.8224
$2p\sigma_u$	-35.6230	-35.6229	-35.6227	-35.6229	-35.6226	-35.6227
$2p\sigma_g$	-35.6230	-35.6229	-35.6227	-35.6229	-35.6226	-35.6227
$2p\pi_u$	-35.6228	-35.6227	-35.6226	-35.6228	-35.6225	-35.6226
$2p\pi_g$	-35.6228	-35.6227	-35.6226	-35.6228	-35.6225	-35.6226
$3s\sigma_g$	-5.0086	-5.0085	-5.0083	-5.0084	-5.0082	-5.0083
$3s\sigma_u$	-5.0077	-5.0076	-5.0073	-5.0074	-5.0073	-5.0074
$3p\sigma_g$	-3.3257	-3.3256	-3.3254	-3.3255	-3.3254	-3.3254
$3p\pi_u$	-3.3187	-3.3186	-3.3185	-3.3186	-3.3184	-3.3185
$3p\pi_g$	-3.3181	-3.3180	-3.3179	-3.3180	-3.3178	-3.3179
$3p\sigma_u$	-3.3181	-3.3181	-3.3178	-3.3179	-3.3178	-3.3178
$3d\sigma_g$	-0.5120	-0.5119	-0.5117	-0.5118	-0.5118	-0.5117
$3d\pi_u$	-0.4993	-0.4992	-0.4991	-0.4992	-0.4990	-0.4991
$3d\delta_g$	-0.4815	-0.4813	-0.4812	-0.4813	-0.4811	-0.4812
$3d\delta_u$	-0.4737	-0.4736	-0.4735	-0.4736	-0.4734	-0.4735
$3d\pi_g$	-0.4590	-0.4589	-0.4586	-0.4588	-0.4586	-0.4587
$3d\sigma_u$	-0.4492	-0.4493	-0.4488	-0.4490	-0.4490	-0.4491
$4s\sigma_g$	-0.2365	-0.2370	-0.2371	-0.2368	-0.2373	-0.2372
$4s\sigma_u$	0.0180	0.0184	0.0187	0.0184	0.0188	0.0187
$4p\pi_u$	0.0823	0.0776	0.0817	0.0820	0.0777	0.0777
$4p\sigma_g$	0.1056	0.1013	0.1045	0.1050	0.1012	0.1012
$4p\pi_g$	0.1706	0.1606	0.1693	0.1700	0.1607	0.1607
energy[b]	-0.79034	-0.79762	-0.80064	-0.79731	-0.80549	-0.79035

[a] f-functions.

[b] total energy, E+3277 au.

Using the $11s8p4d2f(2.89, 0.40)$ basis set, SCF open-shell calculations were performed for some of the low-lying excited states. The ordering of the states, $^3\Sigma_u^+(4s\sigma_g, 4s\sigma_u^*) <^1 \Sigma_u^+(4s\sigma_g, 4s\sigma_u^*) <^3 \Pi_u(3d\pi_g, 4s\sigma_u^*) <^1 \Pi_u(3d\pi_g, 4s\sigma_u^*) <^1 \Delta_u$ $(3d\delta_g, 4s\sigma_u^*)$ and the excitation energies obtained, Table 4–7, are in good agreement with those of Miyoshi *et al.* [27] as calculated under $D_{\infty h}$ symmetry.

Comparison of the SCF-MO energies (Table 4–7) shows that the core orbitals are slightly stabilised (~0.15 au) by the removal of a *d* electron. This reflects the reduction in the penetration of the core by the 4*s* electrons due to the contraction of the 3*d* shell, and is consistent with the findings of Wachters [401] for the atom. This core-valence effect, which would be further altered by the inclusion of relativistic effects, could cause difficulties in the post-HF treatments which employ a "frozen" core to reduce the dimension of the calculation. A change of similar magnitude is observed for the fully occupied 3*d* MOs, whilst the open shells and their complements experience smaller shifts. Again this is synonymous with the presence of a large degree of reorganisation upon excitation.

A crude estimate of the bonding interaction in the *d* shell can be obtained by comparing the separation of the bonding/antibonding pairs of orbitals with the ground state, Table 4–8. For the $^1\Pi_u$ and $^1\Delta_u$ a change in the separation of ~0.06 au is obtained. The slightly larger effect shown for the $^1\Pi_u$ reflects the larger orbital overlap relative of the π relative to the δ. The 3*d* orbitals for the $^{1,3}\Pi_u$ are found to have similar energies. A smaller lowering of the energies of the 3*d* and core MOs for the $^1, 3\Sigma_u^+$ states.

The results of the Mulliken analysis of the SCF wavefunction has been used to indicate the nature of the orbitals. The population distribution for all and the unpaired electrons are given in Table 4–9. Comparisons using the ground state as the model of a closed *d* shell, and the $^3\Sigma_u^+$ as a valence $4s\sigma_g^1 4s\sigma_u^1$ state, allow conclusions to be drawn on the ion-pair nature of the $^1\Sigma_u^+$. The populations of the *s* and *p* AOs for the ground state demonstrate the degree of polarisation, through the inclusion of *p* character for the $4s\sigma_g$ MO. The $^1\Sigma_u^+$ ion-pair has significantly more *p* character (+0.33*e*) than the $^3\Sigma_u^+$, predominantly by replacement of 4*s* electrons. The molecular states corresponding to the $^2S+^2D$ asymptote have more

Table 4–7: SCF MOs and occupation numbers for dicopper at 2.20 Å using the $11s8p4d2f(2.89, 0.40)$ basis (au)

	State					
MO	$^1\Sigma_g^+$	$^1\Sigma_u$	$^3\Sigma_u$	$^1\Pi_u$	$^3\Pi_u$	$^1\Delta_u$
1 ($1s\sigma_u$)	-328.7969 (2)	-328.8397 (2)	-328.8330 (2)	-328.9527 (2)	-328.9514 (2)	-328.9448 (2)
2 ($1s\sigma_g$)	-328.7969 (2)	-328.8397 (2)	-328.8330 (2)	-328.9527 (2)	-328.9514 (2)	-328.9448 (2)
3 ($2s\sigma_u$)	-40.8224 (2)	-40.8642 (2)	-40.8576 (2)	-40.9903 (2)	-40.9893 (2)	-40.9818 (2)
4 ($2s\sigma_g$)	-40.8224 (2)	-40.8642 (2)	-40.8576 (2)	-40.9903 (2)	-40.9893 (2)	-40.9818 (2)
5 ($2p\sigma_u$)	-35.6227 (2)	-35.6652 (2)	-35.6588 (2)	-35.7926 (2)	-35.7916 (2)	-35.7724 (2)
6 ($2p\sigma_g$)	-35.6227 (2)	-35.6652 (2)	-35.6588 (2)	-35.7926 (2)	-35.7916 (2)	-35.7724 (2)
7 ($2p\pi_g$)	-35.6226 (4)	-35.6648 (4)	-35.6578 (4)	-35.7864 (4)	-35.7854 (4)	-35.7839 (4)
9 ($2p\pi_u$)	-35.6226 (4)	-35.6648 (4)	-35.6578 (4)	-35.7864 (4)	-35.7854 (4)	-35.7839 (4)
11 ($3s\sigma_g$)	-5.0083 (2)	-5.0509 (2)	-5.0445 (2)	-5.1640 (2)	-5.1626 (2)	-5.1574 (2)
12 ($3s\sigma_u$)	-5.0074 (2)	-5.0499 (2)	-5.0435 (2)	-5.1630 (2)	-5.1616 (2)	-5.1566 (2)
13 ($3p\sigma_g$)	-3.3254 (2)	-3.3686 (2)	-3.3619 (2)	-3.4757 (2)	-3.4742 (2)	-3.4613 (2)
15 ($3p\pi_u$)	-3.3185 (4)	-3.3627 (4)	-3.3555 (4)	-3.4654 (4)	-3.4639 (4)	-3.4626 (4)
17 ($3p\pi_g$)	-3.3179 (4)	-3.3622 (4)	-3.3550 (4)	-3.4640 (4)	-3.4625 (4)	-3.4627 (4)
18 ($3p\sigma_u$)	-3.3178 (2)	-3.3610 (2)	-3.3542 (2)	-3.4677 (2)	-3.4661 (2)	-3.4542 (2)
19 ($3d\sigma_g$)	-0.5117 (2)	-0.5556 (2)	-0.5535 (2)	-0.6751 (2)	-0.6736 (2)	-0.6435 (2)
20 ($3d\pi_u$)	-0.4991 (4)	-0.5438 (4)	-0.5378 (4)	-0.5627 (4)	-0.5605 (4)	-0.6374 (4)
22 ($3d\delta_g$)	-0.4812 (4)	-0.5261 (4)	-0.5185 (4)	-0.6277 (4)	-0.6261 (4)	-0.4955 (3)
24 ($3d\delta_u$)	-0.4735 (4)	-0.5184 (4)	-0.5106 (4)	-0.6214 (4)	-0.6198 (4)	-0.5471 (4)
26 ($3d\pi_g$)	-0.4587 (4)	-0.5018 (4)	-0.4946 (4)	-0.4601 (3)	-0.4580 (3)	-0.6014 (4)
28 ($3d\sigma_u$)	-0.4491 (2)	-0.4881 (2)	-0.4830 (2)	-0.6172 (2)	-0.6156 (2)	-0.5829 (2)
29 ($4s\sigma_g$)	-0.2372 (2)	-0.3020 (1)	-0.3265 (1)	-0.3193 (2)	-0.3182 (2)	-0.3185 (2)
30 ($4s\sigma_u$)	0.0187 (0)	-0.1294 (1)	-0.1828 (1)	-0.1939 (2)	-0.2007 (2)	-0.1924 (1)
31 ($4p\pi_u$)	0.0777 (0)	0.0628 (0)	0.0641 (0)	0.0516 (0)	0.0526 (0)	0.0487 (0)
33 ($4p\sigma_g$)	0.1012 (0)	0.0625 (0)	0.0909 (0)	0.0687 (0)	0.0698 (0)	0.0713 (0)
34 ($4p\pi_g$)	0.1607 (0)	0.1432 (0)	0.1469 (0)	0.1395 (0)	0.1406 (0)	0.1384 (0)
Total Energy	-3277.79035	-3277.69282	-3277.74207	-3277.63959	-3277.64607	-3277.60834
Excitation energy (eV)	0.0000	2.6538	1.3137	4.1022	3.9259	4.9526

Table 4–8: Separation of d orbitals in dicopper (au)

MOs	State		
	$^1\Sigma_u^+$	$^1\Pi$	$^1\Sigma_u$
$3d\sigma_g - 3d\sigma_u$	-0.0626	-0.0579	-0.0606
$3d\pi_g - 3d\pi_u$	-0.0404	-0.1026	-0.0460
$3d\delta_g - 3d\delta_u$	-0.0087	-0.0063	+0.0516

p character, associated with the occupation of the $4s\sigma_u$ orbital, and f character than the ground state, although the changes are small. The majority of this f character is due to the tighter (higher exponent) function.

Table 4–9: Population analysis at the SCF level for all and unpaired electrons

State	Population			
	s	p	d	f
$^1\Sigma_g^+$	13.7240	24.2332	19.8658	0.1770
$^3\Sigma_u^+$	13.7856	24.1924	19.8366	0.1854
	1.8335	0.1506	0.0052	0.0106
$^1\Sigma_u^+$	13.4638	24.5125	19.8366	0.1854
	1.4471	0.4767	0.0128	0.0334
$^3\Pi_u$	14.5726	24.3816	18.8368	0.2090
	0.7921	0.2188	2.9822	0.0068
$^1\Pi_u$	14.5673	24.3981	18.8252	0.2094
	0.8000	0.2115	2.9817	0.0066
$^1\Delta_u$	14.6462	24.3049	18.8149	0.2340
	0.9417	0.1834	2.8704	0.0064

4.5.3 Direct-CI calculations

The details of the direct-CI calculation are given in Table 4–10. In the present work the eighteen core MOs associated with the $1 - 3s$, $2 - 3p$ are frozen at

the SCF level of treatment, also the MOs corresponding to the core complements and the highest p set and three s sets were discarded in aufbau order. This leads to a total of 70 active MOs for the $11s8p4d$ basis set (the active space consist of 6s, 3p, and 4d MOs), 90 for $11s8p4d1f$ (6s, 4p, 4d, and 1f), and 110 for $11s8p4d2d$ (6s, 5p, 4d, and 2f). The active space is divided into internal and external spaces. The internal space consists of the $3d$ and $4s$ based MOs, 22 electrons in 12 MOs. All the configurations, in the internal space, with the appropriate spin and symmetry were employed as reference functions. The choice of the internal space, and hence the reference configurations, is effectively dictated by the dimensions of the calculations, the present internal space results in up to eighteen reference configurations, and over 2,000,000 CSFs for the larger basis sets. The omission of the $s^2 \rightarrow p^2$ configurations is unfortunate, especially as they have been found to be important in the description of the molecular ground state [365], however, as previously stated, *d-d* correlation is found to have an important contribution to the relative energies of states with different d shell occupancies, therefore it was felt to be necessary that the increased participation of the d-shell be accurately represented.

Calculations were performed for the various basis sets, at 2.20 Å on the singlet Π, and Δ states arising from the $^2S+^2D$ atomic asymptotes, and the Σ_u corresponding to $4s\sigma_u^1 4s\sigma_g^1$ occupancy. These computations used the MOs from the ground state SCF wavefunction. The active space employed was as defined above. This work was performed largely to investigate the effects of the f-functions on the excitation energies. The remaining *ungerade* states arising from the $^2S+^2D$ asymptote were calculated using the $11s8p4d2f(2.89, 0.40)$ basis set, which was found to offer the best description of the excited states.

Additional calculations were performed for the $^{1,3}\Sigma_u^+(4s\sigma_g, 4s\sigma_u)$, $^{1,3}\Pi_u(3d\pi_g, 4s\sigma_u)$, and $^1\Delta_u(3d\delta_g, 4s\sigma_u)$ utilising the MOs from the corresponding open-shell SCF calculations. These will be referred to as parental MO calculations to differentiate them from the computations employing the closed shell ground state MOs. This allows study of the degree of reorganisation associated with the transitions, and thus the feasibility of employing a common MO set in describing these

Table 4–10: Details of direct CI for Cu_2

State	Basis	MO set	Active space int.	Active space ext.	Ref.	C^{2a}	CSFs
$^1\Sigma_g^+$	$11s8p4d2f$(2.89,0.40)	$^1\Sigma_g^+$	12	78	18	0.901	2327260
		$^1\Sigma_g^+$	12	78	18	0.895	1475824
		$^1\Sigma_g^+$	12	66	18	0.886	1057384
	$11s8p4d2f$(1.3375,0.40)	$^1\Sigma_g^+$	12	98	18	0.896	2327260
	$11s8p4d1f$(2.89)	$^1\Sigma_g^+$	12	78	18	0.909	1475824
	$11s8p4d1f$(1.3375)	$^1\Sigma_g^+$	12	78	18	0.901	1475824
	$11s8p4d1f$(0.40)	$^1\Sigma_g^+$	12	78	18	0.895	1475824
	$11s8p4d$	$^1\Sigma_g^+$	12	58	18	0.903	817564
$^1\Sigma_u^+$	$11s8p4d2f$(2.89,0.40)	$^1\Sigma_g^+$	12	98	12	0.894	2324755
		$^1\Sigma_u^+$	12	98	12	0.901	2324755
		$^1\Sigma_g^+$	12	78	12	0.883	1473829
	$11s8p4d2f$(1.3375,0.40)	$^1\Sigma_g^+$	12	98	12	0.888	2324755
	$11s8p4d1f$(2.89)	$^1\Sigma_g^+$	12	78	12	0.900	1473829
	$11s8p4d1f$(1.3375)	$^1\Sigma_g^+$	12	78	12	0.892	1473829
	$11s8p4d1f$(0.40)	$^1\Sigma_g^+$	12	78	12	0.895	1473829
	$11s8p4d$	$^1\Sigma_g^+$	12	58	12	0.888	816079
$^3\Sigma_u^+$	$11s8p4d2f$(2.89,0.40)	$^1\Sigma_g^+$	12	98	12	0.903	3896021
		$^3\Sigma_u^+$	12	98	12	0.906	3896021
		$^1\Sigma_g^+$	12	78	12	0.883	2467159
		$^3\Sigma_u^+$	12	78	12	0.902	2467159
		$^3\Sigma_u^+$	12	66	12	0.894	1766137
	$11s8p4d2f$(1.3375,0.40)	$^1\Sigma_g^+$	12	98	12	0.898	3896021
	$11s8p4d1f$(2.89)	$^1\Sigma_g^+$	12	78	12	0.911	2467159
	$11s8p4d1f$(1.3375)	$^1\Sigma_g^+$	12	78	12	0.903	2467159
	$11s8p4d1f$(0.40)	$^1\Sigma_g^+$	12	78	12	0.897	2467159
	$11s8p4d$	$^1\Sigma_g^+$	12	58	12	0.888	1363185
$^1\Delta_g$	$11s8p4d2f$(2.89,0.40)	$^1\Sigma_g^+$	12	98	8	0.861	2318942
		$^1\Sigma_g^+$	12	78	8	0.845	1469392
	$11s8p4d2f$(1.3375,0.40)	$^1\Sigma_g^+$	12	98	8	0.854	2318942
	$11s8p4d1f$(2.89)	$^1\Sigma_g^+$	12	78	8	0.864	1469392
	$11s8p4d1f$(1.3375)	$^1\Sigma_g^+$	12	78	8	0.856	1469392
	$11s8p4d1f$(0.40)	$^1\Sigma_g^+$	12	78	8	0.845	1469392
	$11s8p4d$	$^1\Sigma_g^+$	12	58	8	0.847	812850

continued on next page

continued from previous page

State	Basis	MO set	Active space int.	Active space ext.	Ref.	C^{2a}	CSFs
$^1\Delta_u$	$11s8p4d2f$(2.89,0.40)	$^1\Sigma_g^+$	12	98	8	0.861	2318942
		$^1\Delta_u$	12	98	8	0.882	2318942
		$^1\Sigma_g^+$	12	78	8	0.844	1469392
		$^1\Delta_u$	12	78	8	0.870	1469392
		$^1\Delta_u$	12	78	8	0.850	1052402
	$11s8p4d2f$(1.3375,0.40)	$^1\Sigma_g^+$	12	98	8	0.854	2318942
	$11s8p4d1f$(2.89)	$^1\Sigma_g^+$	12	78	8	0.864	1469392
	$11s8p4d1f$(1.3375)	$^1\Sigma_g^+$	12	78	8	0.856	1469392
	$11s8p4d1f$(0.40)	$^1\Sigma_g^+$	12	78	8	0.845	1469392
	$11s8p4d$	$^1\Sigma_g^+$	12	58	8	0.846	812850
$^1\Pi_u$	$11s8p4d2f$(2.89,0.40)	$^1\Sigma_g^+$	12	98	8	0.859	2321434
		$^1\Pi_u$	12	98	8	0.883	2321434
		$^1\Sigma_g^+$	12	78	8	0.846	1471172
		$^1\Pi_u$	12	78	8	0.871	1471172
		$^1\Pi_u$	12	66	8	0.854	105762
	$11s8p4d2f$(1.3375,0.40)	$^1\Sigma_g^+$	12	98	8	0.854	2321434
	$11s8p4d1f$(2.89)	$^1\Sigma_g^+$	12	78	8	0.864	1471172
	$11s8p4d1f$(1.3375)	$^1\Sigma_g^+$	12	78	8	0.857	1471172
	$11s8p4d1f$(0.40)	$^1\Sigma_g^+$	12	78	8	0.846	1471172
	$11s8p4d$	$^1\Sigma_g^+$	12	58	8	0.848	813918
$^1\Pi_g$	$11s8p4d2f$(2.89,0.40)	$^1\Sigma_g^+$	12	98	8	0.861	2321434
		$^1\Sigma_g^+$	12	78	8	0.841	1471172
	$11s8p4d2f$(1.3375,0.40)	$^1\Sigma_g^+$	12	98	8	0.851	2321434
	$11s8p4d1f$(2.89)	$^1\Sigma_g^+$	12	78	8	0.862	1471172
	$11s8p4d1f$(1.3375)	$^1\Sigma_g^+$	12	78	8	0.854	1471172
	$11s8p4d1f$(0.40)	$^1\Sigma_g^+$	12	78	8	0.842	1471172
	$11s8p4d$	$^1\Sigma_g^+$	12	58	8	0.843	813918
$^3\Pi_u$	$11s8p4d2f$(2.89,0.40)	$^1\Sigma_g^+$	12	98	8	0.860	3898612
		$^3\Pi_u$	12	98	8	0.882	3898612
$^3\Delta_u$	$11s8p4d2f$(2.89,0.40)	$^1\Sigma_g^+$	12	98	8	0.860	3901580
$2^1\Sigma_u$	$11s8p4d2f$(2.89,0.40)	$^1\Sigma_g^+$	12	98	12	0.861	2324755
$2^3\Sigma_u^+$	$11s8p4d2f$(2.89,0.40)	$^1\Sigma_g^+$	12	98	12	0.859	3896021

[a] weight of reference configurations.

states. The use of a common MO set is desirable if properties are to be computed which involve more than one state simultaneously, such as the spin-orbit interaction between states [342, 406].

Further calculations investigated the effect of reducing the active space. These were performed using the $11s8p4d2f(2.89, 0.04)$ basis set. The MOs corresponding to the tighter of the f-functions were discarded for both ground state and parental MO set calculations, in addition, the MOs due to a d-function were discarded for a set of parental MO computations. These orbitals play an important part in the d-d correlation, therefore it is important to know the effects of their removal, especially given the restrictions on the number of active orbitals in the present version of MRD-CI which would be preferably be employed in multi-reference multi-root study.

4.5.4 The ground state of dicopper

The ground state energies as calculated for the various basis sets, and active spaces are shown in Table 4–11. The inclusion of the f-function causes a marked lowering of the total energy, an effect which is most apparent for α_f=2.89. This would seem to indicate the superiority of this function for the description of the dominant d-d correlation (assuming there is not a large displacement in the position of the minima). That the functions of 2.89 and 0.40 describe different correlation effects is clearly shown by the additivity demonstrated, the energy lowering offered by each function individually relative to the $11s8p4d$ basis are obtained when they are combined. The removal of the f-function from the active space of the $11s8p4d2f(2.89, 0.40)$ returns an energy similar to the $11s8p4d1f(0.40)$ calculations.

The percentage contributions (>0.1 %) to the ground state wavefunction, at the SDCI level are listed in Table 4–12. Comparison is made between the present $11s8p4d2f(2.89, 0.40)$ basis and the results of Bauschlicher [375], and Shim and Gingerich [370] in Table 4–13. In agreement with these earlier studies the single SCF configuration affords an excellent description of the state in the near-

Table 4–11: Energies of Cu_2 $^1\Sigma_g^+$ by SCF and direct CI at 2.20Å

Basis	Active space (int/ext)	Total Energies (au)[a]		
		SCF	SDCI	CI+Davidson
$11s8p4d2f$(2.89,0.40)	(12/66)	-7.79035	-8.189942	-8.235176
$11s8p4d2f$(2.89,0.40)	(12/78)		-8.342467	-8.399982
$11s8p4d2f$(2.89,0.40)	(12/98)		-8.527748	-8.600404
$11s8p4d2f$(1.3375,0.40)	(12/98)	-7.80549	-8.459531	-8.528427
$11s8p4d1f$(2.89)	(12/78)	-7.79731	-8.480137	-8.542841
$11s8p4d1f$(1.3375)	(12/78)	-7.80064	-8.441596	-8.505525
$11s8p4d1f$(0.40)	(12/78)	-7.79762	-8.341076	-8.398190
$11s8p4d$	(12/58)	-7.79034	-8.296677	-8.345569

[a] E+3270 au.

equilibrium region The next most important term is due to $4s\sigma_g^2 \rightarrow 4s\sigma_u^2$, which contrary to the earlier studies is found to exceed $4s\sigma_g^2 \rightarrow 4p\pi_u^2$, however, it should be noted that the present work used the only the former as a reference function whereas Bauschlicher used both, and Shim and Gingerich only used the ground state, therefore the present results carry an inherent bias towards $4s\sigma_u^2$. In total the reference configurations account for ~90 % of the wavefunction.

In agreement with Bauschlicher [375], and contrary to Shim and Gingerich [370], the LUMO is 4*s*-4*s* in nature. Shim and Gingerich reported that the LUMO was mostly $p\sigma$ in character around 2.20 Å.

4.5.5 Excited states

The quality of the reference set can be gauged by the total C^2 values of these configurations in the final wavefunction. The values are listed in Table 4–10. The current reference set including all the states of a particular irreducible representation and spin, generated by the distribution of the electrons amongst the 4*s* and 3*d* shells, gives 88-90 % of the 4*s*-4*s* states, and between 84 and 86 % for the ^2S+^2D states. The weighting of the reference configurations is greatest for the tightest *f*-functions (2.89>1.3375>0.40), and decreases with reduction in the dimension of the active space. The coverage for the parental orbital calculations is significantly

Table 4–12: Percentage contribution of leading configurations to the wavefunction for $^1\Sigma_g^+$ SDCI at 2.20Å.

Calculation								
$11s8p4d$		$11s8p4d1f$			$11s8p4d2f$			
	0.40	1.3375	2.89	1.3375	2.89	2.89	2.89	
(12/58)	(12/78)	(12/78)	(12/78)	(12/98)	(12/66)	(12/78)	(12/98)	Configuration[a]
89.46	88.78	89.52	90.03	88.87	87.84	88.74	89.31	$3d^{10}3d^{10}4s\sigma_g^{2b}$
0.76	0.72	0.75	0.78	0.72	0.67	0.70	0.75	$4s\sigma_g^2 \rightarrow 4s\sigma_u^2$
...	...	...	...	...	0.22	...	...	$3d\delta_g \rightarrow 4d\delta_g$
0.35	0.24	0.23	0.22	0.18	0.34	0.24	...	$4s\sigma_u^2 \rightarrow 4p\pi_g^2$

[a] CSFs relative to the leading configuration.

[b] the leading configuration.

Table 4–13: Comparison of present and literature wavefunctions for the ground state of Cu_2.

Bauschlicher[a]		Shim[b]	Present[c]	
CASSCF	SDCI	SDCI	SDCI	Configuration[d]
94.34	86.94	91.54	89.31	$3d^{10}3d^{10}4s\sigma_g^{2e}$
1.93	1.76	0.66	0.75	$4s\sigma_g^2 \rightarrow 4s\sigma_u^2$
2.97	2.73	1.75	...	$4s\sigma_g^2 \rightarrow 4p\pi_u^2$
0.71	0.51	0.30	...	$4s\sigma_g^2 \rightarrow 4p\pi_g^2$
...	...	0.24	...	$4s\sigma_g^2 \rightarrow 4p\pi_u 4d\pi_u$
...	...	0.23	...	$4s\sigma_g^2 \rightarrow 4s\sigma_u 5s\sigma_u$

[a] from [375]; $(8s6p4d1f)$ basis with $4s4p$ MOs active in the CASSCF, the CI used the CAS wavefunction as n-particle basis.

[b] from [370]; $(8s6p3d)$ basis , 2928 CSF.

[c] $11s8p4d2f(2.89, 0.40)$ basis with 110 active MOs.

[d] CSFs relative to the leading configuration.

[e] the leading configuration.

improved, ~88 % for the d-hole states as calculated with the $11s8p4d2f(2.89, 0.40)$ basis, compared to the calculations employing the ground state MOs.

Table 4–14 and Figure 4–2 show the excitation energies obtained for the different basis sets, using the ground state MOs. The inclusion of f-functions increases the excitation energies of the studied states. This is especially apparent for the d-hole states. The effect is much smaller for the Σ $4s$-$4s$ states. The differences are related to the alteration in the environment of the d electrons and the differential effects associated with the s-d and d-d correlation. Comparison of the natural orbital analyses of the excited states as calculated at 2.20 Å (Table 4–15) show that the $^1\Sigma_g^+ \rightarrow {}^3\Sigma_u^+$ transition has little effect on the d-electrons, whilst $^1\Sigma_g^+ \rightarrow {}^1\Sigma_u^+$ causes a larger reorganisation. The marked increases that occur for the excited states with a d-hole reflect the decrease in d-d correlation associated with the reduction in the number of d-electron. The lower excitation energies obtained with the tightest of the f-functions (2.89) relative to the intermediate function (1.3375) are consistent with the (expected) greater proportion of d-d cor-

Table 4–14: Comparison of excitation energies for basis sets containing different f-functions (eV)

State	Calculation					
	$11s8p4d$		$11s8p4d1f$		$11s8p4d2f$	
		0.40	1.3375	2.89	1.3375	2.89
$^1\Sigma_g^{+a}$	-0.289677	-0.341076	-0.441596	-0.480137	-0.459531	-0.527748
	(-0.345569)	(-0.398190)	(-0.505525)	(-0.542841)	(-0.528427)	(-0.600404)
$^3\Sigma_u^+$	2.2295	2.3184	2.3012	2.2427	2.6168	2.3221
	(2.2837)	(2.3737)	(2.3559)	(2.3040)	(2.4036)	(2.3893)
$^1\Sigma_u^+$	3.3509	3.4565	3.5031	3.4496	3.5422	3.5371
	(3.1217)	(3.3321)	(3.3321)	(3.2716)	(3.3838)	(3.3923)
$^1\Pi_u$	4.2738	4.4897	4.8115	4.6850	5.1678	4.9238
	(3.1048)	(3.3634)	(3.7063)	(3.5390)	(3.8179)	(3.8391)
$^1\Delta_g$	4.5872	4.8152	5.1337	5.0019	5.4962	5.2515
	(3.3866)	(3.6707)	(4.0100)	(3.8400)	(4.1269)	(4.1553)
$^1\Delta_u$	4.7876	5.0205	5.3310	5.1993	5.6971	5.4533
	(3.5900)	(4.2033)	(4.2033)	(4.0358)	(4.3291)	(4.3557)
$^1\Pi_g$	5.2177	5.7616	5.7616	5.6314	6.1305	5.8888
	(3.9727)	(4.5957)	(4.5957)	(4.4984)	(4.7236)	(4.7590)

The terms in parentheses include the Davidson correction.

[a] The ground state total energy, E+3278 au, is given in the first two rows.

relation returned, especially given the contraction of the d-shell of the $4s^23d^9$ state of the atom relative to $4s^13d^{10}$ [335, 382, 403]. It is noted that, given this effect that a more compact f-function may be required for the correct description of the differential correlation, such as the $4f$ STO-3G of Bauschlicher *et al.* [365].

The inclusion of higher "unlinked" clusters through the use of the Davidson correction [63], results in a large lowering of the relative excitation energies of the states with open d-shells. Even taking into account the comparative qualities of the description of the states afforded by the reference configurations, this is a large effect.

The configurations with percentage contributions exceeding 0.1 %, for the various basis sets are listed in Tables 4–16 to 4–21 for each of the states $^1\Sigma_u^+$, $^3\Sigma_u^+$,

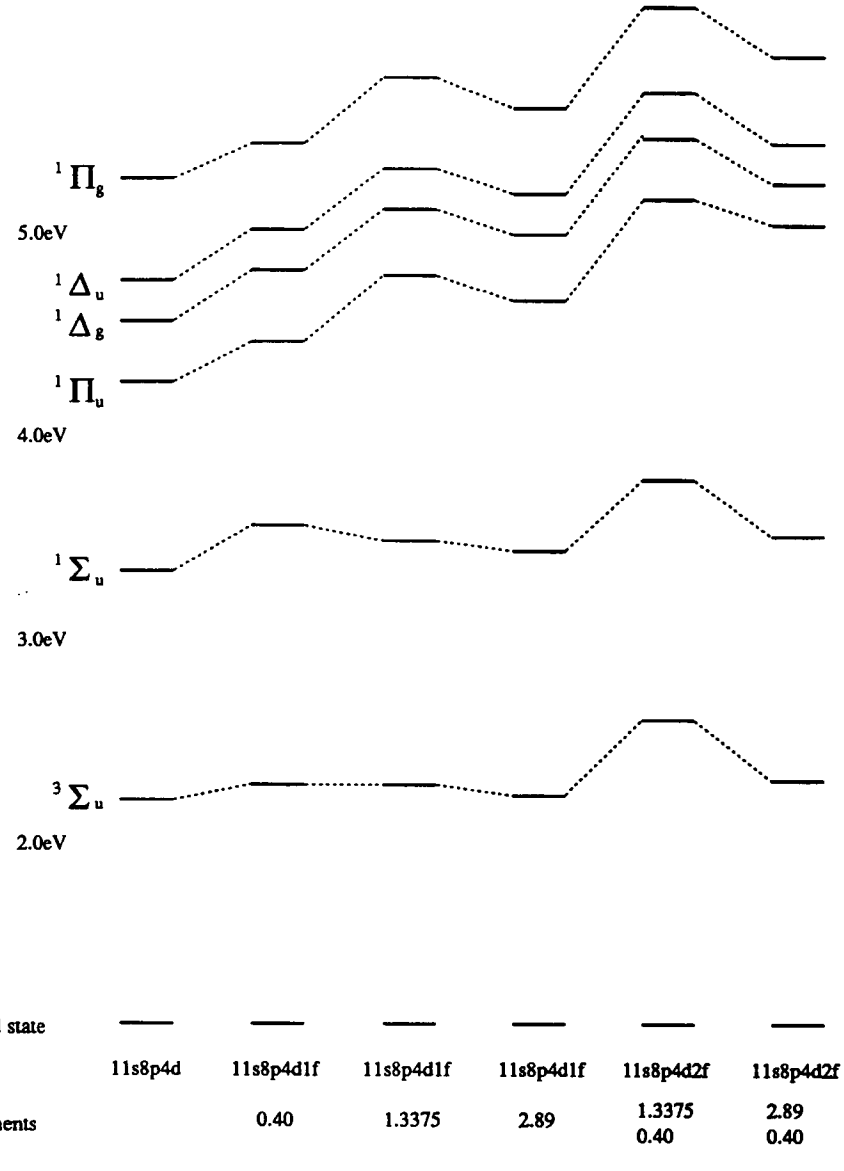

Figure 4–2: Excitation energies of states at the SDCI level for various basis sets

Table 4–15: Natural orbital occupancies at 2.20 Å using the $11s8p4d2f(2.89, 0.40)$ basis.

MO	$^1\Sigma_g^+$	$^3\Sigma_u^+$	$^1\Sigma_u^+$	$^3\Pi_u$	$^1\Pi_u$	$^3\Delta_u$	$^1\Delta_u$	$^1\Pi_g$	$^1\Delta_g$
Orbital occupancies									
$3d\sigma_g$	1.9839	1.9799	1.9835	1.9855	1.9855	1.9854	1.9854	1.9852	1.9855
$3d\pi_u$	3.9660	3.9652	3.9668	3.9052	3.9032	3.9656	3.9656	3.8452	3.9658
$3d\delta_g$	3.9684	3.9696	3.9692	3.9726	3.9726	3.0700	3.0784	3.9722	3.8841
$3d\delta_u$	3.9680	3.9690	3.9690	3.9712	3.9712	3.8797	3.8713	3.9706	3.0654
$3d\pi_g$	3.9680	3.9682	3.9684	3.0397	3.0418	3.9718	3.9718	3.0997	3.9718
$3d\sigma_u$	1.9823	1.9771	1.9819	1.9827	1.9827	1.9830	1.9830	1.9823	1.9831
$4s\sigma_g$	1.9556	0.9957	0.9936	1.9386	1.9357	1.9148	1.9052	1.8828	1.9167
$4s\sigma_u$	0.0229	0.9931	0.9945	1.0234	1.0268	1.0470	1.0566	1.0790	1.0452
$4p\sigma_g$	0.0026	0.0023	0.0039	0.0021	0.0021	0.0022	0.0022	0.0022	0.0022
$4p\pi_u$	0.0128	0.0081	0.0113	0.0103	0.0105	0.0108	0.0108	0.0103	0.0109
$4p\pi_g$	0.0073	0.0064	0.0079	0.0071	0.0071	0.0074	0.0074	0.0073	0.0073
$4p\sigma_u$	0.0058	0.0053	0.0071	0.0074	0.0074	0.0075	0.0074	0.0074	0.0075
$4d\sigma_g$	0.0130	0.0124	0.0134	0.0154	0.0153	0.0146	0.0144	0.155	0.0143
$4d\pi_u$	0.0276	0.0187	0.0175	0.0137	0.0131	0.0131	0.0152	0.0157	0.0151
$4d\delta_g$	0.0210	0.0204	0.0211	0.0186	0.0187	0.0187	0.0172	0.0190	0.0185
$4d\delta_u$	0.0185	0.0181	0.0184	0.0158	0.0158	0.0154	0.0156	0.0161	0.0143
$4d\pi_g$	0.0185	0.0264	0.0256	0.0399	0.0285	0.0296	0.0294	0.0275	0.0294
$4d\sigma_u$	0.0089	0.0094	0.0099	0.0103	0.0104	0.0110	0.0113	0.0108	0.0111
$5s\sigma_g$	...	0.0023	...	0.0027	0.0025	0.0026	0.0026	0.0026	0.0026
$5s\sigma_u$	0.0024	0.0029	...	0.0052	0.0052	0.0052	0.052	0.0054	0.0052
Shell occupancies									
$3d$	19.8366	19.8287	19.8237	18.8568	18.8569	18.8554	18.8554	18.8552	18.8557
$4s$	1.9785	1.9888	1.9880	2.9620	2.9625	2.9618	2.9618	2.9618	2.9619
$4p$	0.0295	0.0220	0.0301	0.0269	0.0270	0.0279	0.0212	0.0272	0.0278
$4d$	0.1061	0.1022	0.1084	0.1023	0.1017	0.1028	0.1027	0.1037	0.1035
$4f$	0.0300	0.0285	0.0311	0.0257	0.0257	0.0257	0.0257	0.0257	0.0257

$^1\Delta_g$, $^1\Delta_u$, $^1\Pi_g$, and $^1\Pi_u$, along with a reduced active space calculation using the $11s8p4d2f(2.89, 0.40)$ basis set. In each case the main configuration is dominant, providing 75-85 % of the wavefunction. The next most important configurations are those required to correctly describe the dissociation of the state. The $^3\Sigma_u^+$ state is well described by $3d^{10}3d^{10}4s\sigma_g^1 4s\sigma_u^1$, this sole configuration yielding 90 % of the wavefunction at r=2.20 Å. The $^1\Sigma_u^+$ ion-pair state has sizable contributions from the $^2S+^2D$ configurations of the same symmetry, $3d\sigma_g 4s\sigma_u$ and $3d\sigma_u 4s\sigma_g$, providing $\sim$ 3.5 % for $11s8p4d2f$, although these decrease with increasing basis set dimension. A similar trend is observed for the other states.

Configurations generated by single electron transitions from the $4s\sigma_g$ and $4s\sigma_u$ to the $4p\sigma$ are important for the $^2S+^2D$ states, with the percentage composition frequently around 1 %. These transitions are associated with the polarisation of the $4s$ orbitals, the importance is attributed to the near degeneracy of the $4s$ and $4p$ orbitals in the atom [365]. Double excitations from the $3d$ orbitals which result in one of the excited electrons remaining within the d-shell often have contributions greater than 0.1 %. This reflects that the calculations were performed under a reduced point group, and that the strict equivalence of electrons in the π and δ was not maintained.

The effect of using the parental MOs (from the corresponding open-shell SCF), in contrast to the SCF closed shell MOs, as the n-particle basis, and of reducing the active space are illustrated in Table 4–22 for the $11s8p4d2f(2.89, 0.40)$ basis set. Also included are the excitation energies of $^3\Pi_u(3d\pi_g, 4s\sigma_u)$, $^3\Delta_u(3d\delta_g, 4s\sigma_u)$, and $^{1,3}\Sigma_u^+(3d\sigma_g, 4s\sigma_u)$ calculated for the closed shell SCF-MO set; these complete the *ungerade* states that are derived from the $^2S+^2D$ atomic asymptote. The contributions to the wavefunctions are listed in Tables 4–23 to 4–24, these are much the same as the other $^2S+^2D$ states. The $^{1,3}\Sigma_u^+(3d\sigma_g, 4s\sigma_u)$ lie well above the the other states arising from $^2S+^2D$, in agreement with the findings of Witko and Beckmann [398]. It is therefore unlikely that any of these is responsible for the low-lying states.

The parental orbital calculations result in substantially lower excitation energies, compared to the SCF closed shell n-particle basis. The lowering, at the SDCI

Table 4–16: Percentage contribution of leading configurations to the wavefunction for $^1\Sigma_u^+$ SDCI at 2.20Å

Calculation							
$11s8p4d$		$11s8p4d1f$			$11s8p4d2f$		
	0.40	1.3375	2.89	1.3375	2.89	2.89	
(12/58)	(12/78)	(12/78)	(12/78)	(12/98)	(12/98)	(12/78)	Configuration[a]
83.06	83.33	85.27	85.73	85.11	85.81	83.31	$3d^{10}3d^{10}4s\sigma_g^1 4s\sigma_u^{1b}$
4.35	3.80	2.91	3.16	2.74	2.66	3.79	$3d\sigma_g \rightarrow 4s\sigma_u$
1.36	1.19	1.00	1.07	0.93	0.90	1.17	$3d\sigma_u \rightarrow 4s\sigma_u$
0.77	0.67	0.57	0.52	0.53	0.46	0.67	$4s\sigma_g \rightarrow 4p\sigma_g$
0.11	0.17	0.09	...	0.10	0.09	0.13	$4s\sigma_g \rightarrow 5s\sigma_g$
0.10	...	...	...	...	...	...	$3d\sigma_u 4s\sigma_u \rightarrow 4s\sigma_g 4p\sigma_g$
0.12	0.10	...	...	...	...	0.10	$3d\sigma_u \rightarrow 4p\sigma_u$
0.11	0.14	0.09	...	0.10	...	0.15	$4s\sigma_u \rightarrow 4p\sigma_u$
0.34	0.24	0.023	0.23	0.19	...	0.24	$4s\sigma_g 4s\sigma_u \rightarrow 4p\pi_u 4p\pi_g$

[a] CSFs relative to the leading configuration.

[b] the leading configuration.

Table 4–17: Percentage contribution of leading configurations to the wavefunction for $^3\Sigma_u^+$ SDCI at 2.20Å

Calculation							
$11s8p4d$		$11s8p4d1f$			$11s8p4d2f$		
	0.40	1.3375	2.89	1.3375	2.89	2.89	
(12/58)	(12/78)	(12/78)	(12/78)	(12/98)	(12/98)	(12/78)	Configuration[a]
90.02	89.25	89.86	90.75	89.47	89.99	89.18	$3d^{10}3d^{10}4s\sigma_g^1 4s\sigma_u^{1\,b}$
0.47	0.44	0.29	0.30	0.29	0.27	0.44	$3d\sigma_u \rightarrow 4s\sigma_u$
0.46	0.48	0.36	0.30	0.37	0.30	0.49	$4s\sigma_u \rightarrow 4p\sigma_u$
...	0.09	...	...	...	...	0.09	$4s\sigma_g \rightarrow 5s\sigma_g$
0.18	0.20	0.15	0.13	0.16	0.13	0.20	$4s\sigma_u \rightarrow 5s\sigma_u$

[a] CSFs relative to the leading configuration.

[b] the leading configuration.

level, is in the region of 0.5 eV for the $4s$-$4s$ states, $^{1,3}\Sigma_u^+$, and greater than 1.5 eV for the d-hole states. This large effect is due to the degree of relaxation in the d-shell and core upon the removal of a d-electron. This is apparent from the contributions to the wavefunctions, where configurations associated with polarisation and reorganisation have significantly lower percentages, and from the SCF orbital analysis (Section 4.5.2) For the Π and Δ, states the single SCF configuration decreases in importance and the configuration required to describe dissociation correspondingly increases, an effect caused by the bias of the SCF wavefunction. Clearly a MCSCF based n-particle basis is desirable in such instances, although given the dimension of the subsequent CI, is is unlikely that a large difference would be found.

The excitation energies of the d-hole states are reduced by the reduction in the active space. In this case, the successive removal of MOs due to the tighter of the two f-functions and the highest exponent d-function, both reduce the percentage of the total d-d correlation returned, an effect which is greater for the ground state. Unfortunately the effect of increasing the active space could not be investigated; given the results for the copper atom, Section 4.5.3, it is possible that the inclusion

Table 4–18: Percentage contribution of leading configurations to the wavefunction for $^1\Delta_g$ SDCI at 2.20Å

Calculation							
$11s8p4d$		$11s8p4d1f$			$11s8p4d2f$		
	0.40	1.3375	2.89	1.3375	2.89	2.89	
(12/58)	(12/78)	(12/78)	(12/78)	(12/98)	(12/98)	(12/78)	Configuration[a]
80.27	80.31	81.05	81.66	80.95	81.57	80.31	$3d\sigma_g^2\pi_u^4\delta_g^4\delta_u^3\pi_g^4\sigma_u^2 4s\sigma_g^2 4s\sigma_u^{1b}$
4.35	4.16	4.48	4.65	4.34	4.46	4.12	$3d\sigma_g^2\pi_u^4\delta_g^3\delta_u^4\pi_g^4\sigma_u^2 4s\sigma_g^1 4s\sigma_u^2$
0.58	0.48	0.42	0.38	0.38	0.32	0.48	$4s\sigma_g \rightarrow 4p\sigma_g$
0.34	0.41	0.30	0.24	0.34	0.28	0.41	$4s\sigma_g \rightarrow 5s\sigma_g$
0.14	...	0.10	0.10	...	...	...	$4s\sigma_g \rightarrow 4d\sigma_g$
0.10	0.16	0.12	0.09	0.15	0.13	0.16	$4s\sigma_g \rightarrow 5p\sigma_g$
0.17	0.16	0.14	0.13	0.14	0.13	0.16	$3d\delta_g\delta_u' \rightarrow 3d\delta_u 4d\delta_g$
0.13	...	0.10	0.10	...	...	...	$3d\delta_g\sigma_u \rightarrow 3d\delta_u 4d\sigma_g$
0.12	0.11	...	...	...	...	0.11	$3d\delta_g 4s\sigma_u \rightarrow 3d\delta_u 4p\sigma_g$
0.18	0.13	0.12	0.11	0.10	...	0.13	$3d\delta_g 4s\sigma_u \rightarrow 3d\delta_u 5s\sigma_g$
0.23	0.19	...	...	...	...	0.19	$3d\delta_g\pi_g \rightarrow 3d\delta_u 4p\pi_g$
0.63	0.30	0.50	0.48	0.24	0.21	0.30	$3d\delta_g\pi_g \rightarrow 3d\delta_u 4d\pi_g$
0.21	...	0.20	0.19	...	...	...	$3d\delta_g\pi_g \rightarrow 3d\delta_u 5d\pi_g$
...	0.31	...	...	0.27	0.25	0.31	$3d\delta_g\pi_g \rightarrow 3d\delta_u 5p\pi_g$
0.16	0.17	0.12	0.11	0.13	0.11	0.17	$3d\delta_g \rightarrow 4d\delta_g$
1.02	1.00	0.76	0.63	0.75	0.61	1.01	$4s\sigma_u \rightarrow 4p\sigma_u$
0.29	0.30	0.23	0.19	0.24	0.20	0.31	$4s\sigma_u \rightarrow 5s\sigma_u$
0.49	0.44	0.39	0.35	0.36	0.31	0.44	$3d\delta_g 4s\sigma_g \rightarrow 3d\delta_u 4p\sigma_u$
0.34	0.23	0.20	0.18	0.19	0.17	0.23	$3d\delta_g 4s\sigma_g \rightarrow 3d\delta_u 5s\sigma_u$
0.26	0.24	0.23	0.11	0.12	0.11	0.24	$3d\delta_g 4s\sigma_g \rightarrow 3d\delta_u 35\sigma_u$
0.22	...	...	...	...	...	...	$4s\sigma_g^2 \rightarrow 4p\pi_g^2$

[a] CSFs relative to the leading configuration.

[b] the leading configuration.

Table 4–19: Percentage contribution of leading configurations to the wavefunction for $^1\Delta_u$ SDCI at 2.20Å

Calculation							
$11s8p4d$		$11s8p4d1f$			$11s8p4d2f$		
	0.40	1.3375	2.89	1.3375	2.89	2.89	
(12/58)	(12/78)	(12/78)	(12/78)	(12/98)	(12/98)	(12/78)	Configuration[a]
79.23	79.28	80.05	80.65	79.96	80.58	79.30	$3d\sigma_g^2\pi_u^4\delta_g^4\delta_u^3\pi_g^4\sigma_u^2 4s\sigma_g^2 4s\sigma_u^{1b}$
5.33	5.14	5.44	5.64	5.30	5.44	5.08	$3d\sigma_g^2\pi_u^4\delta_g^3\delta_u^4\pi_g^4\sigma_u^2 4s\sigma_g^1 4s\sigma_u^2$
0.56	0.47	0.41	0.37	0.37	0.31	0.47	$4s\sigma_g \rightarrow 4p\sigma_g$
0.31	0.36	0.27	0.22	0.30	0.25	0.36	$4s\sigma_g \rightarrow 5s\sigma_g$
0.09	0.14	0.11	0.22	0.14	0.12	0.15	$4s\sigma_g \rightarrow 5p\sigma_g$
0.31	0.31	0.26	0.24	0.26	0.24	0.31	$3d\delta_u^2 \rightarrow 3d\delta_g 4d\delta_g$
0.15	...	0.11	0.11	...	...	...	$3d\delta_u\sigma_u \rightarrow 3d\delta_g 4d\sigma_g$
0.12	0.10	...	...	0.10	...	0.10	$3d\delta_u 4s\sigma_u \rightarrow 3d\delta_g 4p\sigma_g$
0.19	0.13	0.12	0.11	...	...	0.13	$3d\delta_u 4s\sigma_u \rightarrow 3d\delta_g 5s\sigma_g$
0.20	...	...	...	...	...	...	$3d\delta_u\pi_g \rightarrow 3d\delta_g 4p\pi_u$
0.53	0.25	0.41	0.40	0.20	...	0.25	$3d\delta_u\pi_g \rightarrow 3d\delta_g 4d\pi_u$
...	0.26	...	...	0.22	0.21	0.26	$3d\delta_u\pi_g \rightarrow 3d\delta_g 5p\pi_u$
1.00	0.97	0.74	0.61	0.73	0.59	0.98	$4s\sigma_u \rightarrow 4p\sigma_u$
0.28	0.30	0.23	0.19	0.24	0.20	0.30	$4s\sigma_u \rightarrow 5s\sigma_u$
0.55	0.50	0.43	0.39	0.40	0.34	0.50	$3d\delta_u 4s\sigma_u \rightarrow 3d\delta_g 4p\sigma_u$
0.38	0.35	0.30	0.27	0.29	0.26	0.35	$3d\delta_u 4s\sigma_u \rightarrow 3d\delta_g 5s\sigma_u$
0.27	0.25	0.23	0.22	0.22	0.20	0.25	$3d\delta_u 4s\sigma_u \rightarrow 3d\delta_g 5p\sigma_u$
0.09	...	...	...	...	...	...	$3d\delta_u 3d\sigma_g \rightarrow 3d\delta_g 5s\sigma_u$
0.12	0.12	0.10	0.10	0.10	0.10	0.12	$3d\delta_u \rightarrow 4d\delta_u$
0.22	...	...	...	...	...	...	$4s\sigma_g^2 \rightarrow 4p\pi_g^2$

[a] CSFs relative to the leading configuration.

[b] the leading configuration.

Table 4–20: Percentage contribution of leading configurations to the wavefunction for $^1\Pi_u$ SDCI at 2.20Å

Calculation							
$11s8p4d$		$11s8p4d1f$			$11s8p4d2f$		
	0.40	1.3375	2.89	1.3375	2.89	2.89	
(12/58)	(12/78)	(12/78)	(12/78)	(12/98)	(12/98)	(12/78)	Configuration[a]
77.02	77.13	77.94	78.51	77.88	78.49	77.16	$3d\sigma_g^2\pi_u^3\delta_g^4\delta_u^4\pi_g^4\sigma_u^2 4s\sigma_g^2 4s\sigma_u^{1b}$
7.25	7.02	7.36	7.62	7.18	7.37	6.94	$3d\sigma_g^2\pi_u^4\delta_g^4\delta_u^4\pi_g^3\sigma_u^2 4s\sigma_g^1 4s\sigma_u^2$
0.60	0.49	0.49	0.39	0.38	0.32	0.49	$4s\sigma_g \rightarrow 4p\sigma_g$
0.32	0.37	0.28	0.23	0.31	0.26	0.37	$4s\sigma_g \rightarrow 5s\sigma_g$
0.20	...	...	...	...	...	...	$4s\sigma_g \rightarrow 4d\sigma_g$
0.11	0.16	0.12	0.10	0.15	0.13	0.17	$4s\sigma_g \rightarrow 5p\sigma_g$
0.34	0.34	0.28	0.27	0.28	0.26	0.33	$3d\pi_g\delta_u \rightarrow 3d\pi_u 4d\delta_g$
0.20	0.10	0.14	0.14	...	...	0.10	$3d\pi_g\sigma_u \rightarrow 3d\pi_u 4d\sigma_g$
...	0.10	...	...	...	...	0.10	$3d\pi_g\sigma_u \rightarrow 3d\pi_u 5p\sigma_g$
0.11	0.10	...	...	0.10	...	0.10	$3d\pi_g 4s\sigma_u \rightarrow 3d\pi_u 4p\sigma_g$
0.19	0.13	0.12	0.11	...	...	0.13	$3d\pi_g 4s\sigma_u \rightarrow 3d\pi_u 5s\sigma_g$
0.21	...	...	...	...	...	...	$3d\pi_g^2 \rightarrow 3d\pi_u 4p\pi_u$
0.56	0.26	0.43	0.42	0.20	0.20	0,24	$3d\pi_g^2 \rightarrow 3d\pi_u 4d\pi_u$
...	0.28	...	...	0.22	...	0.25	$3d\pi_g^2 \rightarrow 3d\pi_u 5d\pi_u$
0.19	...	0.10	0.09	...	...	...	$3d\pi_g^2 \rightarrow 3d\pi_u 5d\pi_u$
0.97	0.96	0.72	0.60	0.72	0.58	0.96	$4s\sigma_u \rightarrow 4p\sigma_u$
0.27	0.29	0.22	0.18	0.23	0.19	0.29	$4s\sigma_u \rightarrow 5s\sigma_u$
0.64	0.58	0.49	0.44	0.47	0.40	0.58	$3d\pi_g 4s\sigma_g \rightarrow 3d\pi_u 4p\sigma_u$
0.38	0.35	0.30	0.27	0.29	0.25	0.35	$3d\pi_g 4s\sigma_g \rightarrow 3d\pi_u 5s\sigma_u$
0.26	0.24	0.23	0.21	0.21	0.19	0.24	$3d\pi_g 4s\sigma_g \rightarrow 3d\pi_u 35\sigma_u$
0.21	...	...	...		...	...	$4s\sigma_g^2 \rightarrow 4p\pi_u^2$

[a] CSFs relative to the leading configuration.

[b] the leading configuration.

Table 4–21: Percentage contribution of leading configurations to the wavefunction for $^1\Pi_g$ SDCI at 2.20Å

Calculation							
$11s8p4d$		$11s8p4d1f$			$11s8p4d2f$		
	0.40	1.3375	2.89	1.3375	2.89	2.89	
(12/58)	(12/78)	(12/78)	(12/78)	(12/98)	(12/98)	(12/78)	Configuration[a]
82.02	81.93	82.71	83.34	82.57	83.18	81.92	$3d\sigma_g^2\pi_u^4\delta_g^4\delta_u^4\pi_g^3\sigma_u^2 4s\sigma_g^2 4s\sigma_u^{1b}$
2.78	2.65	2.92	3.04	2.80	2.91	2.62	$3d\sigma_g^2\pi_u^3\delta_g^4\delta_u^4\pi_g^4\sigma_u^2 4s\sigma_g^1 4s\sigma_u^2$
0.37	0.52	0.33	0.26	0.41	0.31	0.52	$4s\sigma_g \rightarrow 5s\sigma_g$
0.62	0.44	0.46	0.41	0.37	0.35	0.45	$4s\sigma_g \rightarrow 4p\sigma_g$
0.19	0.11	0.14	0.14	0.09	...	0.11	$4s\sigma_g \rightarrow 4d\sigma_g$
0.12	0.20	0.14	0.11	0.19	0.17	0.20	$4s\sigma_g \rightarrow 5p\sigma_g$
0.30	0.29	0.25	0.24	0.25	0.23	0.29	$3d\pi_u\delta_u \rightarrow 3d\pi_g 4d\delta_g$
0.17	...	0.12	0.12	...	...	...	$3d\pi_u\sigma_u \rightarrow 3d\pi_g 4d\sigma_g$
0.12	0.11	...	...	0.09	...	0.11	$3d\pi_u 4s\sigma_u \rightarrow 3d\pi_g 4p\sigma_g$
0.18	0.13	0.12	0.11	...	...	0.13	$3d\pi_u 4s\sigma_u \rightarrow 3d\pi_g 5s\sigma_g$
0.14	0.11	...	...	...	...	0.11	$3d\pi_u \rightarrow 4p\pi_u$
0.33	0.19	0.19	0.23	0.15	0.13	0.19	$3d\pi_u \rightarrow 4d\pi_u$
...	0.13	0.13	...	0.10	0.19	0.13	$3d\pi_u \rightarrow 5p\pi_u$
0.21	...	...	...	...	...	...	$3d\pi_u\pi_g' \rightarrow 3d\pi_g 4p\pi_u$
0.30	0.14	0.19	0.23	0.11	0.10	0.14	$3d\pi_u\pi_g' \rightarrow 3d\pi_g 4d\pi_u$
...	0.15	...	...	0.13	0.12	0.15	$3d\pi_u\pi_g' \rightarrow 3d\pi_g 4d\pi_u$
0.28	0.30	0.22	0.19	0.24	0.19	0.30	$4s\sigma_u \rightarrow 5s\sigma_u$
1.06	1.03	0.79	0.65	0.78	0.63	1.05	$4s\sigma_u \rightarrow 4p\sigma_u$
0.16	0.15	0.13	0.12	0.13	0.11	0.15	$3d\pi_u 4s\sigma_g \rightarrow 3d\pi_g 5s\sigma_u$
0.24	0.34	0.30	0.28	0.29	0.25	0.34	$3d\pi_u 4s\sigma_g \rightarrow 3d\pi_g 4p\sigma_u$
0.20	0.10	...	...	...	...	0.10	$3d\pi_u 4s\sigma_g \rightarrow 3d\pi_g 5p\sigma_u$
0.22	...	...	...	...	...	...	$4s\sigma_g^2 \rightarrow 4p\pi_u^2$

[a] CSFs relative to the leading configuration.

[b] the leading configuration.

Table 4–22: Comparison of excitation energies for the $11s8p4d2f$(2.89,0.40) for parental and common MO set (eV)

	common MOs		parental MOs		
State	(12/98)	(12/78)	(12/98)	(12/78)	(12/66)
$^1\Sigma_g^+$ [a]	-0.527748	-0.342467	-0.527748	-0.342467	-0.189942
	(-0.600404)	(-0.399982)	(-0.600404)	(-0.399982)	(-0.235176)
$^3\Sigma_u^+$	2.3221	2.3362	1.7791	1.8207	1.8612
	(2.3893)	(2.3904)	(1.9188)	(1.9607)	(1.9969)
$^1\Sigma_u^+$	3.5371	3.4681	3.0054		
	(3.3923)	(3.2730)	(3.0236)		
$^3\Pi_u$	4.8217		3.1071		
	(3.7111)		(2.6903)		
$^1\Pi_u$	4.9238	4.5138	3.2382	2.9431	2.6126
	(3.8391)	(3.3895)	(2.8385)	(2.5086)	(2.1304)
$^1\Delta_g$	5.2515	4.8400			
	(4.1537)	(3.6965)			
$^3\Delta_u$	5.4285				
	(4.3220)				
$^1\Delta_u$	5.4533	5.0455	3.7900	3.5044	3.1766
	(4.3557)	(3.8967)	(3.3762)	(3.0458)	(2.6537)
$^1\Pi_g$	5.8888	5.4803			
	(4.7590)	(4.2850)			
$2^3\Sigma_u^+$	6.1596				
	(5.0281)				
$2^1\Sigma_u^+$	6.3637				
	(5.2786)				

The terms in parentheses include the Davidson correction.

[a] The total ground state energy, E+3278 au, is given in the first two rows.

Table 4–23: Percentage contribution of leading configurations to the wavefunction for Σ_u^+ SDCI at 2.20Å, $11s8p4d2f$

Calculation								
Closed shell				Parental MO				
$^1\Sigma_u^+$ (12/98)	$2^1\Sigma_u^+$ (12/98)	$^3\Sigma_u^+$ (12/98)	$2^3\Sigma_u^+$ (12/98)	$^1\Sigma_u^+$ (12/98)	$^3\Sigma_u^+$ (12/98)	$^3\Sigma_u^+$ (12/78)	$^3\Sigma_u^+$ (12/66)	Configuration[a]
85.81	3.63	89.99	0.31	90.32	89.03	89.69	88.80	$3d^{10}3d^{10}4s\sigma_g^1 4s\sigma_u^{1\,b}$
2.66	74.80	...	76.87	0.30	0.84	0.47	0.56	$3d\sigma_g \rightarrow 4s\sigma_u$
...	7.52	...	8.69	...	...	...	...	$3d\sigma_u 4s\sigma_g \rightarrow 3d\sigma_g 4s\sigma_u$
0.90	0.12	0.27	0.12	...	0.18	...	...	$3d\sigma_u \rightarrow 4s\sigma_u$
0.46	0.37	0.30	0.31	...	...	...	...	$4s\sigma_g \rightarrow 4p\sigma_g$
...	0.53	...	0.63	...	...	...	...	$4s\sigma_u \rightarrow 4p\sigma_u$
...	0.23	0.13	0.25	...	...	...	...	$4s\sigma_g \rightarrow 5s\sigma_g$
...	0.14	...	0.20	...	...	...	...	$4s\sigma_u \rightarrow 5s\sigma_u$
0.09	0.21	...	0.16	...	...	...	...	$4s\sigma_g \rightarrow 5p\sigma_g$
...	0.29	...	0.32	...	...	...	...	$3d\sigma_u 4s\sigma_g \rightarrow 3d\sigma_g 4p\sigma_u$
...	0.18	...	0.20	...	...	...	...	$3d\sigma_u 4s\sigma_g \rightarrow 3d\sigma_g 5s\sigma_u$
...	0.11	...	0.11	...	...	...	...	$3d\sigma_u 4s\sigma_g \rightarrow 3d\sigma_g 5p\sigma_u$
...	0.21	...	0.23	...	...	...	...	$3d\sigma_u \pi_g \rightarrow 3d\sigma_g 4d\pi_u$
...	0.26	...	0.28	...	...	...	...	$3d\sigma_u \pi_g \rightarrow 3d\sigma_g 5p\pi_u$
...	0.12	...	0.23	...	...	...	...	$3d\sigma_u \delta_g \rightarrow 3d\sigma_g 4d\delta_u$

[a] CSFs relative to the leading configuration.

[b] the leading configuration.

Table 4–24: Percentage contribution of leading configurations to the wavefunction for Δ_u SDCI at 2.20Å, $11s8p4d2f$

Calculation					
Closed shell		Parental MO			
$^1\Delta_u$ (12/98)	$^3\Delta_u$ (12/98)	$^1\Delta_u$ (12/98)	$^1\Delta_u$ (12/78)	$^1\Delta_u$ (12/66)	Configuration[a]
80.58	81.32	77.99	77.65	76.79	$3d\sigma_g^2\pi_u^4\delta_g^4\delta_u^3\pi_g^4\sigma_u^2 4s\sigma_g^2 4s\sigma_u^{1b}$
5.44	4.66	10.11	9.20	8.12	$3d\sigma_g^2\pi_u^4\delta_g^3\delta_u^4\pi_g^4\sigma_u^2 4s\sigma_g^1 4s\sigma_u^2$
...	...	0.12	0.13	0.12	$3d\sigma_g^1\pi_u^4\delta_g^4\delta_u^3\pi_g^4\sigma_u^2 4s\sigma_g^1 4s\sigma_u^2$
0.31	0.30	...	...	0.10	$4s\sigma_g \rightarrow 4p\sigma_g$
0.25	0.23	...	...	0.10	$4s\sigma_g \rightarrow 5s\sigma_g$
0.12	0.11	...	...	...	$4s\sigma_g \rightarrow 5p\sigma_g$
0.24	0.24	0.12	0.12	0.17	$3d\delta_u^2 \rightarrow 3d\delta_g 4d\delta_g$
...	0.10	...	...	...	$3d\delta_u\sigma_u \rightarrow 3d\delta_g 4d\sigma_g$
...	...	...	...	0.29	$3d\delta_u\pi_g \rightarrow 3d\delta_g 4p\pi_u$
...	...	...	0.22	0.32	$3d\delta_u\pi_g \rightarrow 3d\delta_g 4d\pi_u$
0.21	0.21	...	0.22	0.30	$3d\delta_u\pi_g \rightarrow 3d\delta_g 5p\pi_u$
0.59	0.77	...	...	...	$3d\sigma_g\delta_u \rightarrow 3d\delta_g 4s\sigma_u$
...	...	...	...	0.10	$4s\sigma_u \rightarrow 4p\sigma_u$
0.20	0.23	...	...	...	$4s\sigma_u \rightarrow 5s\sigma_u$
0.34	0.22	0.10	0.09	0.16	$3d\delta_u 4s\sigma_u \rightarrow 3d\delta_g 4p\sigma_g$
0.26	0.10	0.10	0.11	0.16	$3d\delta_u 4s\sigma_u \rightarrow 3d\delta_g 5s\sigma_g$
0.20	...	...	...	...	$3d\delta_u 4s\sigma_u \rightarrow 3d\delta_g 5p\sigma_g$
...	...	...	0.13	0.18	$3d\delta_u 4s\sigma_g \rightarrow 3d\delta_g 4p\sigma_u$
...	...	...	0.13	0.17	$3d\delta_u 4s\sigma_g \rightarrow 3d\delta_g 5s\sigma_u$
...	...	0.14	0.17	0.20	$3d\delta_u 4s\sigma_g \rightarrow 3d\delta_g 5p\sigma_u$
0.10	...	0.11	0.13	0.17	$3d\delta_u \rightarrow 4d\delta_u$
...	...	...	0.14	0.11	$3d\delta_g \rightarrow 4d\delta_g$
...	...	...	0.09	0.12	$3d\delta_u 3d\delta_g' \rightarrow 3d\delta_g 4d\delta_u$
...	...	...	0.19	0.26	$4s\sigma_g^2 \rightarrow 4p\pi_g^2$

[a] CSFs relative to the leading configuration.

[b] the leading configuration.

Table 4–25: Percentage contribution of leading configurations to the wavefunction for Π_u SDCI at 2.20Å, $11s8p4d2f$

Calculation						
Closed shell		Parental MO				
$^1\Pi_u$ (12/98)	$^3\Pi_u$ (12/98)	$^1\Pi_u$ (12/98)	$^3\Pi_u$ (12/98)	$^3\Pi_u$ (12/78)	$^3\Pi_u$ (12/66)	Configuration[a]
83.18	83.32	83.11	83.37	82.53	81.38	$3d\sigma_g^2\pi_u^4\delta_g^4\delta_u^4\pi_g^3\sigma_u^2 4s\sigma_g^2 4s\sigma_u^{1b}$
2.91	2.66	5.06	4.69	4.47	3.89	$3d\sigma_g^2\pi_u^3\delta_g^4\delta_u^4\pi_g^4\sigma_u^2 4s\sigma_g^1 4s\sigma_u^2$
...	...	0.10	0.11	0.11	0.10	$3d\sigma_g^1\pi_u^3\delta_g^4\delta_u^4\pi_g^4\sigma_u^2 4s\sigma_g^1 4s\sigma_u^2$
0.31	0.26	...	...	...	0.13	$4s\sigma_g \rightarrow 5s\sigma_g$
0.35	0.35	...	...	...	0.10	$4s\sigma_g \rightarrow 4p\sigma_g$
0.17	0.25	...	...	...	...	$4s\sigma_g \rightarrow 5p\sigma_g$
0.23	0.25	0.12	0.24	0.27	0.38	$3d\pi_u\sigma_u \rightarrow 3d\pi_g 4d\sigma_g$
...	...	...	...	...	0.11	$3d\pi_u\sigma_u \rightarrow 3d\pi_g 4d\sigma_g$
...	0.10	...	0.09	...	0.18	$3d\pi_u 4s\sigma_u \rightarrow 3d\pi_g 4p\sigma_g$
...	...	...	...	...	0.15	$3d\pi_u 4s\sigma_u \rightarrow 3d\pi_g 4p\sigma_g$
...	...	...	...	0.11	0.19	$3d\pi_u \rightarrow 4p\pi_u$
0.13	0.14	0.12	0.13	0.17	0.25	$3d\pi_u \rightarrow 4d\pi_u$
0.19	...	0.18	0.15	0.26	0.34	$3d\pi_u \rightarrow 5p\pi_u$
...	...	...	...	0.11	0.17	$3d\pi_u\pi_g' \rightarrow 3d\pi_g 4p\pi_u$
0.10	0.10	0.10	0.10	0.14	0.19	$3d\pi_u\pi_g' \rightarrow 3d\pi_g 4d\pi_u$
0.12	0.12	0.12	0.12	0.14	0.19	$3d\pi_u\pi_g' \rightarrow 3d\pi_g 5p\pi_u$
0.19	0.22	...	...	0.11	...	$4s\sigma_u \rightarrow 5s\sigma_u$
0.63	0.70	...	...	0.11	...	$4s\sigma_u \rightarrow 4p\sigma_u$
0.11	0.10	...	...	...	...	$3d\pi_u 4s\sigma_g \rightarrow 3d\pi_g 5s\sigma_u$
0.25	0.14	...	...	...	...	$3d\pi_u 4s\sigma_g \rightarrow 3d\pi_g 4p\sigma_u$
	...	...	...	...0.19	0.26	$4s\sigma_g^2 \rightarrow 4p\pi_u^2$

[a] CSFs relative to the leading configuration.

[b] the leading configuration.

of the higher virtual MOs could lead to a significant increase in the excitation energies of the d-hole states.

Not surprisingly, the inclusion of the "unlinked" cluster terms in the parental orbital calculations has a much smaller effect for the d-hole states (~0.4 eV) than in the corresponding ground state based computations (~1.1 eV). This reflects the improved zeroth-order description of the states afforded by the parental MOs, and the large degree of reorganisation that occurs accompanying a $3d \rightarrow 4s$ transition, which is not well described at the SDCI level for the ground state MOs. The adequate description of the reorganisation would require that the $d \rightarrow d'$ configurations also be used as references, leading to the inclusion of triply excited states in the calculation. The Davidson correction has little effect on the $^1\Sigma_u^+$ ion-pair state relative to the ground state, however the $^3\Sigma_u^+$ excitation energy is raised.

The natural orbital analysis and orbital occupancies (Table 4–15) support the conclusion that these are effectively singly bonded states. The degree of p-character in the $^1\Sigma_u^+(4s\sigma_u, 4s\sigma_g)$ state would suggest that it is an ion-pair state with a large amount of valence character, rather than vice-versa.

4.5.6 Calculations on atomic copper

During the work on dicopper, calculations were also performed on the atom using the $11s8p4d2f(2.89, 0.40)$ basis set. The absolute and MO energies obtained at the SCF level for the ^2S, ^2D, and $^2P^0$ states are listed in Table 4–26, along with the numerical Hartree-Fock of Martin and Hay [407]. Although the calculations were performed under D_{2h} symmetry, equivalence restrictions were employed for the various shells to maintain "spherical" symmetry. Despite the large basis set used, the results are still found to be far for the Hartree-Fock limit, the absolute energy of the NHF being lower by ~0.15 au. The use of GTOs, which are relatively poor near the nucleus is probably responsible for some of the energy loss. The energy difference obtained for ^2S-^2D separation is in reasonable agreement with the NHF, however, the value for ^2S-^2P is poor. The reason for this discrepancy of almost 1 eV is that the functions used to describe the $4p$ orbital are too tight, as evidenced

Table 4–26: Energies of Cu atom SCF for the $11s8p4d2f$ basis set (au)

MO	State ^2S		^2D		^2P	
$1s$	-328.8078	(2.00)	-329.0491	(2.00)	-328.8625	(2.00)
$2s$	-40.8305	(2.00)	-41.0965	(2.00)	-40.8819	(2.00)
$2p$	-35.6314	(6.00)	-35.8926	(6.00)	-35.6841	(6.00)
$3s$	-5.0168	(2.00)	-5.2663	(2.00)	-5.0702	(2.00)
$3p$	-3.3295	(6.00)	-3.5624	(6.00)	-3.3863	(6.00)
$3d$	-0.4893	(10.00)	-0.6395	(9.00)	-0.5464	(10.00)
$4s$	-0.2384	(1.00)	-0.2854	(2.00)	-0.0284	(0.00)
$4p$	0.0986	(0.00)	0.0695	(0.00)	0.0657	(1.00)
total energy	-1638.887412		-1638.874391		-1638.760960	
excitation energy (eV)	0.0000		0.3543		3.4408	
NHF energy[a]	-1638.9642		-1638.9505		-1638.8657	
excitation energy (eV)	0.00		0.37		2.68	

The terms in parentheses are the orbital occupancies.

[a] numerical Hartree-Fock of Martin and Hay [407].

by the large Mulliken population (0.350) of the most diffuse p function. The most diffuse p in the present basis set has an exponent of 0.069299, this compares to 0.056 which Marian *et al.* [342] estimate to be optimal for the purpose of describing the $3d^{10}4p^1$ state.

The energies of the $3d$ orbitals for the ^2D state are lower than the corresponding values for the ^2S state, this reflects the more compact nature of the d shell associated with the lower number of electrons (d^9 vs. d^{10}). For the $4s$ the energetic penalty due to the increase in electrons (1 to 2) on comparing ^2S to ^2D, is more than compensated by the reduction in the shielding of the nucleus going from d^{10} to d^9, as shown by the increased stability of the orbital. The core orbitals of the ^2D state also occur at lower energies than their ^2S and ^2P counterparts, the ^2P being in the main similar to the ^2S.

The effect of relativity (which is not included in the present computations)

Table 4–27: The effect of relativity on the ^2S state MO energies (au)

MO	non-relativistic	relativistic[a]	difference
$1s$	-328.8078	-332.6545	-3.8467
$2s$	-40.8305	-41.6718	-0.8413
$2p$	-35.6314	-35.8107	-0.1793
$3s$	-5.0168	-5.1565	-0.1397
$3p$	-3.3295	-3.3629	-0.0334
$3d$	-0.4893	-0.4797	0.0096
$4s$	-0.2384	-0.2448	-0.0064

[a] numerical Dirac-Fock of Desclaux [341].

upon the numerical Hartree-Fock is to lower the energy of the ^2D state to below that of the ^2S, by 0.04 eV [342, 407]. The present non-relativistic ^2S MO energies are compared to the numerical Dirac-Fock results of Desclaux [341] in Table 4–27. As expected a considerable lowering in energy is evident for the core orbitals, the valence $3d$ and $4s$ being effected to a much lesser extent. The destabilisation of the $3d$ orbitals upon the inclusion of relativity is due to the contraction of the $4s$ and core orbitals increasing the shielding of the nucleus for this orbital with high angular momentum and relatively little penetration.

The CI calculations on the atomic Cu states employed an active space of 55 orbitals with eleven active electrons. The 1-$3s$, 2-$3p$ AOs were frozen and the fourteen highest energy virtual orbitals were discarded, corresponding to the core complements, two s and one set of p's, The ^2S, ^2D, and ^2P atomic states were computed using n-particle basis sets of the corresponding SCF (parental orbital calculations) and using the ^2S SCF orbitals (a common orbital calculations). Two divisions of the active space were used six internal and 48 external (6/48), and nine internal with 45 external (9/45). The latter, which includes the $4p$ MOs within the internal space allowed the calculation of the ^2P state. The configuration space consisted of those states singly and doubly excited from the reference configurations (Tables 4–28 and 4–29) and from the "internal" states produced by one and two electron excitations from the reference configurations. The dimensions of the calculations are presented in Table 4–29. At this stage in the calculation the

Table 4–28: Reference configurations employed for the calculation of the Cu atom

			$3d$			$4s$	$4p$		
State	a_g	a'_g	b_{2g}	a_u	b_{3g}	a_g	b_{3u}	b_{2u}	b_{1g}
^2S	2	2	2	2	2	1	-	-	-
^2D	2	2	2	2	1	2	-	-	-
	2	2	2	2	1	-	2	-	-
	2	2	2	2	1	-	-	2	-
	2	2	2	2	1	-	-	-	2
^2P	2	2	2	2	2	-	1	-	-

equivalence restrictions were necessarily relaxed, although the effect should not be as pronounced as at the SCF level; a small energy lowering due to the localisation of the hole to a p or a d orbital of a particular symmetry is expected.

The energies obtained for the SDCI, and including the estimate correction for higher than double excitations through the Davidson [63] and Siegbahn [64] corrections, are compared to experiment in Table 4–30. Marian *et al.* [342], using the no-pair method, estimate that the lowering in the ^2S-^2D energy difference due to relativistic effects as 0.43 eV. Therefore comparison for these non-relativistic calculations should be made with a "non-relativistic experimental" value of 1.92 eV. In all cases the parental orbital calculations are found to give the lower absolute and excitation energies. This is especially apparent for the ^2D state, for which a lowering in absolute energy of approximately 0.04 au is obtained, accompanied by a reduction in the ^2S-^2D excitation energy to ~1 eV. Most of the change in the ^2S-^2D energy is returned at the SDCI level, indeed for the parent orbital calculations, the corrections have little differential effect. A study of the important configurations in the CI (Table 4–33 and Tables 4–32, 4–34 for ^2S and ^2P) demonstrates that this is due to the relaxation of the $3d$ and $4s$ orbitals resulting from the $3d \rightarrow 4s$ promotion. For the CI based on the ^2S SCF MOs, there are a large number of configurations associated with transitions of the form $d - d'$ and $s - s'$, which are not present, at least to such a large extent, in the ^2D MO calculation. The transition from the ^2S SCF orbitals to the parent orbital set has a much smaller

Table 4–29: Details of direct CI calculations for the Cu atom using the $11s8p4d2f$ basis set

		Active space				
State	SCF MOs	int.	ext.	Ref.[a]	C^{2b}	CSFs
^2S	^2S	6	48	1(3)	0.950	23347
	^2S	9	45	1(213)	0.950	710216
^2D	^2S	6	48	1(1)	0.896	23199
	^2S	9	45	1(196)	0.898	707688
	^2S	9	45	4(245)	0.898	1507700
	^2D	6	48	1(1)	0.937	23199
	^2D	9	45	4(245)	0.950	1507700
^2P	^2S	9	45	1(191)	0.949	710649
	^2P	9	45	1(191)	0.952	710649

[a] The term in parentheses is the number of states generated within the internal space.

[b] weight of reference states.

effect on the ^2P. The increase in the internal space from six to nine orbitals and the inclusion of the $4p$ orbitals in the generating space, leads to a small lowering of the ^2S absolute energy, with a larger effect for the ^2D. The importance of the $s^2 \rightarrow p^2$ for the ^2D is illustrated by weights of the terms in the CI expansion for this state, ~1 % for the parent orbital calculation.

The excitation energy obtained for the $^2S - ^2P$ is in good agreement with experiment, the remaining discrepancy probably being due to the functions used to represent the $4p$ orbitals, as stated above, although as no values for the expected relativistic correction for this transition are available this effect cannot be ruled out. Including the effects of relativity could be expected to lower the ^2S ground state relative to the ^2P state, improving the agreement with experiment. The $^2S - ^2D$ separation is however considerably less than experiment, ~1 eV if the correction for relativity is made, and, more worrying, than the published results of similar calculations by Werner and Martin [372] and Marian *et al.*[342], Table 4–31. A variety of methods were employed by both groups, including SDCI, the resulting

Table 4–30: Energies calculated for the Cu atom by direct CI

		Energies[a]		
State	MO set[b]	CI	CI+Davidson	CI+Siegbahn
^2S	^2S	-0.164870	-0.178670	-0.179393
		(0.0000)	(0.0000)	(0.0000)
	^2S	-0.165993	-0.180085	-0.180836
		(0.0000)	(0.0000)	(0.0000)
^2D	^2S	-0.081352	-0.119281	-0.123686
		(2.2726)	(1.6160)	(1.5158)
	^2S	-0.090686	-0.128634	-0.132922
		(2.0492)	(1.4000)	(1.3038)
	^2S	-0.090723	-0.127342	-0.131480
		(2.0482)	(1.4352)	(1.3430)
	^2D	-0.121372	-0.141648	-0.142719
		(1.0641)	(1.0074)	(0.9979)
	^2D	-0.132489	-0.144785	-0.146118
		(0.9117)	(0.9606)	(0.9447)
	exptl[c]	(1.49)		
^2P	^2S	-0.026674	-0.043407	-0.044507
		(3.7910)	(3.7310)	(3.7228)
	^2P	-0.032281	-0.045308	-0.045967
		(3.6384)	(3.6674)	(3.6699)
	exptl[c]	(3.81)		

The terms in parentheses are the excitation energies in eV relative to the ^2S state.

[a] relative to -1639 au.

[b] details in Table 4–29.

[c]experimental values from [338].

Table 4–31: Comparison of the present and previous $^2S - ^2D$ excitation energies

Method	Basis	$^2S - ^2D$[a]	Ref.
SDCI	$(16s11p6d2f)/[10s8p4d2f]$	0.9117	-
SDCI+DC	$(16s11p6d2f)/[10s8p4d2f]$	0.9606	-
SDCI+SC	$(16s11p6d2f)/[10s8p4d2f]$	0.9447	-
SDCI	$(16s11p6d3f)/[10s8p4d2f]$	1.56	[342]
SDCI+DC	$(16s11p6d3f)/[10s8p4d2f]$	1.55	[342]
MCPF	$(16s11p6d3f)/[10s8p4d2f]$	1.51	[342]
SDCI	$(15s11p6d2f)/[9s6p4d2f]$	1.52 (1.03)	[372]
SDCI+DC	$(15s11p6d2f)/[9s6p4d2f]$	1.49 (1.00)	[372]
CEPA	$(15s11p6d2f)/[9s6p4d2f]$	1.42 (0.94)	[372]

[a] the energies are in eV.

[b] the terms in parentheses include relativistic effects.

Table 4–32: Percentage contribution of leading configurations to the wavefunction for ^2S SDCI

Calculation		
6/48	9/49	Configuration[a]
95.03	94.78	$3d^{10}4s^{1}$[b]
0.09	0.09	$4s \rightarrow 5s$

[a] CSFs relative to the leading configuration.

[b] the leading configuration.

$^2S - ^2D$ separation is almost independent of method, ranging from 1.40 to 1.56 eV. The basis set used in both studies was similar to the present one in the choice of exponentials and contraction scheme for the s, p, and d functions. Whilst different f polarisation functions were used this should not have the observed effect, therefore differences in basis set can be virtually ruled out as the reason for the discrepancy. This leaves the active set of MOs, it is probable that the discarding of the virtual MOs has, despite the cut-off coinciding with a large gap in the SCF MO energies, had a severely detrimental effect on the present calculation, and by implication the computations on the diatomic.

It is therefore expected on the basis of these results that the excitation energies

Table 4–33: Percentage contribution of leading configurations to the wavefunction for ^2D SDCI

Calculation				
$^2S^a$ (6/48)	$^2S^a$ (9/45)	$^2D^a$ (6/48)	$^2D^a$ (9/45)	Configuration[b]
89.59	87.18	93.69	91.74	$3da_g^2 3da_g'^2 3db_{2g}^2 3da_u^2 3db_{3g}^1 4s^{2b}c$
0.34	0.34	...	...	$3db_{2g} \rightarrow 4db_{2g}$
0.25	0.24	...	...	$3db_{2g} \rightarrow 5db_{2g}$
0.37	0.39	...	...	$3da_u \rightarrow 4da_u$
0.28	0.27	...	...	$3da_u \rightarrow 5da_u$
0.35	0.34	...	...	$3da_g \rightarrow 4da_g$
0.21	0.21	...	...	$3da_g \rightarrow 5da_g$
0.27	0.26	...	...	$3da_g' \rightarrow 4da_g'$
0.20	0.22	...	...	$3da_g' \rightarrow 5da_g'$
0.38	0.37	...	...	$3db_{3g} \rightarrow 4db_{3g}$
0.28	0.28	...	...	$3db_{3g} \rightarrow 5db_{3g}$
1.70	1.84	...	...	$4s \rightarrow 5s$
0.90	0.83	...	...	$4s \rightarrow 6s$
0.12	0.11	...	...	$4s \rightarrow 7s$
0.28	0.88	0.44	1.05	$4s^2 \rightarrow 4pb_{3u}^2$
0.22	0.29	0.22	0.21	$4s^2 \rightarrow 4pb_{3u}, 5pb_{3u}$
0.28	0.90	0.49	0.96	$4s^2 \rightarrow 4pb_{2u}^2$
0.22	0.29	0.25	0.19	$4s^2 \rightarrow 4pb_{2u}, 5pb_{2u}$
0.26	0.79	0.49	1.08	$4s^2 \rightarrow 4pb_{1g}^2$
0.20	0.25	0.25	0.22	$4s^2 \rightarrow 4pb_{1g}, 5pb_{1g}$

[a] n-particle basis.

[b] CSFs relative to the leading configuration.

[c] the leading configuration.

Table 4–34: Percentage contribution of leading configurations to the wavefunction for ^2P SDCI

Calculation		
$^2S^a$ (6/48)	$^2P^a$ (9/45)	Configuration[b]
93.83	94.13	$3d^{10}4pb_{1u}^{1}$ [c]
0.30	0.12	$3da_g \rightarrow 4s$
0.72	0.82	$3da'_g \rightarrow 4s$
0.67	...	$4pb_{1g} \rightarrow 5pb_{1g}$
...	0.11	$3da'_g \rightarrow 3da_g$

[a] n-particle basis.

[b] CSFs relative to the leading configuration.

[c] the leading configuration.

calculated for the transitions in Cu_2 are too low by 0.5 eV, an amount similar to the estimated lowering of the ^2D atomic state relative to the ground state due to relativistic effects. Then why is no such effect observed for the ^2P? It would seem that the ^2S and ^2P are similar enough that no large differential is to be found for the high energy virtual orbitals.

4.6 The spin-orbit interaction for $^2S+^2D$ states

The result of the spin-orbit interaction on the excitation energies was included in a semi-empirical manner following the "atoms-in-molecules" model of Cohen and Schneider [408], and Hay *et al.* [409]. In this treatment the matrix elements coupling the molecular states at infinite separation are determined using the atomic spin-orbit parameters. At this separation the molecular states can be expressed in terms of the atomic states from which they arise. Inherent in this scheme is the assumption that the spin-orbit elements do not change with internuclear separation, an approximation which is valid if the molecular states retain the identity of the atomic states, ie if the bonding interaction remains weak.

The method was originally derived by Cohen and Schneider to describe the low-lying states of the rare gas dimers Ne_2 and Ne_2^+ [408], the results of which are in reasonable agreement with later full *ab initio* calculations [410]. Hay *et al.* applied a similar method to the transition metal dimers Zn_2 and Hg_2 [409]. Further use has included alkali metal dimers [411] and the ion-pair states of CuCl [412].

The spin-orbit interaction is given by one- and two-electron terms as in Equation (4.2) [413,414]. The one-electron term relates to the interaction of the electron's magnetic dipole moment with the magnetic field produced by the the orbital motion in the nuclear electric field; the two-electron term, the spin-other-orbit term, expresses the interaction of the spin of the electron with the magnetic fields produced by the motion of the other electrons. The spin-other-orbit term is, in effect, the shielding of the nuclear field caused by the presence of the other electrons [406].

$$H_{SO} = \frac{e^2\hbar}{8\pi\epsilon_0 m^2 c^2}\left\{\sum_{Ai}\frac{Z_A}{r_{iA}^3}\mathbf{s}_i.(r_{iA}\times\mathbf{p}_i) - \sum_{i\neq j}\frac{1}{r_{ij}^3}(r_{ij}\times\mathbf{p}_i).(\mathbf{s_i}+2\mathbf{s}_j)\right\} \qquad (4.2)$$

The one-electron term, under a central field, can be expressed in terms of the electron spin, $\mathbf{s}_i$, and angular momentum, $\mathbf{l}_i$:

$$H_{SO} = \sum_i \xi_i(r_i) \mathbf{l}_i . \mathbf{s}_i \tag{4.3}$$

Cohen and Schneider proceeded by assuming that the coupling constant, $\xi_i(r_i)$, was the same for all the electrons within a particular shell ($\zeta_{n_i l_i}$) and that any variation in the two-electron terms was negligible. Much of the two-electron contribution is then included through the use of experimentally determined parameters for the atom. This was extended to the molecular case by assuming that the molecular orbitals remain atomic like, leading to Equation (4.4).

$$V_{SO} = \sum_{iA} \zeta^A_{n_i^A l_i^A} \mathbf{l}_i^A . \mathbf{s}_i^A \tag{4.4}$$

The summation running over atoms, A, and the associated electrons, i.

Since the molecular states arise from one atom in ^2S, only the ^2D need be considered. The atomic states are decomposed into space and spin combinations as follows [413], the terms referring to the d-hole in the Cu atom:

$$\begin{array}{lll}
^2D_{5/2} & m_J = \frac{5}{2} & [2^+] \\
 & \frac{3}{2} & \frac{1}{\sqrt{5}} \{[2^-] + 2[1^+]\} \\
 & \frac{1}{2} & \frac{1}{\sqrt{5}} \{\sqrt{2}[1^-] + \sqrt{3}[0^+]\} \\
 & -\frac{1}{2} & \frac{1}{\sqrt{5}} \{\sqrt{3}[0^-] + \sqrt{2}[\underline{1}^+]\} \\
 & & \\
^2D_{3/2} & m_J = \frac{3}{2} & \frac{1}{\sqrt{5}} \{2[2^-] - [1^+]\} \\
 & \frac{1}{2} & \frac{1}{\sqrt{5}} \{\sqrt{3}[1^-] - \sqrt{2}[0^+]\} \\
 & -\frac{1}{2} & \frac{1}{\sqrt{5}} \{\sqrt{2}[0^-] - \sqrt{3}[\underline{1}^+]\}
\end{array}$$

Similarly for the *ungerade* ($-$) and *gerade* ($+$) molecular states:

$$
\begin{aligned}
{}^3\Delta_3 &= \tfrac{1}{\sqrt{2}}\{[2^+]_A[0^+]_B \mp [0^+]_A[2^+]_B\} \\
{}^3\Delta_2 &= \tfrac{1}{\sqrt{2}}\left\{\tfrac{1}{\sqrt{2}}([2^-]_A[0^+]_B + [2^+]_A[0^-]_B) \mp \tfrac{1}{\sqrt{2}}([0^+]_A[2^-]_B + [0^-]_A[2^+]_B)\right\} \\
{}^3\Delta_1 &= \tfrac{1}{\sqrt{2}}\{[2^-]_A[0^-]_B \mp [0^-]_A[2^-]_B\} \\
{}^3\Pi_2 &= \tfrac{1}{\sqrt{2}}\{[1^+]_A[0^+]_B \mp [0^+]_A[1^+]_B\} \\
{}^3\Pi_1 &= \tfrac{1}{\sqrt{2}}\left\{\tfrac{1}{\sqrt{2}}([1^-]_A[0^+]_B + [1^+]_A[0^-]_B) \mp \tfrac{1}{\sqrt{2}}([0^+]_A[1^-]_B + [0^-]_A[1^+]_B)\right\} \\
{}^3\Pi_{0^+} &= \tfrac{1}{\sqrt{2}}\left\{\tfrac{1}{\sqrt{2}}([1^-]_A[0^-]_B - [\underline{1}^+]_A[0^+]_B) \mp \tfrac{1}{\sqrt{2}}([0^-]_A[1^-]_B - [0^+]_A[\underline{1}^+]_B)\right\} \\
{}^3\Pi_{0^-} &= \tfrac{1}{\sqrt{2}}\left\{\tfrac{1}{\sqrt{2}}([1^-]_A[0^-]_B + [\underline{1}^+]_A[0^+]_B) \mp \tfrac{1}{\sqrt{2}}([0^-]_A[1^-]_B + [0^+]_A[\underline{1}^+]_B)\right\} \\
{}^3\Sigma_1 &= \tfrac{1}{\sqrt{2}}\{[0^+]_A[0^+]_B \mp [0^+]_A[0^+]_B\} \\
{}^3\Sigma_{0^-} &= \tfrac{1}{\sqrt{2}}\left\{\tfrac{1}{\sqrt{2}}([0^-]_A[0^+]_B + [0^+]_A[0^-]_B) \mp \tfrac{1}{\sqrt{2}}([0^+]_A[0^-]_B + [0^-]_A[0^+]_B)\right\} \\
{}^1\Delta_2 &= \tfrac{1}{\sqrt{2}}\left\{\tfrac{1}{\sqrt{2}}([2^-]_A[0^+]_B - [2^+]_A[0^-]_B) \mp \tfrac{1}{\sqrt{2}}([0^+]_A[2^-]_B - [0^-]_A[2^+]_B)\right\} \\
{}^1\Pi_1 &= \tfrac{1}{\sqrt{2}}\left\{\tfrac{1}{\sqrt{2}}([1^-]_A[0^+]_B - [1^+]_A[0^-]_B) \mp \tfrac{1}{\sqrt{2}}([0^-]_A[1^+]_B - [0^+]_A[1^-]_B)\right\} \\
{}^1\Sigma_{0^+} &= \tfrac{1}{\sqrt{2}}\left\{\tfrac{1}{\sqrt{2}}([0^-]_A[0^+]_B - [0^+]_A[0^-]_B) \mp \tfrac{1}{\sqrt{2}}([0^+]_A[0^-]_B - [0^-]_A[0^+]_B)\right\}
\end{aligned}
$$

The coupling matrix for the atomic terms, Table 4–35, is derived using the relation $\mathbf{l}.\mathbf{s} = l_z s_z + \frac{1}{2} l^- s^+ + \frac{1}{2} l^+ s^-$, and the molecular coupling matrices, Tables 4–36 to 4–38, are then derived using the above relation for the *d* orbitals, or through the correlation of the molecular states with the corresponding atomic asymptotes.

The results of the treatment for the ground state and parental orbital MOs are listed in Table 4–40; also included are the first-order, or diagonal, energies. The coupling constant used is 817 cm^{-1}, the coupling constant for the ^2D atomic states (Section 4.1). The excitation energies for the states not calculated with the parental orbital set are estimated using the either the lowering of the respective singlet state in the case of $^3\Delta_u$, or the average of the computed states ($^{1,3}\Sigma_u^+$).

This treatment is clearly crude in nature by its very design, neglecting pertur-

Table 4–35: Atomic spin-orbit coupling matrix

	$^2D_{5/2}$	$^2D_{3/2}$
$^2D_{5/2}$	1	0
$^2D_{3/2}$	0	$-\frac{3}{2}$

Table 4–36: Coupling matrix for Ω=0 states

	$^3\Pi_{0+}$	$^1\Sigma_{0+}$	$^3\Pi_{0-}$	$^3\Sigma_{0-}$
$^3\Pi_{0+}$	$-\frac{1}{2}$	$-\frac{\sqrt{3}}{\sqrt{2}}$	0	0
$^1\Sigma_{0+}$	$-\frac{\sqrt{3}}{\sqrt{2}}$	0	0	0
$^3\Pi_{0-}$	0	0	$-\frac{1}{2}$	$\frac{\sqrt{3}}{\sqrt{2}}$
$^3\Sigma_{0-}$	0	0	$\frac{\sqrt{3}}{\sqrt{2}}$	0

Table 4–37: Coupling matrix for Ω=1 states

	$^3\Delta_1$	$^3\Pi_1$	$^1\Pi_1$	$^3\Sigma_1$
$^3\Delta_1$	-1	$\frac{1}{\sqrt{2}}$	$-\frac{1}{\sqrt{2}}$	0
$^3\Pi_1$	$\frac{1}{\sqrt{2}}$	0	$\frac{1}{2}$	$\frac{\sqrt{3}}{\sqrt{2}}$
$^1\Pi_1$	$-\frac{1}{\sqrt{2}}$	$\frac{1}{2}$	0	$-\frac{\sqrt{3}}{\sqrt{2}}$
$^3\Sigma_1$	0	$\frac{\sqrt{3}}{\sqrt{2}}$	$-\frac{\sqrt{3}}{\sqrt{2}}$	0

Table 4–38: Coupling matrix for Ω=2 states

	$^3\Delta_2$	$^1\Delta_2$	$^3\Pi_2$
$^3\Delta_2$	0	-1	$\frac{1}{\sqrt{2}}$
$^1\Delta_2$	-1	0	$-\frac{1}{\sqrt{2}}$
$^3\Pi_2$	$\frac{1}{\sqrt{2}}$	$-\frac{1}{\sqrt{2}}$	$\frac{1}{2}$

Table 4–39: Coupling matrix for Ω=3 states

	$^3\Delta_3$
$^3\Delta_2$	1

Table 4–40: Energies of *ungerade* states of Cu_2 from the $^2S+^2D$ atomic asymptote including the spin-orbit interaction (eV)

State		Ground state MOs			Parental MOs	
		ab initio	diagonal	Spin-orbit	*ab initio*	Spin-orbit
$^3\Pi_u$	0_u^+	3.7111	3.7617	3.7566	2.6903	2.7359
	0_u^-		3.7617	3.7557		2.7350
	1_u		3.7111	3.6880		2.6686
	2_u		3.6605	3.6432		2.6236
$^1\Pi_u$	1_u	3.8391	3.8391	3.8332	2.8385	2.8316
$^3\Delta_u$	1_u	4.3220	4.4233	4.4395	(3.33)	(3.45)
	2_u		4.3220	4.2533		(3.27)
	3_u		4.2207	4.2207		(3.23)
$^1\Delta_u$	2_u	4.3557	4.3557	4.4416	3.3967	3.4703
$^3\Sigma_u^+$	0_u^-	5.0281	5.0281	5.0341	(4.03)	(4.04)
	1_u		5.0281	5.0410		(4.04)
$^1\Sigma_u^+$	0_u^+	5.2786	5.2786	5.2887	(4.28)	(4.28)

The terms in parentheses are estimated, see text for further details.

bations through interactions with other states; this is especially the $^1\Sigma_u^+$ ion-pair state, which can be expected to have an appreciable effect on the the nearby $^3\Pi_{0_u^+}$. However it serves to give an indication of the likely importance of the spin-orbit interaction. The second-order, or off-diagonal, interaction is generally small and most of the spin-orbit effect is returned through the first-order, or diagonal, terms. Little mixing is produced between the states, except for the Ω=2 components of the $^{1,3}\Delta_u$ which interact strongly, the resulting states are linear combinations of the singlet and triplet states, in the ratio 2:1. The second-order spin-orbit effect for these states is of the same magnitude as the first-order effect, ~0.05 eV.

4.7 Comparison with experiment

The results of the present study of the *ungerade* states of dicopper are listed in Table 4–41 along with experimental transition energies. As it is estimated that the 2.20 Å used in this study is approximately 0.07 Å shorter than the ground state equilibrium geometry for this basis set, and assuming that the excited states are described to the same level, a further set of experimental transition energies has been derived from spectroscopic constants for transitions occurring at 2.15 Å(Table 4–41). It should be noted that the $^1\Sigma_u^+(4s\sigma_g, 4s\sigma_u^*)$ and $^1\Pi_u$ states cross in the region of 2.21 Å.

The calculations based upon the ground state MOs yield excitation energies considerably higher than experiment, ~0.5 eV for the $s\sigma_u^1 s\sigma_g^1$ states, and ~1 eV for the $^2S+^2D$ states. The following assignments will be based on the parental orbital calculations, predominantly through comparison with the experimental energies as estimated at 2.15 Å.

The assignments of the low-lying states agrees with the reassessment of the work of Witko and Beckmann [398] given in Section 4.4. Bondybey's assignment of the *a*-state as $^3\Sigma_u^+(4s\sigma_u^1, 4s\sigma_g^1)$ [349] is confirmed. The relatively high energy of the $^1\Sigma_u^+(4s\sigma_u, 3d\sigma_g)$ state strongly argues against this state being either of the *A*- or the *B*-states. Although questions persist regarding the magnitudes of the effects of increasing the active space to include the core-complements, and the inclusion of relativity on ordering of the $^1\Sigma_u^+(4s\sigma_u^1, 4s\sigma_g^1)$ and $^3\Pi_u(4s\sigma_u^1, 3d\pi_g^3)$, these effects are expected to largely cancel. The *A*-state is assigned as $^3\Pi_{0_u^+}$, and the *B*-state as the $^1\Sigma_u^+$ (0_u^+) ion-pair state. The next two excited states may also be assigned with confidence: the *C*-state as $^1\Pi_{1u}$, and the *D* state as $^3\Delta_{1u}$.

The energies of these low-lying states are within 0.2 eV of the experimental values, at 2.15 Å. The current calculations have not included relativistic effects which would be expected to lower the energy of the $^2S+^2D$ states relative to the ground state. The ^2D atomic state is lowered by 0.46 eV relative to the ^2S [342]. Such a large effect would lower the excitation energies to below experiment,

Table 4–41: Comparison of present results with experiment (eV)

	Results				Experiment[a]	
State	Ground state	Parental	Spin-Orbit		T_e(2.22 Å)	2.15 Å
$^3\Sigma_u^+(4s\sigma_u, 4s\sigma_g)$	2.39	1.92			1.91 (a)	
$^3\Pi_u(4s\sigma_u, 3d\pi_g)$	3.71	2.69	2_u	2.62		
			1_u	2.67		
			0_u^+	2.74	2.53 (A)	2.57
			0_u^-	2.74		
$^1\Pi_u(4s\sigma_u, 3d\pi_g)$	3.84	2.84	1_u	2.83	2.71 (C)	2.73
$^1\Sigma_u^+(4s\sigma_u, 4s\sigma_g)$	3.39	3.03			2.70 (B)	2.82
$^3\Delta_u(4s\sigma_u, 3d\delta_g)$	4.32	3.33	3_u	3.23		
			2_u	3.27		
			1_u	3.45	3.17 (D)	3.27
$^1\Delta_u(4s\sigma_u, 3d\delta_g)$	4.36	3.40	2_u	3.47		
$2^3\Sigma_u^+(4s\sigma_u, 3d\sigma_g)$	5.03	4.03	1_u	4.04		
			0_u^-	4.04		
$2^1\Sigma_u^+(4s\sigma_u, 3d\sigma_g)$	5.28	4.28	0_u^+	4.29	3.81 (G)	3.88

[a] see section 4.2

however, as evidenced by the atomic calculations increasing the active space can be expected to raise the excitation energies (Section 4.5.6).

Experimental evidence for the assignments as proposed above comes from lifetime measurements on the low-lying states. As discussed in Section 4.2, the *A*- and *B*-states have significantly shorter fluorescence lifetimes than the *C*- and *D*-states. The shortest lifetime is observed for the *B*-state, which is consistent with the assignment to an ion-pair state which would be expected to be strongly radiatively coupled to the ground state. The mixing of ion- pair character into the *A*-state ($^3\Pi_{0u^+}$) shortens the lifetime with respect to the "pure" $^2S+^2D$ states. Radiative transitions from the *C*- and *D*- states to the ground state are dipole forbidden, and also spin-forbidden for the *D*-state, which has an even longer lifetime than the *C*-state. It is also possible that the ion-pair character introduced into the *A*-, and *B*-states is the cause of the isotopic shifts noted by McCaffrey *et al.* [353], and the unusual vibration spacing [345, 347].

At higher energies the assignment is not clear. Experimentally the *E*-state has

not been positively identified as being due to Cu_2 [343]. Therefore, it would be possible to assign the F-, and G-states to the remaining Σ_u, however, Powers *et al.* [344] reported that these two states perturb each other which is not possible for the calculated states. Further clarification of this region of the experimental spectra requires the accurate treatment of states from higher asymptotes.

4.8 Conclusions and future work

Highly correlated calculations have been performed for the low-lying states of dicopper at, the near-equilibrium geometry of, 2.20 Å, and assignments are proposed on the basis of these results which largely confirm previous theoretical work. The effects of the inclusion of f-functions in the basis on the computed excitation energies have been investigated.

The experimental a-state is confirmed as $^3\Sigma_u^+(4s\sigma_u, 4s\sigma_g)$, the A-state is identified the 0_u^+ component of $^3\Pi_g(4s\sigma_u, 3d\pi_u)$, and the C-state as the corresponding singlet. In agreement with earlier work the $^1\Sigma_u^+(4s\sigma_u, 4s\sigma_g)$ is predicted to arise at considerably lower excitation energies than $^1\Sigma_u^+(4s\sigma_u, 3d\sigma_g)$, and be the B-state. Analysis of the SCF and SDCI wavefunctions supports the conclusion that this state is of ion-pair origin, although the computation of the potential energy surface, including the interactions with other states of the same (0_u^+) symmetry is desirable for confirmation.

A major effect on the computed excitation energies is d-d correlation; the lack of a correct description results in these being calculated too low, although interestingly this leads to in better agreement with experiment. Both diffuse and tight f-functions are required for the correct description of states. The necessity of including a further diffuse s, and even p-functions, for the description of the ion-pair state should be investigated. These are important in the description of the electron attached state. Also the possibility of using a more contracted basis set to reduce the expense of the calculations is suggested.

Large reorganisation energies of about 1 eV are shown to occur for $^2S+^2D$ states. If the treatment is to use ground state MO set, then an adequate description of the reorganisation on excitation is required. This is not forthcoming at the SDCI level and hence will probably require the use of $d \rightarrow d'$ states as reference states or triple excitations within the calculation.

Reasonable agreement if found between experiment and theory for calculations which include both of these effects, although the work on the atom would suggest that this is partially due to the fortuitous cancellation of errors introduced by the truncation of the active space and the lack of a relativistic treatment. For the $^2S+^2D$ states the excitation energy is overestimated. Most of the discrepancy that remains between the present work and experiment is probably due to the exclusion of these effects. Although unlikely to change the conclusions drawn for the low-lying states, an accurate calculation will require the inclusion of these relativistic effects, especially spin-orbit coupling. The determination of the position of $^3\Pi_{1_u}$, here predicted to lie 0.07 eV below the $^3\Pi_{0_u^+}$, is of considerable interest as the state should be experimentally accessible in the matrix, although this is unlikely to be the state observed by Pesič and Weniger [352].

In conclusion, the use of highly correlated calculations which include reorganisation effects are shown to give reasonable results for the excitation energies for dicopper, however, further work is required including excited states for higher asymptotes to assign the spectra below 5 eV. The accurate description of the states will require the inclusion of relativistic effects. Further work is required on the ion-pair state in order to investigate the reasons for the surprisingly short bond length and large binding energy obtained for a bond order of zero, particularly including interactions with nearby states.

Appendix A

Valence, Rydberg and Ion-Pair States

The definition of valence and Rydberg orbitals in the atom is straightforward; valence orbitals are those occupied in the ground state with the maximal principle quantum number, n, and others which share the same principle quantum number; Rydberg orbitals are then those orbitals with a higher value of n. The valence orbitals are responsible for bonding and lone-pairs in the molecular environment. Valence and Rydberg transitions are then defined as excitations which terminate on valence and Rydberg orbitals, respectively; the corresponding valence and Rydberg states are similarly defined. The extension to molecules proceeds using the united atom limit [314], extrapolating the molecular orbitals to the corresponding atomic (or moiety) limits.

The Rydberg orbitals in the molecular environment maintain atomic character due to their diffuse nature, ie the Rydberg electron experiences a central potential due to the effective charge, Z_{eff}, of the molecular core, comprising the nuclei and other electrons. The Rydberg electron is electrostatically bound to the core due to the imperfect shielding of the nuclei by the other electrons. The Rydberg states form a series converging to the ionisation potential of the core-hole orbital, the excitation energies given by a formula similar to atomic hydrogen (with charge Z_{eff}). Relative to the IP, $n = \infty$, this is,

$$IP - T_e = \frac{R_H Z_{eff}^2}{(n-\delta)^2}$$

Defining the term value (effectively the IP of the Rydberg state), where R_H is the Rydberg constant ($\sim$13.595 eV), and $(n - \delta)$ is the effective quantum number of the state, here δ is the quantum defect. Ignoring any interactions with other states the separations between Rydberg states are greatest for $\Delta n = 1$, and decrease for orbital angular momenta, $\Delta l = 1$, and spin, $\Delta s = 1$. The Z_{eff} is determined by the ability of the molecular-core electrons to shield the nuclear charge. In the atom this can be shown to vary considerably depending on the core-hole orbital, electrons in low angular momentum, low principle quantum number orbitals are significantly more effective at shielding the nuclei. For molecules this effect is smaller, and the Z_{eff} values is normally taken as one. The value of δ, and hence $(n - \delta)$, is also dependent upon the degree of shielding of the nucleus, particularly the degree of penetration of the core by the Rydberg orbital, which characterises the angular momentum of the Rydberg electron ($s > p > d > f$). Therefore the n/δ can be used to identify Rydberg series. Since the Rydberg electron is so distant from the nuclei in the molecule, the molecular core electrons of the Rydberg state are similar in electronic state to the corresponding ionic state. Thus the vibrational fine structure of Rydberg states matches that of the UV-photoelectron spectra of the corresponding cation.

Ion-pair states may be defined as those molecular states which correlate under the united atom limit to a pair of ions [336]. Alternative definitions revolve around the molecular state dissociating to give a pair of ions rather than neutral fragments, these are however complicated by need to define if this hypothetical process is non-adiabatic or adiabatic. The non-adiabatic approach is similar to the united atoms definition, the molecular orbitals deforming smoothly to atomic orbitals, or orbitals localised on the moieties, as $R \rightarrow \infty$. If the adiabatic definition is used the molecule stays in the same eigenstate, however the underlying configuration may change. Characteristic of a pure ion-pair state is the Coulombic form $(1/r)$ of the attractive limb of the potential energy surface.

In reality molecular states are combinations of valence, Rydberg, and ion-pair character; the states are intimately mixed. Strong mixing can be found between states in the same energy range which differ by no more than two electrons and

have the same spin, particularly if the states have similar density distributions and the electronic angular momentum is maintained.

Appendix B

Further details of MRD-CI calculations on propyne

Included in this section are tabular summaries of the present MRD-CI calculations in C_s symmetry.

Table B–1: Propyne ground state CI calculations

Basis	Leading terms[b]	C^2	MRDCI energy[a]	λ	MR-CISD energy[a]	Full-CI energy[a]
DZ	scf (0.886)	0.9130	-116.0930	1.060	-116.0982	-116.1176
DZP	scf (0.884)	0.9009	-116.2458	0.832	-116.2705	-116.3048
DZP_l	scf (0.886)	0.9048	-116.1398	0.806	-116.1668	-116.1937
TZ	scf (0.894)	0.8938	-116.1338	0.773	-116.1398	-116.1698
TZ2P	scf (0.886)	0.8922	-116.2373	0.786	-116.2719	-116.3096
DZ+R(3s2p2d)	scf (0.887)	0.9123	-116.0925	0.946	-116.0986	-116.1182
DZP_l+R(3s2p2d)	scf (0.892)	0.9156	-116.0745	0.883	-116.0828	-116.0995
DZP_l+R(3s2p2d)[c]	scf (0.885)	0.9042	-116.1380	0.825	-116.1573	-116.1834

[a] all energies are expressed in au.

[b] scf - ground state SCF configuration, the terms in parenthesis are the C_i^2 values.

[c] larger calculation with 83 active MOs

Table B–2: Propyne DZ+R(3s2p2d) CI calculation in C_S symmetry, $^1A'$ states.

State	Open Shells	C_i^2	C^2	MRDCI energy	λ	MR-CISD energy	Full-CI energy	Transition energy
1	$11a'(s)$, $17a'(s)$	0.291, 0.205						
	$10a'(s)$, $12a'(p_z)$	0.152, 0.121	0.9057	-115.7228	0.762	-115.8182	-115.8424	7.5048
2	$12a'(p_z)$, $23a'(p_z)$	0.485, 0.206						
	$19a'(d_{z2})$, $11a'(s)$	0.070, 0.069	0.8975	-115.7271	0.798	-115.7960	-115.8225	8.0457
3	$25a'(v)$, $9a''(v)$, $8a''(p_x)$	0.206, 0.205, 0.125						
	$22a'(p_y)$, $3a''(p_x)$, $13a'(p_y)$	0.122, 0.087, 0.084	0.9219	-115.7092	0.835	-115.8000	-115.8180	8.1686
4	$3a''(p_x)$, $13a'(p_y)$	0.278, 0.275						
	$8a''(p_x)$, $22a'(p_y)$	0.163, 0.163	0.9101	-115.6960	0.805	-115.7906	-115.8133	8.2976
5	$13a'(p_y)$, $3a''(p_x)$, $25a'(v)$	0.196, 0.189, 0.172						
	$9a''(v)$, $22a'(p_y)$, $8a''(p_x)$	0.172, 0.057, 0.054	0.9183	-115.6886	0.821	-115.7820	-115.8019	8.6084
6	$14a'(d_{z2})$, $19a'(d_{z2})$, $23a'(p_z)$	0.543, 0.227, 0.058	0.9041	-115.6881	0.739	-115.7697	-115.7942	8.8179
7	$15a'(d_{yz})$, $20a'(d_{yz})$	0.690, 0.101	0.9112	-115.6771	0.763	-115.7658	-115.7881	8.9829
8	$4a''(d_{xz})$, $6a''(d_{xz})$	0.674, 0.108	0.9125	-115.6740	0.787	-115.7660	-115.7880	8.9863
9	$23a'(p_z)$, $12a'(p_z)$, $19a'(d_{z2})$	0.418, 0.230, 0.108	0.8949	-115.6774	0.764	-115.7558	-115.7839	9.0953
10	$10a'(s)$, $17a'(s)$,$19a'(d_{z2})$	0.537, 0.142, 0.079	0.9065	-115.6708	0.773	-115.7573	-115.7807	9.1852
11	$16a'(d_{x2-y2})$, $21a'(d_{x2-y2})$	0.474, 0.322						
	$20a'(d_{yz})$	0.081	0.9145	-115.6622	0.819	-115.7580	-115.7787	9.2360
12	$8a''(p_x)$, $3a''(p_x)$	0.521, 0.324	0.9109	-115.6519	0.796	-115.7469	-115.7694	9.4912
13	$11a'(s)$, $17a'(s)$, $18a'(s)$	0.380, 0.187, 0.137	0.9069	-115.6480	0.832	-115.7439	-115.7675	9.5427
14	$7a''(d_{xy})$, $5a''(d_{xy})$, $6a''(d_{xz})$	0.409, 0.351, 0.103	0.9147	-115.6586	0.763	-115.7472	-115.7671	9.5553
15	$22a'(p_y)$, $13a'(p_y)$	0.517, 0.321	0.9113	-115.6516	0.781	-115.7439	-115.7657	9.5917
16	$5a''(d_{xy})$, $6a'(d_{xy})$	0.533, 0.270	0.9154	-115.6310	0.872	-115.7402	-115.7618	9.6989
17	$16a'(d_{x2-y2})$, $21a'(x^2-y^2)$	0.403, 0.336						
	$20a'(d_{yz})$	0.128	0.9140	-115.6350	0.796	-115.7348	-115.7562	9.8503
18	$20a'(d_{yz})$, $6a''(d_{xz})$, $20a'(d_{yz})$	0.358, 0.194, 0.103	0.9112	-115.6407	0.766	-115.7308	-115.7527	9.9457
19	$6a''(d_{xz})$, $20a'(d_{yz})$	0.319, 0.157						
	$4a''(d_{xz})$, $8a''(d_{xy})$	0.107, 0.099	0.9131	-115.6382	0.781	-115.7297	-115.7512	9.9882
20	$17a'(s)$, $18a'(s)$, $24a'(s)$	0.330, 0.320, 0.226	0.9019	-115.6015	0.894	-115.6889	-115.7104	11.6976

Table B–3: Propyne DZ+R(3s2p2d) CI calculation in C_S symmetry, $^1A''$ states

State	Open Shells	C_i^2	C^2	MRDCI energy	λ	MR-CISD energy	Full-CI energy	Transition energy
1	$11a'(s)$, $17a'(s)$, $10a'(s)$	0.313, 0.292, 0.139	0.8980	-115.7177	0.768	-115.8211	-115.8483	7.3436
2	$9a''(v)$, $25a'(v)$, $8a''(p_x)$	0.467, 0.249, 0.057	0.9303	-115.7181	0.836	-115.8077	-115.8233	8.0247
3	$12a'(p_z)$, $19a'(d_{z2})$, $23a'(p_z)$	0.737, 0.082, 0.054	0.8945	-115.7048	0.700	-115.7901	-115.8180	8.1699
4	$25a'(v)$, $9a''(v)$, $22a'(p_y)$ $13a'(p_y)$, $8a''(p_x)$	0.376, 0.185, 0.098 0.068, 0.055	0.9271	-115.7090	0.827	-115.8008	-115.8172	8.1898
5	$3a''(p_x)$, $9a''(v)$, $8a''(p_x)$	0.563, 0.151, 0.145	0.9199	-115.6905	0.791	-115.7842	-115.8035	8.5644
6	$13a'(p_y)$, $25a'(v)$, $22a'(p_y)$	0.520, 0.181, 0.154	0.9202	-115.6877	0.806	-115.7830	-115.8021	8.6007
7	$14a'(d_{z2})$, $19a'(d_{z2})$ $10a'(s)$, $17a'(s)$	0.304, 0.284 0.195, 0.055	0.8990	-115.6620	0.789	-115.7623	-115.7894	9.0641
8	$10a'(s)$, $14a'(d_{z2})$ $17a'(s)$, $18a'(s)$	0.426, 0.125 0.120, 0.100	0.8989	-115.6658	0.711	-115.7617	-115.7878	9.1195
9	$4a''(d_{xz})$, $7a''(d_{xy})$, $5a''(d_{xy})$	0.567, 0.185, 0.096	0.9158	-115.6824	0.782	-115.7618	-115.7821	9.1451
10	$21a'(d_{x2-y2})$, $16a'(d_{x2-y2})$ $15a'(d_{yz})$	0.409, 0.284 0.191	0.9162	-115.6798	0.791	-115.7614	-115.7816	9.1587
11	$5a''(d_{xy})$, $4a''(d_{xz})$ $7a''(d_{xy})$, $6a''(d_{xz})$	0.488, 0.191 0.142, 0.059	0.9170	115.6776	0.780	-115.7594	-115.7794	9.2206
12	$15a'(d_{yz})$, $16a'(d_{x2-y2})$ $20a'(d_{yz})$	0.520, 0.221 0.106	0.9175	-115.6738	0.769	-115.7583	-115.7781	9.2559
13	$23a'(p_z)$, $18a'(s)$	0.525, 0.168	0.9015	-115.6164	0.974	-115.7397	-115.7658	9.5903
14	$14a'(d_{z2})$, $23a'(d_{z2})$, $19a'(p_z)$	0.359, 0.247, 0.099	0.9003	-115.6404	0.748	-115.7397	-115.7656	9.5957
15	$8a''(p_x)$, $3a''(p_x)$, $22a'(p_y)$	0.481, 0.187, 0.120	0.9190	-115.6463	0.779	-115.7441	-115.7637	9.6466
16	$22a'(p_y)$, $13a'(p_y)$, $8a''(p_x)$	0.464, 0.207, 0.132	0.9192	-115.6452	0.784	-115.7429	-115.7623	9.6837
17	$21a'(d_{x2-y2})$, $16a'(d_{x2-y2})$	0.441, 0.348	0.9157	-115.6522	0.785	-115.7397	-115.7537	9.9202
18	$7a''(d_{xy})$, $5a''(d_{xy})$	0.535, 0.271	0.9166	-115.6520	0.766	-115.7322	-115.7523	9.9576
19	$6a''(d_{xz})$	0.689	0.9197	-115.6346	.784	-115.7270	-115.7482	10.1235
20	$20a'(d_{yz})$, $15a'(d_{yz})$	0.659, 0.093	0.9195	-115.6345	0.789	-115.7267	-115.7459	10.1304

Table B–4: Propyne DZP$_I$+R(3s2p2d) CI calculation in C_S symmetry, ^{1}A$'$ states.

State	Open Shells	C_i^2	C^2	MRDCI energy	λ	MR-CISD energy	Full-CI energy	Transition energy
1	11a$'(s)$, 17a$'(s)$, 12a$'(p_z)$	0.331, 0.199, 0.095						
	22a$'(p_z)$, 10a$'(s)$, 18a$'(s)$	0.094, 0.071 0.062	0.9076	-115.7056	0.795	-115.8095	-115.8309	7.3085
2	9a$''(v)$, 25a$'(v)$, 23a$'(p_y)$	0.254, 0.252, 0.109						
	8a$''(p_x)$, 13a$'(p_y)$, 3a$''(p_x)$	0.099, 0.062, 0.060	0.9310	-115.6905	0.893	-115.7975	-115.8120	7.8231
3	12a$'(p_z)$, 19a$'(d_{z2})$	0.573, 0.100						
	17a$'(s)$, 22a$'(p_z)$	0.060, 0.057	0.9075	-115.7011	0.822	-115.7822	-115.8035	8.0533
4	13a$'(p_y)$, 3a$''(p_x)$	0.281, 0.271						
	23a$'(p_y)$, 8a$''(p_x)$	0.183, 0.156	0.9163	-115.6739	0.800	-115.7726	-115.7909	8.4052
5	14a$'(d_{z2})$, 19a$'(d_{z2})$	0.471, 0.310	0.9053	-115.6633	0.802	-115.7597	-115.7825	8.6254
6	3a$''(p_x)$, 13a$'(p_y)$, 25a$'(v)$	0.245, 0.197, 0.137						
	9a$''(v)$, 8a$''(p_x)$, 23a$'(p_y)$	0.136, 0.082, 0.077	0.9249	-115.6679	0.798	-115.7656	-115.7815	8.6525
7	15a$'(d_{yz})$, 20a$'(d_{yz})$	0.533, 0.271	0.9181	-115.6470	0.877	-115.7587	-115.7775	8.7611
8	5a$''(d_{xy})$ 7a$''(d_{xy})$	0.428, 0.411	0.9210	-115.6395	0.851	-115.7488	-115.7662	9.0691
9	16a$'(d_{x^2-y^2})$, 21a$'(d_{x^2-y^2})$	0.327, 0.292						
	4a$''(d_{xz})$, 6a$''(d_{xz})$	0.123, 0.114	0.9196	-115.6430	0.818	-115.7481	-115.7657	9.0826
10	4a$''(d_{xz})$, 6a$''(d_{xz})$	0.303, 0.192						
	16a$'(d_{x^2-y^2})$, 21a$'(d_{x^2-y^2})$	0.152, 0.095	0.9195	-115.6419	0.775	-115.7411	-115.7582	9.2860
11	22a$'(p_z)$, 12a$'(p_z)$, 19a$'(d_{z2})$	0.419, 0.155, 0.124	0.9034	-115.6486	0.739	-115.7326	-115.7550	9.3749
12	10a$'(s)$, 17a$'(s)$	0.243, 0.167						
	11a$'(s)$, 18a$'(s)$	0.120, 0.113	0.9121	-115.6421	0.770	-115.7343	-115.7536	9.4120
13	14a$'(d_{z2})$, 22a$'(p_z)$, 19a$'(d_{z2})$	0.314, 0.231, 0.203	0.9056	-115.6308	0.785	-115.7243	-115.7468	9.5985
14	8a$''(p_x)$, 3a$''(p_x)$	0.546, 0.322	0.9183	-115.6289	0.779	-115.7266	-115.7444	9.6622
15	23a$'(p_y)$, 13a$'(p_y)$	0.507, 0.353	0.9185	-115.6302	0.774	-115.7268	-115.7443	9.6662
16	10a$'(s)$, 11a$'(s)$	0.453, 0.289	0.9172	-115.6282	0.753	-115.7210	-115.7390	9.8108
17	5a$''(d_{xy})$ 7a$''(d_{xy})$	0.458, 0.420	0.9203	-115.6125	0.790	-115.7137	-115.7308	10.0338
18	21a$'(d_{x^2-y^2})$, 16a$'(d_{x^2-y^2})$	0.460, 0.406	0.9188	-555.6157	0.756	-115.7126	-115.7299	10.0583
19	6a$''(d_{xz})$, 4a$''(d_{xz})$	0.394, 0.371	0.9183	-115.6134	0.742	-115.7061	-115.7233	10.2381
20	17a$'(s)$, 21a$'(s)$, 18a$'(s)$	0.439, 0.214, 0.204	0.9088	-115.5932	0.744	-115.6819	-115.6996	10.8814

Table B–5: Propyne DZP$_I$+R(3s2p2d) CI calculation in C_S symmetry, ^{1}A″ states.

State	Open Shells	C_i^2	C^2	MRDCI energy	λ	MR-CISD energy	Full-CI energy	Transition energy
1	$9a''(v)$, $25a'(v)$, $8a''(p_x)$	0.555, 0.087, 0.062	0.9384	-115.7006	0.882	-115.8023	-115.8210	7.5771
2	$11a'(s)$, $17a'(s)$, $10a'(s)$ $18a'(s)$, $24a'(s)$	0.297, 0.283, 0.122 0.115, 0.065	0.9086	-115.6921	0.745	-115.7960	-115.8166	7.6973
3	$25a'(v)$, $13a'(p_y)$ $23a'(p_y)$, $20a'(d_{yz})$	0.408, 0.143 0.122, 0.097	0.9352	-115.6881	0.886	-115.7971	-115.8105	7.8633
4	$12a'(p_z)$, $19a'(d_{z2})$, $22a'(p_z)$	0.715, 0.109, 0.062	0.9036	-115.6796	0.730	-115.7708	-115.7928	8.3449
5	$3a''(p_x)$, $9a''(v)$, $8a''(p_x)$,	0.605, 0.135, 0.101	0.9243	-115.6754	0.819	-115.7748	-115.7912	8.3882
6	$13a'(p_y)$, $23a'(p_y)$ $25a'(v)$, $20a'(d_{yz})$	0.551, 0.198 0.071, 0.052,	0.9270	-115.6695	0.836	-115.7695	-115.7850	8.5588
7	$4a''(d_{xz})$, $6a''(d_{xz})$, $9a''(v)$	0.606, 0.178, 0.079	0.9199	-115.6621	0.845	-115.7521	-115.7696	8.9762
8	$14a'(d_{z2})$, $19a'(d_{z2})$, $10a'(s)$	0.263, 0.261, 0.159	0.9089	-115.6425	0.745	-115.7469	-115.7676	9.0328
9	$5a''(d_{xy})$ $7a''(d_{xy})$	0.591, 0.274	0.9192	-115.6570	0.802	-115.7471	-115.7646	9.1121
10	$21a'(d_{x2-y2})$, $16a'(d_{x2-y2})$ $15a'(d_{yz})$	0.445, 0.373 0.080	0.9230	-115.6534	0.851	-115.7469	-115.7633	9.1497
11	$15a'(d_{yz})$, $20'(d_{yz})$, $25a'(v)$	0.432, 0.256, 0.117	0.9249	-115.6506	0.842	-115.7440	-115.7599	9.2407
12	$10a'(s)$, $19a'(p_z)$ $14a'(d_{z2})$, $17a'(s)$,	0.455, 0.135 0.117, 0.109	0.9082	-115.6366	0.754	-115.7376	-115.7585	9.2801
13	$6a''(d_{xz})$, $4a''(d_{xz})$	0.537, 0.253	0.9179	-115.6323	0.841	-115.7221	-115.7402	9.7772
14	$8a''(p_x)$, $3a''(p_x)$	0.586, 0.155	0.9250	-115.6269	0.762	-115.7236	-115.7391	9.8065
15	$14a'(d_{z2})$, $19a'(d_{z2})$, $22a'(p_z)$	0.345, 0.291, 0.137	0.9077	-115.6188	0.715	-115.7163	-115.7366	9.8746
16	$11a'(s)$, $10a'(s)$,	0.521, 0.161	0.9101	-115.6154	0.740	-115.7147	-115.7348	9.9252
17	$7a''(d_{xy})$, $5a''(d_{xy})$	0.597, 0.266	0.9198	-115.6283	0.778	-115.7173	-115.7345	9.9331
18	$20a'(d_{yz})$, $15a'(d_{yz})$	0.450, 0.359	0.9236	-115.6233	0.801	-115.7112	-115.7272	10.1316
19	$21a'(d_{x2-y2})$, $16a'(d_{x2-y2})$	0.388, 0.382	0.9228	-115.6262	0.777	-115.7108	-115.7267	10.1444
20	$22a'(p_z)$, $18a'(s)$, $14a'(d_{z2})$	0.489, 0.116, 0.122	0.9104	-115.5988	0.610	-115.6807	-115.6977	10.9338

Table B–6: Propyne DZP$_I$+R(3s2p2d) CI calculation in C_S symmetry, ^{3}A$'$ states.

State	Open Shells	C_i^2	C^2	MRDCI energy	λ	MR-CISD energy	Full-CI energy	Transition energy
1	$9a''(v)$, $25a'(v)$	0.437, 0.362	0.9368	-115.7492	0.905	-115.8715	-115.8849	5.8405
2	$25a'(v)$, $9a''(v)$	0.419, 0.344	0.9421	-115.7141	0.879	-115.8345	-115.8463	6.8895
3	$17a'(s)$, $11a'(s)$, $18a'(s)$	0.276, 0.275, 0.130						
	$24a'(s)$, $10a'(s)$	0.106, 0.093	0.9096	-115.6914	0.815	-115.8178	-115.8394	7.0767
4	$12a'(p_z)$, $19a'(d_{z2})$, $22a'(p_z)$	0.679, 0.123, 0.080	0.9151	-115.6785	0.815	-115.7861	-115.8057	7.9936
5	$3a''(p_x)$, $8a''(p_x)$	0.340, 0.189						
	$13a'(p_y)$, $23a'(p_y)$	0.175, 0.134	0.9150	-115.6702	0.842	-115.7849	-115.8045	8.0263
6	$13a'(p_y)$, $3a''(p_x)$	0.326, 0.217						
	$23a'(p_y)$, $8a''(p_x)$	0.201, 0.085	0.9164	-115.6666	0.737	-115.7637	-115.7818	8.6464
7	$10a'(s)$, $14a'(d_{z2})$	0.466, 0.100	0.9097	-115.6332	0.808	-115.7533	-115.7749	8.8341
8	$19a'(d_{z2})$, $14a'(d_{z2})$	0.275, 0.267						
	$10a'(s)$, $18a'(s)$	0.105, 0.099	0.9121	-115.6411	0.770	-115.7533	-115.7732	8.8799
8	$15a'(d_{yz})$, $21a'(d_{x2-y2})$	0.517, 0.150						
	$20a'(d_{yz})$, $16a'(d_{x2-y2})$	0.119, 0.080	0.9157	-115.6515	0.823	-115.7541	-115.7732	8.8799
10	$16a'(d_{x2-y2})$, $21a'(d_{x2-y2})$	0.463, 0.198						
	$15a'(d_{yz})$, $20a'(d_{yz})$	0.097, 0.089	0.9166	-115.6492	0.818	-115.7541	-115.7730	8.8832
11	$5a''(d_{xy})$, $4a''(d_{xz})$, $7a''(d_{xy})$	0.704, 0.112, 0.077	0.9132	-115.6452	0.822	-115.7565	-115.7670	9.0485
12	$4a''(d_{xz})$, $6a''(d_{xz})$, $5a''(d_{xy})$	0.475, 0.247, 0.107	0.9128	-115.6484	0.804	-115.7437	-115.7630	9.1562
13	$14a'(d_{z2})$, $19a'(d_{z2})$	0.274, 0.240						
	$22a'(p_z)$, $12a'(p_z)$	0.203, 0.123	0.9150	-115.6178	0.782	-115.7351	-115.7546	9.3804
14	$23a'(p_y)$, $13a'(p_y)$, $8a''(p_x)$	0.311, 0.259, 0.158	0.9162	-115.6257	0.771	-115.7316	-115.7503	9.5012
15	$21a'(d_{x2-y2})$, $16a'(d_{x2-y2})$	0.542, 0.314	0.9120	-115.6221	0.820	-115.7277	-115.7482	9.5605
16	$20a'(d_{yz})$, $6a''(d_{xz})$, $15a'(d_{yz})$	0.363, 0.213, 0.115	0.9133	-115.6176	0.810	-115.7229	-115.7425	9.7158
17	$8a''(p_x)$, $3a''(p_x)$	0.372, 0.192						
	$23a'(p_y)$, $13a'(p_y)$	0.161, 0.107	0.9158	-115.6234	0.710	-115.7159	-115.7338	9.9509
18	$6a''(d_{xz})$, $20a'(d_{yz})$, $4a''(d_{xz})$	0.341, 0.221, 0.139	0.9126	-115.6166	0.786	-115.7126	-115.7319	10.0019
19	$17a'(s)$, $24a'(s)$	0.447, 0.205	0.9112	-115.5833	0.773	-115.6995	-115.7180	10.3804
20	$17a'(s)$, $24a'(s)$	0.477, 0.429	0.9138	-115.5373	0.555	-115.6202	-115.6310	12.7493

Table B–7: Propyne DZP$_l$+R(3s2p2d) CI calculation in C_S symmetry, $^3A''$ states.

State	Open Shells	C_i^2	C^2	MRDCI energy	λ	MR-CISD energy	Full-CI energy	Transition energy
1	$9a''(v)$, $25a'(v)$	0.497, 0.266	0.9376	-115.7127	0.861	-115.8321	-115.8449	6.9276
2	$17a'(s)$, $11a'(s)$, $18a'(s)$	0.295, 0.219, 0.143						
	$24a'(s)$, $10a'(s)$	0.106, 0.103	0.9129	-115.6842	0.829	-115.8137	-115.8344	7.2145
3	$25a'(v)$, $9a''(v)$, $23a'(p_y)$	0.440, 0.212, 0.079	0.9374	-115.6876	0.858	-115.8081	-115.8211	7.5751
4	$12a'(p_z)$, $19a'(d_{z2})$, $22a'(p_z)$	0.624, 0.140, 0.119	0.9117	-115.6748	0.792	-115.7762	-115.7959	8.2601
5	$6a''(d_{xz})$, $4a''(d_{xz})$	0.435, 0.332						
	$7a''(d_{xy})$, $9a''(v)$	0.059, 0.057	0.9139	-115.6458	0.858	-115.7688	-115.7897	8.4296
6	$13a'(p_y)$, $3a''(p_x)$	0.311, 0.221						
	$23a'(p_y)$, $8a''(p_x)$	0.153, 0.145	0.9174	-115.6623	0.756	-115.7696	-115.7876	8.4859
7	$3a''(p_x)$, $13a'(p_y)$, $8a''(p_x)$	0.302, 0.233, 0.148						
	$23a'(p_y)$, $25a'(v)$, $9a''(v)$	0.080, 0.068, 0.057	0.9186	-115.6583	0.793	-115.7667	-115.7848	8.5639
8	$10a'(s)$	0.572	0.9108	-115.6279	0.856	-115.7500	-115.7710	8.9387
9	$5a''(d_{xy})$, $7a''(d_{xy})$	0.511, 0.332	0.9178	-115.6496	0.814	-115.7512	-115.7696	8.9778
10	$22a'(p_z)$, $12a'(p_z)$	0.447, 0.180	0.9110	-115.6201	0.871	-115.7455	-115.7671	9.0459
11	$19a'(d_{z2})$, $14a'(d_{z2})$, $18a'(s)$	0.443, 0.159, 0.081						
	$10a'(s)$, $2a'(p_z)$	0.063, 0.058	0.9102	-115.6366	0.765	-115.7459	-115.7657	9.0830
12	$15a'(d_{yz})$, $20a'(d_{yz})$	0.611, 0.246	0.9313	-115.6322	0.835	-115.7467	-115.7611	9.2088
13	$16a'(d_{x^2-y^2})$, $21a'(d_{x^2-y^2})$	0.692, 0.168	0.9130	-115.6262	0.772	-115.7381	-115.7574	9.3096
14	$23a'(p_y)$, $8a''(p_x)$	0.289, 0.229						
	$13a'(p_y)$, $3a''(p_x)$	0.148, 0.136	0.9185	-115.7179	0.773	-115.7236	-115.7418	9.7340
15	$7a''(d_{xy})$, $5a''(d_{xy})$	0.438, 0.373	0.9163	-115.6225	0.780	-115.7196	-115.7380	9.8359
16	$23a'(p_y)$, $8a''(p_x)$	0.228, 0.212						
	$3a''(p_x)$, $13a'(p_y)$	0.146, 0.134	0.9172	-115.6195	0.689	-115.7186	-115.7359	9.8932
17	$20a'(d_{yz})$, $15a'(d_{yz})$	0.506, 0.216	0.9314	-115.6013	0.822	-115.7197	-115.7343	9.9387
18	$4a''(d_{xz})$, $6a''(d_{xz})$	0.483, 0.246	0.9160	-115.6165	0.744	-115.7077	-115.7259	10.1649
19	$11a'(s)$, $10a'(s)$	0.430, 0.134	0.9175	-115.6017	0.688	-115.7053	-115.7227	10.2527
20	$14a'(d_{z2})$, $22a'(p_z)$, $19a'(d_{z2})$	0.591, 0.124, 0.107	0.9169	-115.5982	0.651	-115.6961	-115.7129	10.5199

Table B–8: Oscillator Strengths Calculated for DZP$_I$+R in C_S symmetry

A′ symmetry			A″ symmetry		
Transition	Energy /au	Oscilator Strength	Transition	Energy /au	Oscilator Strength
1 (s)	7.3085	0.007	1 (v)	7.5771	0.022
2 (v)	7.8231	0.091	2 (s)	7.6973	0.011
3 (z)	8.0533	0.171	3 (v)	7.8633	0.487
4 (y)	8.4052	1.090	4 (z)	8.3449	0.062
5 (z^2)	8.6254	0.928	5 (x)	8.3882	0.000
6 (x)	8.6525	0.064	6 (y)	8.5588	0.005
7 (yz)	8.7611	0.718	7 (xz)	8.9762	0.043
8 (xy)	9.0691	0.015	8 (z^2)	9.0328	0.005
9 (x^2-y^2)	9.0826	0.058	9 (xy)	9.1121	0.003
10 (xz)	9.2860	0.151	10 (x^2-y^2)	9.1497	0.014
11 (z)	9.3749	0.015	11 (yz)	9.2407	0.007
12 (s)	9.4130	0.045	12 (s)	9.2801	0.012
13 (z^2)	9.5985	0.877	13 (xz)	9.7772	0.052
14 (x)	9.6622	0.796	14 (x)	9.8065	0.073
15 (y)	9.6662	0.926	15 (z^2)	9.8746	0.032
16 (xy)	9.8108	0.007	16 (s)	9.9252	0.001
17 (x^2-y^2)	10.0338	0.071	17 (xz)	9.9331	0.037
18 (xz)	10.0583	0.020	18 (yz)	10.1316	0.066
19 (z^2)	10.2381	0.019	19 (xy)	10.1444	0.009
20 (s)	10.8814	0.879	20 (z)	10.9338	0.199

Appendix C

Further details of MRD-CI calculations on furan

This section contains further details of the present MRD-CI calculations. The tabulated data includes the energies obtained at various stages within the calculations, the diagonaliser energy (MRD-CI), the energy extrapolated to include the estimated effects of a configurations singly and doubly excited from the reference configurations (MR-CISD), and the full-CI energy as computed incorporating the Davidson correction for multiply excited states. The excitation energy relative to the ground state is given in eV. Also included are descriptions of the roots and the C^2 values.

Table C–1: Furan ground state CI calculations

Basis	Leading terms[b]	C^2	MRDCI energy[a]	λ	MR-CISD energy[a]	Full-CI energy[a]
DZ+R(3s2p2d)	scf (0.872)	0.8870	-228.9265	0.718	-228.9791	-229.0232
DZP_l	scf (0.875)	0.8879	-228.9180	0.746	-229.0400	-229.0869
DZP_l+R(3s2p2d)	scf (0.881)	0.8980	-228.8750	0.753	-228.9489	-228.9818
DZP_h+R(3s2p2d)	scf (0.882)	0.8996	-228.8698	0.757	-228.9435	-228.9755

[a] all energies are expressed in au.

[b] scf - SCF configuration, the terms in parenthesis are the C_i^2 values.

Table C–2: Furan DZ+R(3s2p2d) CI calculation , $^1A_1$ states.

State	Open Shells	C_i^2	C^2	MRDCI energy	λ	MR-CISD energy	Full-CI energy	Transition energy
1	$7b_1(\pi_4^*)$, $4a_2(\pi_5^*)$	0.462, 0.242	0.9053	-228.4681	0.800	-228.7343	-228.7734	6.7952
2	$2a_2(d_{xy})$, $3a_2(d_{xy})$	0.643, 0.240	0.8943	-228.4790	0.739	-228.6983	-228.7425	7.6383
3	$3b_1(p_x)$, $6b_1(p_x)$	0.572, 0.218	0.9005	-228.4391	0.749	-228.6825	-228.7249	8.1151
4	$4b_1(d_{xz})$	0.790	0.8998	-228.4194	0.765	-228.6735	-228.7179	8.3059
5	$3a_2(d_{xy})$, $2a_2(d_{xy})$	0.600, 0.242	0.8943	-228.4475	0.737	-228.6719	-228.7166	8.3411
6	$6b_1(p_x)$, $3b_1(p_x)$	0.588, 0.238	0.9008	-228.3939	0.741	-228.6450	-228.6879	9.1228
7	$4a_2(\pi_5^*)$, $7b_1(\pi_4^*)$	0.351, 0.216						
	$7b_1^2(\pi_4^{*2})1a_2^0(\pi_3^0)$, $5b_1(d_{xz})$	0.115, 0.063	0.8736	-228.3863	0.693	-228.6285	-228.6820	9.2824
8	$5b_1(d_{xz})$	0.726	0.9054	-228.3541	0.667	-228.5971	-228.6359	10.5371
9	$7b_1^2(\pi_4^{*2})1a_2^0(\pi_3^0)$,	0.334						
	$7b_1(\pi_4^*)1b_1(\pi_1)$, $4a_2(\pi_5^*)$	0.224, 0.212	0.8574	-228.3261	0.756	-228.5766	-228.6400	10.4263

Table C–3: Furan DZ+R(3s2p2d) CI calculation , $^1B_1$ states.

State	Open Shells	C_i^2	C^2	MRDCI energy	λ	MR-CISD energy	Full-CI energy	Transition energy
1	$7b_2(p_y)$, $10b_2(p_y)$	0.733, 0.127	0.8998	-228.4834	0.746	-228.7328	-228.7749	6.7553
2	$8b_2(d_{yz})$, $9b_2(d_{yz})$	0.795, 0.061	0.8996	-228.4590	0.763	-228.7149	-228.7589	7.2132
3	$10b_2(p_y)$, $7b_2(p_y)$	0.669, 0.108	0.8976	-228.4184	0.817	-228.7075	-228.7529	7.3536
4	$15a_1(s)$, $10a_1(s)$	0.336, 0.202						
	$11a_1(s)$	0.172	0.8836	-228.4309	0.700	-228.6952	-228.7472	7.5102
5	$12a_1(p_z)$, $19a_1(p_z)$	0.704, 0.101	0.8769	-228.4398	0.687	-228.6723	-228.7270	8.0599
6	$13a_1(d_{x^2-y^2})$, $10a_1(s)$	0.460, 0.138						
	$16a_1(d_{x^2-y^2})$	0.122	0.8798	-228.3960	0.697	-228.6542	-228.7077	8.5832
7	$14a_1(d_{z^2})$, $19a_1(p_z)$	0.692, 0.086	0.8787	-228.4072	0.685	-228.6504	-228.7044	8.6745
8	$9b_2(d_{yz})$, $8b_2(d_{yz})$	0.741, 0.059	0.8995	-228.4017	0.724	-228.6596	-228.7005	8.7809
9	$10a_1(s)$, $15a_1(s)$	0.435, 0.203						
	$13a_1(d_{x^2-y^2})$	0.162	0.8802	-228.3920	0.700	-228.6473	-228.7009	8.7696
10	$19a_1(p_z)$, $12a_1(p_z)$	0.580, 0.083	0.8759	-228.3805	0.671	-228.6224	-228.6780	9.3913
11	$16a_1(d_{x^2-y^2})$, $16a_1(d_{x^2-y^2})$	0.633, 0.172	0.8759	-228.3606	0.572	-228.5796	-228.6296	10.7105
12	$18a_1(d_{z^2})$	0.748	0.8820	-228.3450	0.690	-228.6067	-228.6569	9.9660
13	$11a_1(s)$, $15a_1(s)$	0.665, 0.126	0.8839	-228.3485	0.725	-228.6210	-228.6718	9.5608
14	$17a_1(s)$, $20a_1(s)$	0.400, 0.293						
	$15a_1(s)$	0.120	0.8807	-228.3125	0.587	-228.5463	-228.5930	11.7054

Table C–4: Furan DZ+R(3s2p2d) CI calculation , $^1B_2$ states.

State	Open Shells	C_i^2	C^2	MRDCI energy	λ	MR-CISD energy	Full-CI energy	Transition energy
1	$5b_1(d_{xz})$, $6b_1(p_x)$, $3b_1(p_x)$	0.432, 0.219, 0.105	0.9043	-228.4819	0.749	-228.7345	-228.7747	6.7609
2	$3b_1(p_x)$, $5b_1(d_{xz})$, $6b_1(p_x)$	0.287, 0.255, 0.255	0.9040	-228.4705	0.802	-228.7451	-228.7881	6.3955
3	$7b_1(\pi_4^*)$, $5b_1(d_{xz})$, $4b_1(d_{xz})$	0.320, 0.288, 0.170	0.9065	-228.4550	0.737	-228.7073	-228.7457	7.5501
4	$3b_1(p_x)$, $6b_1(p_x)$	0.448, 0.324	0.9062	-228.4308	0.776	-228.6945	-228.7348	7.8462
5	$5b_1(d_{xz})$, $4a_2(\pi_5^*)$, $7b_1(\pi_4^*)$	0.311, 0.297, 0.209	0.9024	-228.4184	0.716	-228.6602	-228.7005	8.7801
6	$2a_2(d_{xy})$, $3a_2(d_{xy})$	0.649, 0.190	0.8993	-228.4294	0.742	-228.6562	-228.6989	8.8246
7	$3a_2(d_{xy})$, $2a_2(d_{xy})$	0.653, 0.178	0.8993	-228.3950	0.730	-228.6224	-228.6647	9.7498
8	$4a_2(\pi_5^*)$, $7b_1(\pi_4^*)$	0.440, 0.291	0.8936	-228.4068	0.686	-228.6107	-228.6558	9.9973

Table C–5: Furan DZ+R(3s2p2d) CI calculation , $^1A_2$ states.

State	Open Shells	C_i^2	C^2	MRDCI energy	λ	MR-CISD energy	Full-CI energy	Transition energy
1	$10a_1(s)$, $11a_1(s)$	0.423, 0.268						
	$15a_1(s)$, $17a_1(s)$	0.107, 0.073	0.8901	-228.4782	0.767	-228.7554	-228.8041	5.9606
2	$12a_1(p_z)$, $19a_1(p_z)$	0.790, 0.050	0.8905	-228.4824	0.737	-228.7268	-228.7742	6.7750
3	$13a_1(d_{x^2-y^2})$, $16a_1(d_{x^2-y^2})$	0.752, 0.064	0.8958	-228.4467	0.778	-228.7255	-228.7722	6.8305
4	$14a_1(d_{z^2})$	0.800	0.8923	-228.4552	0.741	-228.7060	-228.7528	7.3560
5	$10a_1(s)$, $15a_1(s)$	0.401, 0.143						
	$17a_1(s)$, $11a_1(s)$	0.137, 0.104	0.8883	-228.4389	0.759	-228.7009	-228.8041	7.4416
6	$19a_1(p_z)$	0.668	0.8930	-228.4075	0.772	-228.6915	-228.7390	7.7336
7	$7b_2(p_y)$, $10b_2(p_y)$	0.731, 0.110	0.8993	-228.4297	0.745	-228.6861	-228.7295	7.9911
8	$17a_1(s)$, $11a_1(s)$	0.352, 0.346	0.8883	-228.4096	0.739	-228.6750	-228.7231	8.1664
9	$9b_2(d_{yz})$, $8b_2(d_{yz})$	0.738, 0.113	0.8996	-228.4184	0.734	-228.6593	-228.7021	8.7360
10	$9b_2(d_{yz})$, $7b_2(p_y)$	0.620, 0.092						
	$10b_2(p_y)$, $8b_2(d_{yz})$	0.070, 0.067	0.8996	-228.3774	0.765	-228.6528	-228.6975	8.8611
11	$16a_1(d_{x^2-y^2})$	0.605	0.8911	-228.3954	0.701	-228.6531	-228.6980	8.8484
12	$18a_1(d_{z^2})$, $16a_1(d_{x^2-y^2})$	0.554, 0.139	0.8976	-228.3968	0.629	-228.6264	-228.6706	9.5951
13	$10b_2(p_y)$	0.647	0.9015	-228.3691	0.690	-228.6276	-228.6698	9.6157
14	$15a_1(s)$, $17a_1(s)$	0.510, 0.264	0.8977	-228.3625	0.687	-228.6004	-228.7231	10.4227

Table C–6: Furan DZP$_I$+R(3s2p2d) CI calculation , $^1A_1$ states.

State	Open Shells	C_i^2	C^2	MRDCI energy	λ	MR-CISD energy	Full-CI energy	Transition energy
1	$7b_1(\pi_4^*)$, $4a_2(\pi_5^*)$	0.427, 0.271	0.9365	-228.4665	0.894	-228.7165	-228.7381	6.6322
2	$2a_2(d_{xy})$, $3a_2(d_{xy})$	0.634, 0.236	0.9043	-228.4742	0.767	-228.6647	-228.6970	7.7503
3	$3b_1(p_x)$, $6b_1(p_x)$	0.533, 0.258	0.9081	-228.4363	0.788	-228.6502	-228.6824	8.1481
4	$4b_1(d_{xz})$, $5b_1(d_{xz})$	0.768, 0.084	0.9068	-228.4162	0.825	-228.6415	-228.6758	8.3269
5	$3a_2(d_{xy})$, $2a_2(d_{xy})$	0.590, 0.233	0.9022	-228.4425	0.745	-228.6333	-228.6665	8.5806
6	$6b_1(p_x)$, $3b_1(p_x)$	0.509, 0.287	0.9072	-228.3930	0.760	-228.6069	-228.6393	9.3196
7	$4a_2(\pi_5^*)$, $7b_1(\pi_4^*)$,$5b_1(d_{xz})$	0.327, 0.165, 0.159						
	$6b_1(p_x)$, $7b_1^2(\pi_4^{*2})1a_2^0(\pi_3^0)$	0.059, 0.051	0.8952	-228.3868	0.731	-228.6010	-228.6379	9.3597
8	$7b_1^2(\pi_4^{*2})1a_2^0(\pi_3^0)$, $7b_1(\pi_4^*)1b_1(\pi_1)$	0.363, 0.213						
	$4a_2(\pi_5^*)$, $7b_1^2(\pi_4^{*2})2b_2^0(\pi_2^0)$	0.158, 0.053	0.8995	-228.3218	0.866	-228.5813	-228.6202	9.8396
9	$5b_1(d_{xz})$, $7b_1(\pi_4^*)$, $4b_1(d_{xz})$	0.576, 0.163, 0.057	0.9073	-228.3652	0.725	-228.5849	-228.6174	9.9160

Table C–7: Furan DZP$_I$+R(3s2p2d) CI calculation , $^1B_1$ states.

State	Open Shells	C_i^2	C^2	MRDCI energy	λ	MR-CISD energy	Full-CI energy	Transition energy
1	$7b_2(p_y)$, $10b_2(p_y)$	0.758, 0.119	0.9058	-228.4836	0.792	-228.7051	-228.7379	6.6386
2	$10b_2(p_y)$, $9b_2(d_{yz})$	0.457, 0.194						
	$7b_2(p_y)$, $10a_1(s)$	0.099, 0.089	0.9039	-228.4176	0.875	-228.6990	-228.7374	6.6517
3	$8b_2(d_{yz})$, $9b_2(d_{yz})$	0.739, 0.130	0.9082	-228.4555	0.831	-228.6920	-228.7250	6.9884
4	$10a_1(s)$, $11a_1(s)$	0.406, 0.188						
	$11a_1(s)$, $10b_2(p_y)$	0.115, 0.063	0.8978	-228.4248	0.744	-228.6813	-228.7193	7.1430
5	$12a_1(p_z)$, $19a_1(p_z)$	0.711, 0.084	0.8901	-228.4385	0.738	-228.6462	-228.6864	8.0398
6	$9b_2(d_{yz})$, $8b_2(d_{yz})$	0.517, 0.124						
	$10b_2(p_y)$	0.230	0.9107	-228.4119	0.811	-228.6539	-228.6855	8.0645
7	$13a_1(d_{x^2-y^2})$, $16a_1(d_{x^2-y^2})$	0.607, 0.189	0.8929	-228.4039	0.763	-228.6347	-228.6747	8.3585
8	$14a_1(d_{z^2})$	0.748	0.8915	-228.4076	0.767	-228.6326	-228.6733	8.3949
9	$16a_1(d_{x^2-y^2})$, $16a_1(d_{x^2-y^2})$	0.416, 0.233						
	$19a_1(p_z)$	0.183	0.8923	-228.3702	0.762	-228.6107	-228.6517	8.9835
10	$10a_1(s)$, $15a_1(s)$	0.363, 0.241						
	$11a_1(s)$	0.153	0.8975	-228.3852	0.718	-228.6044	-228.6406	9.2854
11	$19a_1(p_z)$, $16a_1(d_{x^2-y^2})$	0.486, 0.201						
	$12a_1(p_z)$	0.115	0.8890	-228.3764	0765	-228.6104	-228.6502	9.9740
12	$18a_1(d_{z^2})$	0.730	0.8917	-228.3588	0.710	-228.5763	-228.6141	10.0054
13	$11a_1(s)$, $15a_1(s)$	0.494, 0.235	0.9021	-228.3450	0.649	-228.5497	-228.5810	12.0326

Table C–8: Furan DZP$_l$+R(3s2p2d) CI calculation , $^1B_2$ states.

State	Open Shells	C_i^2	C^2	MRDCI energy	λ	MR-CISD energy	Full-CI energy	Transition energy
1	$3b_1(p_x)$, $6b_1(p_x)$, $7b_1(\pi_4^*)$	0.493, 0.292, 0.059	0.9216	-228.4812	0.824	-228.7083	-228.7371	6.6589
2	$7b_1(\pi_4^*)$, $5b_1(d_{xz})$	0.364, 0.273						
	$3b_1(p_x)$, $4b_1(d_{xz})$	0.135, 0.094	0.9131	-228.4658	0.828	-228.6994	-228.7290	6.8788
3	$b_1(d_{xz})$, $7b_1(\pi_4^*)$	0.650, 0.207	0.9182	-228.4886	0.787	-228.6703	-228.6984	7.7115
4	$6b_1(p_x)$, $3b_1(p_x)$	0.551, 0.264	0.9207	-228.4329	0.827	-228.6665	-228.6943	7.8244
5	$5b_1(d_{xz})$, $7b_1(\pi_4^*)$, $4b_1(d_{xz})$	0.561, 0.183, 0.132	0.9191	-228.4159	0.764	-228.6380	-228.6657	8.6020
6	$2a_2(d_{xy})$, $3a_2(d_{xy})$	0.615, 0.234	0.9029	-228.4239	0.765	-228.6198	-228.6534	8.9357
7	$4a_2(\pi_5^*)$	0.737	0.8852	-228.4045	0.716	-228.5915	-228.6335	9.4773
8	$3a_2(d_{xy})$, $2a_2(d_{xy})$	0.609, 0.210	0.9011	-228.3916	0.756	-228.5888	-228.6227	9.7713

Table C–9: Furan DZP$_l$+R(3s2p2d) CI calculation , $^1A_2$ states.

State	Open Shells	C_i^2	C^2	MRDCI energy	λ	MR-CISD energy	Full-CI energy	Transition energy
1	$15a_1(s)$, $11a_1(s)$	0.327, 0.267						
	$10a_1(s)$	0.167	0.9131	-228.4829	0.834	-228.7320	-228.7631	5.9500
2	$12a_1(p_z)$, $19a_1(p_z)$	0.736, 0.092	0.9066	-228.4780	0.841	-228.7123	-228.7463	6.4096
3	$13a_1(d_{x2-y2})$, $16a_1(d_{x2-y2})$	0.511, 0.240	0.9142	-228.4434	0.816	-228.6887	-228.7192	7.1378
4	$14a_1(d_{z2})$, $18a_1(d_{z2})$	0.714, 0.107	0.9122	-228.4424	0.804	-228.6788	-228.7097	7.4047
5	$18a_1(d_{z2})$, $14a_1(d_{z2})$	0.558, 0.142						
	$19a_1(p_z)$	0.101	0.9090	-228.4062	0.874	-228.6700	-228.7039	7.5628
6	$10a_1(s)$, $15a_1(s)$	0.603, 0.175	0.9117	-228.4381	0.798	-228.6718	-228.7027	7.5944
7	$13a_1(d_{x2-y2})$, $16a_1(d_{x2-y2})$	0.413, 0.303	0.9134	-228.4104	0.835	-228.6631	-228.6941	7.8292
8	$7b_2(p_y)$, $10b_2(p_y)$	0.517, 0.201	0.9026	-228.4327	0.780	-228.6564	-228.6914	7.9007
9	$8b_2(d_{yz})$, $9b_2(d_{yz})$	0.773, 0.061	0.9040	-228.4115	0.848	-228.6517	-228.6879	7.9987
10	$19a_1(p_z)$, $16a_1(d_{x2-y2})$	0.512, 0.152						
	$19a_1(p_z)$	0.134	0.9058	-228.4178	0.7402	-228.6380	-228.6696	8.4954
11	$11a_1(s)$, $15a_1(s)$	0.559, 0.111	0.9153	-228.4094	0.732	-228.6291	-228.6568	8.8442
12	$17a_1(s)$, $15a_1(s)$	0.442, 0.214						
	$20a_1(s)$	0.153	0.9146	-228.3740	0.726	-228.6022	-228.6300	9.5722
13	$9b_2(d_{yz})$	0.790	0.9046	-228.3552	0.584	-228.5253	-228.5516	11.7063

References

[1] E. Schrödinger. *Collected Papers on Wave Mechanics.* Blackie and Sons, London, New York (trans. J. F. Shearer and W. M. Deans), 1928.

[2] M. Born and J. R. Oppenheimer. *Ann. Phys.*, **84**, 457, 1927.

[3] P. Carsky and M. Urban. *Ab Initio Calculations; Methods and Applications in Chemistry.* Springer-Verlag, Berlin, Heidelberg and New York, 1980.

[4] G. L. Malli. In J. Maruani, editor, *Molecules in Physics, Chemistry and Biology Vol. II*, page 85. Reidel, New York, 1988.

[5] K. Balasubramanian. *J. Phys. Chem.*, **93**, 6585, 1989.

[6] F. Hund. *Z. Phys.*, **51**, 759, 1928.

[7] R. S. Mulliken. *Phys. Rev.*, **32**, 186, 1928.

[8] R. S. Mulliken. *Phys. Rev.*, **32**, 761, 1928.

[9] C. C. J. Roothaan. *Rev. Mod. Phys.*, **23**, 69, 1951.

[10] C. C. J. Roothaan. *Rev. Mod. Phys.*, **32**, 179, 1960.

[11] R. McWeeny and B. T. Pickup. *Rep. Prog. Phys.*, **43**, 1065, 1980.

[12] J. A. Pople and R. K. Nesbet. *J. Chem. Phys.*, **22**, 571, 1954.

[13] R. K. Nesbet. *Proc. R. Soc. London, Ser. A*, **230**, 312, 1955.

[14] A. Szabo and N. S. Ostlund. *Modern Quantum Chemistry; Introduction to Advanced Electronic Structure Theory.* Macmillan, New York, 1982.

[15] A. T. Amos and G. G. Hall. *Proc. R. Soc. London, Ser. A*, **263**, 483, 1961.

[16] P.-O. Löwdin. *Phys. Rev.*, **97**, 1474, 1955.

[17] J. S. Andrews, D. Jayatilaka, R. G. A. Bone, N. C. Handy, and R. D. Amos. *Chem. Phys. Lett.*, **183**, 423, 1991.

[18] J. C. Slater. *Phys. Rev.*, **36**, 57, 1930.

[19] S. F. Boys. *Proc. R. Soc. London, Ser. A*, **200**, 542, 1950.

[20] I. Shavitt. In B. Alder, S. Fernbach, and M. Rotenberg, editors, *Methods in Computational Physics Vol. II.* Academic Press, New York, 1963.

[21] J. Almlöf and P. R. Taylor. *J. Chem. Phys.*, **86**, 4070, 1987.

[22] J. Almlöf, K. Faegri, and K. Korsell. *J. Comput. Chem.*, **3**, 385, 1982.

[23] P. Knowles. In R. G. Evans and S. Wilson, editors, *Supercomputational Science*, page 211. Plenum, New York, 1990.

[24] G. Das and A. C. Wahl. *J. Chem. Phys.*, **44**, 87, 1966.

[25] L. Engelbrecht and B. Liu. *J. Chem. Phys.*, **78**, 3097, 1983.

[26] P. A. Cox, M. Bénard, and A. Veillard. *Chem. Phys. Lett.*, **87**, 159, 1982.

[27] E. Miyosho, H. Tatewaki, and T. Nakamura. *J. Chem. Phys.*, **78**, 815, 1983.

[28] R. D. Amos. *J. Chem. Soc., Faraday Trans. II*, **83**, 1595, 1987.

[29] P.-O. Löwdin. *Adv. Chem. Phys.*, **2**, 207, 1959.

[30] C. W. Bauschlicher Jr. and Langhoff S. R. *Adv. Chem. Phys.*, **76**, 103, 1990.

[31] M. Kotani, A. Ameniya, E. Ishiguro, and T. Kinaura. *Tables of Molecular Integrals.* Marazen, 1963.

[32] P. Pauncz. *Spin Eigenfunctions: Construction and Use.* Plenum, New York, 1978.

[33] S. Wilson. *Electron Correlation in Molecules.* Claredon, Oxford, 1984.

[34] J. Paldus. *The Unitary Group for the Evaluation of Electronic Matrix Elements.* Springer-Verlag, Berlin, 1981.

[35] P. J. Knowles and H.-J. Werner. *Chem. Phys. Lett.*, **145**, 514, 1988.

[36] J. K. L. MacDonald. *Phys. Rev.*, **43**, 830, 1933.

[37] J. C. Slater. *Phys. Rev.*, **34**, 1293, 1929.

[38] J. C. Slater. *Phys. Rev.*, **38**, 1109, 1931.

[39] J. Paldus. *J. Chem. Phys.*, **61**, 5321, 1974.

[40] V. R. Saunders and J. H. van Lenthe. *Mol. Phys.*, **48**, 923, 1983.

[41] P. E. M. Siegbahn. *Chem. Phys. Lett.*, **109**, 417, 1984.

[42] P. J. Knowles. *Chem. Phys. Lett.*, **155**, 513, 1989.

[43] R. J. Harrison and N. C. Handy. *Chem. Phys. Lett.*, **95**, 386, 1983.

[44] M. J. M. Bernal and S. F. Boys. *Phil. Trans. R. Soc.*, **A245**, 139, 1952.

[45] C. F.Bender and E. R. Davidson. *J. Chem. Phys.*, **47**, 4972, 1967.

[46] C. F.Bender and E. R. Davidson. *Phys. Rev.*, **183**, 23, 1969.

[47] J. L. Whitten and M. Hackmeyer. *J. Chem. Phys.*, **51**, 5584, 1969.

[48] J. L. Whitten. *J. Chem. Phys.*, **56**, 5458, 1972.

[49] L. R. Kahn, P. J. Hay, and I. Shavitt. *J. Chem. Phys.*, **61**, 3530, 1974.

[50] R. J. Buenker and S. D. Peyerimhoff. *Theor. Chim. Acta*, **35**, 33, 1974.

[51] S. D. Peyerimhoff and R. J. Buenker. *Adv. Quantum Chem.*, **9**, 69, 1975.

[52] R. J. Buenker, S. D. Peyerimhoff, and W. Butscher. *Mol. Phys.*, **35**, 771, 1978.

[53] P. E. M. Siegbahn. *J. Chem. Phys.*, **75**, 2314, 1981.

[54] P. E. M. Siegbahn. *Chem. Phys.*, **66**, 443, 1982.

[55] H.-J. Werner and E.-A. Reinsch. *J. Chem. Phys.*, **76**, 3144, 1982.

[56] H.-J. Werner and P. J. Knowles. *J. Chem. Phys.*, **89**, 5803, 1988.

[57] C. F. Jackels and I. Shavitt. *Theor. Chim. Acta*, **58**, 81, 1981.

[58] R. J. Bartlett and D. M. Silver. *Int. J. Quantum Chem. Symp.*, **9**, 183, 1975.

[59] R. J. Bartlett, I. Shavitt, and Purvis G. D. *J. Chem. Phys.*, **71**, 281, 1979.

[60] R. J. Bartlett. *Annu. Rev. Phys. Chem.*, **32**, 359, 1981.

[61] R. J. Bartlett, S. J. Cole, G. D. Purvis, W. C. Elmer, H. C. Hsien, and I. Shavitt. *J. Chem. Phys.*, **87**, 6579, 1987.

[62] R. Ahlrichs. *Theor. Chim. Acta*, **35**, 59, 1974.

[63] S. R. Langhoff and E. R. Davidson. *Int. J. Quantum Chem.*, **8**, 61, 1974.

[64] P. E. M. Siegbahn. *Chem. Phys. Lett.*, **55**, 386, 1978.

[65] J. A. Pople, R. Seeger, and R. Krishnan. *Int. J. Quantum Chem.*, **11**, 149, 1977.

[66] M. R. A. Blomberg and P. E. M. Siegbahn. *J. Chem. Phys.*, **78**, 5682, 1983.

[67] R. Ahlrichs, P. Scharf, and C. Ehrhardt. *J. Chem. Phys.*, **82**, 890, 1985.

[68] R. J. Gdanitz and R. Ahlrichs. *Chem. Phys. Lett.*, **143**, 413, 1988.

[69] D. P. Chong and S. R. Langhoff. *J. Chem. Phys.*, **84**, 5606, 1986.

[70] R. J. Buenker and S. D. Peyerimhoff. *Theor. Chim. Acta*, **39**, 217, 1975.

[71] R. J. Buenker. In P. G. Burton, editor, *Proceedings of the Workshop on Quantum Chemistry and Molecular Physics.* Woolongong Univ. Pres, 1980.

[72] R. J. Buenker. In R. J. Bartlett, editor, *Studies in Physical and Theoretical Chemistry.* Elsevier, Amsterdam, 1982.

[73] R. J. Buenker and R. A. Phillips. *J. Mol. Struct. (Theochem)*, **123**, 291, 1985.

[74] M. Dupuis, D. Spangler, and J. J. Wendoloski. *NRCC Software Catalog, Vol. 1, GAMESS, Program QC01*, 1980.

[75] M. F. Guest. *GAMESS: User Guide and Reference Manual*, 1989.

[76] Z. Gershgorn and I. Shavitt. *Int. J. Quantum Chem*, **2**, 751, 1968.

[77] I. Shavitt. *Chem. Phys. Lett.*, **192**, 135, 1992.

[78] C. F. Bunge. *Phys. Rev.*, **168**, 92, 1968.

[79] S. R. Langhoff and E. R. Davidson. *J. Chem. Phys.*, **64**, 4699, 1976.

[80] P. G. Burton, R. J. Buenker, P. J. Bruna, and S. D. Peyerimhoff. *Chem. Phys. Lett.*, **95**, 379, 1983.

[81] D. B. Knowles, J. R. Alvarezcollado, G. Hirsch, and R. J. Buenker. *J. Chem. Phys.*, **92**, 585, 1990.

[82] H.-J. Werner. *Adv. Chem. Phys.*, **69**, 1, 1987.

[83] R. Shepard. *Adv. Chem. Phys.*, **69**, 63, 1987.

[84] D. R. Hartree, W. Hartree, and B. Swirles. *Phil. Trans. Roy. Soc. (London)*, **A238**, 299, 1939.

[85] D. W. Smith and O. W. Day. *J. Chem. Phys.*, **62**, 113, 1975.

[86] K. Ruedenberg, L. M. Cheung, and S. T. Elbert. *Int. J. Quantum Chem.*, **16**, 1069, 1979.

[87] B. O. Roos. *Adv. Chem. Phys.*, **69**, 100, 1987.

[88] J. Olsen, B. O. Roos, P. Jorgensen, and H. J. Aa. *J. Chem. Phys.*, **89**, 2185, 1989.

[89] J. Hinze. *J. Chem. Phys.*, **59**, 6424, 1973.

[90] B. Levy and G. Berthier. *Int. J. Quantum Chem.*, **2**, 307, 1968.

[91] M. R. Hoffmann, D. J. Fox, J. F. Gaw, Y. Osamura, Y. Yamaguchi, R. S. Grew, G. Fitzgerald, H. F. Schaefer, P. J. Knowles, and N. C. Handy. *J. Chem. Phys.*, **80**, 2660, 1984.

[92] T. C. Chang and W. H. E. Schwarz. *Theor. Chim. Acta*, **44**, 45, 1977.

[93] B. O. Roos, P. Taylor, and P. E. M. Siegbahn. *Chem. Phys.*, **48**, 157, 1980.

[94] E. Dalgaard and P. Jorgensen. *J. Chem. Phys.*, **69**, 3833, 1978.

[95] B. H. Lengsfield. *J. Chem. Phys.*, **77**, 4073, 1982.

[96] K. K. Docken and J. Hinze. *J. Chem. Phys.*, **57**, 4928, 1972.

[97] H.-J. Werner and W. Meyer. *J. Chem. Phys.*, **74**, 5794, 1981.

[98] P.J. Knowles, G. J. Sexton, and N. C. Handy. *Chem. Phys. Lett.*, **72**, 337, 1982.

[99] K. Hirao. *Chem. Phys. Lett.*, **190**, 374, 1992.

[100] K. Hirao. *Chem. Phys. Lett.*, **196**, 397, 1992.

[101] W. D. Laidig and R. J. Bartlett. *Chem. Phys. Lett.*, **104**, 424, 1984.

[102] W. D. Laidig, P. Saxe, and R. J. Bartlett. *J. Chem. Phys.*, **86**, 887, 1987.

[103] M. R. Hoffmann and J. Simons. *J. Chem. Phys.*, **88**, 993, 1988.

[104] R. J. Bartlett. *J. Phys. Chem.*, **93**, 1697, 1989.

[105] C. Møller and M. S. Plesset. *Phys. Rev.*, **46**, 618, 1934.

[106] K. A. Brueckner and C. A. Levinson. *Phys. Rev.*, **97**, 1344, 1955.

[107] K. A. Brueckner. *Phys. Rev.*, **100**, 36, 1955.

[108] J. Goldstone. *Proc. R. Soc. London, Ser A*, **239**, 267, 1957.

[109] H. P. Kelly. *Adv. Chem. Phys.*, **14**, 129, 1969.

[110] S. Wilson and D. M. Silver. *Phys. Rev. A*, **14**, 1949, 1976.

[111] D. J. Baker, D. Moncrieff, and S. Wilson. In R. G. Evans and S. Wilson, editors, *Supercomputational Science.* Plenum, New York, 1990.

[112] L. Brillouin. *Act. Sci. Ind.*, **71**, 159, 1934.

[113] N. C. Handy, P. J. Knowles, and K. Somasundram. *Theor. Chim. Acta*, **86**, 87, 1985.

[114] R. H. Nobes, J. A. Pople, L. Radom, N. C. Handy, and P. J. Knowles. *Chem. Phys. Lett.*, **138**, 481, 1987.

[115] R. D. Amos, J. S. Andrews, N. C. Handy, and P. J. Knowles. *Chem. Phys. Lett.*, **185**, 256, 1991.

[116] P. J. Knowles, J. S. Andrews, R. D. Amos, N. C. Handy, and J. A. Pople. *Chem. Phys. Lett.*, **186**, 130, 1991.

[117] W. J. Lauderdale, J. F. Stanton, T. Gauss, J. D. Watts, and R. J. Bartlett. *Chem. Phys. Lett.*, **187**, 21, 1991.

[118] T. J. Lee and D. Jayatilaka. *Chem. Phys. Lett.*, **201**, 1, 1993.

[119] S. J. Cole and R. J. Bartlett. *J. Chem. Phys.*, **86**, 873, 1987.

[120] F. Coester. *Nucl. Phys.*, **7**, 421, 1958.

[121] F. Coester and H. Kümmel. *Nucl. Phys.*, **17**, 477, 1960.

[122] J. A. Pople, R. Krishnan, H. B. Schlegel, and J. S. Binkley. *Int. J. Quantum Chem.*, **14**, 545, 1978.

[123] R. J. Bartlett and G. D. Purvis. *Int. J. Quantum Chem.*, **14**, 561, 1978.

[124] R. J. Bartlett and G. D. Purvis. *Phys. Scr.*, **21**, 255, 1980.

[125] G. D. Purvis and R. J. Bartlett. *J. Chem. Phys.*, **76**, 1910, 1982.

[126] J. Noga and R. J. Bartlett. *J. Chem. Phys.*, **86**, 7041, 1987.

[127] J. Cizek and J. Paldus. *Int. J. Quantum Chem.*, **5**, 359, 1971.

[128] H. Kümmel, K. H. Lührmann, and J. G. Zabolitzky. *Phys. Rep. C*, **36**, 1, 1978.

[129] J. Paldus, J. Cizek, and B. Jeziorski. *J. Chem. Phys.*, **90**, 4356, 1989.

[130] J. Cizek. *J. Chem. Phys.*, **45**, 4256, 1966.

[131] G. E. Scuseria, A. C. Schiener, T. J. Lee, J. E. Rice, and H. F. Schaefer. *J. Chem. Phys.*, **86**, 2881, 1987.

[132] R. J. Bartlett, H. Sekino, and G. D. Purvis. *Chem. Phys. Lett.*, **98**, 66, 1983.

[133] Y. S. Lee, S. A. Kucharski, and R. J. Bartlett. *J. Chem. Phys.*, **81**, 5906, 1984.

[134] M. Urban, J. Noga, S. J. Cole, and R. J. Bartlett. *J. Chem. Phys.*, **83**, 4041, 1985.

[135] J. Noga, R. J. Bartlett, and M. Urban. *Chem. Phys. Lett.*, **134**, 126, 1987.

[136] W. Meyer. *J. Chem. Phys.*, **58**, 1017, 1973.

[137] M. Rittby and R. J. Bartlett. *J. Phys. Chem.*, **92**, 3033, 1988.

[138] S. A. Kucharski, A. Balková, and R. J. Bartlett. *Theor. Chim. Acta*, **80**, 321, 1991.

[139] H. Nakatsuji and K. Hirao. *J. Chem. Phys.*, **68**, 2053, 1978.

[140] K. Hirao and H. Nakatsuji. *J. Chem. Phys.*, **69**, 4548, 1978.

[141] H. Nakatsuji. *Chem. Phys. Lett.*, **59**, 362, 1978.

[142] D. Mukherjee and P. K. Mukherjee. *Chem. Phys.*, **39**, 325, 1979.

[143] K. Emrich. *Nucl. Phys. A*, **351**, 397, 1981.

[144] K. Emrich and J. G. Zabolitzky. *Nucl. Phys. A*, **351**, 439, 1981.

[145] M Takahashi and J. Paldus. *J. Chem. Phys.*, **85**, 1486, 1986.

[146] J. Geertsen, M. Rittby, and R. J. Bartlett. *Chem. Phys. Lett.*, **164**, 57, 1989.

[147] B. Jeziorski and H. J. Monkhorst. *Phys. Rev. A*, **24**, 1668, 1981.

[148] D. Mukhopadhyay, S. Mukhopadhyay, R. Chaudhuri, and D. Mukherjee. *Theor. Chim. Acta*, **80**, 441, 1991.

[149] S. S. Z. Adnan, S. Bhattacharyya, and D. Mukherjee. *Mol. Phys.*, **39**, 519, 1980.

[150] S. Ghosh, D. Mukherjee, and S. N. Bhattacharyya. *Chem. Phys.*, **72**, 161, 1982.

[151] S. Ghosh, D. Mukherjee, and S. N. Bhattacharyya. *Mol. Phys.*, **43**, 173, 1982.

[152] H. Nakatsuji. *Acta Chim. Hungaria*, **129**, 719, 1992.

[153] I. Lindgren and D. Mukherjee. *Phys. Rep.*, **151**, 93, 1987.

[154] R. Offermann, W. Ey, and H. Kümmel. *Nucl. Phys. A*, **273**, 349, 1976.

[155] R. Offermann, W. Ey, and H. Kümmel. *Nucl. Phys. A*, **273**, 368, 1976.

[156] D. Mukherjee, R. K. Moitra, and A. Mukhopadyay. *Mol. Phys.*, **33**, 955, 1977.

[157] I. Lindgren. *Int. J. Quantum Chem. Symp.*, **12**, 33, 1978.

[158] W. Kutzelnigg. *J. Chem. Phys.*, **80**, 822, 1984.

[159] L. Stolarczyk and H. J. Monkhorst. *Phys. Rev. A*, **32**, 725, 1985.

[160] L. Stolarczyk and H. J. Monkhorst. *Phys. Rev. A*, **32**, 743, 1985.

[161] A. Haque and U. Kaldor. *Chem. Phys. Lett.*, **117**, 347, 1985.

[162] A. Haque and U. Kaldor. *Chem. Phys. Lett.*, **120**, 261, 1985.

[163] L. Stolarczyk and H. J. Monkhorst. *Phys. Rev. A*, **37**, 1908, 1988.

[164] L. Stolarczyk and H. J. Monkhorst. *Phys. Rev. A*, **37**, 1926, 1988.

[165] B. Jeziorski and J. Paldus. *J. Chem. Phys.*, **90**, 2714, 1989.

[166] M. Rittby, S. Pal, and R. J. Bartlett. *J. Chem. Phys.*, **90**, 3214, 1989.

[167] U. Kaldor. *Theor. Chim. Acta*, **80**, 427, 1991.

[168] M. Barysz, H. J. Monkhorst, and L. Z. Stolarczyk. *Theor. Chim. Acta*, **80**, 483, 1991.

[169] L. Meissner and R. J. Bartlett. *J. Chem. Phys.*, **92**, 561, 1990.

[170] C. M. Rittby and R. J. Bartlett. *Theor. Chim. Acta*, **80**, 469, 1991.

[171] A. Balková, S. A. Kucharski, L. Meissner, and R. J. Bartlett. *Theor. Chim. Acta*, **80**, 335, 1991.

[172] D. Mukherjee. *Chem. Phys. Lett.*, **125**, 207, 1986.

[173] D. Mukherjee, W. Kutzelnigg, and S. Koch. *J. Chem. Phys.*, **87**, 5911, 1987.

[174] W. Kutzelnigg, D. Mukherjee, and S. Koch. *J. Chem. Phys.*, **87**, 5902, 1987.

[175] L. Meissner, L. Kucharski, and R. J. Bartlett. *J. Chem. Phys.*, **91**, 6187, 1989.

[176] W. C. Maguire, R. A. Hanel, D. E. Jennings, V. G. Kunde, and R. E. Samuelson. *Nature*, **292**, 683, 1981.

[177] F. J. Lovas, D. R. Johnson, D. Buhl, and L. E. Sneyder. *Astrophys. J.*, **209**, 1550, 1976.

[178] W. M. Irvine, B. Hoglund, P. Friberg, J. Aslene, and J. Elder. *Astrophys. J.*, **248**, L113, 1981.

[179] P. S. Martin, K. Yates, and I. G. Csizmadia. *Can. J. Chem.*, **67**, 2178, 1989.

[180] G. Herzberg. *Infra-Red and Raman Spectra of Polyatomic Molecules.* D. Van Nostrand, New York, 1945.

[181] R. Trambarulo and W. Gordy. *J. Chem. Phys.*, **18**, 1613, 1950.

[182] R. D. Nelson, D. R. Lide, and A. A. Maryott. *Selected Values of Electric Dipole Moments.* National Bureau of Standards, 1967.

[183] P. M. Burrel, B. Bjarnov, and R. H. Schwendeman. *J. Mol. Spectrosc.*, **82**, 193, 1980.

[184] G. Herzberg, F. Patat, and H. Verlerger. *J. Phys. Chem.*, **41**, 123, 1937.

[185] G. Herzberg and B. P. Stoicheff. *Nature*, **175**, 79, 1955.

[186] C. W. Bauschlicher and S. R. Langhoff. *Chem. Phys. Lett.*, **193**, 380, 1992.

[187] B. P. Stoicheff. *Tetrahedron*, **17**, 135, 1962.

[188] J. L. Duncan. *Spectrochim. Acta*, **20**, 1197, 1964.

[189] J. L. Duncan, D. C. McKean, P. D. Mallison, and R. D. McCulloch. *J. Mol. Spectrosc.*, **46**, 232, 1973.

[190] L. Pauling, H. D. Springall, and K. J. Palmer. *J. Am. Chem. Soc.*, **61**, 927, 1939.

[191] L. F. Thomas, E. I. Sherrard, and J. Sheridan. *Trans. Faraday Soc.*, **51**, 619, 1955.

[192] A. Dubrulle, D. Boucher, J. Burie, and J. Demaison. *J. Mol. Spectrosc.*, **72**, 158, 1978.

[193] C. C. Costain. *J. Chem. Phys.*, **29**, 864, 1958.

[194] R. S. Mulliken, C. A. Rieke, and W. G. Brown. *J. Am. Chem. Soc.*, **63**, 41, 1941.

[195] W. Tsang. *Int. J. Chem. Kinet.*, **10**, 687, 1978.

[196] D. F. McMillen and D. M. Golden. *Annu. Rev. Phys. Chem.*, **33**, 493, 1982.

[197] K. B. Wiberg. *J. Am. Chem. Soc.*, **101**, 2204, 1979.

[198] K. B. Wiberg. *J. Am. Chem. Soc.*, **102**, 1229, 1980.

[199] R. K. Thomas and H. W. Thompson. *Spectrochim. Acta, Part A*, **24**, 1337, 1968.

[200] R. K. Thomas and H. W. Thompson. *Spectrochim. Acta, Part A*, **24**, 1353, 1968.

[201] J. W. Russel, M. Murphy, T. R. Faulkner, and S. Sugai. *Spectrochim. Acta, Part A*, **27**, 119, 1971.

[202] J. L. Duncan, I. J. Wright, and D. Ellis. *J. Mol. Spectrosc.*, **37**, 394, 1971.

[203] R. Anttila, S. Jaakkonen, and T. Sahlström. *Spectrochim. Acta, Part A*, **28**, 1615, 1972.

[204] J. L. Duncan, D. C. McLean, and G. D. Nivellini. *J. Mol. Struct.*, **32**, 255, 1976.

[205] S. Kondo and Y. Koga. *J. Chem. Phys.*, **69**, 4022, 1978.

[206] N. F. Henfrey and B. A. Thrush. *J. Mol. Spectrosc.*, **113**, 426, 1985.

[207] N. F. Henfrey and B. A. Thrush. *J. Mol. Spectrosc.*, **121**, 139, 1987.

[208] L. C. Baylor, E. Weitz, and P. Hofmann. *J. Chem. Phys.*, **90**, 615, 1989.

[209] C. Meyer and M. Sergent-Rozey. *J. Mol. Spectrosc.*, **83**, 343, 1980.

[210] N. F. Henfrey and B. A. Thrush. *J. Mol. Spectrosc.*, **121**, 150, 1987.

[211] T. Al Adlouni and G. Garner. *J. Mol. Spectrosc.*, **127**, 186, 1988.

[212] M. V. Andreocci, P. Bitchev, P. Carusi, and A. Furlani. *J. Electron Spectrosc. Relat. Phenom.*, **16**, 25, 1979.

[213] K. Kimura, S. Kutsumata, Y. Achiba, T. Yamazaki, and S. Iwata. *Handbook of He(I) Photoelectron Spectra of Fundamental Organic Molecules.* Japan Scientific Societies Press, Tokyo, Halsted Press, New York, 1981.

[214] G. Bieri and L. Åsbrink. *J. Electron Spectrosc. Relat. Phenom.*, **20**, 149, 1980.

[215] P. R. Keller, J. W. Taylor, T. A. Carlson, and F. A. Grimm. *J. Electron Spectrosc. Relat. Phenom.*, **33**, 333, 1984.

[216] W. von Niessen, L. S. Cederbaum, J. Schirmer, G. H. F Diercksen, and W. P. Kraemer. *J. Electron Spectrosc. Relat. Phenom.*, **28**, 45, 1982.

[217] H. Bock and B. G. Ramsey. *Angew. Chem., int. edit. Engl.*, **12**, 734, 1973.

[218] W. Ensslin, H. Bock, and G. Becker. *J. Am. Chem. Soc.*, **96**, 2757, 1974.

[219] D. W. Turner, C. Baler, and C. R. Brundle. *Molecular Photoelectron Spectroscopy.* Wiley-Interscience, London, 1970.

[220] P. Carlier, J. E. Dubois, P. Masclet, and G. Mouvier. *J. Electron Spectrosc. Relat. Phenom.*, **7**, 77, 1975.

[221] B. Ciommer, K. M. Nguyen, H. Schwarz, G. Frenking, G. Kwiatkowski, and E. Illenberger. *Chem. Phys. Lett.*, **104**, 216, 1984.

[222] J. C. Giordan. *J. Am. Chem. Soc.*, **105**, 6544, 1983.

[223] J. C. Hemminger, B. G. Wicke, and W. Klemperer. *J. Chem. Phys.*, **65**, 2798, 1976.

[224] O. Nomura and S. Iwata. *J. Chem. Phys.*, **74**, 6830, 1981.

[225] C. K. Ingold and G. W. King. *J. Chem. Soc.*, page 2702, 1953.

[226] K. K. Innes. *J. Chem. Phys.*, **22**, 863, 1954.

[227] P. D. Foo and K. K. Innes. *Chem. Phys. Lett.*, **22**, 439, 1973.

[228] R. W. Wetmore and H. F. Schaeffer III. *J. Chem. Phys.*, **69**, 1648, 1978.

[229] S. P. So, R. W. Wetmore, and H. F. Schaeffer III. *J. Chem. Phys.*, **73**, 5706, 1980.

[230] P. G. Wilkinson. *J. Mol. Spectrosc.*, **2**, 387, 1958.

[231] W. E. Kammer. *Chem. Phys.*, **5**, 408, 1974.

[232] D. Demoulin. *Chem. Phys.*, **11**, 329, 1975.

[233] M. Perić, R. J. Beunker, and S. D. Peyerimhoff. *Mol. Phys.*, **53**, 1177, 1984.

[234] W. C. Price and A. D. Walsh. *Trans. Faraday Soc.*, **41**, 381, 1945.

[235] T. Nakayama and K. Watanabe. *J. Chem. Phys.*, **40**, 558, 1964.

[236] C. R. Bowman and W. D. Miller. *J. Chem. Phys.*, **42**, 681, 1965.

[237] D. F. Dance and I. C. Walker. *J. Chem. Soc., Faraday Trans. II*, **70**, 1426, 1974.

[238] R. S. Stradling, M. A. Baldwin, A. G. Loudon, and A. Maccoll. *J. Chem. Soc., Faraday Trans. II*, **72**, 871, 1976.

[239] W. M. Flicker, O. A. Mosher, and A. Kuppermann. *J. Chem. Phys.*, **69**, 3311, 1978.

[240] C. Fridh. *J. Chem. Soc., Faraday Trans. II*, **74**, 2193, 1978.

[241] S. Hamai and F. Hirayama. *J. Chem. Phys.*, **71**, 2934, 1979.

[242] G. Herzberg. *Molecular Spectra and Molecular Structure. III. Electronic Spectra and Electronic Structure of Polyatomic Molecules.* Van Nostrand Reinhold, New York, 1966.

[243] W. C. Price. *Phys. Rev.*, **47**, 444, 1935.

[244] M. B. Robin. *Higher Excited States of Polyatomic Molecules, Vol. II.* Academic, New York, 1975.

[245] T. C. Betts and V. McKoy. *J. Chem. Phys.*, **60**, 2947, 1973.

[246] S. Trajmar, J. K. Rice, P. S. P. Wei, and A. Kuppermann. *Chem. Phys. Lett.*, **1**, 703, 1968.

[247] S. Trajmar, J. K. Rice, and A. Kuppermann. *Adv. Chem. Phys.*, **18**, 15, 1970.

[248] M. Fujii, A. Haijima, and M. Ito. *Chem. Phys. Lett.*, **150**, 380, 1988.

[249] A. Galli, P. Harteck, and R. R. Reeves Jr. *J. Phys. Chem.*, **71**, 2719, 1967.

[250] K. Seki and H. Okabe. *J. Phys. Chem.*, **96**, 3345, 1992.

[251] S. Satyapal and R. Bersohn. *J. Phys. Chem.*, **95**, 8004, 1991.

[252] L. J. Stief, V. J. DeCarlo, and W. A. Payne. *J. Chem. Phys.*, **54**, 1913, 1971.

[253] W. A. Payne and L. J. Stief. *J. Chem. Phys.*, **56**, 3333, 1972.

[254] G. W. King and C. K. Ingold. *Nature*, **169**, 1101, 1952.

[255] J. M. Hollas and T. Sutherley. *Mol. Phys.*, **21**, 183, 1971.

[256] D. F. Dance and I. C. Walker. *Chem. Phys. Lett.*, **18**, 601, 1973.

[257] M. Jungen. *Chem. Phys.*, **2**, 367, 1973.

[258] D. Demoulin and M. Jungen. *Theor. Chim. Acta.*, **34**, 1, 1974.

[259] M. Herman and R. Colin. *Phys. Scr.*, **25**, 275, 1982.

[260] M. N. R. Ashfold, R. N. Dixon, J. D. Prince, and B. Tutcher. *Mol. Phys.*, **56**, 1185, 1985.

[261] W. E. Kammer. *Chem. Phys. Lett.*, **6**, 529, 1970.

[262] H. Lischka and A. Karpfen. *Chem. Phys.*, **102**, 77, 1986.

[263] M. Perić, S. D. Peyerimhoff, and R. J. Buenker. *Mol. Phys*, **62**, 1339, 1987.

[264] J. O. Jensen, G. F. Adams, and C. F. Chabalowski. *Chem. Phys. Lett.*, **172**, 379, 1990.

[265] J. O. Jensen, G. F. Adams, and C. F. Chabalowski. *J. Chem. Phys.*, **94**, 1332, 1991.

[266] S. Huzinaga. *J. Chem. Phys.*, **42**, 1293, 1965.

[267] T. H. Dunning. *J. Chem. Phys.*, **53**, 2823, 1970.

[268] T. H. Dunning. *J. Chem. Phys.*, **55**, 716, 1971.

[269] I. C. Walker, M. H. Palmer, and A. Hopkirk. *Chem. Phys.*, **141**, 365, 1990.

[270] M. H. Palmer, I. C. Walker, M. F. Guest, and A. Hopkirk. *Chem. Phys.*, **147**, 19, 1990.

[271] I. C. Walker and M. H. Palmer. *Chem. Phys.*, **153**, 169, 1991.

[272] M. H. Palmer and I. C. Walker. *Chem. Phys.*, **157**, 187, 1991.

[273] R. D. Amos and J. E. Rice. *CADPAC: The Cambridge Analytic Derivatives Package*, issue 4.0, 1987.

[274] V. Kellö, M. Urban, J. Noga, and G. H. F. Diercksen. *J. Am. Chem. Soc.*, **106**, 5864, 1984.

[275] H. Honjou, J. Pacansky, and M. Yoshimime. *J. Am. Chem. Soc.*, **107**, 5332, 1985.

[276] M. F. Powell, M. R. Peterson, and I. G. Csizmadia. *J. Mol. Struct. (Theochem)*, **92**, 323, 1983.

[277] P. C. Hariharan and J. A. Pople. *Chem. Phys. Lett.*, **16**, 217, 1972.

[278] D. A. Dixon and B. E. Smart. *J. Phys. Chem.*, **93**, 7772, 1989.

[279] N. Koga and M. Morokuma. *J. Am. Chem. Soc.*, **113**, 1907, 1991.

[280] E. D. Simandiras, J. E. Rice, T. J. Lee, R. D. Amos, and N. C. Handy. *J. Chem. Phys.*, **88**, 3187, 1988.

[281] J. D. Brown. *Biochemistry.* Harper and Row, New York, 1983.

[282] P. Vogel. *Bull. Soc. Chim. Belg.*, **99**, 395, 1990.

[283] F. M. Dean. *Adv. Heterocylcic Chem.*, **31**, 237, 1982.

[284] F. M. Dean. *Adv. Heterocylcic Chem.*, **30**, 167, 1982.

[285] B. Bak, D. Christensen, W. R. Dixon, L. Hansen-Nygaard, J. R. Andersen, and M. Schottländer. *J. Mol. Spectrosc.*, **9**, 124, 1962.

[286] P. B. Liescheski and D. W. H. Rankin. *J. Mol. Struct*, **196**, 1, 1989.

[287] F. Mata, M. C. Martin, and G. O. Sørensen. *J. Mol. Struct.*, **48**, 157, 1978.

[288] R. Fourme. *Acta Crystallogr., Sect B*, **28**, 2984, 1972.

[289] F. R. Cordell and J. E. Boggs. *J. Mol. Struct. (Theochem)*, **165**, 175, 1988.

[290] M. H. Palmer. *Structure and Reactions of Heterocyclic Compounds.* Arnold, London, 1967.

[291] T. G. Schamlz, C. L. Norris, and W. H. Flygare. *J. Am. Chem. Soc.*, **95**, 7961, 1973.

[292] J. H. D. Eland. *J. Mass Spectrom. Ion Phys.*, **2**, 471, 1969.

[293] P. J. Derrick, L. Åsbrink, O. Edqvist, and E. Lindholm. *Spectrochim. Acta*, **27A**, 2525, 1971.

[294] P. J. Derrick, L. Åsbrink, O. Edqvist, B. Ö. Jonsson, and E. Lindholm. *Int. J. Mass Spectrom. Ion. Phys.*, **6**, 161, 1971.

[295] P. Dechant, A. Schweig, and W. Thiel. *Angew. Chem., int. edit. Engl*, **12**, 308, 1973.

[296] J. A. Sell and A. Kuppermann. *Chem. Phys. Lett.*, **61**, 355, 1979.

[297] G. Bieri, L. Åsbrink, and W. von Niessen. *J. Electron Spectrosc. Relat. Phenom.*, **27**, 129, 1982.

[298] L. Klasinc, A. Sabljić, G. Kluge, J. Rieger, and M. Scholz. *J. Chem. Soc., Perkin Trans. II*, page 539, 1982.

[299] R. Seth-Smith, M. Anselment, L. F. DiMauro, J. M. Fryre, and T. J. Sears. *J. Chem. Phys.*, **87**, 4435, 1987.

[300] A. D. O. Bawagan, B. J. Olsson, K. H. Tan, J. M. Chen, and B. X. Yang. *Chem. Phys.*, **164**, 283, 1992.

[301] M. H. Palmer and A. J. Gaskell. *Theor. Chim. Acta*, **26**, 357, 1972.

[302] P. Siegbahn. *Chem. Phys. Lett.*, **8**, 245, 1971.

[303] W. von Niessen, W. P. Kraemer, and L. S. Cederbaum. *J. Electron Spectrosc. Relat. Phenom.*, **8**, 179, 1976.

[304] M. Hehenberger. *Chem. Phys. Lett.*, **46**, 117, 1977.

[305] L. Åsbrink, C. Fridh, and E. Lindholm. *J. Electron Spectrosc. Relat. Phenom.*, **16**, 65, 1979.

[306] K.-H. Thunemann, R. J. Buenker, and W. Butscher. *Chem. Phys.*, **47**, 313, 1980.

[307] G. De Alti and P. Decleva. *Chem. Phys. Lett.*, **77**, 413, 1981.

[308] H. Nakatsuji, O. Kitao, and T. Yonezawa. *J. Chem. Phys.*, **83**, 723, 1985.

[309] U. Gelius, C. J. Allen, G. Johansson, H. Siegbahn, D. A. Allison, and K. Siegbahn. *Phys. Scr.*, **3**, 237, 1971.

[310] L. W. Pickett. *J. Chem. Phys.*, **8**, 293, 1940.

[311] B. Nordén, R. Håkansson, P. B. Pedersen, and E. W. Thulstrup. *Chem. Phys.*, **33**, 355, 1978.

[312] J. L. Roebber, D. P. Gerrity, R. Hemley, and V. Vaida. *Chem. Phys. Lett.*, **75**, 104, 1980.

[313] L. Nyulászi. *J. Mol. Struct.*, **273**, 133, 1992.

[314] M. B. Robin. *Higher Excited States of Polyatomic Molecules, Vol. III.* Academic, New York, 1985.

[315] I. C. Walker. Private communication.

[316] E. H. van Veen. *Chem. Phys. Lett.*, **41**, 535, 1976.

[317] W. M. Flicker, O. A. Mosher, and A. Kuppermann. *J. Chem. Phys.*, **64**, 1315, 1976.

[318] W. M. Flicker, O. A. Mosher, and A. Kuppermann. *Chem. Phys. Lett.*, **38**, 489, 1976.

[319] A. Kuppermann, W. M. Flicker, and O. A. Mosher. *Chem. Rev.*, **79**, 77, 1979.

[320] W. C. Price and A. D. Walsh. *Proc. R. Soc. London, Ser. A*, **179**, 201, 1941.

[321] L. W. Pickett, N. J. Hoeflich, and T-C Liu. *J. Am. Chem. Soc.*, **73**, 4865, 1951.

[322] K. Watanabe and T. Nakayama. *J. Chem. Phys.*, **29**, 48, 1958.

[323] C. D. Cooper, A. D. Willianson, J. C. Miller, and R. N. Compton. *J. Chem. Phys.*, **73**, 1527, 1980.

[324] N. Solony, F. W. Birss, and J. B. Greeshields. *Can. J. Chem.*, **43**, 1569, 1965.

[325] J. Del Bene and H. F. Jaffé. *J. Chem. Phys.*, **48**, 1807, 1968.

[326] P. C. Mishra and K. Jug. *Theor. Chim. Acta*, **61**, 559, 1982.

[327] G. Buemi, F. Zuccarello, and G. Romeo. *J. Mol. Struct. (Theochem)*, **94**, 115, 1983.

[328] P. Ertl and J. Leska. *J. Mol. Struct. (Theochem)*, **165**, 1, 1988.

[329] F. R. Cordell and J. E. Boggs. *J. Mol. Struct. (Theochem)*, **35**, 163, 1981.

[330] I. G. John and L. Radom. *J. Am. Chem. Soc.*, **100**, 3981, 1978.

[331] F. Török, Á. Hegedüs, and P. Pulay. *Theor. Chim. Acta*, **32**, 145, 1972.

[332] V. K. Yadav, A. Yadav, and R. Poirier. *J. Mol. Struct. (Theochem)*, **199**, 101, 1989.

[333] G. de Brouckère, W. C. Nieuwpoort, R. Broer, and G. Berthier. *Mol. Phys.*, **45**, 649, 1982.

[334] G. De Alti, P. Decleva, and A. Lisini. *Chem. Phys.*, **90**, 231, 1984.

[335] M. D. Morse. *Chem. Rev.*, **86**, 1049, 1986.

[336] K. P. Lawley and R. J. Donovan. *J. Chem. Soc. Faraday Trans.*, **89**, 1885, 1993.

[337] E. U. Condon and G. H. Shortley. *The Theory of Atomic Spectra.* University Press, Cambridge, 1963.

[338] U.S. National Bureau of Standards. *Atomic Energy Levels as Derived from the Analysis of Optical Spectra, NSRDS-NBS 35 Volume II.* U.S. Dept. Commerce, 1970.

[339] E. A. Rohlfing and J. J. Valentini. *J. Chem. Phys.*, **84**, 6560, 1986.

[340] D. G. Leopold, J. Ho, and W. C. Linederger. *J. Chem. Phys.*, **86**, 1715, 1987.

[341] J. P. Deslaux. *At. Data Nucl. Data*, **12**, 311, 1973.

[342] C. M. Marian, D. Hippe, B. A. Hess, and S. D. Peyerimhoff. *Theor. Chim. Acta*, **81**, 375, 1992.

[343] R. H. Page and C. S. Gudeman. *J. Chem. Phys.*, **94**, 39, 1991.

[344] D. E. Powers, S. G. Hansen, M. E. Geusic, D. L. Michalopoulos, and R. E. Smalley. *J. Chem. Phys.*, **78**, 2866, 1983.

[345] R. S. Ram, C. N. Jarman, and P. F. Bernath. *J. Mol Spectrosc.*, **156**, 468, 1992.

[346] N. Åslund, R. F. Barrow, W. G. Richards, and D. N. Travis. *Arkiv. Fysik.*, **30**, 171, 1965.

[347] M. Doverstål, B. Lindgren, U. Sassenberg, and H. Yu. *Chem. Phys. Lett.*, **192**, 283, 1992.

[348] J. Lochet. *J. Phys. B*, **11**, L55, 1978.

[349] V. E. Bondybey, G. P. Schwarz, and J. H. English. *J. Chem. Phys.*, **78**, 11, 1983.

[350] B. Kleman and S. Lindqvist. *Arkiv. Fysik.*, **8**, 333, 1954.

[351] J. Ruamps. *Compt. Rend.*, **238**, 1489, 1954.

[352] D. S. Pesič and S. Weniger. *C. R. Acad. Sci., Ser B*, **273**, 602, 1971.

[353] J. G. McCaffrey, R. R. Bennett, M. D. Morse, and W. H. Breckenridge. *J. Chem. Phys.*, **91**, 92, 1989.

[354] D. R. Preuss, S. A. Pace, and J. L. Gole. *J. Chem. Phys.*, **71**, 3553, 1979.

[355] D. E. Powers, S. G. Hansen, M. E. Geusic, A. C. Pulu, J. B. Hopkins, M. A. Duncan, P. R. R. Langridge-Smith, and R. E. Smalley. *J. Phys. Chem.*, **86**, 2556, 1982.

[356] J. L. Gole, J. H. English, and V. E. Bondybey. *J. Phys. Chem.*, **86**, 2560, 1982.

[357] P. C. Cartwright. PhD thesis, University of Edinburgh, 1989.

[358] R. E. Steele. *J. Mol. Spectrosc.*, **61**, 477, 1976.

[359] G. A. Ozin, S. A. Mitchell, and J. Garcia-Prieto. *J. Chem. Phys.*, **86**, 473, 1982.

[360] V. E. Bondybey. *J. Chem. Phys.*, **77**, 3771, 1982.

[361] A. D. Sappey, J. E. Harrington, and J. C. Weisshaar. *J. Chem. Phys.*, **91**, 3854, 1989.

[362] S. S. S. Rao and S. V. K. Rao. *Indian J. Pure Appl. Phys.*, **16**, 923, 1978.

[363] N. L. Singh. *Phys. Rev.*, **99**, 1624, 1955.

[364] G. A. Bishea, N. Marak, and M. D. Morse. *J. Chem. Phys.*, **95**, 5618, 1991.

[365] C. W. Bauschlicher Jr., S. P. Walch, and P. E. M. Siegbahn. *J. Chem. Phys.*, **76**, 6015, 1982.

[366] K. Raghavachari, K. K. Sunil, and K. D. Jordan. *J. Chem. Phys.*, **83**, 4633, 1985.

[367] K. K. Sunil, K. D. Jordan, and K. Raghavachari. *J. Phys. Chem.*, **89**, 457, 1985.

[368] H. Tatewaki and M. Sekiya. *J. Chem. Phys.*, **85**, 5895, 1986.

[369] H. Partridge, K. W. Richman, and E. A. McCullough. *Theor. Chim. Acta*, **74**, 151, 1988.

[370] I. Shim and K. A. Gingerich. *J. Chem. Phys.*, **79**, 2903, 1983.

[371] P. Scharf, S. Brode, and R. Ahlrichs. *Chem. Phys. Lett.*, **113**, 447, 1985.

[372] H.-J. Werner and R. L. Martin. *Chem. Phys. Lett.*, **113**, 451, 1985.

[373] M. Pélissier. *J. Chem. Phys.*, **79**, 2099, 1983.

[374] R. L. Martin. *J. Chem. Phys.*, **78**, 5840, 1983.

[375] C. W. Bauschlicher Jr., S. P. Walch, and P. E. M. Siegbahn. *J. Chem. Phys.*, **78**, 3347, 1983.

[376] L. Pauling. *J. Chem. Phys.*, **78**, 3346, 1983.

[377] S. R. Langhoff and C. W. Bauschlicher Jr. *J. Chem. Phys.*, **84**, 4485, 1986.

[378] G. H. Jueng and J. C. Barthelat. *J. Chem. Phys.*, **78**, 2097, 1983.

[379] H. Stoll, P. Fuentealba, M. Dolg, J. Flad, L. v. Szentpaly, and H. Preuss. *J. Chem. Phys.*, **79**, 5532, 1983.

[380] H. Stoll, P. Fuentealba, P. Schwerdtfeger, J. Flad, L. v. Szentpaly, and H. Preuss. *J. Chem. Phys.*, **81**, 2732, 1984.

[381] S. P. Walch, C. W. Bauschlicher Jr., B. O. Roos, and C. J. Nelin. *Chem. Phys. Lett.*, **103**, 175, 1983.

[382] K. K. Sunil and K. D. Jordan. *Chem. Phys. Lett.*, **128**, 363, 1986.

[383] C. W. Bauschlicher. *Chem. Phys. Lett.*, **97**, 204, 1983.

[384] C. Kölmel and R. Ahlrichs. *J. Phys. Chem.*, **94**, 5536, 1990.

[385] M. Pelissier. *J. Chem. Phys.*, **75**, 775, 1981.

[386] R. D. Cowan and D. C. Griffin. *J. Opt. Soc. Am.*, **66**, 1010, 1976.

[387] J. Harris and R. O. Jones. *J. Chem. Phys.*, **70**, 830, 1979.

[388] B. Delley, D. E. Ellis, A. J. Freeman, E. J. Baerends, and D. Post. *Phys. Rev. B*, **27**, 2132, 1983.

[389] G. S. Painter and F. W. Averill. *Phys. Rev. B*, **28**, 5536, 1983.

[390] F. W. Averill and G. S. Painter. *Phys. Rev. B*, **32**, 2141, 1985.

[391] K. A. Jackson. *Phys. Rev. B*, **47**, 9715, 1993.

[392] K. Kobayashi, N. Kurita, H. Kumahora, and K. Tago. *Phys. Rev. A*, **43**, 5810, 1991.

[393] R. O. Jones and O. Gunnarsson. *Rev. Mod. Phys.*, **61**, 689, 1989.

[394] T. Ziegler, J. G. Snijders, and E. J. Baerends. *J. Chem. Phys.*, **74**, 1271, 1981.

[395] P. Joyes and M. Leleyter. *J. Phys. B*, **6**, 150, 1973.

[396] A. B. Anderson. *J. Chem. Phys.*, **68**, 1744, 1978.

[397] G. A. Ozin, H. Huber, D. McIntosh, S. Mitchell, J. G. Norman, and L. Noodlemann. *J. Am. Chem. Soc.*, **101**, 3504, 1979.

[398] M. Witko and H.-O. Beckmann. *Mol. Phys.*, **47**, 945, 1982.

[399] A. T. Amos, P. A. Brook, and S. A. Moir. *J. Phys. Chem.*, **92**, 733, 1988.

[400] P. J. Hay. *J. Chem. Phys.*, **66**, 4377, 1977.

[401] A. J. H. Wachters. *J. Chem. Phys.*, **52**, 1033, 1970.

[402] S. P. Walch and C. W. Bauschlicher Jr. *Chem. Phys. Lett.*, **105**, 171, 1984.

[403] S. P. Walch and C. W. Bauschlicher Jr. In R. J. Bartlett, editor, *Comparison of Ab Initio Quantum Chemistry with Experiment for Small Molecules.* D. Reidel, 1985.

[404] H.Tatewaki. Private communication.

[405] D. Hippe and S. D. Peyerimhoff. *Mol. Phys.*, **76**, 293, 1992.

[406] W. G. Richards, H. P. Trivedi, and D. L. Cooper. *Spin-orbit Coupling in Molecules.* Clarendon, Oxford, 1981.

[407] R. L. Martin and P. J. Hay. *J. Chem. Phys.*, **75**, 4539, 1981.

[408] J. S. Cohen and B. Schneider. *J. Chem. Phys.*, **61**, 3230, 1974.

[409] P. J. Hay, T. H. Dunning Jr., and R. C. Raffenetti. *J. Chem. Phys.*, **65**, 2679, 1976.

[410] F. Grein and S. D. Peyerimhoff. *J. Chem. Phys.*, **87**, 4684, 1987.

[411] F. Spiegelmann, D. Pavolini, and J. P. Daudey. *J. Phys. B*, **22**, 2465, 1989.

[412] N. W. Winter and D. L. Huestis. *Chem. Phys. Lett.*, **133**, 311, 1987.

[413] J. C. Slater. *Quantum Theory of Atomic Structure, Vol. II.* McGraw-Hill, New York, 1960.

[414] T. Itoh. *Rev. Mod. Phys.*, **37**, 159, 1965.

Publications:

- The Electronic States of the Azines. VI. 1,3,5-Triazine, Studied by VUV Absorption, Near-Threshold Electron Energy-Loss Spectroscopy and Ab Initio Multireference Configuration-Interaction Calculations.
  I. C. Walker, M. H. Palmer, and C. C. Ballard, *Chem. Phys.*, **167**, 61-75, 1992.

Chemical Physics 167 (1992) 61–75
North-Holland

The electronic states of the azines. VI. 1.3.5-triazine, studied by VUV absorption, near-threshold electron energy-loss spectroscopy and ab initio multi-reference configuration interaction calculations

Isobel C. Walker
Department of Chemistry, Heriot-Watt University, Riccarton, Edinburgh EH14 4AS, Scotland, UK

Michael H. Palmer and Charles C. Ballard
Department of Chemistry, University of Edinburgh, West Mains Road, Edinburgh EH9 3JJ, Scotland, UK

Received 2 April 1992; in final form 10 July 1992

The results of large-scale ab initio CI calculations on the electronic states of 1.3.5-triazine, using a multi-reference multi-root CI (MRD-CI) method are related to new VUV absorption and low-energy electron energy-loss (EEL) measurements, leading to detailed spectral assignments. Vertical transition energies are computed to within 0.6 eV for all and 0.3 eV for most of the low-lying electronic states. The computations are extended to cationic states and to the evaluation of ground state molecular electronic properties of the molecule.

1. Introduction

We have previously reported the results of spectroscopic experiments (VUV absorption and near-threshold electron energy-loss, EEL) together with multi-reference CI calculations on pyridine [1] and each of the three diazines [2–4]. We have now extended this work to 1.3.5-triazine, in order to further our understanding of spectroscopic and other electronic properties of the azabenzenes.

An extended VUV absorption spectrum for 1.3.5-triazine has been reported [5] as has an EEL spectrum (3.25–17 eV) recorded for electrons of 150 eV incident-energy [6]. In these, $\pi\pi^*$ states are located at (vertical transition energies) 5.7 eV ($^1A_2''$), 6.86 eV ($^1A_1'$) and 7.76 eV ($^1E'$). Other investigators have been concerned with the detailed analysis of these $\pi\pi^*$ bands [7,8]. At least two $n\pi^*$ states, $^1E''$ and $^1A_2''$, contribute to electronic excitation spectra around 4–5 eV [5,6]. The lower-lying of these, $^1E''$ (which is S_1) has been explored using a variety of techniques [9,10–20] and the band origin reliably positioned at 3.827 eV (30869 cm^{-1}) [14,20]. The lowest triplet state $^3E''$ has been estimated to lie about 0.5 eV below the corresponding singlet [19,20]. No other low-lying triplet state has been located by experiment. The origin of the $6e' \rightarrow 3sa_1'$ Rydberg transition is 6.916 eV [6,8,21]; accompanying vibrational structure matches that in the lowest photoelectron band [6]. Other proposed Rydberg-state origins are 9.37 eV ($1e''3p$) and 8.60 eV ($6e'4s$) [6].

In this work, we have extended the measured VUV spectrum and present it along with new EEL spectra recorded under conditions favourable for the detection of optically forbidden transitions. We consider detailed assignment of the spectroscopic states using the results of multi-reference, multi-root configuration interaction calculations, as previously applied [1–4]. Few high-order computations on the electronic states of 1.3.5-triazine have been reported. π-electron only calculations have focused upon the low-lying $\pi\pi^*$ states [22–25]. The results from refs.

Correspondence to: I.C. Walker, Department of Chemistry, Heriot-Watt University, Riccarton, Edinburgh EH14 4AS, Scotland, UK.

[23,25] are particularly noteworthy for accurate assignment of all three bands. When σ electrons are included [26–28], the agreement with experiment is variable. A study on π-electron delocalisation in azines led to the surprising conclusion [29] that the delocalisation energy of 1,3,5-triazine is 10% higher than that of benzene and the other azines. In an important series of papers on nπ* states Goodman et al. [10–12] have drawn attention to some of the factors involved in an MO interpretation of these. These will be discussed below in relation to the present theoretical work.

We consider, also, the assignment of the photoelectron spectrum (PES) of 1,3,5-triazine [6,30] and, in addition, compute some ground-state electronic properties. Because of its high symmetry, few of these have been determined experimentally.

2. Experimental methods and results

2.1. VUV absorption

The VUV spectrum of fig. 1 was recorded at the SERC synchrotron source, Daresbury, using procedures which have been previously detailed [1–3]. The data are presented on an energy (eV) abscissa for direct comparison with the scattered-electron results and photoelectron data. Over the range of overlap, the present VUV spectrum is concordant with that of ref. [5], including absolute intensities. We have extended the measured spectral range at the high energy end from about 9 to 11.8 eV; however, the lowest absorption band (nπ*) lies below our onset energy.

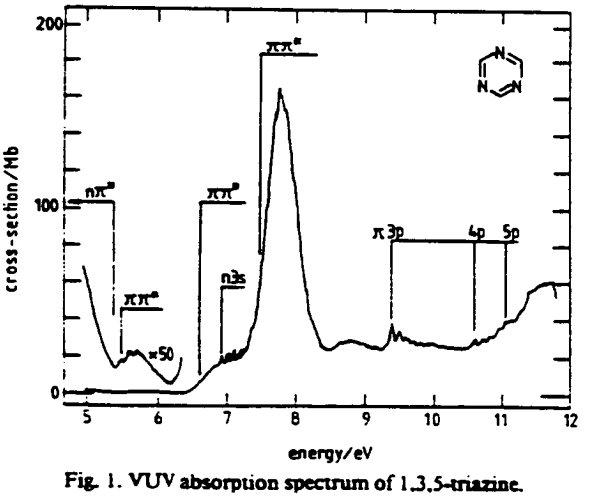

Fig. 1. VUV absorption spectrum of 1,3,5-triazine.

The known ππ* absorptions ($^1A_2'$, $^1A_1'$ and $^1E'$ in ascending order, see above) are marked on fig. 1. Fig. 2 shows these ππ* bands on expanded scales. In each of them weak vibrational structure, ascribed to excitation of vibrational mode ν_1 (symmetry a_1', 0.123 eV in the ground state [9], ≈0.1 eV here) can be discerned. There is no doubt about the location of the lowest Rydberg state (e'3s, $^1E'$), origin 6.971 eV, which is both one-photon and two-photon allowed [21]. In the two-photon absorption spectrum, vibrational fine structure has been interpreted as excitation of, predominantly, a degenerate (e') vibration, ν_6 (a ring-breathing mode, 0.084 eV in the ground state [9]) together with the totally symmetric modes ν_1, (0.123 eV in the ground state) and ν_{12} (0.141 eV in the ground state) [21]. Comparison of the observed fine structure with that in the $(6e')^{-1}$ PES

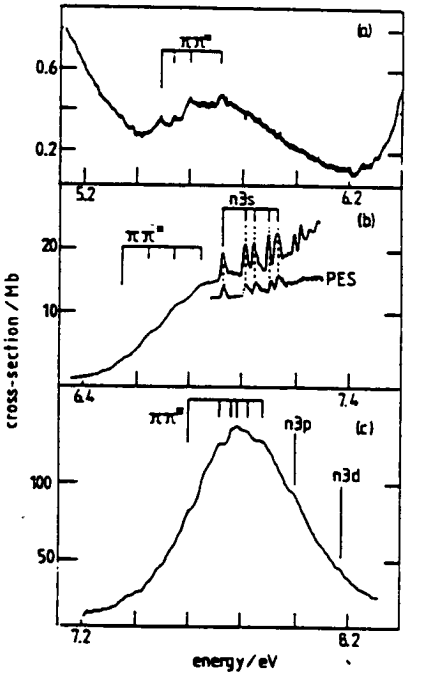

Fig. 2. Absorption bands of 1,3,5-triazine. (a) ππ* ($^1A_2'$). (b) ππ* ($^1A_1'$) and n3s ($^1E'$). PES is a trace of the $(6e')^{-1}$ band in the photoelectron spectrum, taken from ref. [6]. This illustrates that the structures at 7.187 and 7.213 eV are not of the n3s band. (c) ππ* ($^1E'$).

band suggests that two relatively intense absorptions, at 7.187 and 7.213 eV respectively, do not belong to the $^1E'$ Rydberg state (fig. 2b). We return to these following presentation of the theoretical data.

Transitions at 9.365 and 10.603 eV (fig. 3a) are linked to the $^2E''$ ionisation limit (11.69 eV [6]) and assigned $^1e''3p$ and $^1e''4p$ respectively, from the quantum defects (0.52 and 0.48 respectively). This is in agreement with Fridh et al. [6]. Our tentative assignment for the $^1e''5p$ member of this series is 11.046 eV, quantum defect 0.41 (fig. 3a). In these, the active vibration is thought to be ν_{12}.

The broad band spanning 8.5–9.2 eV carries weak structure (fig. 3b). The e'4s Rydberg state is expected to lie around 8.6 eV, as proposed by Fridh et al. [6]. Considering the expected vibrational substructure, our preferred origin is 8.680 eV, quantum defect 0.80 (fig. 3b). Also the maximum at 8.902 eV appears to be the origin of a Rydberg state associated with IP_2 (figs. 3a and 3b). The quantum defect, 0.79, is typical of an s-type state (e''3s, $^1E''$). However, as this is optically forbidden, there must be doubt in this assignment and the possibility that it is e''3p, with an anomolously high quantum defect, should be considered. We label an absorption maximimum at 9.077 eV as e'4d, from the quantum defect (0.18). The associated e'3d state is expected around 8.2 eV. In fact, there is a very weak maximum at 8.16 eV, on the high-energy side of the intense $^1\pi\pi^*$ band (fig. 2c). Another weak maximum at 7.97 eV (fig. 2c) is tentatively labelled e'3p (quantum defect 0.42). Finally, we note that the Rydberg structures between 8.5 and 9.2 eV sit on a broad hump which is present, also, in near-threshold EEL spectra (below and fig. 4(i)), suggesting an underlying valence state. We identify the maxima at 8.65 and 8.72 eV respectively (fig. 3b) with this valence state. It will be shown later that the present theoretical data are consistent with a $\pi\pi^*$ in this energy region.

Spectral data are tabulated in table 1.

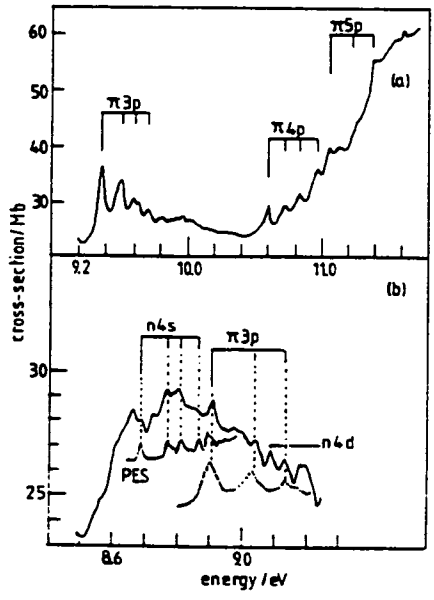

Fig. 3. Absorption bands of 1,3,5-triazine (a) Rydberg states associated with IP_2 (b) Rydberg states. PES is a trace of the $(6e')^{-1}$ band in the photoelectron spectrum taken from ref. [6]. The other trace is of the π3p VUV absorption band of (a).

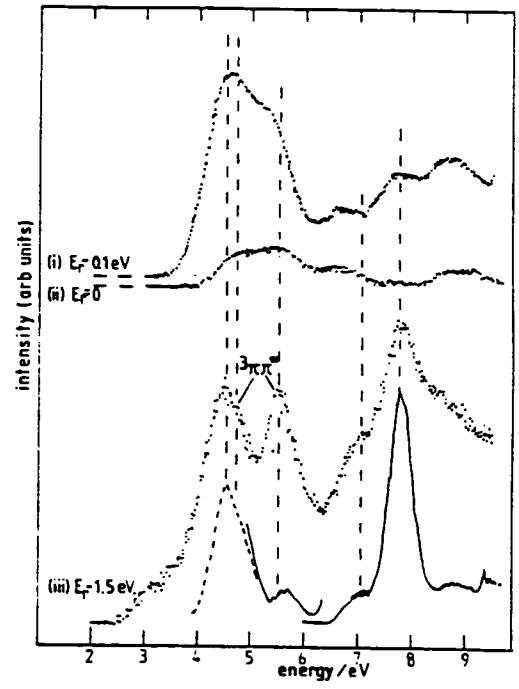

Fig. 4. Spectra of 1,3,5-triazine (i)–(iii) EEL spectra recorded at the indicated residual electron energies, E_r. The signal in (ii) is of negative ions, formed in resonant dissociative attachment processes, and these contribute, also, to the spectrum of (i). The lowest trace is the VUV absorption spectrum, in which the profile of the first absorption band has been taken from ref. [5].

Table 1
Present spectral energies and assignments for 1,3,5-triazine

Valence states			Rydberg states			
energy (eV)	Δ [a]	type	energy (eV)	Δ [a]	type	quantum defect
4.7 [b]		$^3\pi\pi^*$	6.917		^{1}n3s	0.90
5.52 [b]		$^3\pi\pi^*$	6.950	0.033		
			6.967	0.050		
5.479			7.003	0.086		
5.527	0.048		7.034	0.117		
5.585	0.106		7.088	0.171		
5.702	0.213		7.120	0.203		
6.55		$^1\pi\pi^*$	7.153	0.236		
6.65	0.10		7.167	0.250		
6.74	0.19					
6.86	0.31		8.680		^{1}n4s	0.80
			8.718	0.038		
7.187		^{1}nπ^*	8.756	0.076		
7.213	0.026		8.790	0.110		
7.589		$^1\pi\pi^*$	7.97		^{1}n3p	0.42
7.706	0.117					
7.771	0.182		8.161		^{1}n3d	0.29
7.858	0.267		9.077		^{1}n4d	0.18
8.652		$^1\pi\pi^*$	8.902		$^1\pi$3p	0.7
8.718	0.066		9.030	0.128		
			9.124	0.222		
			9.365		$^1\pi$3p	0.52
			9.501	0.136		
			9.595	0.230		
			9.704	0.339		
			10.593		$^1\pi$4p	0.48
			10.718	0.125		
			10.820	0.227		
			10.966	0.373		
			11.046		$^1\pi$5p	0.41
			11.268	0.122		
			11.392	0.246		

[a] Δ = vibrational spacing, see text. [b] EEL, all other energies from VUV spectra.

2.2. Electron energy-loss (EEL)

The EEL spectra illustrated (fig. 4) were recorded in a trapped electron spectrometer which has been described [1–3].

1,3,5-triazine was unusual among the azabenzenes in that it was found to undergo dissociative electron attachment (eq. (1a), see below) via a number of resonant (anionic) states ([AB^-]) starting around 4.2 eV.

$$e + AB \rightarrow [AB^-] \begin{cases} \nearrow A + B^-, & (1a) \\ \searrow AB^* + e. & (1b) \end{cases}$$

The dissociation processes were detected through collection of (unidentified) negative ions (B^- above) in the absence of a trapping potential, that is under conditions such that scattered electrons were not collected. The negative ion signal is shown in fig. 4(ii). The dissociating anion states (located about 4.7, 5.5,

6.6, 8.7 and 9.2 eV) are likely to be excited (2-particle, 1-hole) resonances. Another resonant state, which causes a broad maximum in the total electron scattering cross-section centred near 4.0 eV has been assigned as a ground-state shape resonance (1-particle state) [31].

In fig. 4(i), recorded with a trapping potential of about 0.1 V, negative ions are present along with scattered electrons of residual energy (E_r) 0–0.1 eV; the latter dominate. The resonances revealed in dissociative attachment are likely, also, to decay with autoionisation to the parent (1-particle, 1-hole) states (eq. (1b)). Such resonant, inelastic scattering will account for the relatively large excitation cross-sections observed at 4–6 eV and about 9 eV at low residual electron energies (fig. 4(i)).

Resonant inelastic scattering also complicates the interpretation of the spectrum of fig. 4(iii). In this, only scattered electrons of residual energy ≈ 1.5 eV are recorded [1]. The broad energy-loss band around 3 eV happens for electrons of incident energy around 4.5 eV, which is a resonance region (fig. 4(ii)), and the molecule is excited indirectly via the resonance (eq. (1b)). The final state of the molecule is either a highly vibrationally excited electronic ground state or a low-lying triplet. In order to establish whether or not there is a triplet state spanning 3 eV, we have looked carefully, at low E_r values, for evidence of direct electron energy-loss around 3 eV but without success. In general, the electron energy-loss onset for E_r values below about 1 eV, precedes the optical onset (fig. 4) by about 0.5 eV. Thus, we are sure of triplet state excitation within about 0.5 eV of the optical onset, but the existence of a triplet around 3 eV cannot be settled from the present work.

At higher energy-losses, with $E_r \approx 1.5$ eV, the EEL peaks (fig. 4(iii)) broadly match the VUV absorption bands (fig. 2), but with different relative intensities. However, comparison of peak maxima between different EEL spectra, and with optical data, indicates energy regions where optically forbidden states contribute to inelastic electron scattering (fig. 4). In particular, E_{max} for the second band is 5.5 eV while that in optical absorption is 5.7 eV and there is a weak shoulder at 4.7 eV in EEL ($E_r \approx 1.5$ eV). These data (table 1) are related to computed results in sections 3 and 4.

3. Theoretical methods and basis sets

We continue the policy of using three basis sets, each focused upon a different aspect of the azine properties [1–4]. A double zeta (DZ) basis of the Huzinaga/Dunning-type [32] was employed to identify the low-lying singlet and triplet states of valence character and to study cationic states relevant to assignment of the photoelectron spectrum. This basis set was augmented by molecule-centre-based [3s,2p,2d] Rydberg functions (DZ+R) for the main assignments of the optical and EEL electronic spectra. Finally, we utilized a triple zeta valence+ polarisation basis (TZVP) for an SCF+(all-valence electron) CI study of the $X\ ^1A_1'$ ground state electronic properties of the molecule. Further details of these are contained in section 5 of ref. [4]. Here, it will suffice to note that that total GTO bases are DZ (66), DZ+R (87) and TZVP (138) with numbers of MOs/active electrons in the CI as 43/24, 61/24 and 100/30, respectively. All calculations with the DZ and TZVP bases were at the computed equilibrium geometry, as is standard practice. For consistency with our previous studies, the molecule lies in the yz plane. This will allow direct comparison of particular Rydberg states between the azines. In the present instance, this does not conform with normal point group conventions where $C_3(z)$ is out of plane, but is consistent with ref. [9]. In the DZ+R work, up to 20 roots of each symmetry in the C_{2v} subset were obtained and up to about 50 main reference configurations which, when quadruple open-shell spin combinations (configuration state functions, CSFs) are taken into account, gave about 70 main reference 20 root calculations; these are 70M20R in the MRD-CI terminology [33].

The highest point group accessible in MRD-CI is D_{2h} and hence 1,3,5-triazine was treated in C_{2v} with the identities A_1 ($A_1'+E'$), A_2 ($A_1''+E''$), B_1 ($A_2''+E''$) and B_2 ($A_2'+E'$). The MOs are symmetric (s) and antisymmetric (a) with respect to the xz plane. In D_{3h} symmetry, the SCF single configuration occupancy (all electron) is $1e'^2-6e'^2$, $1a_1'^2-5a_1'^2$, $1a_2'^2$, $1a_2''^2$, $1e''^4$ and all of these have a relationship to the molecular orbitals (MOs) of benzene [9,34,35]. The molecular orbitals of lone-pair (LP) type in the (SCF) ground state transform as ($a_1'+e'$) while the π MOs are ($a_2''+e''$). Excited states will fall into two types,

valence and Rydberg, with the valence states arising from transitions from LP/π to low-lying π^* (benzene-like $1e_{2u}$, here 2e") and σ^* MOs. The linear combinations of MOs in D_{3h} for low-lying excitations can be derived by consideration of the $n\pi^*$ and $\pi\pi^*$ processes occurring.

The lone-pair (LPn) are $5a_1'$ ($n_1+n_2+n_3=n_0$) and 6e' ($n_1+n_2-2n_3=n_s$; $n_2-n_1=n_a$) with π MOs $1a_2''+1e''$ ($\pi_s+\pi_a$). If coupling of other levels can be ignored at this stage (but see below) then the 6 D_{3h} states are given by

$$A_2' = \pi_s\pi_a^* - \pi_a\pi_s^*, \quad (2)$$

$$A_1' = \pi_s\pi_s^* + \pi_a\pi_a^*, \quad (3)$$

$$E' = \pi_s\pi_a^* + \pi_a\pi_s^* \quad \text{and} \quad \pi_s\pi_s^* - \pi_a\pi_a^*, \quad (4)$$

$$A_2'' = n_s\pi_s^* + n_a\pi_a^*, \quad (5)$$

$$A_1'' = n_s\pi_a^* - n_a\pi_s^*, \quad (6)$$

$$E'' = n_s\pi_a^* + n_a\pi_s^* \quad \text{and} \quad n_s\pi_s^* - n_a\pi_a^*. \quad (7)$$

The relationships of the $\pi\pi^*$ states $(1e'')^3(2e'')^1$ to those of benzene are $A_2' = B_{2u}$, $A_1' = B_{1u}$ and $E' = E_{1u}$ [22,23].

4. Theoretical results

4.1. Comparison with other structural data

Early investigation of 1,3,5-triazine by X-ray diffraction showed the molecule to have D_{3h} symmetry [36–38]. With this, and an assumed C–H bond length of 1.084 Å, the moments of inertia from the rotational Raman spectrum yield $r_0(CN) = 1.338$ Å, $\angle NCN = 127°$, $\angle CNC = 113°$ [39]. The results of combined electron diffraction (ED), IR/Raman studies and ab initio force field calculations led to [40] an r_g/r_α structure (also D_{3h}), CN 1.338 Å, CH 1.106 Å, $\angle CNC = 113.9°$ and $\angle HCN = 116.9°$. A number of other electronic structure calculations have produced D_{3h} structures in close agreement with the above results and in particular with $\angle NCN$ exceeding $\angle CNC$ [41,42]. These and other computations will be referred to subsequently, but it is worth noting that split-valence ab initio calculations on the σ and π cations show Jahn–Teller distortion of the ring structures away from D_{3h}. Thus the adiabatic IPs could well refer to elongated molecules, where the equilateral triangles of 3C/3N are distorted to isosceles triangle [43] in the cations.

The results of the present molecular total energies are compared with previous calculations [29,35,44–47] in table 2. In general, former work is restricted to SCF calculations. Some obvious differences [35,47] in DZ basis calculations which are not at equilibrium are apparent from table 2. Thus, the results in ref. [47] were obtained with the same basis as used in the present work but with short C–H bond lengths. This will have some effect upon the calculated ionisation energies [47]. The earlier study [35] used a relatively short expansion of GTOs, with consequent impact upon total energy.

Perhaps because of the high symmetry, the structure of 1,3,5-triazine has been studied at equilibrium with a number of basis sets (table 3). In general, the C–N bond length decreases with increase in basis set from 1.354 Å (STO-3G) [43] to 1.318 Å (6-31G**) [29]. The experimental data seem quite clear that 1.338 Å will fit both Raman [40] and electron diffraction [41] data. In all calculations, the internal bond angle is larger at C that at N.

4.2. Assignment of the PES

The most highly resolved PES of triazine is that of Fridh et al. [6]. The 10–18 eV region can be described in terms of 5 bands (A–E) (fig. 5). The most extensive previous theoretical work is the TDA/GF study [47]. In comparisons with data in refs. [6,47] it should be noted that [6] uses the MO nomenclature of pyridine (up to $11a_1$ $7b_2$ $2b_1$ $1a_2$) as well as the 1,3,5-triazine D_{3h} sequencing (eq. (8)) while ref. [47] uses a valence shell only numbering. Some identities are thus as follows: (i) 6e' (present, [6]), 4e' [47], ($11a_1+7b_2$) [6]; and (ii) $5a_1'$ (present, [6]), $3a_1'$ [47], $8a_1$ [6]. The present results are expressed in terms of orbital occupancy in table 4 and are shown graphically in fig. 5. The best fit of the band A–D centroids (E lies beyond the GF limit) is given by the GF calculations. Preliminary results obtained by the SAC-CI method are also shown in fig. 5. The MRD-CI study shows the same phenomenon as our previous azine studies [2–4], namely, highly selective lowering of the IPs of LP (and σ states generally)

Table 2
Total energies by basis set for 1,3,5-triazine ground state

Basis set	Method	Energy (au)	Ref.
DZ	SCF(r_e)	−278.56266	this work
DZ	CI(1M1R 30e)	−279.10819	this work
DZ	CASSCF(10e) (15416 conf.)	−278.68324	this work
DZ+R	SCF	−278.56443	this work
(DZ+3s2p2d)	CI(11M1R 24e)	−278.92368	this work
TZVP	SCF(r_e)	−278.77460	this work
	CI (30e) (215177 CSF)	−279.43670	this work
STO-3G	SCF(r_e)	−275.13795	[44]
3-21G	SCF(r_e)	−277.10111	[44]
4-31G	SCF(r_e)	−278.2334	[45]
DZ	SCF	−278.567	[46]
DZ	SCF	−278.309	[35]
DZ	SCF	−278.48651	[47]
6-31G	SCF(r_e)	−278.53526	[44]
6-31G*	SCF	−278.69285	[42]
6-31G**	SCF(r_e)	−278.70076	[44]
6-31G**	MP2(r_e)	−279.55806	[29]
6-31G**	MP3(r_e)	−279.57013	[29]

Table 3
Comparison of equilibrium structures from ab initio calculations and experimental data

Method	Ref.	Bond length (Å)		Angle (deg) NCN
		CN	CH	
SCF-DZ	this work	1.3362	1.0788	123.749
SCF-TZVP	this work	1.3154	1.0739	125.459
STO-3G	[43]	1.354	1.091	126.4
4-21G	[43]	1.327	1.065	123.4
4-21G	[41]	1.332	1.067	123.9
4-21G*	[41]	1.325	1.073	126.3
6-31G	[42]	1.353	1.091	126.4
3-21G	[48]	1.330	–	124.0
6-31G**	[29]	1.318	–	125.6
ED [a]	[40] (r_a)	1.338	1.106	126.1
X-ray	[37,38]	1.319	(1.00)	126.8
Raman	[39]	1.338	(1.084)	127.0

[a] ED denotes electron diffraction.

while the π states are well reproduced. Thus ionisation from 6e′, $5a_1'$ and $1a_2'$ are computed to be lower in IP than found experimentally.

We also performed CASSCF calculations of the lowest $^2E'$ and $^2E''$ states. A subset of 10 electrons (9 in ions) in 9 MOs was used, which yielded $^2E'$ 10.428 eV and $^2E''$ 11.411 eV (2220 CSF for the ions). The wavefunctions show some contamination of higher states relative to the immediate one-electron processes and are shown in eqs. (8)–(11), where "a" and "s" refer to antisymmetric and symmetric e-type MOs, and terms with the same occupancy but differ-

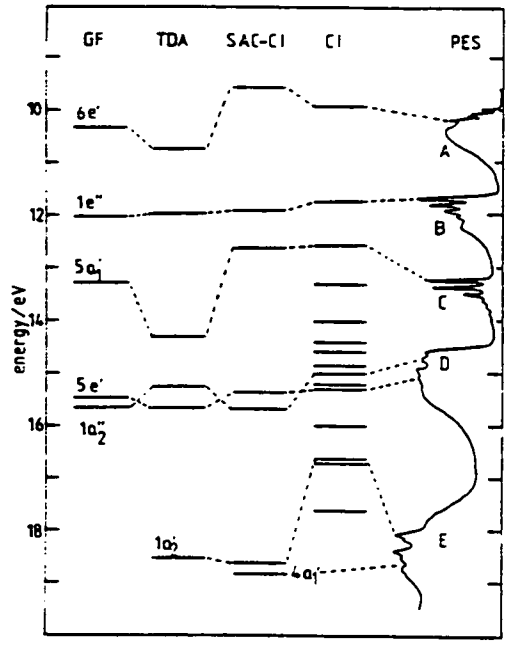

Fig. 5. Ionisation energies and cationic states of 1,3,5-triazine comparison of computed data with an experimental spectrum (PES) taken from ref. [6]. GF is the Green's function, TDA the Tamm–Dancoff calculations [47]. SAC-CI and CI – this work.

Table 4
Computed ionisation potentials (eV) with DZ basis set

Energy (eV)	Orbital occupancy
9.877	$(6e')^3$
11.731	$(1e")^3$
12.589	$(5a_1')^1$
13.341	$(6e')^2(2e")^1$
14.036	$(6e')^2(2e")^1$
14.355	$(6e')^2(2e")^1$
14.572	$(1e")^2(6e')^3(2e")^1$
14.862	$(1e")^2(6e')^3(2e")^1$
14.958	$(1a_2")^1$
15.218	$(1e")^2(6e')^3(2e")^1$
15.294	$(5e')^3$
16.045	$(5a_1')^1(6e')^3(2e")^1$
16.639	$(1a_2')^1$
16.715	$(5a_1')^1(6e')^3(2e")^1$
17.617	$(1e")^2(2e")^1$

ent spin combinations have been gathered together. The CASSCF energies for $1\,^2E'$ and $1\,^2E"$ are closer to experiment than the CI values.

The SCF and CASSCF X $^1A_1'$ ground state:

$$\Psi_{SCF} = 1a_1'^2\,5a_1'^2\,1e'^4\,6e'^0\,1a_2'^2\,1a_2"^0\,1e"^0\,, \quad (8)$$

$$\Psi_{CASSCF} = 0.955\Psi_{SCF} - 0.235\Psi[(1e_a")^2(2e_a")^2] - 0.106\Psi[(1e_a")^1(1e_s")^1(2e_a")^1(2e_s")^1]\,. \quad (9)$$

The CASSCF X $^2E'$ ground state:

$$\Psi_{CASSCF} = 0.940\Psi[(6e')^3] + 0.276\Psi[(1e")^3(6e')^3(2e")^3] - 0.109\Psi[(1e_a")^2(6e')^3(2e_a")^2]\,. \quad (10)$$

The CASSCF X $^2E"$ ground state:

$$\Psi_{CASSCF} = 0.949\Psi[(1e")^3] - 0.173\Psi[(1e_a")^1(1e_s")^1(2e_a")^1] - 0.114\Psi[(1e")^1(2e_s")^2]\,. \quad (11)$$

The present study confirms that the adiabatic IPs [6] at 10.01 (A), 11.69 (B) and 13.26 (C) eV (fig. 5) are indeed $1\,^2E'$, $1\,^2E"$ and $1\,^2A_1'$ states, respectively. Furthermore, band D is clearly $1\,^2A_2" + 2\,^2E'$ (if shake-up states are omitted from the terminology) but, as with ref. [47], the order of states is uncertain. Band E is $1\,^2A_2' + 2\,^2A_1'$, again of uncertain order and, in agreement with ref. [6], the fine structure must be associated with $2\,^2A_1'$.

4.3. Calculated excited states and relation to experiment

4.3.1. Valence states

Principal results for the MRD-CI studies are given in table 5 (DZ basis set, singlet and triplet states; DZ+R basis, singlet states only).

For the $^1\pi\pi^*$ states, the DZ basis set gives $^1A_2'$ 5.48 eV (5.7 eV measured), $^1A_1'$ 7.52 eV (6.86 eV measured) and $^1E'$ 7.89 eV (7.76 eV measured). The state order is correct and the energies good for the first and third states. Addition of the Rydberg functions slightly increased the $^1A_2'$ state energy (5.59 eV), making it very close to the experimental value. However, the energies of the two higher states were lowered, that for $^1E'$ excessively (to 7.25 eV) bringing it below the $^1E_1'$ state (now 7.41 eV). Thus, it was difficult to get the correct balance of valence and Rydberg functions in these states. The basis set used seemed to exaggerate the Rydberg character of the E' state. Arguments were presented above for a valence

Table 5
Excitation energies (eV) for low-lying singlet (^1S) and triplet (^3T) states of 1,3,5-triazine

Open shells		Energy (eV)				
		calculated [a]			experiment	
		(^1S)		(^3T) DZ	^1S	^3T
		DZ	DZ+R			
Valence states						
$n\pi^*$						
$e'e''$	A_2''	4.237	4.139	3.439	4.58 [d]	≈ 3 [c]?
	A_1''	4.402	4.252	3.510		
	E''	4.459	4.030	3.656	3.83 [e]	≈ 3.3 [c]
$a_1' \pm e'a_2$	E''	7.359	7.080	6.524		
	E''	7.885		7.840		
$e'e''$	A_2''	9.312	7.747	8.746	7.19 [b]	
	E''	9.471		8.282		
	A_1''	9.928		9.352		
$(e''b')^6(e'')^2$	A_2''	10.075		9.396		
$\pi\pi^*$						
$e''e''$	A_2'	5.481	5.595	5.206	5.7 [b]	4.7 [c]
	A_1'	7.522	7.406	4.523	6.86 [b]	
	E'	7.893	7.252	5.386	7.76 [b]	5.52 [c]
$a_2''e'' \pm e''a_2''$	E'	9.2	10.032	8.161	8.65 [b]	
	E'	11.601		10.617		
$n\sigma^*$						
$e'a_1'$	E'	10.026		9.568		
$e'e'$	A_1'	10.737		10.154		
	A_2'	10.739		9.201		
	E'	10.763		10.531		
	Type		**DZ+R**		**Experiment**	
Rydberg states						
$n\pi^*$						
$e'e'' \pm e'e''$	$A_2''(xx, xy)$		7.021			
	$E''(xz, xy)$		7.861			
	$A_1''(xz, xy)$		8.582			
	$A_2''(x)$		7.502		7.97 [b]	
	$E''(x)$		7.396			
$a_1'e'' \pm e'a_2''$	$A_1(x)$		8.433			
$e'e'' \pm e'a_2'$	$E''(xz, xy)$		8.627			
	$E''(xz, xy)$		9.537			
$n\sigma^*$						
$e''na_1'$	$E''(s)$		8.270			
	$E''(s)$		9.457			
$e''ne'$	$A_2''(y, z)$		8.786		8.90 [b]	
	$E''(y, z)$		9.736			
	$A_1''(y, z)$		9.658			

(Continued on next page)

Table 5 (continued)

	Type		DZ+R	Experiment
$n\sigma^*$				
$e'na_1'$	$E'(s)$		6.599	6.92 [b]
	$E'(s)$		8.819	8.68 [b]
	$E'(s)$		9.430	
$e'na_1'$	$E'(x^2)$		8.130	8.16 [b]
$e'e' \pm e'e'$	$E'(yz, y^2-z^2)$		8.475	
	$A_1'(yz)$		7.911	
	$A_1'(yz)$		8.651	
$e'e'$	$A_2'(y, z)$	7.328		
	$A_1'(y, z)$	8.049		
	$E'(y, z)$	8.912		
$n\pi^*$				
$e''a_2''$	$E'(x)$		9.407	9.36 [b]
	$E'(x)$		10.857	10.59 [b]
$e''e'' \pm e''e''$	$E'(xz, xy)$		10.448	
	$A_1'(xz)$		10.172	

[a] This work. [b] Present VUV. [c] Present EEL. [d] Ref. [5]. [e] Refs. [19,20].

state underlying the Rydberg state transitions at 8.5–9.2 eV (figs. 3b and 4(i)). We propose a $\pi\pi^*$ ($^1E'$) assignment, calculated at 9.2 eV (DZ, table 5).

For the $^1n\pi^*$ states, both basis sets predict three to lie near 4 eV excitation energy. Of these, only the $^1A_2''$ component has non-zero oscillator strength. We assume this to be dominant in VUV absorption and so assign it to the 4.58 eV transition [5] and fig. 4; calculated values are 4.24 eV (DZ) and 4.14 eV (DZ+R). The extended basis set correctly predicts $^1E''$ to be lowest-lying of the $^1n\pi^*$ states. Its measured origin is 3.827 eV which compares with calculated vertical excitation energies of 4.46 eV (DZ) and 4.03 eV (DZ+R). The third (optically forbidden) state in this group, $^1A_1''$ (calculated energy 4.40 eV (DZ) and 4.25 eV (DZ+R)), has not yet been located by experiment. A higher optically allowed ($^1A_2''$) state is to be expected. Such a state was computed at 7.75 eV with the DZ+R basis, having been lowered dramatically from the DZ value of 9.31 eV. This implies Rydberg character. As pointed out above, two relatively sharp (and Rydberg-like) optical bands at 7.187 and 7.213 eV (fig. 2a) appear not to belong to the nearby e'3s state and we now suggest that they arise from excitation of this fourth $n\pi^*$ state.

Brinen and Goodman [10] have noted that, as well as the $(e')^3(e'')^1$ MO composition leading to $E''+A_1''+A_2''$ states, further interactions could perturb these E'' states. If we adopt the nomenclature of ref. [10], with the identities for the inner lone-pair level ($5a_1'$, n_0), the degenerate levels ($6e'$, $n_1/n_{(1)}$) and ($1e''$, $\pi_1/\pi_{(1)}$) then (unnormalised) states of each symmetry of the types shown could emerge as follows:

$$A_2'' = n_0^2 n_{(1)}^2 n_1^1 \pi_2^1 + n_0^2 n_1^2 n_{(1)}^1 \pi_{(2)}^1 , \quad (12)$$

$$A_1'' = n_0^2 n_{(1)}^2 n_1^1 \pi_2^1 - n_0^2 n_1^2 n_{(1)}^1 \pi_{(2)}^1 , \quad (13)$$

$$E_1'' = n_0^2 n_{(1)}^2 n_1^1 \pi_{(2)}^1 + n_0^1 n_{(1)}^2 n_1^2 \pi_2^1 , \quad (14a)$$

$$E_1'' = n_0^2 n_1^2 n_{(1)}^1 \pi_2^1 + n_0^1 n_{(1)}^2 n_1^2 \pi_{(2)}^1 , \quad (14b)$$

$$E_2'' = n_0^2 n_{(1)}^2 n_1^1 \pi_{(2)}^1 - n_1^2 n_{(1)}^2 n_0^1 \pi_2^1 , \quad (15a)$$

$$E_2'' = n_0^2 n_1^2 n_{(1)}^1 \pi_2^1 - n_1^2 n_{(1)}^2 n_0^1 \pi_{(2)}^1 \quad (15b)$$

First, we note that there was no evidence in the calculated states ($1A_2'' + 1A_1'' + 1E''$) of interactions with configurations derived from $n_0(5a_1')$ except at a minute level. Second, a more substantial interaction occurs in $2E''/3E''$, namely a perturbation of the $5a_1' 2e''$ state by $6e'2a_2''$. Finally, the symmetry designations of ref. [10] A_2'', A_1'', E'' (eqs. (12)–(15)) do not follow those of eqs. (5)–(7), whereas the latter obey the standard conventions with the irreducible representations in D_{3h} [#1]. It is interesting to note in

[#1] We are grateful to Dr. K.P. Lawley for discussion on this point.

this context, that the inner π-MO, $1a_2''$, participates in similar interactions with $2a_2''$ in the 2E′ and 3E′ states through the combinations $(1a_2''2e'')+(1e''2a_2'')$. All of these interactions are mirrored in the singlet and triplet manifolds.

In the triplet manifold, we calculate three $^3n\pi$ states to lie below S_1 and within 0.3 eV of each other. This is generally consistent with available experimental data. As discussed in section 2.2, it is not clear whether or not any of these contribute to the observed electron energy-loss band at 3 eV (fig. 4(iii)). Three $^3\pi\pi$ states emerge at 4.53, 5.20 and 5.39 eV respectively. From these, we assign the shoulder at 4.7 eV in EEL and the maximum at 5.5 eV (fig. 4(iii)) to $^3\pi\pi^*$ excitation. A third, relatively low-energy triplet state ($^3n\pi$, $^3E''$) is calculated at 6.52 eV. This may contribute to near-threshold electron energy-loss at 6.5 eV (fig. 4(i)). As pointed out above, from experiment, triplet states appear to lie close to optically allowed states and the present theoretical work supports this view.

4.3.2. Rydberg states

Calculated energies for singlet Rydberg states are listed in table 5. The computed value for the first of these, n3s (E″), is 6.6 eV which compares with a measured energy of 6.92 eV. The corresponding n4s state is calculated to lie at 8.82 eV, in reasonable agreement with the experimental estimate of 8.68 eV (ref. [6], and this work).

Rydberg states of type e′3p (i.e. associated with IP_1, 10.01 eV, $(6e')^{-1}$) are expected, from quantum defects, around 7.5 eV and hence obscured in the VUV by the strong $\pi\pi^*$ absorption. The only such state to have been located by spectroscopy is that at 7.97 eV, assigned from the present optical data (fig. 2c). As seen in table 5, calculated energies which may be identified with states of this type are in reasonable agreement with expectation. The same is generally true for e′3d states. The computed energy of an optically allowed component, 8.13 eV (table 5) agrees well with a proposed experimental energy, 8.16 eV (fig. 2c). However, a computed energy of 7.02 eV for an (e′3d) state of symmetry $^1A_2''$ (table 5) is low by more than 1 eV.

Of the Rydberg states relating to IP_2 (11.69 eV, $(1e'')^{-1}$) only a few are optically allowed. As discussed above, a transition at 8.90 eV in the VUV spectrum (fig. 3b) has the mark of a Rydberg state e″3s, $^1E''$ (computed energy 8.27 eV) but its intensity is high for an optically forbidden process. On the other hand e″$3p_{y,z}$ components ($^1A_2''$) are calculated to lie at 8.79 eV, close to the observed 8.90 eV energy. An allowed excitation, terminating in a p_x-type orbital, is calculated at 9.41 eV which compares with an observed value of 9.36 eV (fig. 3a).

5. Ground state electronic properties

Present computed results are collected in table 6. Owing to the high symmetry of the molecule, few experimental data are available for comparison. In principle, we might expect data on second moments of the charge distribution to arise from microwave (MW) experiments on monodeutero-1,3,5-triazine, where the small dipole moment, as in monodeuterobenzene [48] should allow MW study. The magnetic shielding at the *N* nuclei is remarkably similar to that in pyrimidine [2], where the *N* atoms also have a meta-orientation. The ^{14}N nuclear quadrupole coupling is 4.572 MHz with asymmetry parameter (η) 0.443 [49]. It has generally been assumed that the three components χ_{zz}, χ_{yy} and χ_{xx}, which by definition have $|\chi_{zz}| \geq |\chi_{yy}| \geq |\chi_{xx}|$, have the orientation radial (*R*, pointing out from the ring centre), *T* (tangential) and *Π* at N, with derived values of −4.572, +1.273 and +3.299, respectively [50]. In other papers of this series [1–4], we have noted that the TZVP basis set yields a value of the ^{14}N nuclear quadrupole coupling constant (Q_N) of 5.0111 MHz au^{-1} [4]. The computed ^{14}N nuclear quadrupole coupling constants (SCF/CI) for the free molecule are −5.410/−5.228 (*R*), +1.762/1.787 (*T*) and +3.684/+3.441 MHz (*Π*). As with the other azines [1–4], these values are higher in magnitude that the condensed phase (77 K) data [50], but the orientation of the *R*, *T*, *Π* components match the assumed set [50]. In the crystal, the molecules lie (stepwise) in parallel sheets with the shortest intermolecular contacts C–C 3.31 and N–N 3.17 Å [37]. Thus there is no intermolecular H bonding.

In the absence of experimental information on any of the second moments of the charge distribution or magnetic susceptibility, it seems appropriate to review the changes as the benzene ring is modified by replacement of CH by N. The diamagnetic susceptibility (electronic term total) shows that the out-of-

Table 6
Calculated one-electron properties for the ground state of 1,3,5-triazine at r_e from the TZVP basis set – atomic properties evaluated at the N C H nuclei, molecular properties at the centre of mass [a]

			SCF	CI
Atomic	potential (esu cm^{-1})			
	at N		−166.4894	−166.4905
	at C		−132.7932	−132.9842
	at H		−9.7604	−9.7642
	magnetic shielding (ppm)			
	at N	z^2	−328.8991	−328.9508
		y^2	−336.2608	−336.1638
		x^2	−311.6178	−311.6694
	at C	z^2	−265.3546	−265.7891
		y^2	−268.0480	−268.6142
		x^2	−245.6829	−245.8024
	at H	z^2	−35.6732	−35.6246
		y^2	−16.6571	−16.7088
		x^2	−4.9332	−4.9525
	electric field (10^8 dyne esu^{-1})			
	at N	z	0.0092	0.0089
		y	0.0053	0.0051
	at C	z	−0.0013	−0.0017
		y	−0.0008	−0.0010
	at H	z	−0.0018	−0.0024
		y	−0.0010	−0.0014
	force at nucleus (au)			
	at N	z	0.3741	0.3623
		y	0.2160	0.2092
	at C	z	−0.0454	−0.0589
		y	−0.0262	−0.0340
	at H	z	−0.0106	−0.0141
		y	−0.0061	−0.0081
	electric field gradient at ^{14}N			
	principal axis [b]	R	1.0796	1.0433
		T	−0.3444	−0.3566
		Π	−0.7352	−0.6867
		η	0.362	0.316
	electric field gradient at ^{2}H			
	principal axis [c]	q	0.1575	0.1571
		B	−0.3229	−0.3227
		Π	0.1654	0.1656
		η	0.024	0.026

(Continued on next page)

Table 6 (continued)

		SCF	CI
Molecular	quadrupole moment (esu cm^2)		
	z^2 (=y^2)	−0.4506	−0.5317
	x^2	0.9013	1.0634
	second moments (10^{-16} cm^2)		
	electronic z^2 (=y^2)	−49.4951	−49.5347
	x^2	−7.1192	−7.1109
	total z^2 (=y^2)	−7.3716	−7.4082
	x^2	−7.1192	−7.1104
	diamagnetic susceptibility (10^{-6} emu mol^{-1})		
	electronic z^2 (=y^2)	−240.1902	−240.3085
	x^2	−419.9730	−420.2840
	total z^2 (=y^2)	−61.4781	−61.5964
	x^2	−62.5488	−62.8598

[a] For consistency with excited state studies in the azines [1–4,9], the molecule lies in the yz plane.
[b] R, T and Π correspond to principal axes pointing in a radial, tangential and π direction respectively.
[c] q and π correspond to in-plane and out-of-plane π components, while B refers to the component along the CH bond.

plane component (x^2) is about 5% lower for each of the diazines relative to benzene or pyridine [1–4], and this trend is continued with a further 5% drop for 1,3,5-triazine. The in-plane values decline in the same sequence but the effects are smaller. The experimental values for pyridine and benzene are similar [51]. The magnetic susceptibility anisotropy [52] has been used as a measure of aromatic character. It is defined as the difference between the out-of-plane and average of the in-plane values of magnetic susceptibility. In the present series, the values are little changed by CI being ($\times 10^{-6}$ emu mol^{-1}) pyridine (−203), diazines (−191) and 1,3,5-triazine (−180) and supporting the contention that there is a lowering of aromatic character as CH is replaced by N and in contrast to ref. [29].

The second moments of the electronic charge distribution, also determined from MW spectroscopy in suitable cases, have long been known to be well represented by SCF calculated values [53]. The present series of TZVP basis set calculations, with and without CI, show that the results are very accurate for pyridine [53,54], leading to confidence that those computed for the higher azines are of predictive value. The total values of the second moments (generally) include the nuclear components; since these are zero for the out-of-plane component (c^2 in MW, here x^2), it is not surprising that the x^2 values are markedly smaller in magnitude. However, as CH is replaced by N in $C_nH_nN_{6-n}$, the value of x^2 (in units of 10^{-16} cm^2) shows a decline, thus −8.50 (n=6), −8.0 (n=5), −7.6 (n=4), and −7.1 (n=3) [55].

In the special case of the molecular quadrupole moments, the sign of the out-of-plane value ($\langle|3x^2-r^2|\rangle$, table 6) changes in the series, with values (in units of 10^{-26} esu cm^2) −8.95 (n=6), −5.0 (n=5), −2.5±0.3 (n=4), and +0.90 (n=3).

6. Concluding remarks

Excitation energies of the low-lying excited states of 1,3,5-triazine have been calculated to within 0.6 eV for all, and to within 0.3 eV for most, relative to experimental vertical values. The largest discrepancy between computed and measured energies are for the second and third $\pi\pi^*$ states. These results confirm that the three low-lying $^1n\pi^*$ states of 1,3,5-triazine all lie within the energy region spanned by the first optical absorption band. Within this group, the singlet–triplet splitting is about 0.5 eV (but the possibility of a $^3n\pi^*$ state around 3 eV has arisen from the electron

impact experiments). The lowest $^3\pi\pi^*$ state is in this same energy region. We have proposed spectral energies for a fourth low-lying $^1n\pi^*$ state (about 7.2 eV) as well as a fourth $^1\pi\pi^*$ state (about 8.5 eV).

The paucity of observed Rydberg-excited states is accounted for by the fact that only a few are optically allowed and, these, in general, lie in congested spectral regions.

The GF calculations lead to the best interpretation of the ionisation potentials, where MRD-CI produces low IPs for n-type ionisations, as found previously for other azines.

Of the ground state properties considered here, the ^{14}N nuclear quadrupole coupling is the only one to have been determined by experiment and is well reproduced by the present calculations. Further experimental work in this area is necessary.

Acknowledgement

We thank Dr. M.F. Guest for developments to the MRD-CI module in GAMESS, Dr. A. Hopkirk for support and assistance at the Daresbury Laboratory, the SERC for the award of beam time at the Synchrotron Source, Daresbury and a studentship (to CCB) and the Computer Board for the provision of computing facilities.

References

[1] I.C. Walker, M.H. Palmer and A. Hopkirk, Chem. Phys. 141 (1990) 365.
[2] M.H. Palmer, I.C. Walker, M.F. Guest and A. Hopkirk, Chem. Phys. 147 (1990) 19.
[3] I.C. Walker and M.H. Palmer, Chem. Phys. 153 (1991) 169.
[4] M.H. Palmer and I.C. Walker, Chem. Phys. 157 (1991) 187.
[5] A. Bolovinos, P. Tsekeris, J. Philis, E. Pantos and G. Andritsopoulos, J. Mol. Spectry. 103 (1984) 240.
[6] C. Fridh, L. Asbrink, B.O. Jonsson and E. Lindholm, Intern. J. Mass Spectrom. Ion Phys. 8 (1972) 85.
[7] F. Halverson and R.C. Hirt, J. Chem. Phys. 19 (1951) 711.
[8] J.S. Brinen, R.C. Hirt and R.G. Schmitt, Spectrochim. Acta 18 (1962) 863.
[9] K.K. Innes, I.G. Ross and W.R. Moomaw, J. Mol. Spectry. 132 (1988) 492.
[10] J.S. Brinen and L. Goodman, J. Chem. Phys. 31 (1959) 482.
[11] J.S. Brinen and L. Goodman, J. Chem. Phys. 35 (1961) 1219.
[12] L. Goodman, J. Mol. Spectry. 6 (1961) 109.
[13] Y. Udagawa, M. Ito and S. Nagakura, J. Mol. Spectry. 39 (1971) 400.
[14] J.D. Webb, K.M. Swift and E.R. Bernstein, J. Chem. Phys. 73 (1980) 4891.
[15] M. Heaven, T. Sears, V.E. Bondybey and T.A. Miller, J. Chem. Phys. 75 (1981) 5271.
[16] A.E.W. Knight and C.S. Parmenter, Chem. Phys. 43 (1979) 257.
[17] N. Olha and H. Baba, Chem. Phys. Letters 84 (1981) 308.
[18] H. Saigusa and E.C. Lim, J. Chem. Phys. 78 (1983) 91.
[19] J.B. Palix and S.D. Colson, Chem. Phys. Letters 119 (1985) 38.
[20] P.U. de Haag, W.L. Meerts and J.T. Hougen, Chem. Phys. 151 (1991) 371.
[21] R.L. Whetter and E.R. Grant, J. Chem. Phys. 81 (1984) 691.
[22] R. Pariser and R.G. Parr, J. Chem. Phys. 21 (1953) 767.
[23] N. Mataga and K. Nishimoto, Z. Physik. Chem. NF 13S (1957) 140.
[24] W.R. Carper and J. Stengl, Mol. Phys. 15 (1968) 121.
[25] I. Fischer-Hjalmars and M. Sundbom, Acta Chem. Scand. 22 (1968) 607.
[26] M. Sundbom, Acta Chem. Scand. 25 (1971) 487.
[27] R. Sen and S. Bhattacharyya, Indian J. Pure Appl. Phys. 24 (1986) 348.
[28] K. Jug and G. Hahn, J. Comput. Chem. 4 (1983) 410.
[29] K.B. Wiberg, D. Nakaji and C.M. Breneman, J. Am. Chem. Soc. 111 (1989) 4178.
[30] R. Gleiter, E. Heilbronner and V. Hornung, Helv. Chim. Acta 55 (1972) 255.
[31] I. Nenner and G.J. Schulz, J. Chem. Phys. 62 (1975) 1714.
[32] T.H. Dunning, J. Chem. Phys. 55 (1971) 716.
[33] R.J. Buenker, in: Proceedings of the Workshop on Quantum Chemistry and Molecular Physics, Wollongong, Australia (1980), ed. P.G. Burton (Wollongong Univ. Press, 1980); Studies in physical and theoretical chemistry, Vol. 21, ed. R. Carbo (Elsevier, Amsterdam, 1982); R.J. Buenker and R.A. Phillips, J. Mol. Struct. 123 (1985) 291.
[34] M.H. Palmer, A.J. Gaskell and R.H. Findlay, J. Chem. Soc. Perkin Trans. II (1974) 778.
[35] J. Almlof, B. Roos, U. Wahlgren and H. Johansen, J. Electron Spectry. Relat. Phenom. 2 (1973) 51.
[36] L.A. Siegal and E.F. Williams, J. Chem. Phys. 22 (1954) 1147.
[37] P.J. Wheatley, Acta Cryst. 8 (1955) 224.
[38] P.F. Price, E.N. Matsen and W.T. Delany, Acta Cryst. A 34 (1978) 194.
[39] J.E. Lancaster and B.P. Stoicheff, Can. J. Phys. 34 (1956) 1016.
[40] W. Pyckout, I. Callaerts, C. Van Alsenoy, H.J. Geise, A. Almenningen and R. Seip, J. Mol. Struct. 147 (1986) 321.
[41] F. Pang, P. Pulay and J.E. Boggs, J. Mol. Struct. 88 (1982) 79.
[42] O. Mo, J.L.G. De Paz and M. Yanez, J. Mol. Struct. 150 (1987) 135.

[43] H. Kato, K. Hirao and K. Yamashita, J. Mol. Struct. 88 (1982) 265.
[44] Y. Osamura, M. Unno and K. Hashimoto, J. Am. Chem. Soc. 109 (1987) 1370.
[45] E. Fos, J. Vilarrasa and J. Fernandez, J. Org. Chem. 50 (1985) 4894.
[46] F. Mulder, G. van Dijk and C. Huizoon, Mol. Phys. 38 (1979) 577.
[47] W. von Niessen, W.P. Kraemer and G.H.F. Diercksen, Chem. Phys. 41 (1979) 113.
[48] J.S. Murray, J.M. Seminario and P. Politzer, J. Mol. Struct. 187 (1989) 95.
[49] L. Guibe and E.A.C. Lucken, Mol. Phys. 10 (1966) 273.
[50] E.A.C. Lucken, Nuclear quadrupole coupling constants (Academic Press, London, 1969) p. 233.
[51] J.H.S. Wang and W.H. Flygare, J. Chem. Phys. 52 (1970) 5636.
[52] D.H. Sutter and W.H. Flygare, J. Amer. Chem. Soc. 91 (1969) 4063.
[53] M.H. Palmer, R.H. Findlay and A.J. Gaskell, J. Chem. Soc. Perkin Trans. II (1974) 420.
[54] R.C. Benson and W.H. Flygare, J. Am. Chem. Soc. 92 (1970) 7523.
[55] M.H. Palmer and I.C. Walker, Chem. Phys. 133 (1989) 113.